Modelling, simulation and control of the filtration process in a submerged anaerobic membrane bioreactor treating urban wastewater

ÁNGEL ROBLES MARTÍNEZ

EDITORIAL
UNIVERSITAT POLITÈCNICA DE VALÈNCIA

UNIVERSITAT POLITÈCNICA DE VALÈNCIA

DEPARTAMENTO DE INGENIERÍA HIDRÁULICA Y MEDIO AMBIENTE

MODELLING, SIMULATION AND CONTROL OF THE FILTRATION PROCESS IN A SUBMERGED ANAEROBIC MEMBRANE BIOREACTOR TREATING URBAN WASTEWATER

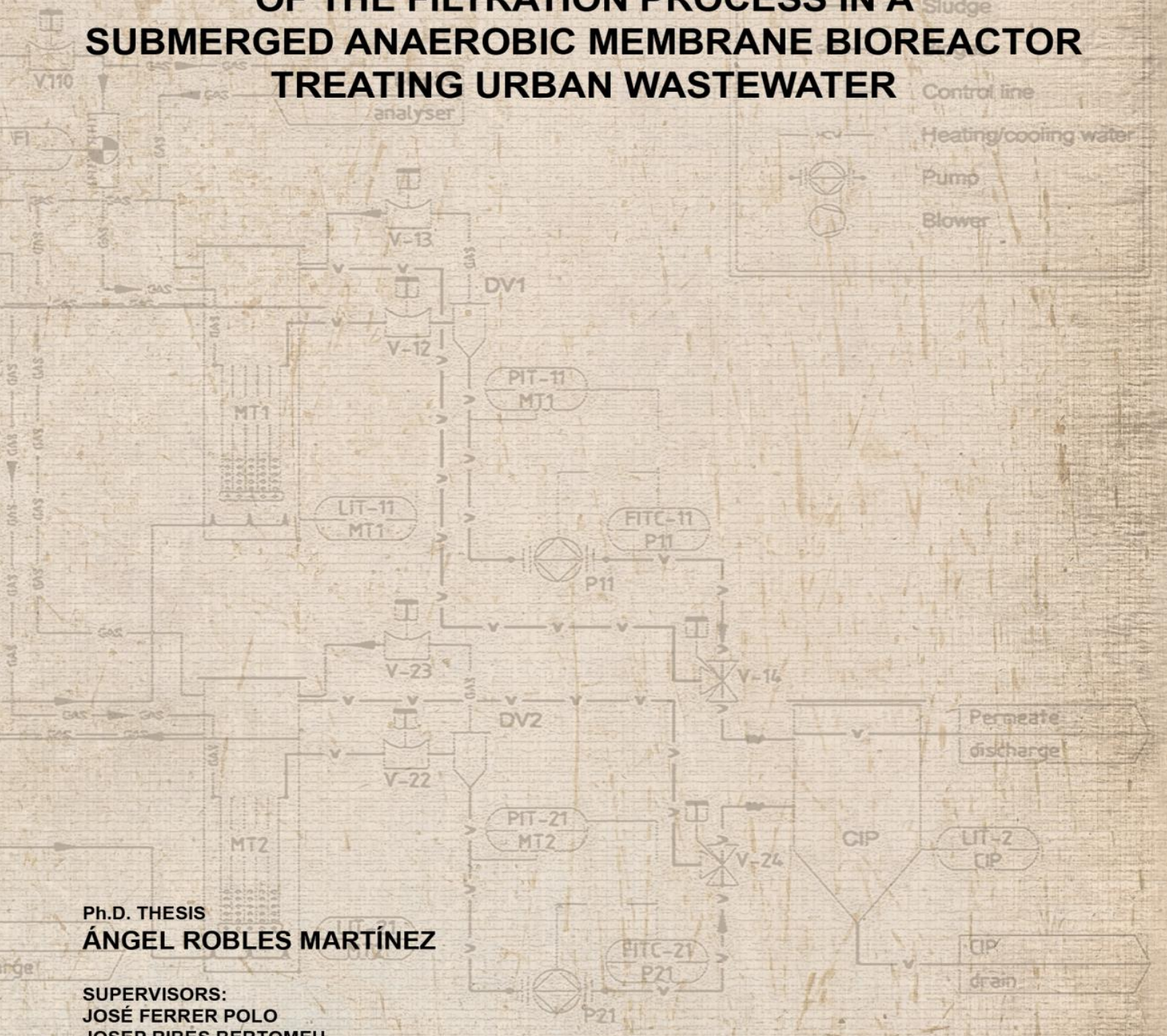

Ph.D. THESIS

ÁNGEL ROBLES MARTÍNEZ

SUPERVISORS:
JOSÉ FERRER POLO
JOSEP RIBES BERTOMEU
MARÍA VICTORIA RUANO GARCÍA

NOVEMBER 2013

Department of Hydraulic Engineering and Environment

UNIVERSITAT
POLITÈCNICA
DE VALÈNCIA

Modelling, simulation and control of the filtration process in a submerged anaerobic membrane bioreactor treating urban wastewater

This thesis is submitted in partial fulfilment of the requirements for the Degree of Doctor of Philosophy

Ph.D. THESIS
ÁNGEL ROBLES MARTÍNEZ

SUPERVISORS:
JOSÉ FERRER POLO
JOSEP RIBES BERTOMEU
MARÍA VICTORIA RUANO GARCÍA

NOVEMBER 2013

Collection Doctoral Thesis

First Edition, 2013

Telf.: 963 877 012 / www.lalibreria.upv.es

ISBN: 978-84-9048-176-9 (printed version)

A mí madre...

ACKNOWLEDGEMENTS

En estas líneas deseo plasmar mi más sincero agradecimiento a todas aquellas personas que de una forma u otra me han ofrecido su apoyo y confianza durante estos cuatro años de mi vida…

En primer lugar quisiera agradecer a la doctora Aurora Seco y a mi tutor y director de tesis el doctor José Ferrer, por confiar en mí y brindarme la oportunidad de crecer tanto personal como profesionalmente. Gracias por concederme la beca pre-doctoral que ha permitido este trabajo.

A los doctores Mª Victoria Ruano y Josep Ribes, por haber sido más que directores de tesis y haberme enseñado mucho más de lo que refleja este documento. Me habéis brindado vuestra amistad, me habéis hecho reír, y me habéis sabido dar el ánimo que en tantos momentos he necesitado. Gracias por confiar tanto en mí.

Al Ministerio de Ciencia e Innovación, por la beca concedida durante estos cuatro años, dentro del programa de ayudas a la Formación de Personal Investigador (FPI).

I would like to thank Jean-Philippe Steyer and Eric Latrille for giving me the chance to learn with them and welcoming me into their research group during six months. Of course, I also want to thank so amazing people I met in the Laboratoire de Biotechnologie de l'Environnement in Narbonne: Cecilia, Salomé, Abigail, Carlos, Quentin, Florian, Benoit, Sofian, Nico, and so on.

A los doctores Ramón Barat y Joaquín Serralta, que vieron algo en mí cuando era alumno de máster. Vosotros plantasteis la semilla de esta tesis doctoral, y me habéis ayudado y guiado durante mis inicios en la docencia universitaria.

A Freddy, mi *partner* en este duro camino, por hacer más llevaderas las duras horas de trabajo tanto en el despacho como en la planta, por ofrecerme su amistad, y como no, ¡por aguantarme!. Siempre podrás contar conmigo. Y a Ángela, por su gran ayuda en el diseño de las portadas de esta tesis.

A Laura C. y Juan Bautista, por aportar tantas risas y buenos momentos mientras luchábamos contra el SAnMBR. El trabajo se hace ameno a vuestro lado.

A Javier Claros, por ser sin duda pieza imprescindible en esta aventura. Gracias por ofrecerme distintos (y similares) puntos de vista que tanto me han enseñado. Siempre tendrás mi amistad y apoyo incondicional.

A Alberto, Luís, Paqui y Daniel A., por brindarme la oportunidad de aprender y de reír junto a vosotros. Sabéis muy bien como amenizar un menú de cafetería con vuestro buen humor.

A Emérita, con quien (junto a Freddy y Javier C.) tanto he reído en esos mini *breaks* de despacho. Y a Nuria, que tiene esa capacidad innata de hacerte sonreír y sacar el lado bueno de las cosas.

A Antonio, Dani G., Ana R., Ruth, Álex y Tao, por tantos y tantos buenos momentos almorzando, comiendo, merendando y ¡hasta cenando!. Gracias por hacerme reír y darle alegría a la UPV.

A todos los compañeros del "labo" en Burjassot: Marcela, Laura S., Sara, Rafa, Brenda, Ana P., Javier E., Silvia, Mónica, Joana, Patri… por acogerme como a uno más tanto dentro como fuera de la UV.

A mis amigos, Patri, JuanMa, Sandra, Mikel, Eva, Pablo, Ester, Victor, Cristian… por estar toda una vida a mi lado y por ser mi familia. Os quiero.

A mi familia, por apoyarme tanto. Y ante todo a mi madre, por guiarme en la vida. Sin ti nada de esto habría sido posible. Te llevaré siempre conmigo mamá, te quiero.

ABSTRACT

Submerged anaerobic MBRs (SAnMBRs) are considered as a candidate technology to improve sustainability in wastewater treatment field, broadening the range of application of anaerobic biotechnology to low-strength wastewaters (*e.g.* urban ones) or extreme environmental conditions (*e.g.* low operating temperatures). This alternative technology is more sustainable (rather than aerobic-based technologies) because wastewater turns into a renewable source of energy and nutrients, whilst providing a recyclable water resource. SAnMBRs not only has the main advantages of MBRs (*i.e.* high quality effluent, and reduced space requirements) but also the main advantages of anaerobic processes. In this regard, low sludge production can be obtained due to the low biomass yield of anaerobic organisms, low energy demand is required since aeration is not needed, and methane is produced – a renewable energy source that improves the energy balance in this system. Mention must also be made of the potential nutrient recovery from wastewater either when the effluent can be used for direct irrigation or when it must be further treated by using nutrient recovery technologies.

The main aim of this Ph.D. thesis is therefore to investigate the potential of SAnMBR as core technology for urban wastewater treatment at ambient temperature. Specifically, this thesis focusses on the following aspects: (1) set-up, calibration and start-up of the required instrumentation, control, and automation (ICA) system; (2) identification of the key operating parameters affecting membrane performance; (3) modelling and simulation of the filtration process; and (4) development of different control strategies aimed to optimise filtration process under the minimum operating cost.

In this research work, an ICA system is proposed for SAnMBRs, which is required for enabling suitable and stable process performance towards perturbations. Membrane performance in the studied SAnMBR system was comparable to aerobic full-scale MBR plants. After more than two years of continuous operation no significant irreversible fouling problems were detected, and low fouling rates were observed even when MLTS was high (up to 25 g L^{-1}). A resistance-in-series-based filtration model is presented, which was able to accurately reproduce the filtration process. Moreover, a knowledge-based supervisory controller for filtration is proposed, which resulted in high energy savings during membrane scouring, low physical cleaning downtimes of total operating time, and low average operating costs.

This Ph.D. thesis is enclosed in a national research project funded by the Spanish Ministry of Science and Innovation entitled "*Using membrane technology for the energetic recovery of wastewater*

organic matter and the minimization of the sludge produced" (MICINN project CTM2008-06809-C02-01/02). To obtain representative results that could be extrapolated to full-scale plants, this research work was carried out in an SAnMBR system featuring industrial-scale hollow-fibre membrane units that was operated using effluent from the pre-treatment of the Carraixet WWTP (Valencia, Spain).

RESUM

El reactor anaerobi de membranes submergides (SAnMBR) està considerat com una tecnologia candidata per a millorar la sostenibilitat en el sector de la depuració d'aigües residuals i suposa una extensió en l'aplicabilitat de la biotecnologia anaeròbia al tractament d'aigües residuals amb baixa càrrega (p.e. aigua residual urbana) o a condicions mediambientals extremes (p.e. baixes temperatures d'operació). Aquesta tecnologia alternativa de tractament d'aigües residuals és més sostenible que les tecnologies aeròbies actuals ja que transforma l'aigua residual en una font renovable d'energia i nutrients, a més de proporcionar un recurs d'aigua reutilitzable. SAnMBR no solament presenta els principals avantatges dels reactors de membranes (*i.e.* efluent d'elevada qualitat, i poques necessitats d'espai), sinó que també presenta els avantatges dels processos anaerobis. En aquest sentit, la tecnologia SAnMBR presenta una baixa producció de fangs degut a la baixa taxa de creixement dels microorganismes implicats en la degradació de la matèria orgànica, presenta una baixa demanda energètica gracies a l'absència de aeració, i permet la generació de metà, el qual representa una font d'energia renovable que millora el balanç energètic net del sistema. Cal destacar també el potencial de recuperació de nutrients de l'aigua residual bé quan l'efluent és destinat directament a irrigació o bé quan aquest ha de ser tractat prèviament mitjançant tecnologies de recuperació de nutrients.

L'objectiu principal d'aquesta tesi doctoral és avaluar la viabilitat de la tecnologia SAnMBR com a procés basic en el tractament d'aigües residuals urbanes a temperatura ambient. Concretament, aquesta tesi se centra en les següents tasques: (1) establiment, calibració i posada en marxa del sistema d'instrumentació, control i automatització necessari; (2) identificació dels paràmetres d'operació clau que afecten al procés de filtració; (3) modelació i simulació del procés de filtració; i (4) desenvolupament d'estratègies de control per a l'optimització del procés de filtració, considerant els costos d'operació i manteniment del procés.

En aquest treball d'investigació es proposa un sistema d'instrumentació, control i automatització per a SAnMBR, el qual va ser essencial per poder mantindre un comportament adequat i estable del sistema front a possibles pertorbacions. El comportament de les membranes va ser comparable a l'observat en sistemes MBR aerobis a escala industrial. Després de més de dos anys d'operació ininterrompuda, no es van detectar problemes significatius associats a l'embrutiment irreversible de les membranes, fins i tot operant a elevades concentracions de sòlids en el licor mescla (valors de fins a 25 g L^{-1}). En aquest treball es presenta un model de filtració (basat en el model de resistències en sèrie) que va permetre simular el procés de filtració de forma adequada. D'altra banda, es proposa un

control supervisor basat en un sistema expert que va permetre reduir el consum energètic associat a la neteja física de les membranes, disminuir el percentatge de temps destinat a la neteja física respecte del total d'operació, i, en general, un menor cost operacional del procés de filtració.

Aquesta tesi doctoral està integrada en un projecte nacional d'investigació, subvencionat pel Ministeri de Ciència i Innovació (MICINN), amb títol "*Modelació de l'aplicació de la tecnologia de membranes per a la valorització energètica de la matèria orgànica de l'aigua residual i la minimització dels fangs produïts*" (MICINN, projecte CTM2008-06809-C02-01/02). Per a obtenir resultats representatius que puguen ser extrapolats a plantes reals, aquesta tesi doctoral s'ha dut a terme utilitzant un sistema SAnMBR que incorpora mòduls comercials de membrana de fibra buida. A més, aquesta planta és alimentada amb l'efluent del pretractament de la EDAR del Barranc del Carraixet (València, Espanya).

RESUMEN

El reactor anaerobio de membranas sumergidas (SAnMBR) está considerado como tecnología candidata para mejorar la sostenibilidad en el sector de la depuración de aguas residuales, ampliando la aplicabilidad de la biotecnología anaerobia al tratamiento de aguas residuales de baja carga (p.ej. agua residual urbana) o a condiciones medioambientales extremas (p.ej. bajas temperaturas de operación). Esta tecnología alternativa de tratamiento de aguas residuales es más sostenible que las tecnologías aerobias actuales ya que el agua residual se transforma en una fuente renovable de energía y nutrientes, proporcionando además un recurso de agua reutilizable. SAnMBR no sólo presenta las principales ventajas de los reactores de membranas (*i.e.* efluente de alta calidad, y pocas necesidades de espacio), sino que también presenta las ventajas de los procesos anaerobios. En este sentido, la tecnología SAnMBR presenta una baja producción de fangos debido a la baja tasa de crecimiento de los microorganismos implicados en la degradación de la materia orgánica, presenta una baja demanda energética debido a la ausencia de aireación, y permite la generación de metano, el cual representa una fuente de energía renovable que mejora el balance energético neto del sistema. Cabe destacar el potencial de recuperación de nutrientes del agua residual bien cuando el efluente es destinado directamente a irrigación, o bien cuando debe ser tratado previamente mediante tecnologías de recuperación de nutrientes.

El objetivo principal de esta tesis doctoral es evaluar la viabilidad de la tecnología SAnMBR como proceso básico en el tratamiento de aguas residuales urbanas a temperatura ambiente. Concretamente, esta tesis se centra en las siguientes tareas: (1) implementación, calibración y puesta en marcha del sistema de instrumentación, control y automatización necesario; (2) identificación de los parámetros de operación clave que afectan al proceso de filtración; (3) modelación y simulación del proceso de filtración; y (4) desarrollo de estrategias de control para la optimización del proceso de filtración, considerando los costes de operación y mantenimiento.

En este trabajo de investigación se propone un sistema de instrumentación, control y automatización para SAnMBR, el cual fue esencial para mantener un comportamiento adecuado y estable del sistema frente a posibles perturbaciones. El comportamiento de las membranas fue comparable a sistemas MBR aerobios a escala industrial. Tras más de dos años de operación ininterrumpida, no se detectaron problemas significativos asociados al ensuciamiento irreversible de las membranas, incluso operando a elevadas concentraciones de sólidos en el licor mezcla (valores de hasta 25 g L^{-1}). En este trabajo se presenta un modelo de filtración (basado en el modelo de resistencias en serie) que permitió simular de

forma adecuada el proceso de filtración. Por otra parte, se propone un control supervisor basado en un sistema experto que consiguió reducir el consumo energético asociado a la limpieza física de las membranas, disminuir el porcentaje de tiempo destinado a la limpieza física respecto al total de operación, y, en general, un menor coste operacional del proceso de filtración.

Esta tesis doctoral está integrada en un proyecto nacional de investigación, subvencionado por el Ministerio de Ciencia e Innovación (MICINN), con título *"Modelación de la aplicación de la tecnología de membranas para la valorización energética de la materia orgánica del agua residual y la minimización de los fangos producidos"* (MICINN, proyecto CTM2008-06809-C02-01/02). Para obtener resultados representativos que puedan ser extrapolados a plantas reales, esta tesis doctoral se ha llevado a cabo utilizando un sistema SAnMBR que incorpora módulos comerciales de membrana de fibra hueca. Además, esta planta es alimentada con el efluente del pre-tratamiento de la EDAR del Barranco del Carraixet (Valencia, España).

TABLE OF CONTENTS

MAIN NOMENCLATURE AND ABBREVIATION

A	*membrane area*
Alk	*carbonate alkalinity*
AnR	*anaerobic reactor*
BRF	*biogas recycling flow*
CH_4	*methane*
CIP	*clean in place*
COD	*chemical oxygen demand*
COD_S	*soluble COD*
COD_T	*total COD*
DV	*degasification vessel*
ET	*equalisation tank*
EPS	*extracellular polymeric substances*
EPS_C	*carbohydrate fraction of EPS*
EPS_P	*protein fraction of EPS*
F-R	*filtration-relaxation*
FR	*fouling rate*
FR_C	*FR related to cake-layer formation*
FS	*flat sheet*
HF	*hollow fibre*
HRT	*hydraulic retention time*
HS^-	*total sulphide expressed as HS^-*
J	*transmembrane flux*
J_{20}	*20 ºC-normalised J*
J_C	*critical flux*
$J_{20,C}$	*20 ºC-normalised J_C*
K	*permeability*
K_{20}	*20 ºC-normalised K*
LMH	*litre per square metre of membrane per hour*
MA	*methanogenic Archaea*
MBR	*membrane bioreactor*
MLTS	*mixed liquor total solids*
MT	*membrane tank*
NH_4-N	*ammonium measured as nitrogen*
OLR	*organic loading rate*
OPC	*OLE for process control*
PID	*proportional-integrative-derivative*

PLC	*programmable logic controller*
PO_4-P	*orthophosphate measured as phosphorous*
R_C	*cake-layer resistance*
R_I	*irreversible layer resistance*
R_M	*membrane resistance*
R_T	*total membrane resistance*
RF	*rotofilter*
SAeMBR	*submerged aerobic MBR*
SAnMBR	*submerged anaerobic MBR*
SCADA	*supervisory control and data acquisition*
SGD_m	*specific gas demand per membrane area*
SGD_p	*specific gas demand per permeate volume*
SMP	*soluble microbiological products*
SMP_C	*carbohydrate fraction of SMP*
SMP_P	*protein fraction of SMP*
SRB	*sulphate reducing bacteria*
SO_4-S	*sulphate measured as sulphur*
SRF	*sludge recycling flow*
SRT	*sludge retention time*
T	*temperature*
TS	*total solids*
TSS	*total suspended solids*
TMP	*transmembrane pressure*
VFA	*volatile fatty acids*
VS	*volatile solids*
VSS	*volatile suspended solids*
WWTP	*wastewater treatment plant*
α_C	*specific cake resistance*
α_I	*specific irreversible fouling resistance*
μ	*dynamic viscosity*

CHAPTER 1:

Introduction: Application of membrane technology to the anaerobic treatment of urban wastewater

1.1 State of the art of urban wastewater treatment

Nowadays, most of the electricity, up to 80%, is generated from fossil fuels [1.1]. Dependency on these fuels is one of the key issues in global environmental sustainability because it causes considerable amounts of carbon dioxide to be released into the atmosphere, something which cannot be ignored due to the global warming it causes. Hence, electricity consumption is a key element in the overall environmental performance of a WWTP [1.2; 1.3].

Urban wastewater treatment (WWT) is an energy-intensive activity whose operating energy requirements vary considerably from one WWTP to another depending on the type of influent, treatment technology and required effluent quality. Table 1.1 shows the typical energy footprint of the main processes involved in the urban wastewater treatment. As this table illustrates, the energy related to biological treatment is in the range of 0.25 – 2.5 kWh m^{-3}. This energy consumption mainly depends on regional parameters, such as climate, water availability, water use and population density.

Table 1.1. Typical energy footprint of the main processes involved in the urban wastewater treatment [1.4; 1.5; 1.6].

Operation	**Energy consumption (kWh m^{-3})**
Preliminary treatment	0.16 - 0.30
Trickling filters	0.24 - 0.40
Activated sludge	0.25 - 0.60
Activated sludge with nitrification	0.30 - 1.40
MBR	0.50 - 2.50

Currently, most urban WWTPs use aerobic processes that consume considerable amounts of energy when performing acceptable biological treatment. Specifically, some studies indicate that bioreactor aeration could account for up to 60% of total WWTP energy consumption [1.7; 1.8]. Moreover, the cost related to wastewater treatment is expected to increase due to increasing restrictions for treated water discharging and sludge disposal, which means a significant challenge in wastewater treatment field. Furthermore, there will be additional charges based on regulations related to the mitigation of greenhouse gas emissions penalising both energy consumption and sludge production [1.9].

It is, therefore, particularly important to implement new energy-saving technologies involving a significant change of paradigm in the urban wastewater treatment field towards a sustainable treatment process from an economic, social and environmental point of view. These new energy-saving technologies must reduce the overall WWTP carbon footprint and improve environmental sustainability. From a sustainability point of view, aerobic urban WWT does not exploit the potential energy contained in the organic matter and the fertiliser value of nutrients. In contrast, in anaerobic processes wastewater becomes a raw material from which very useful resources such as energy, nutrients and reusable water could be obtained. In this regard, anaerobic biological processes have been recognised as the most suitable pathway towards sustainable wastewater treatment systems [1.10; 1.11; 1.12].

1.2 Anaerobic treatment of urban wastewater

1.2.1 Main processes involved

The potentials of anaerobic technology for urban wastewater treatment have been widely assessed during the last 20 years [1.13]. The anaerobic treatment of urban wastewater is based on the same biological, physical and chemical processes than the anaerobic digestion (AD) of sludge. AD is a multistep process in which complex organic materials are converted to simpler compounds without an external electron acceptor such as oxygen or nitrate.

Figure 1.1 shows the main processes involved in the anaerobic treatment of sulphate-loaded urban wastewater. These processes are the following:

- ***Extracellular hydrolysis*** of complex organic particulates to simple sugars, amino acids and long-chain organic fatty acids.
- ***Acidogenesis*** of these sugars, amino acids and long-chain organic fatty acids to produce organic acids and alcohols. Acidogenesis includes ***acetogenesis*** process, in which the organic acids and alcohols are converted to hydrogen and acetic acid.
- ***Hydrogenotrophic methanogenesis***, in which hydrogen is converted to methane using CO_2 by hydrogenotrophic methanogenic *Archaea* (MA).
- ***Acetotrophic methanogenesis***, in which acetate is converted to methane producing CO_2 by acetotrophic MA.
- ***Sulphate reduction***, in which sulphate reducing bacteria (SRB) compete with MA for the available substrate reducing the sulphate present in the wastewater to sulphide.

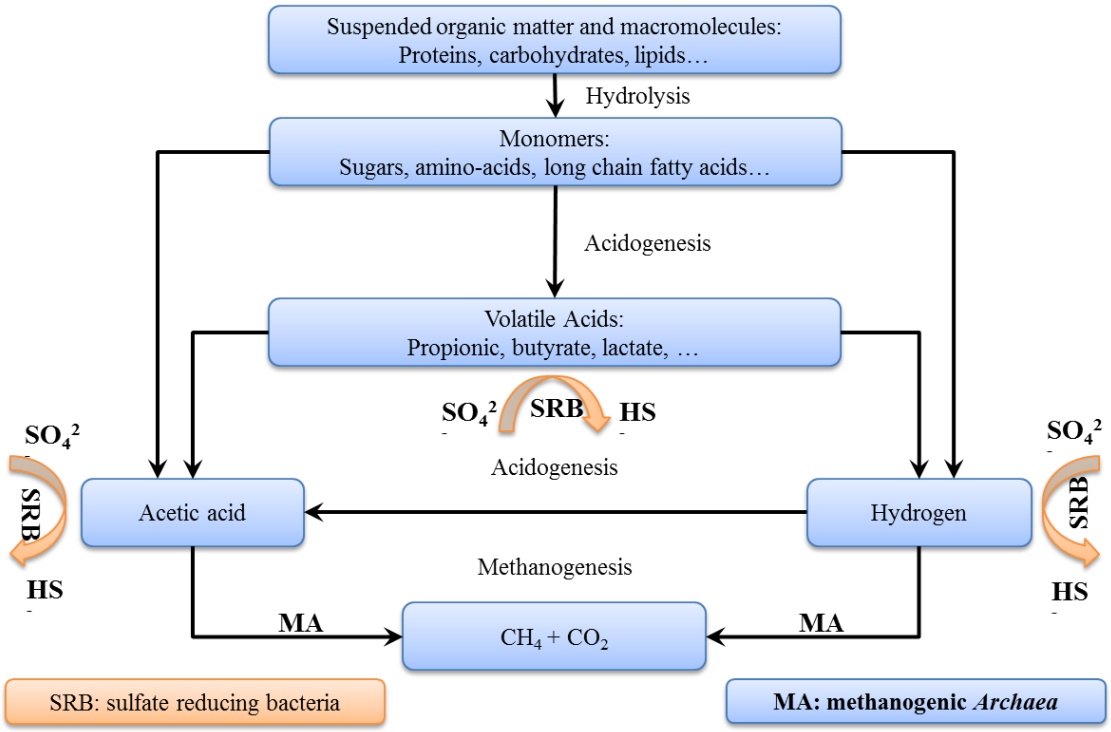

Figure 1.1 Main processes involved in the anaerobic treatment of sulphate-loaded wastewater.

1.2.2 Anaerobic vs. aerobic treatment

A significant driver encourages anaerobic urban wastewater treatment as an alternative of aerobic-based conventional options, mainly due to the following sustainable advantages (some of these are illustrated in Figure 1.2):

- Low sludge production. Only 10 – 20% of the organic matter is assimilated into biomass, reducing therefore sludge production. Sludge production is up to ten times lower than in aerobic treatment [1.14].
- Pathogens reduction. The produced sludge is mostly stabilised.
- Low energy demand. Anaerobic processes do not require oxygen supply, which significantly reduces the energy consumption related to wastewater treatment.
- Energy recovery from the organic matter content in wastewater. Organic matter is converted into biogas, which can be used as energy resource (see Figure 1.3).
- The possibility of nutrient recovery from wastewater, which could be reused for agricultural purposes.
- High capacity to treat slowly degradable substrates mainly at high concentrations, but also at low/medium concentrations.
- Reduction of odours in closed-air configurations.

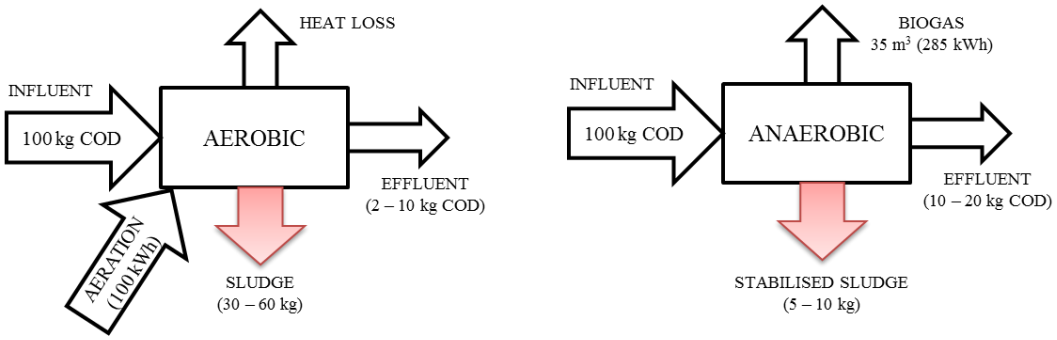

Figure 1.2 Comparison of aerobic and anaerobic treatment [1.15].

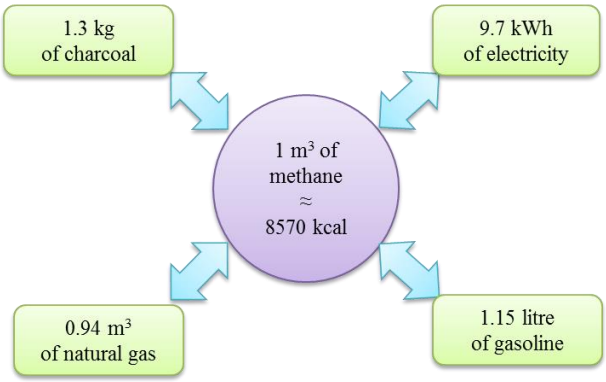

Figure 1.3 Energetic equivalence of methane [1.15].

Nevertheless, anaerobic processes also present some drawbacks that must be addressed:

- The low sludge production is closely linked to the slow growth of anaerobic microorganisms. Consequently, anaerobic processes require high operating temperature and/or long sludge retention time (SRT).
- The anaerobic biomass is highly sensitive to process overloads and disturbances due to several causes, such as acidification, presence of free ammonia or H_2S.
- The anaerobic sludge presents low settleability, which involves operating with high reaction volumes.

These drawbacks are the reasons why the current research on anaerobic processes aims not only to extend their applicability, but also to optimise their performance and enhance their robustness towards perturbations [1.15].

Concerning the low settleability of anaerobic sludge, it is of special interest to control SRT when treating low-strength wastewater, *i.e.* minimising the loss of biomass in the effluent since this loss is not compensated with the biomass growth inside the reactor [1.13; 1.16]. In this regard, different

anaerobic technologies have been developed, in which higher biomass retention is achieved by the use of the capacity of forming anaerobic granular biomass or by means of attached growth reactors. Some of the most commonly studied systems are the anaerobic filters [1.17], the up-flow anaerobic sludge blanket (UASB) reactors [1.18] and the granular sludge bed reactors (EGBRs). At present, above the 80% of the full-scale anaerobic installations are reactors in which biomass retention is attained by the formation of sludge granules [1.14]. However, the applicability of these technologies for low-strength wastewater treatment (*e.g.* urban ones) is limited since the low amount of biogas produced per cubic metre of treated water does not allow increasing the ambient temperature. On this point, these technologies have been only used for urban wastewater treatment in warm weather countries where the low organic load is compensated with the high ambient temperatures. Instead, for mild and cold weathers, the low temperatures and the low organic loads of the urban wastewaters make technologies of this type technically unfeasible.

Hence, the current challenge for the anaerobic treatment of urban wastewater at ambient temperature is to achieve effective solid-liquid separation in order to control SRT thus improving effluent quality. In this regard, membrane technology can overcome the limitation of anaerobic processes for urban wastewater treatment at ambient temperature since the filtration process provides complete SRT control.

Anaerobic membrane bioreactors (AnMBRs) are therefore considered as a candidate to improve sustainability in the treatment of wastewaters broadening the range of application of anaerobic biotechnology to low-strength wastewaters or low operating temperatures.

1.3 Membrane technology for wastewater treatment

Membrane bioreactor (MBR) technology was introduced in the late 1960s coinciding with the availability of the first industrial-scale ultrafiltration (UF) and microfiltration (MF) membranes. The first aerobic MBR (AeMBR) was developed commercially by Dorr-Oliver [1.19] for application to ship-board sewage treatment [1.20]. It consisted of an activated sludge bioreactor and a crossflow membrane filtration loop. Due to the poor economics of the first MBR generation, they only found applications in niche areas such as, for instance, isolated trailer parks or ski resorts [1.21]. The MBR breakthrough came in the late 1980s when Yamamoto *et al*. [1.22] proposed submerging the membranes directly in the bioreactor. Nowadays, submerged MBR is one of the most promising technologies in the wastewater treatment field.

The full-scale application of membrane technology to urban wastewater treatment has increased widely in the last decades due to the industrial production of membranes capable to work with high flows, and the production of more compact, cheap and exchangeable membrane modules. Indeed, worldwide implementation is becoming increasingly active due to the adoption of low pressure driven submerged membranes (*i.e.* hollow-fibre (HF) and flat-sheet (FS)) requiring lower operating energy demands than traditional sidestream systems [1.23]. Table 1.2 shows some of the currently operating full-scale AeMBR plants worldwide.

Table 1.2 Example of the current operating full-scale AeMBR plants worldwide [1.24]. *Nomenclature: **PDF**: peak-design flow; **MLD**: millions of liters per day*.

Project	**Supplier**	**Date**	**PDF (MLD)**
Brightwater, WA	GE	2011	170
Qinghe, China	OW/MRC	2011	150
North Las Vegas, NV	GE	2011	133
Yellow River, GA	GE	2011	111
Shiyan Shendinghe, China	OW/MRC	2009	110
Aquaviva, Cannes, France	GE	2012	106
Busan City, Korea	GE	2012	100
Guangzhou, China	Memstar	2010	100
Wenyuhe, Beijing, China	Asahi/OW	2007	100
Johns Creek, GA	GE	2009	94
Beixiaohe, China	Siemens	2008	78
Al Ansab, Muscat, Oman	Kubota	2009	78
Peoria, AZ	GE	2008	76
Cleveland Bay, Australia	GE	2007	75
Lusail, Qatar	GE	2008	60
Sabadell, Spain	Kubota	2009	55
San Pedro del Pinatar, Spain	GE	2007	48
Syndial, Italy	GE	2005	47

Specifically, European MBR market was estimated to be nearly 57$ million in 2004 and is expected to have sustainable growth in the near future [1.25]. UK/Ireland, France, Germany, Iberia, Benelux and Italy are the major players in European MBR market [1.26; 1.27] (see Figure 1.4). MBR market in USA and Canada is also expected to grow in the next decade mainly due to revenue from membrane

based water purification, desalination and wastewater treatment [1.28]. It has been estimated that the market will double every 7 years [1.29].

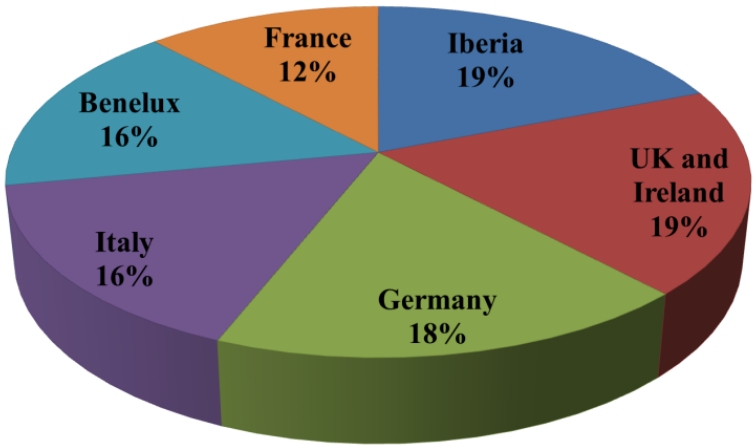

Figure 1.4 European MBR market [1.27]

The main benefits of using MBR technology instead of conventional activated sludge systems (CAS) for urban wastewater treatment are the following:

- Obtaining solid- and microorganism-free effluent (high effluent quality).
- Reducing the footprint of the WWTP.
- Reducing the operating problems related to foaming.
- Decoupling hydraulic retention time (HRT) and SRT (*i.e.* high SRT can be achieved without increasing the reactor volume).
- Intensifying the organic matter removal process due to a higher microbial biodiversity in the reactor (retention of the low-growth rate microorganisms).

As mentioned above, membrane technology has shown a high capability for obtaining high effluent quality. This is particularly important when considering reuse options [1.30; 1.31; 1.32]. All the microorganisms remain inside the system (even if those are forming flocs or not), which provides perfect control of SRT and high effluent quality [1.33]. Controlling the SRT of the process allows the growth of species that would be simply washed out in other systems [1.34] without increasing the operating temperature. This fact increases the possibility of application of MBR technologies for a high diversity of wastewaters, including wastewaters with persistent pollutants. For example, Hwu *et al.* [1.35] found that microorganisms responsible for the oleic acid degradation could not be kept in EGBR systems.

1.3.1 Classification of MBR systems

Two MBR configurations can be defined based on how the membranes are integrated with the bioreactor: sidestream and submerged (see Figure 1.5).

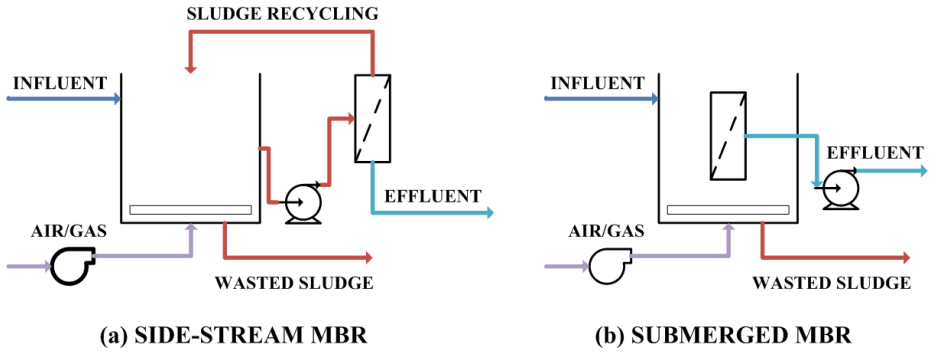

Figure 1.5 Configurations of a membrane bioreactor: **(a)** sidestream and **(b)** submerged.

In sidestream MBRs (see Figure 1.5a), the membrane modules are placed outside the reactor, and the mixed liquor circulates at high velocity over a recirculation loop that contains the membrane. The main constraint of sidestream configuration is the high energy requirements, due to the high operational transmembrane pressures (TMP) and the significant volumetric flow required to achieve the desired cross-flow velocities [1.14]. Indeed, pumping requirements for sidestream aerobic MBRs account for 60 to 80 % of the total energy consumption [1.36]. The main advantage of sidestream configuration is that the membranes are physically cleaned due to the cross-flow velocity applied over the membrane surface.

In submerged (or immersed) MBRs (see Figure 1.5b), the membranes are directly immersed in the mixed liquor (either in the reactor or in a separate membrane tank). Submerged MBR configuration involves lower energy requirements in comparison with sidestream configurations since permeate is obtained by vacuum filtration. However, submerged MBRs operate at lower transmembrane fluxes (J) thus requiring larger membrane surfaces for a given treatment flow. In order to minimise fouling in submerged configurations an amount of air/gas is introduced/recycled to the system from the bottom of the membranes.

As mentioned before, most of the new commercial applications of MBR technology for urban wastewater treatment are based on submerged configuration. This is mainly due to the low cost and

suitable fouling control that is achieved by combining low-pressure filtration and membrane scouring by air/gas sparging [1.23].

1.3.2 Membrane technology applied to anaerobic wastewater treatment

The first application of membranes in anaerobic wastewater treatment was reported in 1978 [1.37]. It consisted of an external cross-flow membrane applied to the treatment of a septic tank effluent. On the other hand, the first commercially-available AnMBR was developed by Dorr-Oliver in the early 1980s, which was known as membrane anaerobic reactor system (MARS). It was designed for high-strength whey processing wastewater treatment and consisted of a completely mixed suspended growth anaerobic reactor and a crossflow membrane filtration loop. Nevertheless, this system was only tested at pilot scale due to the high membrane acquisition and operating costs. Since then, many pilot- and laboratory-scale investigations about the application of this technology to industrial wastewater treatment have been carried out. Nowadays, several full-scale plants are treating industrial wastewaters [1.38]. However, the application of AnMBR technology for urban wastewater treatment has been less reported [1.39].

Figure 1.6 shows an example of the possible configurations of a submerged AnMBR (SAnMBR).

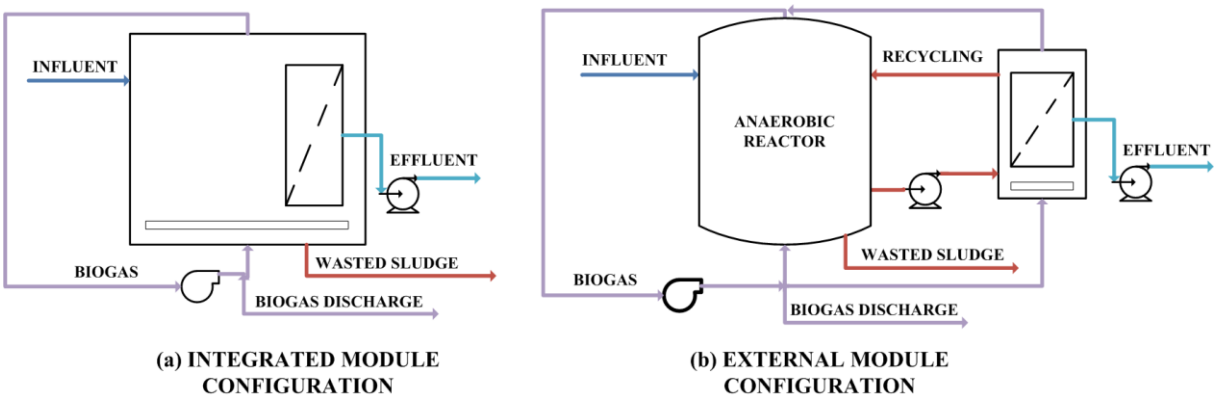

Figure 1.6 Configurations of a submerged anaerobic membrane bioreactor: **(a)** integrated and **(b)** external.

The opportunity to develop an MBR concept with the advantage of a clarified effluent with improved energy balance and very low sludge production has placed SAnMBR as a potential technology to accomplish the challenges that urban wastewater treatment will face in the near future. However, as an emerging technology there are still some barriers or challenging issues that limit their widespread practical application. Thus, further breakthroughs in these challenges should be pursued [1.39]. As regards the filtration process, the necessity of working at high SRTs for anaerobic treatment of low-

strength wastewaters at ambient temperature could lead to high mixed liquor total solids (MLTS) concentrations, which is one of the main operating restrictions in filtration-based technology [1.23]. High MLTS levels favour membrane fouling, which decreases membrane permeability (K) and increases operating and maintenance costs [1.40]. Therefore, since the operating costs in SAnMBR technology are mainly determined by the energy required for membrane operation [1.23], further research is needed to minimise membrane fouling thus allowing optimising this technology.

Membrane fouling can be reduced by different strategies (see, for instance, Vallero *et al*. [1.41]; Liao *et al*. [1.42]; Dvořák *et al*. [1.43]), such as the following: optimising the frequency and duration of the physical cleaning stages (back-flushing and relaxation); optimising the air/gas sparging intensity for membrane scouring; or operating under sub-critical filtration conditions (which are bounded by the so-called critical flux). However, the effect of these operational variables on membrane fouling is not accurately evaluated at lab scale since it strongly depends on the membrane size [1.44]. Specifically in HF membranes the HF length is the main design parameter.

Among the reported AnMBR studies for wastewater treatment, most of them have been assessed at laboratory or bench scale (see Table 1.3). Nevertheless, no references have been found in the literature concerning the application of SAnMBR technology for urban wastewater treatment using industrial-scale membrane units. Therefore, further studies are needed on modelling, simulation and control in SAnMBR technology using industrial-scale membrane modules to facilitate the design and implementation of this technology at full-scale.

Table 1.3 Main characteristics of AnMBR studies for wastewater treatment using HF and FS membrane modules [1.45]. *Nomenclature:* ***J_{20}****: transmembrane flux ;* ***TMP****: transmembrane pressure;* ***MF****: microfiltration;* ***UF****: ultrafiltration;* ***HF****: hollow-fibre;* ***FS****: flat-sheet;* ***Da****: Dalton; and* ***BRF****: biogas recycling flow.*

Filtration range	**Membrane type**	**Pore size (μm)**	**Area (m^2)**	**J_{20} (LMH)**	**TMP (kPa)**	**BRF (L min^{-1})**	**Reference**
MF	FS	0.4	0.1	2 - 10	23	5	[1.46]
MF	FS	0.4	0.1	1.5 - 2	-	2 - 5	[1.47]
MF	FS	0.4	0.1	10 - 20	0 - 30	5	[1.48]
UF	HF	0.1	0.46	-	-		[1.49]
UF	HF	100 kDa	5.02	-	-		[1.50]
MF	FS	70 kDa	0.03	4.7 - 5.7	< 30	0.75	[1.51]
MF/UF	FS	MF: 100 kDa; UF: 30 kDa	0.026	4 - 12	-	-	[1.51]
UF	FS	70 kDa	0.03	4.35 - 4.85	43.5	-	[1.51]
MF	FS	0.4	0.1	10 - 20	10 - 30	5	[1.52]
-	FS	0.45	0.236	5.3	-	-	[1.53]
MF	FS	0.45	0.118	4.3 - 7.9	< 30	-	[1.54]
-	HF	0.1	0.091	7 - 10	10 - 35		[1.55]
-	FS	0.2	0.003	80 - 450	20 - 125	-	[1.56]
MF	FS	0.3	0.03	1.6 - 6.3	30	0.25 - 0.75	[1.57]
MF	FS	70 kDa	0.03	1.8 - 8.1	< 30	0.75	[1.58]
MF	FS	70 kDa	0.03	5.3 - 9.2	35	0.15 - 0.75	[1.59]
-	FS	70 kDa	0.03	4.8 - 9.1	< 40	0.75	[1.60]
-	HF	0.04	0.094	-	-		[1.61]
MF	FS	0.4	0.12	2 - 12	< 50	-	[1.62]
-	HF	0.4	0.05	24	-		[1.63]
MF	FS	0.4	0.1	3 - 7.2	17.5	5	[1.64]
MF	FS	0.4	0.1	-	-	5	[1.65]
-	FS	-	0.351	20 - 30	-	-	[1.66]
-	FS	0.4	0.1	5 - 8	33 - 41	5.5	[1.67]
-	HF	0.4	0.1	-	45		[1.68]
MF	FS	0.3	0.03	4.6 - 10.1	< 30	0.3 - 0.75	[1.69]
-	HF	0.4	0.12	1.3 - 3.5	-		[1.70]

1.4 Membrane fouling in MBR technology

As mentioned before, membrane fouling is a challenging issue that limit the widespread practical application of SAnMBR technology [1.39]. Therefore, since the operating costs in SAnMBR systems are mainly determined by the energy required for membrane operation [1.23], further research is required in developing energy efficient fouling control strategies based on optimising both hydrodynamic conditions and physical cleaning procedures.

Limited attempts to enhance membrane operation by optimising both air/gas sparging intensity and membrane operating mode (relaxation, back-flushing, etc.) have been reported [1.21]. On the other hand, research on bulk characteristics may improve significantly the understanding of fouling mechanisms and control methods in SAnMBRs.

1.4.1 Classification of membrane fouling

Different classifications of the fouling types can be found in the literature. Regarding its nature, fouling can be classified in:

- Reversible: corresponding to the fouling that appears during filtration and that can be removed by physical cleaning from the membrane surface (membrane scouring by air/gas sparging, back-flushing, etc.).
- Residual: corresponding to the persistent reversible fouling that requires enhanced physical cleaning.
- Irreversible: corresponding to the fouling that cannot be removed physically from the membrane surface, requiring of chemical cleaning protocols.
- Irrecoverable: corresponding to the fouling that cannot be removed neither physically nor chemically from the membrane surface.

With reference to its origin, fouling can be classified in:

- Particulate: fouling is caused by the bulk particles that build-up a cake-layer on the membrane surface. In many cases, cake-layer formation linked with removable fouling is considered as the major contributor to membrane fouling in MBR technology [1.71].
- Inorganic: fouling is caused by the precipitation of several inorganic compounds, inorganic colloids and crystals on membrane and pore surfaces, such as struvite, $CaCO_3$, $CaSO_4$ and $MgCO_3$ [1.72]. In general, membrane fouling in MBRs is mainly governed by biofouling and

organic fouling rather than by inorganic fouling, although all of them take place simultaneously during membrane filtration of activated sludge [1.71].

- Organic: fouling is caused by the accumulation and adsorption of different organic biopolymers (*i.e.* proteins and polysaccharides) on the membrane surface. Fouling due to extracellular polymeric substances (EPS) and/or soluble microbial products (SMP) can be considered a subset of both organic fouling and biofouling [1.72].
- Biofouling: fouling as a result of the interactions between membrane surface and bulk components [1.72]. Biofouling refers to the deposition, growth and metabolism of flocs on the membranes, which finally form a biofilm.

Table 1.4 Classification of Fouling [1.73]

Definition	Fouling Rate (mbar min^{-1})	Cleaning frequency	Cleaning Method
Cake, reversible or removable fouling	0.1 - 1	10 min	Physical cleaning (*e.g.* relaxation, back-flushing)
Residual fouling	0.01 - 0.1	1 - 2 weeks	Maintenance cleaning (*e.g.* chemically enhanced back-flushing)
Irreversible fouling	0.001 - 0.01	6 - 12 months	Chemical cleaning
Irrecoverable fouling	0.0001 - 0.001	several years	Cannot be removed

1.4.2 Main factors affecting membrane fouling

Membrane fouling in MBR technology is influenced by several factors, which can be divided into four groups: feed characteristics, bulk characteristics, operating conditions, and membrane and module design. Figure 1.7 summarises some of these factors as well as some key interactions between them. Whilst some parameters directly affect membrane fouling, others result in a subsequent mitigation of fouling propensity. The complex interactions between these parameters complicate the understanding of membrane fouling [1.21].

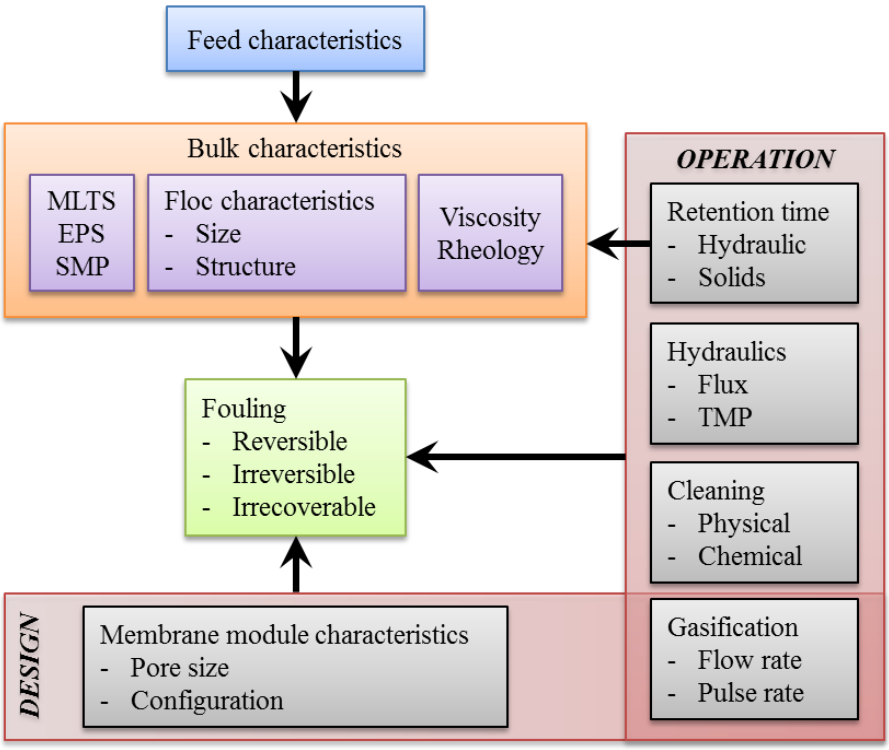

Figure 1.7 Main factors affecting fouling in submerged membrane bioreactors (adapted from [1.23]).

1.4.2.1 Feed characteristics

Fouling in MBR technology is mostly affected by the interactions between membrane and bulk characteristics rather than wastewater per se [1.74]. Nevertheless, some feed characteristics such as salinity can affect membrane fouling. Feed characteristics mainly affect membrane fouling due to changes in the bulk physical-chemical properties [1.75; 1.76]. Therefore, fouling propensity due to feed characteristics is indirectly taken into consideration during the biomass characterisation [1.21].

1.4.2.2 Bulk characteristics

1.4.2.2.1 MLTS concentration

MLTS is usually considered one key factor affecting membrane fouling. Indeed, increasing MLTS concentration results in a considerable negative impact on membrane permeability [1.77; 1.78; 1.79]. Different studies have reported various empirical mathematical expressions describing membrane performance which include solids concentration. Nevertheless, contradictory findings about the effect of this parameter on membrane filtration have been also reported [1.21; 1.71].

1.4.2.2.2 Viscosity

Commonly to conventional activated sludge processes, bulk viscosity is closely related to the mixed liquor suspended solids (MLSS) concentration. Bulk viscosity affects bubble size thus affecting membrane scouring by air/gas sparging. A threshold MLSS concentration has been reported (around 10 – 17 g L^{-1} depending on operating conditions) above which bulk viscosity tends to increase exponentially with MLSS [1.80], increasing therefore fouling rate propensity.

1.4.2.2.3 Extracellular polymeric substances (EPS)

EPS have been reported not only as the major bulk component keeping the floc in a three-dimensional matrix, but also as a key membrane foulant in MBR systems [1.21].

The "EPS" term entails different types of macromolecules such as polysaccharides, proteins, lipids and other polymeric compounds which have been found at or outside the cell surface and in the intercellular space of microbial aggregates [1.81]. EPS functions include aggregation of bacterial cells in flocs, activated sludge liquors and biofilms, formation of a protective barrier around the bacteria, water barrier, and adhesion to surfaces [1.82]. Hence, EPS can be responsible for the creation of additional flux resistances in membrane filtration processes.

Generally, EPSs are differentiated considering whether they are linked to the biological cell floc (eEPS) or not. In the second case, EPSs are soluble in the bulk supernatant and are defined SMPs. SMPs consist in different soluble materials produced by active secretion, shedding of cell surface material or cell lysis. A simplified representation of EPS, eEPS and SMP is shown in Figure 1.8.

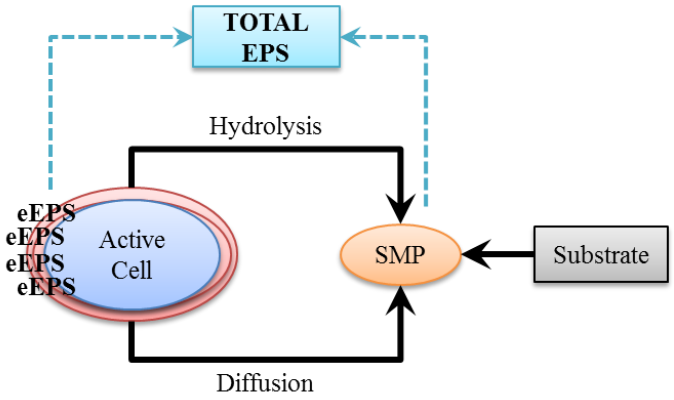

Figure 1.8 Simplified representation of EPS, eEPS and SMP [1.21].

It is worth pointing out that the concentration of eEPS is directly dependent on the extractive method applied for their determination. One of the extraction methods most commonly used is the cation exchange resin (CER) method proposed by Frølund *et al*. [1.83]. Typically, the solution containing eEPS is characterised by its relative content of protein (eEPSp) and carbohydrate (eEPSc). Carbohydrates and proteins are commonly determined by photometry according to the methodology proposed by Dubois *et al*. [1.84] and Lowry *et al*. [1.85], respectively.

1.4.2.2.4 Soluble microbial products (SMP)

Bound EPS cannot be considered as the sole cause of membrane fouling due to the complex nature of sludge suspension. In this regard, the influence of SMP on membrane fouling has attracted much attention in the last years [1.86; 1.87; 1.88] since SMP easily accumulate in MBRs, which results in poor filterability of the sludge suspension [1.71]. SMPs are defined as soluble cellular components that are either released during cell lysis, diffused through the cell membrane, lost during synthesis, or excreted for some purpose [1.21].

Several researchers suggest that SMP concentration significantly affects membrane fouling [1.89; 1.90; 1.91]. During filtration, SMPs are adsorbed on the membrane surface and/or block membrane pores. Moreover, SMPs favour the formation of a gel layer on the membrane surface which acts as a secondary membrane, increasing hydraulic resistance to permeate flow.

1.4.2.3 Operating conditions

1.4.2.3.1 Hydraulics and cleaning

Since J and TMP are interrelated, one of them might be fixed for operating and design purposes. Conventional pressure-driven filtration commonly operates at fixed J controlling TMP by means of the cleaning frequency (*i.e.* physical and/or chemical cleaning frequency). Physical cleaning commonly entails membrane scouring by air/gas sparging, back-flushing (reversing the transmembrane flow) and relaxation (membrane scouring by air/gas sparging without permeating). Chemical cleaning can be performed either in-situ or ex-situ, generally by means of sodium hypochlorite and/or nitric acid. On the other hand, chemically enhanced back-flushing protocols can be also periodically applied, in which a low amount of chemical reagents is added to the back-flushing permeate.

As mentioned before, physical cleaning (which is immediate and less likely to degrade the membranes) is used to remove reversible fouling from the membrane surface, whilst chemical cleaning (more time-consuming and likely to degrade the membranes) is applied for removing irreversible fouling component. It is worth pointing out that physical cleaning protocols are less effective than chemical ones.

1.4.2.3.2 Sludge retention time (SRT)

SRT, which ultimately controls biomass characteristics, is probably the most important operating parameter affecting fouling propensity in MBRs [1.21]. Operating at high SRTs involves high MLTS, which commonly decreases membrane permeability [1.79]. On the other hand, as mentioned before, increasing MLTS concentration could also result in high fouling propensities due to increasing bulk viscosity, which reduces the efficiency of membrane scouring by air/gas sparging [1.92]. On the contrary, operating at low SRTs could lead to high membrane fouling propensities due to increasing EPS/SMP production [1.21]. Therefore, SRT must be carefully selected in order to optimise filtration in MBR technology.

1.4.2.3.3 Air/gas sparging intensity

Air/gas sparging is the most commonly applied strategy to induce shear stress on the membrane surface in submerged MBR configuration. Indeed, most of the recent studies on hydrodynamic conditions in MBR technology aimed to optimise air/gas sparging intensity for membrane scouring [1.21].

Basically, air/gas sparging induces local shear transients and liquid flow fluctuations near the membrane surface that increase back transport phenomenon. These induced local shear transients prevent particle deposition over the membrane surface. Moreover, air/gas sparging affects lateral movement (or sway) in HF configuration, also preventing particle deposition. This sway also helps overcoming membrane clogging associated with high packing densities in HF bundles. All these effects contribute, therefore, to a significant reduction in fouling propensity.

1.4.2.4 Membrane and module design

1.4.2.4.1 Membrane pore size

The membrane pore size has a significant effect on membrane fouling depending on feed characteristics, particularly in particle size distribution. Submerged MBR configuration commonly entails MF (symmetric membranes with pore size from 0.1 to 0.5 μm) and UF (asymmetric membranes with pore size from 0.02 to 0.1 μm) membranes [1.93]. Although UF technology involves higher energy requirements, this type of membranes retains more colloidal organic matter. Moreover, some authors have observed that microfiltration membranes are prone to develop fouling due to macrocolloids incrustation [1.94].

1.4.2.4.2 Membrane configuration

Membrane performance is highly influenced by membrane configuration, *i.e.* the geometry and the way it is structured and oriented in relation to the flow of water, as well as the way the individual discrete membrane units themselves are housed in containers to produce modules [1.23]. Ideally, membrane modules should promote turbulence to favour cake layer detachment. In contrast, ideal membrane module configurations may also present high packaging density, which negatively affects membrane turbulence. On the contrary, low packing densities are usually related to high investment costs.

1.4.3 Fouling control strategies

The key operating challenge in AnMBR technology is to optimise membrane operation in order to minimise any kind of membrane fouling and thereby increase the membrane lifespan. Among different fouling control strategies, physical cleaning protocols (*e.g.* air/gas sparging, back-flushing and relaxation) are the most commonly applied.

Physical cleaning protocols are required to ensure continuous process performance. It is expected that physical cleaning effectiveness will tend to decrease over time due to the accumulation of irreversible fouling on the membrane surface. Therefore, different chemical cleaning protocols may also be applied. As mentioned before, chemical cleaning protocols usually include maintenance cleaning and chemical recovery. Maintenance cleaning is used to maintain design permeability and helps to reduce the frequency of chemical recovery. Chemical recovery is generally conducted when further filtration

is no longer feasible because reaching unsustainable TMP levels. Nevertheless, continuous application of chemical cleaning protocols is not recommended since they negatively affect membrane lifespan [1.95]. Table 1.5 summarises some of the fouling control protocols published for bench-scale AnMBR studies for urban WWT.

Table 1.5 Fouling control protocols in published bench-scale AnMBR studies for urban WWT (Adapted from Smith *et al.* [1.96]). *Nomenclature:* ***PE:*** *Polyethylene;* ***PVDF****: polyvinylidene fluoride;* ***PTFE****: polytetrafluoroethylene;* ***PES****: polyethersulfone; and* ***GAC:*** *granular activated carbon.*

Bioreactor Configuration	**Membrane information**	**Fouling control**	**Reference**
UASB + Submerged membranes	0.03 μm PE submerged HF	Periodic oxic cleaning with 5% NaOCl	[1.97]
EGSB + Submerged membranes	0.1 μm PE submerged HF	Back-flushing and relaxation; periodic chemical cleaning with 0.03% NaOCl	[1.98]
Submerged AnMBR	0.4 μm submerged HF/0.4 μm PE chloride submerged FS	Biogas sparging	[1.99]
Completely mixed anaerobic reactor	0.1 μm PVDF cross flow tubular	Cross-flow; weekly cleaning with 0.1% w/w NaOH and disinfectant	[1.100]
Jet flow anaerobic reactor	100 kDa cross flow	Cross-flow	[1.101]
Completely mixed anaerobic reactor	1 μm PTFE cross flow tubular	Cross-flow; periodic chemical cleaning with NaOCl	[1.102]
Completely mixed anaerobic reactor	0.2 μm cross flow HF	Periodic back-flushing; chemical cleaning with 0.1 M NaOH, 1% H_2O_2 and 1% HCl; and periodic back-flushing	[1.104]
Completely mixed anaerobic reactor	1 μm PTFE cross flow tubular	Periodic back-flushing	[1.103]
Up-flow anaerobic reactor	100 kDa cross flow coated PVDF and 30 kDa cross flow polyetherimine	Cross-flow	[1.105]
Completely mixed anaerobic reactor	0.1 μm PES submerged FS	Biogas sparging	[1.54]
UASB + cross-flow membranes	100 kDa cross flow PVDF tubular	Cross-flow; NaOCl cleaning every 6 hours	[1.106]
Two-stage fluidised bed MBR	0.1 μm PVDF submerged HF	GAC fluidisation; periodic back-flushing and/or NaOCl/NaOH cleaning	[1.55]
Submerged AnMBR	0.2 μm PES submerged FS	Biogas sparging and back-flushing	[1.107]

1.4.3.1 Air/gas sparging intensity

As previously commented, the operating energy demand could be a potential weakness for the feasibility of full-scale SAnMBR systems. In this respect, much effort has been focused in the last years on optimising gas sparging intensity in SAnMBR technology since the energy involved in this process remains the higher factor over total operating costs. Gas sparging intensity is commonly expressed as specific gas demand per square metre of membrane area (SGD_m) or as specific gas demand per cubic metre of treated water (SGD_P). Both parameters are useful to monitor energy consumption in SAnMBR systems. Table 1.6 summarises common air sparging intensities in AeMBR technology for urban wastewater treatment using industrial-scale membrane modules. It is important to highlight that there is still a lack of data regarding SGD_m and SGD_P in SAnMBR technology entailing industrial-scale membrane modules.

Table 1.6 Summary of full-scale plant data for aerobic urban wastewater treatment [1.23]. *Nomenclature: **FS**: Flat-sheet; **HF**: hollow-fibre; **J**: transmembrane flux; **K**: membrane permeability; **SAD_m**: specific air demand per membrane area; **SAD_P**: specific air demand per permeate volume.*

Technology	J (LMH)	K (LMH bar^{-1})	SAD_m (Nm^3 h^{-1} m^{-2})	SAD_P
FS	19.4	261	0.57	27.5
HF	19.5	104	0.30	15.4

1.4.3.2 Back-flushing

Back-flushing has been reported as a successful way for removing not only most of the reversible fouling due to pore blocking and cake layer build-up, but also clogging near the membrane surface. Back-flushing is commonly controlled by its frequency, duration and flux. Several studies have assessed these back-flushing characteristics on membrane fouling removal. For instance, Jiang *et al.* [1.108] reported that back-flushing presenting low frequency but long duration (600 s filtration/45 s backwashing) is more efficient than more frequent back-flushing with short durations (200 s filtration/15 s backwashing). Although higher fouling amounts are expected to be removed if increasing back-flushing duration and frequency, optimising this operating stage is essential for minimising energy consumption while maximising the treatment efficiency of membranes [1.21].

1.4.3.3 Sustainable operating flux

Sustainable flux in MBR technology is defined as the flux at which the decrease in permeability is operationally acceptable (*i.e.* it is possible to operate at reasonable TMP and fouling rate values) [1.109]. Flux sustainability is commonly assessed in the long-term. In these long-term trials the flux is determined by setting different J values lower than the critical one [1.110], which is experimentally determined in the short term. Indeed, sustainable flux can also be defined as sub-critical flux by default.

1.4.3.3.1 Critical Flux

One such fouling control strategy aimed to optimise filtration whilst minimising investment and operating costs is based on using membranes in sub-critical filtration conditions [1.109]. These conditions are limited by the critical flux (J_C): a quantitative filtration parameter defined firstly as "the flux below which no fouling occurs" [1.111], as "the flux below which a decline of flux with time does not occur; above it, fouling is observed" [1.112], or as "a flux below which there is no fouling by colloidal particles" [1.113].

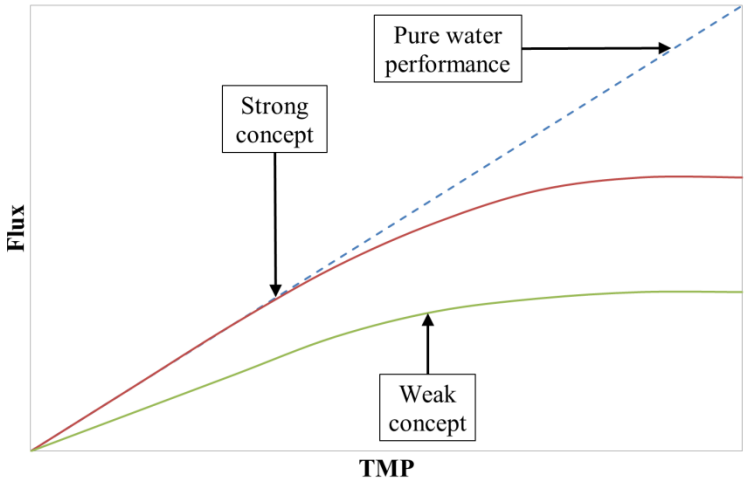

Figure 1.9 Schematic representation of the strong and weak definitions of the critical flux.

On the basis of these conditions, two different concepts have been defined. In the "strong" concept, critical flux (J_{CS}) is defined as the flux below which membrane performance is equal to its ability to treat clean water under same operating conditions (see Figure 1.9). For the "weak" concept, it is assumed that there is a very rapid fouling on start-up filtration periods, thus the flux–TMP relationship

is below that of the pure water line (see Figure 1.9). Therefore, the critical flux (J_{CW}) is the point at which this line becomes non-linear [1.112].

1.5 Filtration process modelling in MBR technology

Understanding and optimising a complex system such as a membrane bioreactor (MBR) is a difficult and time-consuming task mainly because of the large number of sub-processes taking place simultaneously, which generally are highly dependent one upon each other. Mathematical modelling is a powerful tool for studying such complex systems [1.114].

Mathematical modelling attempts enabling the prediction of the behaviour of a system from a set of parameters and initial conditions. Modelling techniques (including statistical methods, computer simulation, system identification, and sensitivity analysis) have become very important tools in the urban wastewater treatment field as they allow designing and optimising WWTPs. Mathematical modelling in wastewater treatment aims at providing an accurate and fast image of the real behaviour of the system under different dynamic operating conditions. In this regard, mathematical models allow foreseeing the most adequate process performance under given operating conditions.

The main applications of mathematical models can be summarised in:

- Investigation: mathematical models allow representing the results obtained in laboratory or pilot scale, predicting the process performance towards perturbations.
- Design: mathematical models allow the design of new facilities, as well as to assess the influence of several factors on the performance of the plant.
- Operation and control: mathematical models allow designing and testing different control strategies aimed to optimise the process performance.
- Diagnosis: mathematical models allow interpreting the historic data, detecting possible operating problems and proposing different operating and/or structural modifications.

Depending on the background, mathematical models can be classified as follows [1.121]:

- Mechanistic or physiological models (white-box models): these models describe a given process on the basis of physical, chemical and biological laws. The white-box concept means that every detail in the model has a mechanistic explanation, commonly attempting to include as many details as possible. White-box models use to be complex models that result in accurate predictions of the modelled variables when the model parameters are appropriately calibrated.

- Phenomenological, empirical or heuristic models (black-box models): these models are based on empiricism rather than laws. A black-box model has not necessarily a structure compatible with the underlying physical, chemical or biological realism. Indeed, the main characteristic of models of this type is that they assume no knowledge of physical or internal relationships between the system inputs and outputs other than the observable responses in the outputs that inputs produce. Therefore, black-box models relate system inputs and outputs by applying the simplest possible mathematical expression. These models cannot represent situations for which they have not been previously calibrated. The utility of these models lies in identifying possible problems of a previously calibrated system using real operating data.
- Semi-empirical models (grey-box models): these models involve both mechanistic and phenomenological characteristics. These models appear from the necessity of developing simple models incorporating the process know-how. Therefore, the main advantages of this type of models are the physical interpretability and the mathematical identificability of the parameters included in the modelling approach. Depending on the degree of description and complexity, these models approximate one or another of the two previous modelling approaches.

Most of the mathematical models used in the urban wastewater treatment field are semi-empirical, but including a certain high degree of complexity, which approximates mechanistic models.

As mentioned before, computerised models make possible to perform many virtual experiments in a short space of time. This is clearly advantageous toward slow and costly lab experiments. Nevertheless, two important aspects must be taken into account for good modelling practice: (1) the mathematical model might be built from experimental data; and (2) the model must be adequately calibrated and validated from experimental data in order to maintain its realism. The typical steps required in a model building exercise are shown in Figure 1.10.

As Figure 1.10 shows, the following steps can be defined for good modelling practice [1.114]:

- Defining the goal of the modelling study: this step is essential to avoid building useless models (*e.g.* constructing overly complex or simple models).
- Collecting a priori knowledge (*e.g.* existing process knowledge, models, etc.) and experimental data about the studied system.
- Deciding on the model framework (*e.g.* white, black or grey modelling, type of equations (algebraic, ordinary or partial differential), system boundaries, etc.).
- Selecting the model structure if there is still more than one possibility.

- Calibrating the model (*i.e.* estimating the value for the model parameters and confronting the model with experimental data).
- Validating the model in order to test whether the model is capable to predict data sets other than the one used in the calibrating step.

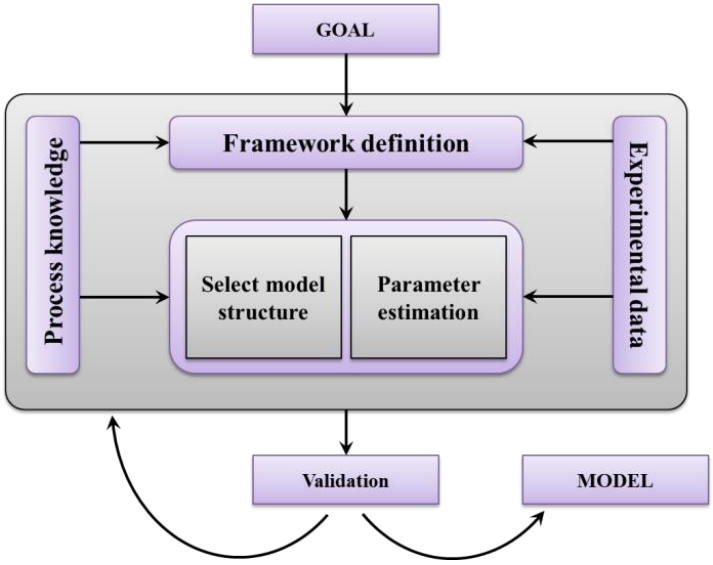

Figure 1.10 Different steps in any model building exercise needed to develop a validated model ready for further application. [1.114].

1.5.1 State of the art of filtration modelling

MBR modelling studies focusses on biological processes rather than filtration. Nevertheless, it is worth pointing out not to overlook the fouling process since mathematical modelling of filtration in MBR technology is essential for operating optimisation.

The biological processes involved in MBR systems can be successfully modelled by using either classical models [1.115; 1.116] or plant-wide models [1.117; 1.118]. As for the modelling of the filtration processes (in addition to the modelling of integrated processes, i.e. biological + filtration processes), several empirical/semi-empirical models have been proposed [1.114; 1.119; 1.120] to express the relationship between sludge characteristics and/or operating conditions, and membrane fouling.

Different modelling approaches to describe the influence of different fouling mechanisms on membrane permeability have been applied to MBR technology, being the Carman-Kozeny equation, the Darcy's law, and the resistance-in-series concept the most commonly used.

1.5.1.1 Carman-Kozeny equation

Each porous medium in low-pressure filtration is assumed to consist of "ideal", straight, cylindrical pores in which flow is assumed to be laminar (Reynolds number (*Re*) < 2000). Hence, the liquid flow can be described as a Hagen-Poiseuille flow (*i.e.* the flow is driven through the medium by a difference in transmembrane hydraulic pressure; the flow through the pore has a parabolic profile; and the liquid is assumed to be Newtonian). The Hagen-Poiseuille equation was adapted by Carman-Kozeny (**Eq. 1.1**) to incorporate pore diameter (d_p, m^2) and medium thickness (δ, m) into this pore-flow filtration model.

$$J = \frac{\varepsilon^3 \cdot d_p^2}{72 \cdot (1-\varepsilon)^2 \cdot \tau \cdot \mu \cdot \delta} \cdot TMP \qquad \textbf{Eq. 1.1}$$

where:

- τ is the medium tortuosity.
- μ is the permeate viscosity.
- ε is the porosity (dimensionless) $= \frac{Total\ pores\ volume}{Total\ porous\ media\ volume}$

However, the Carman-Kozeny equation requires a great deal of effort in order to correctly determine specific characteristics of the filter medium. In addition, these characteristics are time-dependant because some depend on different operating factors such as transmembrane pressure. It is, therefore, advisable to minimise the number of parameters to be included in the model.

1.5.1.2 Resistance-in-series based models

Most of the filtration models in MBR technology describe the flux through each in-series medium using Darcy's law of filtration as theoretical modelling starting point (**Eq. 1.2**). In Darcy's law the permeate volume (V_P) is driven through each medium by a difference in TMP. This law enables the total filtration resistance R_T to be calculated combining different partial resistances related to different fouling mechanisms.

$$J = \frac{1}{A}\frac{dV_P}{dt} = \frac{TMP}{\mu \cdot R_T} \qquad \textbf{Eq. 1.2}$$

where:

- A is the membrane area.

Different partial resistances can be found in the literature, which have been applied to model filtration in MBR technology, such as the following:

- R_M is the clean membrane resistance.
- R_C is the cake layer resistance.
- R_{STA} is the standard pore blocking resistance.
- R_{COM} is the complete pore blocking resistance.
- R_{INT} is the intermediate blocking resistance.
- R_P is the pore blocking resistance.
- R_{REV} is the resistance caused by reversible fouling.
- R_{IRRV} is the resistance caused by irreversible fouling.
- R_{IRRC} is the resistance caused by irrecoverable fouling.
- R_{CD} is the dynamic sludge film resistance.
- R_{SC} is the stable sludge cake resistance.
- R_F is the fouling resistance.
- R_B is the biofilm resistance.

Apart from the clean membrane resistance, which is a time invariant characteristic of the membrane itself, separate models are required for estimating each of the above-mentioned partial resistance components, either based on the exact mechanism taking place near the membrane surface, or on a semi-empirical calibration basis [1.114].

Table 1.7 summarises some of the resistance-in-series-based filtration models applied in MBR technology found in the recent literature, including the resistance-in-series decomposition of their respective model structure. Broekmann et al. [1.122] modelled the pore blocking and cake formation in membrane filtration taking into account the adhesive forces between the particles and the membrane surface, and also the impact of the particle and membrane pore size distributions. Busch et al. [1.123] created a model of submerged HF membrane filtration that incorporated the geometry and hydrodynamics of the system. Li and Wang [1.126] proposed a "comprehensive mathematical model for membrane fouling in a submerged MBR" that includes the impact of shear intensity on membrane scouring. Ludwig et al. [1.128] proposed a dynamic model for simulating submerged membranes on

the basis of the standard parameters usually measured in filtration processes (MLTS and cross flow aeration). And Sarioglu et al. [1.129] proposed a "resistance-in-series" membrane filtration model that considers overall membrane resistance in terms of three distinct components: intrinsic membrane resistance, accumulated solids resistance and membrane fouling resistance.

Table 1.7 Overview of the different possible decompositions of the filtration resistance used in the literature (Adapted from Naessens *et al*. [1.114]).

Resistance in series decomposition	Reference
$R = R_M + R_C + R_P + R_{IRRV}$	[1.122]
$R = R_M + R_C + R_P + R_B$	[1.123]
$R = R_M + R_C + R_{STA} + R_{COM} + R_{INT}$	[1.124]
$R = R_M + R_C + R_F$	[1.125]
$R = R_M + R_P + R_{CD} + R_{CS}$	[1.126]
$R = R_M + R_C + R_B$	[1.127]
$R = R_M + R_C + R_F$	[1.128]
$R = R_M + R_C + R_F$	[1.129]

All these models have been developed and validated in AeMBRs. Therefore, further research on modelling and simulation of filtration in SAnMBR technology is needed.

1.6 Filtration process control in MBR technology

Instrumentation, control and automation (ICA) is now an established and recognised area of technology in the wastewater treatment field. This has been possible not only because of the necessity of minimising operating costs and/or resources in WWTPs, but also due to the combination of a number of factors [1.15]:

- Instrumentation technology is today much more mature. More advanced instruments as on-line in-situ sensors are now regularly used.
- Actuators have also improved over the years. For instance, frequency converters to module the rotatory speed in pumps and compressors are commonly used, which allow a better controllability of the plant.
- Computing power can be currently considered almost "free".
- Control theory and automation technology offer powerful tools (*e.g.* benchmarking models) for evaluating different control strategy performances.

- Improved software packages are available for data acquisition and plant supervision (*e.g.* supervisory control and data acquisition (SCADA) and process control systems). Data-processing tools are mostly borrowed from multivariate statistics and soft computing (neural networks and fuzzy systems).
- Advanced dynamic models applied to wastewater treatment have been developed and there are commercial simulators available to condense the knowledge of plant dynamics (*e.g.* DESASS: DEsign and Simulation of Activated Sludge Systems [1.130]).

ICA can be defined as follows [1.131]:

- Instrumentation: group of elements and/or equipment aimed for on-line monitoring the main control parameters of the process, and group of final control elements that can be manipulated for conducting established actions.
- Control: group of control algorithms aimed to optimise the process performance. These algorithms can be classic controllers (*e.g.* on-off and proportional-integral-derivative (PID)) or advanced controllers (*e.g.* model-based or artificial intelligence based: fuzzy-logic, neural-networks).
- Automation: group of elements capable of conducting automatically the actions established by the control algorithm over the final control elements, as well as the elements responsible for transmitting and/or transforming the on-line measurements. This group can be defined as the interaction or union between instrumentation and control.

Figure 1.11 illustrates the interactions between the different elements of ICA.

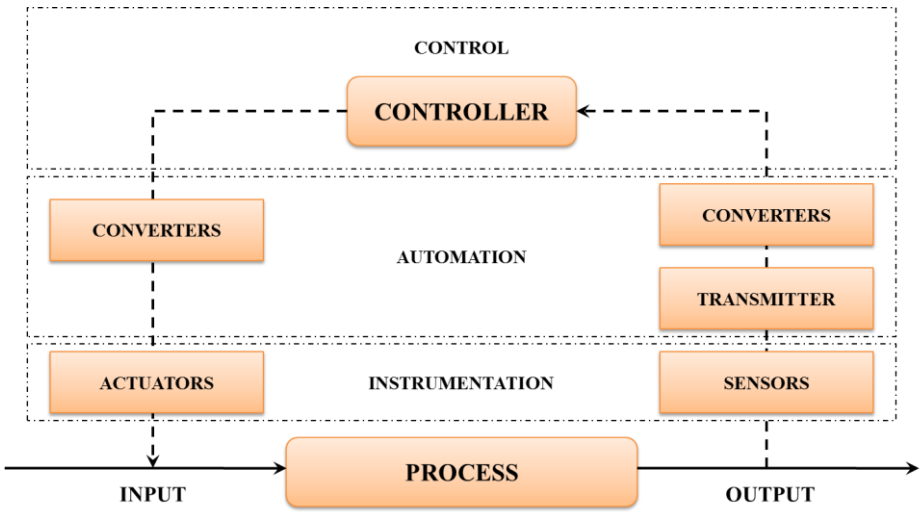

Figure 1.11 Simplified interactions between the different elements of ICA.

1.6.1 Control in wastewater treatment

The main aim of WWTP control lies in accomplishing with established standards under the minimum operating cost. Therefore, the design of a control system must consider several factors, such as energy consumption, reagents consumption, and/or investment and maintenance costs.

Different levels of control can be applied in the wastewater treatment field, which can be mainly classified in four levels [1.15]:

- Level 1. *Manual adjustments based on manual samplings and laboratory measurements*. This is the simplest level.
- Level 2. *Manual adjustment of control based on on-line measurements*. In this level the control system is adjusted manually based on on-line measurements existing in the SCADA system. These on-line measurements can be obtained from either permanent probes or mobile monitoring stations. This level allows the operator to observe the process dynamics assessing, therefore, the effect of the previously applied control actions.
- Level 3. *Lower-layer control*. This level consists in simple on-line closed-loop controllers (*e.g.* PID and on-off control) implemented through SCADA and/or PLC systems. It usually consists in Simple Input Simple Output structures (SISO). Due to the limited calculation and programming potential of standard SCADA/PLC systems, only simple control algorithms based on real-time measurements (on-line monitoring) are usually included in this level.
- Level 4. *Upper-layer control.* This is the most advanced and complex level, including different advanced control systems (*e.g.* fuzzy logic, neural network, model-based control, etc.) aimed to enhance the standard operation of a SCADA/PLC system. It usually consists in Multiple Input Multiple Output structures (MIMO).This level also includes supervisory control systems, on-line tuning protocols and performance reporting.

The general procedure for designing a control system is shown in Figure 1.12. The first step consists in defining the aim of the controller to be implemented in the WWTP. Then, the aim is transformed into a control strategy that could be implemented on an industrial scale under the minimum cost. The control strategy is developed on the basis of an adequate control structure. The next step consists in adjusting the main parameters that define the control system by simulation and experimentation. Finally, the controller can be implemented and validated in the real plant.

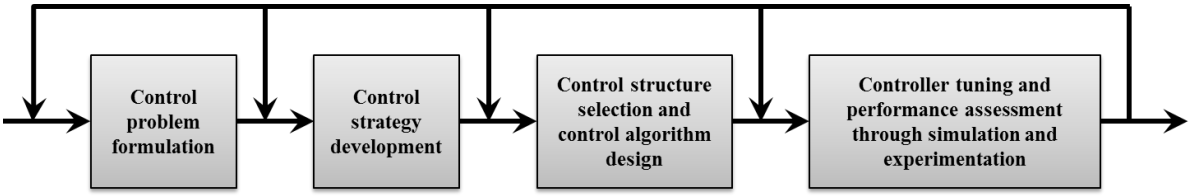

Figure 1.12 General proceeding for designing a control system [1.15].

1.6.1.1 Control structure selection

As mentioned above, the first step for developing a controller consists in defining the aim of the controller to be implemented. In this respect, manipulated and controlled variables of the controller must be selected. The manipulated variables will be those that can be adjusted in a determined operating interval, either manually or automatically. A WWTP is characterised by a limited number of manipulated variables, mainly corresponding to internal flow rates. It is important to highlight that selecting appropriately the manipulated variables is a key point in the development of a control system. Inadequate manipulated variables can result in a worsening of the performance of the WWTP. On the other hand, the control variables will be those that can be on-line monitored.

According to the number of inputs and outputs, a control system can be classified as follows:

- SISO: single-input-single-output control structure
- SIMO: single-input-multiple-output control structure
- MISO: multiple-input-single-output control structure
- MIMO: multiple-input-multiple-output control structure

Once the control inputs and outputs have been selected, the control structure may be defined. In this respect, a control system can be generally classified as follows:

- Feedback control
- Feedforward control
- Combined feedback-feedforward control

On the other hand, depending on the mode the control action is taken, a control system can be classified as follows:

- Open-loop control: the control action is not based on any feedback or measurement, rather based on disturbance or time.
- Closed-loop control: the control action is based on disturbance measurements.

1.6.1.1.1 Feedback control

Feedback controllers are closed-loop controllers where the control action aims to compensate the error (ε) between the controlled variable and its set point. Therefore, feedback control takes corrective actions when the controlled variable deviates from the reference input. Oppositely to feedforward control, feedback control does not require a detailed model for the process and/or high knowledge degree of the controlled process dynamics. Since the control action is applied when an error on the controller variable is observed, feedback control is not advisable for controlling processes with large time delays.

1.6.1.1.2 Feedforward control

Feedforward control allows applying the control action before identifying a deviation of the controlled variable from the reference set-point. The action of open-loop controllers of this type is mainly conducted by detecting perturbations on an input variable different to the controlled one. Therefore, unlike feedback control, feedforward control acts before the error is observed in the control variable. Nevertheless, models are required for the controlled process. The accuracy of the disturbance measurements and the precision of the model finally determine the robustness of feedforward control.

1.6.1.1.3 Combined feedback-feedforward control

It consists in a combination of feedback and feedforward control (see Figure 1.13). This kind of controller allows enhancing the system when the feedback control variables and the feedforward perturbation variables are adequately selected. In this case, feedforward control allows fast actions due to accounting for different process perturbations.

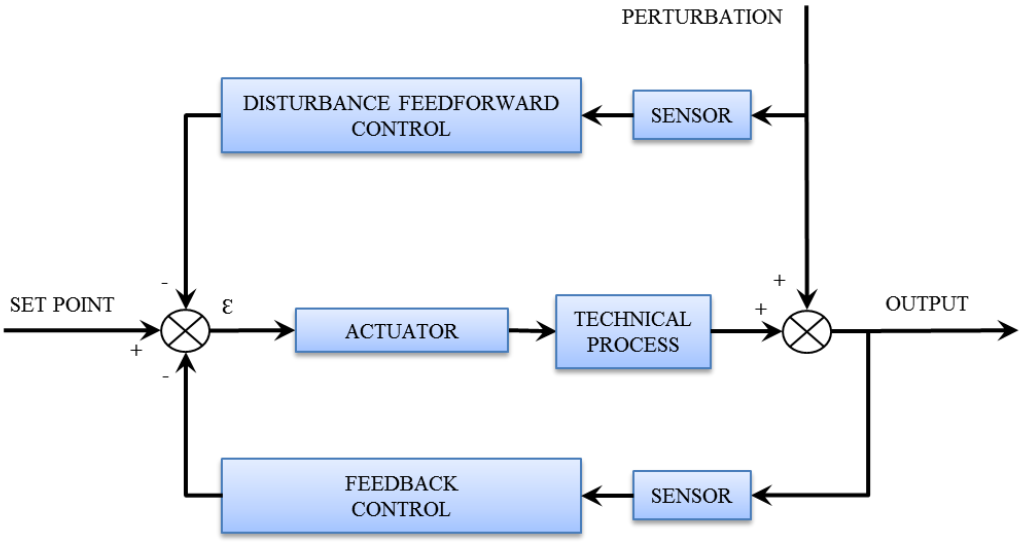

Figure 1.13 Block diagram of a combined feedback-feedforward control structure.

1.6.1.2 Control algorithm design

Once the control structure is selected, the algorithm to be included in the controller must be established. The main control laws used in the urban wastewater treatment field are the following:

- On-off control
- PID control
- Advanced control: fuzzy-logic control, neural networks, model-based control, adaptive control, etc.

1.6.1.2.1 On-off control

On-off controllers are simple, inexpensive feedback controls in which the controller keeps the controlled variable within a given operating range by switching the actuator between two stages (mainly on and off) according to a sensor measurement and a control law. Therefore, the control variable can only take two values (u_{max} and u_{min}) depending on the control error (ε).

1.6.1.2.2 Proportional-integral-derivative (PID) control

PID control is the most generic controller used in industrial systems since they have proven its effectiveness in several applications. PID controllers attempt to minimise the error on the controlled variable by adjusting a given manipulated variable. It is a control method in which the control output is proportional to the error (proportional action), its time history (integral action), and the rate at which

it is changing (derivative action). Indeed, the control action is established on the basis of the single control actions included in the control structure:

- Proportional action: It establishes the value of the control output proportionally to the error. It allows minimising the control offset only when controlling stable and robust systems.
- Integral action: It is proportional to both magnitude and duration of the error and is based on the continuous integration of the accumulated error over time. It accelerates the controlled variable towards its set-point and eliminates the residual steady state offset resulting from the proportional control action. The integral control action results in inappropriate control responses when controlling systems with large response times.
- Derivative action: The aim of this action is the future prevision and compensation of the control offset by examining the change rate of the error. Thus, the derivative action tries to correct the controller behaviour before the error is produced (*e.g.* decelerating the control response when approximating to the corresponding set point). The main constraint of this control action is the possible accentuation of control noise.

The final structure of a PID-based controller is built by combining the above-mentioned individual PID control actions. The general PID control structure can be defined as follows:

$$u\,(t) = K_P \cdot \left(\varepsilon\,(t) + \frac{1}{\tau_I} \cdot \int_0^t \varepsilon\,(t) \cdot dt + \tau_D \cdot \frac{d\varepsilon\,(t)}{dt} \right) \qquad \textbf{Eq. 1.3}$$

where:

- $u\,(t)$ is the control output at time t.
- $\varepsilon\,(t)$ is the control error at time t.
- K_P is the proportional gain (usually dimensionless), which determinates how strong the proportional term is.
- τ_I is the integral time (it has units of time), which determinates how fast the integral term is.
- τ_D is the derivative time (it has units of time), which determinates how fast the derivative term is.

The simple structure of PID control represents both its strength and weakness since its simplicity is sometimes limiting due to the complexity of the controlled system. There are several processes (especially in wastewater treatment) whose variability and instability impede a satisfactory performance of PID controllers. To solve this limitation, different advanced controllers have been applied in the wastewater treatment field. Moreover, as processing plants become increasingly

complex in order to increase efficiency and reduce costs, there might be greater incentives for using advanced control systems.

1.6.1.2.3 Advanced control algorithms

Model-based control

Model-based control aims to adjust different manipulated variables (simultaneously) in order to minimise the error between controlled variables and corresponding set points. It is based on predicted responses of the controlled system by applying an appropriate model. Traditionally, linear models were used for this purpose, but currently, more sophisticated non-linear models are being applied, which are capable of handling multivariable processes.

Model-based control algorithms are usually based on the following elements:

- Predictive model
- Objective function
- Optimising algorithm

As the model is the core of the controller, it may accomplish the following requirements for real-time optimisation [1.132]: (1) robustness (i.e. it always finds a solution); (2) fast problem solving; (3) in certain operating conditions, it always reaches the same solution, even from different starting points; and (4) ability to identify system constraints. Moreover, the model applied should be capable of fully capturing process dynamics.

Fuzzy-logic-based control

Fuzzy-logic allows transforming the practical knowledge of a human operator (mainly qualitative) to mathematical language. Fuzzy-logic allows working simultaneously with numerical data and logical terms. The logical terms are less accurate than numerical data but proportionate useful information from the human reasoning.

Oppositely to crisp (classical-logic) reasoning, which uses only the “equal” and “not equal” concepts (operates on discrete values of either 0 (false) or 1 (true)), fuzzy reasoning is based on the concept of membership grade: the crisp true/false duality is softened by the membership grade which can vary continuously between 0 (no similarity) to 1 (full similarity). Therefore, if classical logic is the science

of the formal and normative principles of the reasoning, fuzzy logic refers to the formal principles of the approximate reasoning, whose boundaries correspond to crisp reasoning.

Fuzzy logic allows formulating mathematically imprecise expressions such as "very open" or "little open". Thus, it is possible to represent the human reasoning by means of a programming language, which allows quantifying those imprecise descriptions that are commonly used in the quotidian language. Moreover, applying fuzzy-logic calculations enables designing nonlinear controllers, without a detailed knowledge of the operating point nonlinearity, as would be required for a classical control design.

Therefore, the main advantages of fuzzy control are the following:

- No detailed mathematical model is required.
- Human experience can be easily incorporated.
- It is robust.
- It can adapt to process changes.
- Only with a limited number of rules it can control very complex systems.
- It presents tolerance with the imprecision.
- It presents capacity for modelling non-linear problems.

A fuzzy set is mathematically defined by the following expression:

$$A = \{\mu_A(x): X \rightarrow [0,1]\} \qquad \textbf{Eq. 1.4}$$

where:

- A is the fuzzy set.
- X is the support: interval of values $X \in \mathcal{R}$ of interest for the independent variable x.
- x is the value of the linguistic variable $x \in X$. A linguistic variable can be defined through a number of linguistic labels over the same support.
- $\mu_A(x)$ is the membership function of x to the linguistic label A. This function is the operational definition of the fuzzy set A. Indeed, the fuzzy approach generalises the membership concept through the membership function $\mu(x)$.

The membership function of a given fuzzy set represents the degree of truth for each value of $x \in X$ inside the interval [0, 1] of the element x to the fuzzy set A. Therefore, the degree of truth of the element x is not a discreet value in the interval {0, 1} but gradual in the enclosed interval [0, 1]. The

linguistic labels of a given fuzzy set (*e.g.* "very high" or "zero") define the support of said fuzzy set. Thus, the membership functions associated with these linguistic labels may cover the rank of numerical variation of the physical variable.

Several mathematical representations can be applied to a membership function, such as triangular, trapezoidal, singleton or bell-shaped (see Figure 1.14). One key advantage of the fuzzy sets is that the characteristic parameters of the selected membership functions can be arbitrarily established [1.133].

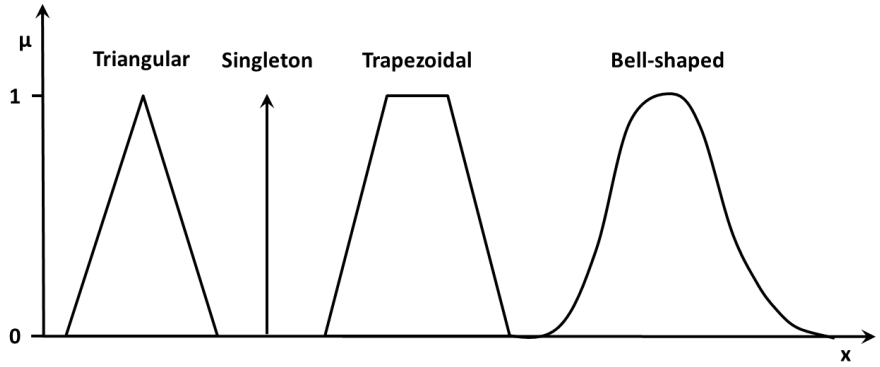

Figure 1.14 Various types of membership functions representing fuzzy sets [1.134].

Figure 1.15 shows the basic structure of a fuzzy-logic control algorithm.

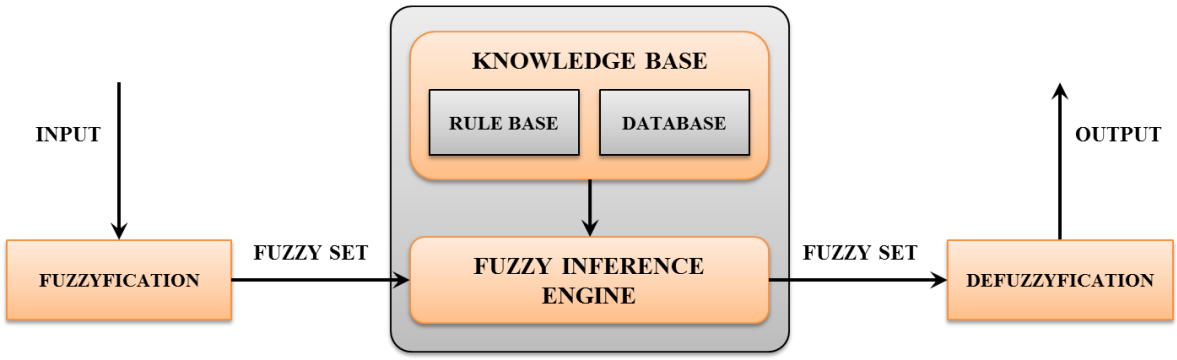

Figure 1.15 Basic structure of a fuzzy-logic controller.

Fuzzy-logic control can be divided in the following 5 stages:

1. Physical input of the control system.

This stage is analogous to any control algorithm. It corresponds to the input of the on-line measured variables to the controller.

2. Fuzzification.

This stage comprises the transformation of the input physical variables from stage 1 to linguistic variables. In this stage, the input fuzzy sets are defined and it is decided how to logically quantify the control inputs (defining the linguistic labels of each linguistic variable). *Fuzzification* involves the determination of the similarity of a given data to a set of predefined membership functions. Given a numerical value *x* (crisp information), *fuzzification* computes its degree of truth with respect to the predefined membership functions (frame of cognition).

3. Inference.

Once the degrees of truth of the input linguistic variables to its respective labels are obtained, the inference engine is conducted. The inference engine relates the degrees of truth of the input fuzzy sets with the degrees of truth of the defined output fuzzy sets. To this aim, the following information is applied:

- Database. This database corresponds to the number of linguistic labels of each input and output linguistic variable, jointly with the number of parameters that define the membership function of each fuzzy set. Therefore, in this stage the group of output fuzzy sets covering the rank of variation of the output physical variable must be defined.
- Rule base. Given an antecedent and a consequent, the degree of truth of the consequent is deduced (implied) by the degree of truth of the antecedent. Thus, a rule base including *if-then* implications must be defined. It actually defines the control strategy.

The fuzzy inference engine is conducted by means of the determination of the degree of fulfilment of each one of the defined rules in the rule base. This degree of fulfilment corresponds to the degree of truth of the output variable *x* to the corresponding fuzzy set. The inference methods more commonly used are the *Max-Min* operator (see Eq. 1.5) proposed by Mamdani [1.135] and the *Max-Prod* operator (see Eq. 1.6) proposed by Larsen [1.136].

$$\mu_B(y) = \min\left[\mu_{A1}(x_1), \mu_{A2}(x_2)\right] \qquad \textbf{Eq. 1.5}$$

where:

- $\mu_B(y)$ is the degree of truth of the output y to the output fuzzy set *B*.
- $\mu_{A1}(x_1)$ is the degree of truth of the input x_1 to the input fuzzy set *A1*.
- $\mu_{A2}(x_2)$ is the degree of truth of the input x_2 to the input fuzzy set *A2*.

$$\mu_B(y) = \mu_{A1}(x_1) \cdot \mu_{A2}(x_2) \qquad \textbf{Eq. 1.6}$$

If more than two fuzzy rules interacts on the same output fuzzy set, it is used the logical operator "or", which applies the union between the two rules (see Eq. 1.7).

$$\mu_B(y) = Max(\mu_B(y)_1, \mu_B(y)_2) \qquad \textbf{Eq. 1.7}$$

where:

- $\mu_B(y)_i$ is the degree of truth of the output variable y to the fuzzy set *B* for each of the fuzzy rules (*i*=1,2,…n) considered in the controller.

4. Defuzzification.

This stage comprises the transformation of each output linguistic variable to a numerical value (output physical variable). To obtain this output scalar value one of the following mathematical methods is commonly applied [1.137]:

Centre of gravity method (usually applied in Mamdani fuzzy models). It uses the following equation to determine the value of the physical output variable:

$$\hat{y} = \frac{\int y \cdot \mu(y) \cdot dy}{\int \mu(y) \cdot dy} \qquad \textbf{Eq. 1.8}$$

where:

- $\hat{y}$ is the value of the physical output variable

Weighted average defuzzifier method (usually applied in Sugeno fuzzy models). It uses the following equation to determine the value of the physical output variable:

$$\hat{y} = \frac{\sum_{i=1}^{n} c_i \cdot \mu(y_i)}{\sum_{i=1}^{n} \mu(y_i)} \qquad \textbf{Eq. 1.9}$$

where:

- c_i is the singleton value of the corresponding output singleton membership

5. Physical output of the control system.

This stage is analogous to any control algorithm. Once the value of the output physical variable of the controller is obtained, this value is commanded to the corresponding actuator.

1.6.2 State of the art of filtration control

The energy consumption during filtration involves the major term of the operational cost in MBR technology (up to the 75% [1.138]). Two types of terminology are commonly used for classifying the control systems for filtration in MBR technology: (1) one related to the nature of the controlled and manipulated variables; and (2) other strictly related to the nature of the controller [1.139]. In the first case, the control systems for filtration in MBR technology usually involve the regulation of air/gas scouring, membrane operating stages (including flux, duration and frequency of the stages that comprise the operating mode) and chemical cleaning (see Figure 1.16). In the second case, the control systems are simply classified as open-loop or closed-loop control.

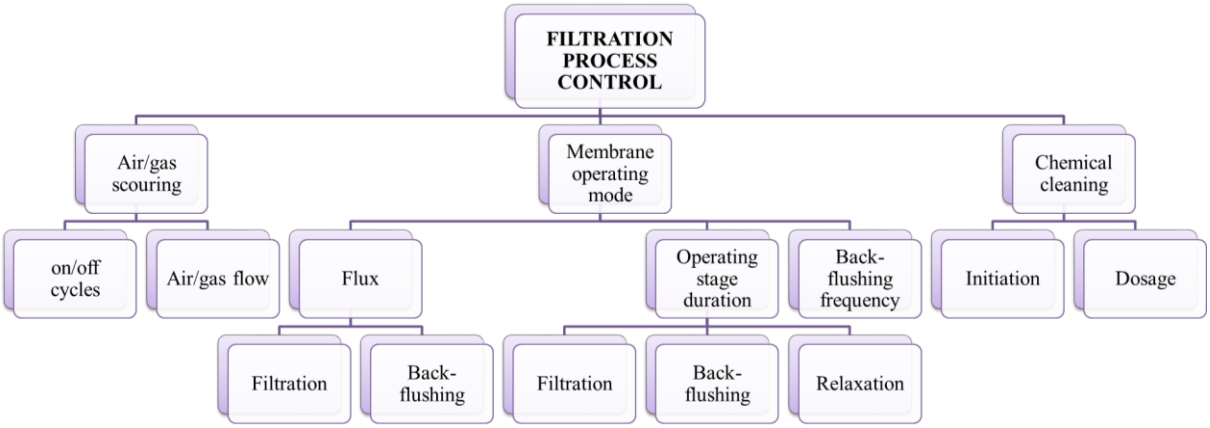

Figure 1.16 Main filtration variables controlled in MBR technology (Adapted from Ferrero *et al*. [1.139]).

Different control systems have been developed and validated for AeMBRs, even at full-scale. However, no specific controllers have been developed and validated using industrial-scale membranes in SAnMBR systems. Therefore, further research is needed to develop control strategies aimed to optimise filtration in SAnMBR systems on an industrial-scale. Table 1.8 summarises some of the currently implemented control systems for filtration in MBR technology. As Table 1.8 shows, the main currently implemented control systems for filtration in MBR technology entail controlling aeration, TMP, filtration resistance, permeate flux and fouling rate by manipulating aeration/gasification flow, permeate flux, permeation and relaxation duration, back-flushing duration and initiation, maintenance and recovery chemical cleaning initiation, TMP and cross-flow velocity. It is worth pointing out that membrane scouring by air/gas sparging is a key control variable in both open-loop and closed-loop control systems.

Table 1.8 Implemented control systems for filtration in MBR technology (Adapted from Ferrero *et al*. [1.139]).

Control type	**Controlled variable**	**Manipulated variable**	**Reference**
Open-loop	Aeration on/off and intensity		[1.140]
Open-loop	Aeration on/off and intensity		[1.141]
Open-loop	Aeration on/off		[1.142]
Open-loop	Aeration on/off		[1.143]
Open-loop	Aeration intensity		[1.144; 1.145]
Open-loop	Aeration intensity		[1.146]
Open-loop	Aeration intensity		[1.147]
Closed-loop	TMP	Gasification flow and permeate flux	[1.148]
Closed-loop	TMP	Back-flushing duration and initiation	[1.149; 1.150]
Closed-loop	TMP	Aeration flow; permeation and relaxation duration; and permeate flux	[1.151]
Closed-loop	Resistance	Aeration on/off and flow; permeation, relaxation and back-flushing duration; back-flushing initiation; permeate flux; and maintenance and recovery chemical cleaning initiation	[1.152; 1.153]
Closed-loop	Resistance	Permeate flux and duration; back-flushing flux; and aeration on/off	[1.154; 1.155]
Closed-loop	Resistance and permeate flux	TMP and cross-flow velocity	[1.156]
Closed-loop	Permeability	Aeration flow; and back-flushing and relaxation initiation	[1.157; 1.158]
Closed-loop	Permeability	Aeration flow	[1.159; 1.160; 1.161; 1.162]
Closed-loop	Permeate flux	Back-flushing initiation	[1.163]
Closed-loop	Permeate production	Aeration flow; and back-flushing and relaxation duration	[1.164; 1.165; 1.166]
Closed-loop	Fouling rate	Aeration flow	[1.167]

1.7 Sensitivity analysis

WWTP models are used for many applications/purposes including plant design, optimisation and control. In this regard, it is generally accepted that WWTP modelling and simulation represents a powerful tool for control systems design and tuning. However, the model predictions are not free from uncertainty as these models are an approximation of reality (abstraction), and are typically built on a considerable number of assumptions. In this sense, the application of a model requires determining the values of the parameters that represent the performance of the specific process to be simulated. However, some models present a large number of parameters, which does infeasible to experimentally calibrate the whole set of parameters [1.168; 1.169; 1.170]. Therefore, the most important model inputs must be found out in order to make feasible a suitable calibration of overparameterised models. The parameters to calibrate will be those that are sensitive, that is, that present the greater influence in model outputs. In this sense, sensitivity analysis provides useful information for the modellers as this technique attempts to quantify how a change in the model input factors affects the model outputs.
Similarly, fuzzy-logic-based controllers usually contain quite a number of parameters which complicates their calibration. So far, these control systems have been tuned by trial and error methods, based on technical knowledge on the process and controller performance. Whatever the optimisation method is applied, the fine-tuning of these controllers requires a previous selection of the most important parameters to be adjusted in each particular application. Thus sensitivity analysis tools have been also applied to find an adequate control parameter subset for facilitating fine-tuning fuzzy controllers applied to wastewater treatment [1.171].

1.7.1 Sensitivity analysis strategies

Sensitivity analysis strategies have been recognised as a suitable mathematical tool for determining the most influential parameters of a model/controller [1.168; 1.169; 1.172].

The sensitivity function of a model output y with respect to an input factor θ can be defined by the following expression:

$$S(t) = \frac{\partial y(t)}{\partial \theta} \qquad \textbf{Eq. 1.10}$$

where:

- $y(t)$ is the model output at time t.
- θ is the input factor of the model.
- $S(t)$ is the sensitivity of the model output y to the input factor θ at time t.

Different sensitivity analysis strategies have been applied in the literature typically classified in two main categories:

- Local sensitivity analysis, which is based on the local effect of the inputs on the model outputs. The corresponding sensitivities are determined for one specific set of parameter values, also called the nominal parameter set (*i.e.* one point in the parameter space).
- Global sensitivity analysis, where a sampling method is taken and the uncertainty range given in the input reflects the uncertainty on the output. These techniques evaluate the sensitivity function in many different points in the parameter space.

Most of the local sensitivity analysis strategies [1.173; 1.174] assume that the relation between the input factors and the output variables is linear. Therefore, the relative importance of each input factor is obtained by applying fixed variation of each input factor around a given nominal value, keeping constant the value of the rest of inputs.

On the other hand, global sensitivity analysis strategies are suitable when the model is non-linear and/or the uncertainty of the inputs is significant. The main disadvantage of using global sensitivity analysis strategies instead of local ones is the considerable increase of computational demand.

1.7.1.1 Global sensitivity analysis

The global sensitivity analysis techniques most widely applied can be classified as follows [1.175]:

- Fourier amplitude sensitivity test (FAST) method [1.176] and FAST extended [1.177]. These methods are based on variance analysis methods from the calculation of the total indexes of sensitivity (TSIs). These indexes measure not only the main first order effects of each individual parameter or parameter subset, but also greater order ones. The method is capable to evaluate the influence of the parameters in the interval of variation considered and the interactive effects between them.
- Monte Carlo procedure. It is based on randomly generating combinations of input factors to evaluate model outputs. From these combinations, Monte Carlo procedure determines the uncertainty in the model predictions and the contribution of each input factor to this uncertainty. In general, Monte Carlo procedures comprise 5 steps:
    - Selecting the variance range and distribution of each input factor.
    - Generating a random combination of values for the input factors in the determined working space. To this aim, Monte Carlo procedures can use different sampling

strategies, such as random sampling, stratified sampling (*e.g.* Latin hypercube sampling) and semi-random sampling.
    - Evaluating the model output for each combination of values for the input factors.
    - Uncertainty analysis (*i.e.* analysing the value of the output and its variance).
    - Sensitivity analysis. This last step consists in applying a sensitivity analysis strategy (*e.g.* correlation coefficient determination, regression analysis, FAST method, etc.).
- Screening methods. These techniques are defined as one-factor-at-a-time (OAT) methods of global sensitivity analysis. In these techniques the so-called elementary effects of input factors to model outputs are evaluated. An example of this type of techniques is the Morris screening method [1.178].

The selection of a global sensitivity analysis methodology is mainly based on the total computational cost, taking into account: (1) the computational demand derived from the model simulations; (2) the number of input factors to be evaluated; and (3) the computational cost derived from the selected sensitivity analysis technique. The application of FAST and Monte Carlo procedures remains limited to models where the number of parameters is not too high and the computational demand of model simulations is relatively low (in the order of minutes). On the other hand, the Morris screening method is characterised by being a simpler global technique that presents a computational cost lower than the rest of global sensitivity analysis methodologies [1.179].

The Morris screening method

Numerous applications of the Morris screening method can be found in the literature for the selection of the most influential parameters in different types of models [1.172; 1.179; 1.180; 1.181]. On the other hand, different applications can be found for determining the most influential parameters in fuzzy-logic controllers [1.182; 1.183].

The Morris screening method [1.178] consists in obtaining a given number of representative matrixes of input combinations using an efficient random sampling strategy. From these matrixes the elementary effects of each input factor to model outputs are determined under the minimum possible computational cost. Finally, the mean (μ) and standard deviation (σ) of the elementary effects calculated for each input factor are used for selecting the most influential parameters of the model/controller.

The procedure for determining the elementary effects described by Morris can be summarised as follows:

- The interval of variation of each input factor X_i (i=1,2..*k*) is divided in *p* levels. Initially it is assumed that the distribution of each input factor is uniform in the interval [0,1], being these values converted latter in real distributions. Therefore, the input working space (ω) representative of the group of possible input factors is defined by *k* dimensions divided in *p* levels.
- Then, the elementary effects of the input factor X_i for a given value in the parameter vector $X=(X_1, X_2 \ldots X_k)$ can be defined as follows:

$$d_i(X) = \left(\frac{y(X_1,...,X_{i-1}, X_i + \Delta, X_{i+1},...,X_k) - y(X)}{\Delta} \right) \text{ for } X \in \omega, \text{ and } X_i \in [0, (1-\Delta)]. \qquad \textbf{Eq. 1.11}$$

where:

- $y(X)$ is the model output for the combination of input factors, X.
- $d_i(X)$ is the elementary effect of the input factor i on the output variable y.
- Δ is defined as shown in Eq. 1.12.

$$\Delta = \frac{p}{2(p-1)} \qquad \textbf{Eq. 1.12}$$

- In order to calculate the distribution of *r* elementary effects of each input *i* (F_i) a random sampling strategy is proposed. Specifically, to obtain one elementary effect per parameter one matrix (known as "trajectory") is generated from an specific design [1.178] of dimensions $(k+1)\cdot k$, where each row represents one combination of values for the parameters X, obtained from a random sampling in ω. Therefore, a total of *r* trajectories of $(k+1)$ values of X are required for obtaining *r* elementary effects for each input factor, that is, a total of $r\cdot(k+1)$ model evaluations will be necessary. Selecting the number of trajectories to be evaluated is a critical step for obtaining adequate estimations of the sensitivity measures [1.184].
- Finally, after evaluating the model $r\cdot(k+1)$ times, the *r* elementary effects of each input factor are calculated using Eq. 1.11. From this, the basic statistics of each distribution F_i are calculated (*i.e.* μ and σ).

In order to enhance the Morris screening method, Saltelli *et al*. [1.185] proposed the use of the absolute values of the elementary effects to calculate the mean ($\mu*$) as additional sensitivity statistic.

From σ and $\mu*$ it is possible to determine the most influential parameters of the model as follows (Figure 1.17):

- Low $\mu*$ and σ values indicate negligible effects of the input factor to model outputs.
- High $\mu*$ values and low σ values indicate linear and additive effects of the input factor to model outputs.
- High $\mu*$ and σ values indicate non-linear or interactive effects of the input factor to model outputs. The Morris screening method does not differentiate between these both effects because of being a method based on first order sensitivity.

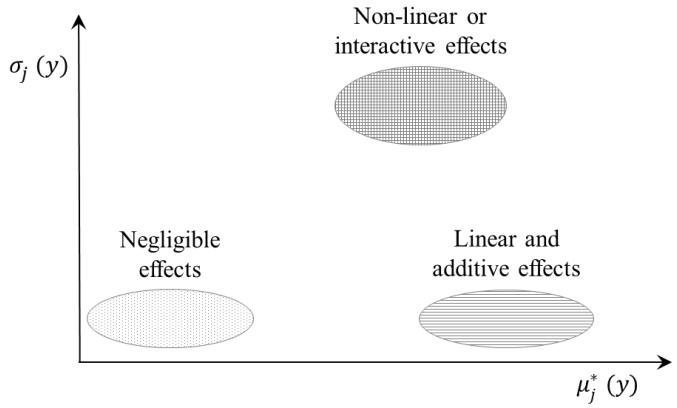

Figure 1.17 Theoretical disposition of means $\boldsymbol{\mu_j^*(y)}$ and standard deviations $\boldsymbol{\sigma_j}$ $\boldsymbol{(y)}$ of the effects distribution.

Campolongo *et al*. [1.186] proposed a modification of the Morris screening method by improving the sampling strategy. It consisted in selecting the *r* trajectories in such a way as to maximise their dispersion in ω. At first, a high number of random Morris trajectories (*M*) are generated (*M* = 500 ~ 1000 trajectories) and then the highest spread *r* trajectories are chosen. This spread is defined following the definition of geometric distance between a couple of trajectories *m* and *l*, which is defined by the following equation:

$$d_{ml} = \left\{ \sum_{i=1}^{k+1} \sum_{j=1}^{k+1} \sqrt{\sum_{z=1}^{k} \left[X_i^m(z) - X_i^l(z) \right]^2} \right. \text{ for } m \neq l\text{; otherwise } d_{ml} = 0. \qquad \textbf{Eq. 1.13}$$

where:

- $X_i^m\ (z)$ is the z^{th} coordinate of the i^{th} point of the m^{th} Morris trajectory.
- d_{ml} is the geometric distance between a couple of trajectories *m* and *l*.

Consequently, the best combination of *r* trajectories from *M* is selected by maximising the distance d_{ml} among them, and thus, the quantity *D*, which is the sum of all the distances d_{ml} between couple of trajectories belonging to the combination.

This *D* quantity must be calculated for each possible combination of *r* trajectories. Consequently, the evaluation of all the possible combinations results in a high computational demand. To solve this combinatorial problem, Ruano *et al*. [1.183] developed an alternative methodology which does not take into account all the possible combinations, but it gets with low computational demand a combination of *r* trajectories out of *M* that are really close to the highest spread ones.

1.8 Scope and outline of this thesis

On the basis of the current research found in the literature it is expected that combining membrane filtration and anaerobic biological process will represent a sustainable and cost-effective technology for the anaerobic treatment of urban wastewater at ambient temperature conditions. Within this research line, the main objective of this Ph.D. thesis is to investigate the feasibility of filtration process in SAnMBR technology for urban wastewater treatment at ambient temperature. To this aim, this thesis is focussed on modelling, simulation and control of filtration process in SAnMBRs. To obtain representative results that could be extrapolated to full-scale plants, this research work was carried out in an SAnMBR system featuring industrial-scale HF membrane units that was operated using effluent from the pre-treatment of the Carraixet WWTP (Valencia, Spain).

This Ph.D. thesis is enclosed in a national research project funded by the Spanish Ministry of Science and Innovation entitled “Using membrane technology for the energetic recovery of wastewater organic matter and the minimization of the sludge produced” (MICINN project CTM2008-06809-C02-01/02).

This Ph.D. thesis is presented as a series of chapters that represent journal papers (compendium of papers). According to the aim of this Ph.D. thesis, the following series of objectives were defined:

a) Set-up, calibration and start-up of the required ICA for SAnMBR systems treating urban wastewater (developed in *Chapter 2*). This objective involves the following:

- Evaluating the performance of ICA in the SAnMBR plant (diagnosis) in order to identify possible operating problems and therefore apply the required modifications (operating conditions and/or facilities), and the corresponding ICA adaptations.

- Analysing the possible correlations between the plant performance and the on-line measures from the different probes installed in the plant.

b) Identification of the key operating parameters affecting membrane performance in SAnMBR systems treating urban wastewater (developed in *Chapters 3, 4, 5 and 6*). This objective involves the following:

- Identifying the critical filtration conditions at different MLTS levels and gas sparging intensities.
- Assessing the effect of different process variables related to the membrane operating mode on the filtration process.
- Assessing the effect of different biological and physico-chemical bulk characteristics on the filtration process.

c) Modelling and simulation of the filtration process in SAnMBR systems treating urban wastewater (developed in *Chapters 7, 8 and 9*). This objective involves the following:

- Developing and calibrating a model for filtration in SAnMBR systems entailing industrial-scale HF membrane units.
- Validating the model using both short-term and long-term experimental data.
- Sensitivity analysis assessment of the developed filtration model.

d) Development of different control strategies aimed to optimise filtration in SAnMBR systems treating urban wastewater on an industrial scale (developed in *Chapters 10 and 11*). This objective involves the following:

- Development, calibration and validation of an advanced controller (knowledge-based) for filtration in the SAnMBR plant fitted with industrial-scale HF membrane units.
- Identifying the influential parameters of the developed advanced controller and the optimal initial values through mathematical analysis techniques (Morris screening method and Monte Carlo procedure) in order to facilitate its calibration by optimisation algorithms.
- Developing a model-based supervisory controller (linked to the advanced controller) aimed to optimise membrane performance under the minimum operating cost

1.9 References

1.1 X.M. Guo, E. Trably, E. Latrille, H. Carrère, J.P. Steyer, Hydrogen production from agricultural waste by dark fermentation: A review, Int. J. Hydrog. Energy 35 (2010), 10660–10673.

1.2 A. Gallego, A. Hospido, MT. Moreira, G. Feijoo, Environmental performance of wastewater treatment plants for small populations, Resour. Conser. Recy. 52 (2008), 931–940.

1.3 G. Rodriguez–Garcia, M. Molinos–Senante, A. Hospido, F. Hernández–Sancho, M.T. Moreira, G. Feijoo, Environmental and economic profile of six typologies of wastewater treatment plants, Water Res. 45 (2011), 5997–6010.

1.4 A. Meda, P. Cornel, Energy and water: relationships and recovery potential, IWA Water and Energy conference, Amsterdam, The Netherlands, 10–12 November 2010.

1.5 P. Cornel, A. Meda, S. Bieker, Wastewater as a source of energy, nutrients and service water, Treatise of Water Science, Editor: Peter Wilderer, Elsevier Verlag, 2011.

1.6 V. Lazarova, KH. Choo, P. Cornel, Water–energy interactions in water reuse, IWA Publishing, London, UK, 2012.

1.7 Metcalf & Eddy Inc., 2003. Wastewater Engineering: Treatment and Reuse, 4th edition, New York, McGraw–Hill.

1.8 F. Hernandez–Sancho, M. Molinos–Senante, R. Sala–Garrido, Energy efficiency in Spanish wastewater treatment plants: A non–radial DEA approach, Sci. Total Environ. 409 (2011), 2693–2699.

1.9 P.F. Greenfield, D.J. Batstone, Anaerobic digestion: Impact of future greenhouse gases mitigation policies on methane generation and usage, Water Sci. Technol. 52 (2005), 39–47.

1.10 G. Zeeman, G. Lettinga, The role of anaerobic digestion of domestic sewage in closing the water and nutrient cycle at community level, Water Sci. Technol. 39 (1999), , 187–194.

1.11 G. Lettinga, J.B. Van Lier, J.C.L. Van Buuren, G. Zeeman, Sustainable development in pollution control and the role of anaerobic treatment, Water Sci. Technol. 44 (2001), 181–188.

1.12 W. Verstraete, P. Van de Caveye, V. Diamantis, Maximum use of resources present in domestic "used water", Bioresour Technol. 100 (2009), 5537–5545.

1.13 G. Lettinga, S. Rebac and G. Zeeman, Challenge of psychrophilic anaerobic wastewater treatment, Trends Biotechnol. 19 (2001), 363–370.

1.14 D. Jeison, Anaerobic membrane bioreactors for wastewater treatment: feasibility and potential applications, PhD Thesis, Universidad de Wageningen, Holanda, 2007.

1.15 G. Olsson, M.K. Nielsen, Z. Yuan, A. Lynggaard–Jensen, J.P. Steyer, Instrumentation, Control and Automation in Wastewater Systems–IWA Scientific and technical report Nº15, 2005.

1.16 P. Lant, K. Hartley, Solids characterisation in an anaerobic migrating bed reactor (AMBR), sewage treatment system, Water Res. 41 (2007), 2437–2448.

1.17 J.C. Young, P.L. McCarty, The anaerobic filter for wastewater treatment, J. Wat. Poll. Cont. Fed. 41 (1967), 160–166.

1.18 G. Lettinga, A.F.M. Vanvelsen, S.W. Hobma, W. Dezeeuw, A. Klapwijk, Use of the Upflow Sludge Blanket (USB), Reactor Concept for Biological Wastewater Treatment, Especially for Anaerobic Treatment, Biotechnol. Bioeng. 22 (1980), 699–734.

1.19 I. Bemberis, P. J. Hubbard, F. B. Leonard, Membrane sewage treatment systems potential for complete wastewater treatment, In: American Society for Agricultural Engineering Winter Meeting, 71/878 (1971), 1–28.

1.20 J. Bailey, I. Bemberis, J. Presti, Phase I Final Report e Shipboard sewage treatment system, General Dynamics Electric Boat Division NTIS, 1971.

1.21 P. Le–Clech, V. Chen, T.A.G. Fane, Fouling in membrane bioreactors used in wastewater treatment, J. Membr. Sci. 284 (2006), 17–53.

1.22 K. Yamamoto, M. Hiasa, T. Mahmood, T. Matsuo, Direct solid–liquid separation using hollow fiber membrane in an activated–sludge aeration tank, Water Sci. Technol. 21 (1989), 43–54.

1.23 S. Judd, C. Judd, The MBR Book: Principles and Applications of Membrane Bioreactors for Water and Wastewater Treatment, 2nd edition, Elsevier, ISBN: 978–0–08–096682–3, 2011.

1.24 S. Judd, The MBR site, July 2011, http://www.thembrsite.com.

1.25 R.R. Singhania, G. Christophe, G. Perchet, J. Troquet, C. Larroche, Immersed membrane bioreactors: An overview with special emphasis on anaerobic bioprocesses, Bioresource Technol. 122 (2012), 171-180.

1.26 Frost and Sullivan, European Membrane Bioreactor Market, Market research, 2003.

1.27 Frost and Sullivan, Strategic Analysis of the European Membrane Bioreactor Markets, Market research, 2005.

1.28 Frost and Sullivan, US and Canada Membrane Bioreactor Markets, Market research, 2004.

1.29 S. Judd, The status of membrane bioreactor technology, Trends Biotechnol. 26 (2008), 109–116.

1.30 L. Innocenti, D. Bolzonella, P. Pavan, F. Cecchi, Effect of sludge age on the performance of a membrane bioreactor. Influence on nutrient and metals removal, Desalination 146 (2002), 467–474.

1.31 P. Cote, M. Masini, D. Mourato, Comparison of membrane options for water reuse and reclamation, Desalination 167 (2004), 1–11.

1.32 R. Liu, X. Huang, L. Chen, X. Wen, Y. Qian, Operational performance of a submerged membrane bioreactor for reclamation of bath wastewater, Process Biochem. 40 (2005), 125–130.

1.33 B.K. Ince, O. Ince, P.J. Sallis, G.K. Anderson, Inert COD production in a membrane anaerobic reactor treating brewery wastewater, Water Res. 34 (2000), 3943–3948.

1.34 R.M. Ben Aim, M.J. Semmens, Membrane bioreactors for wastewater treatment and reuse: a success story, Water Sci. Technol. 47 (2002), 1–5.

1.35 C.S. Hwu, J.B. van Lier, G. Lettinga, Physicochemical and biological performance of expanded granular sludge bed reactors treating long–chain fatty acids, Process Biochem. 33 (1998), 75–81.

1.36 M. Gander, B. Jefferson, S. Judd, Aerobic MBRs for domestic wastewater treatment: a review with cost considerations. Sep. Purif. Technol. 18 (2000), 119–130.

1.37 H.E. Grethlein, Anaerobic digestion and membrane separation of domestic wastewater, J. Water Pollut. Control Fed. 50 (1978), 754–763.

1.38 R.K. Dereli, M.E. Ersahin, H. Ozgun, I. Ozturk, D. Jeison, F. van der Zee, J.B. van Lier, Potentials of anaerobic membrane bioreactors to overcome treatment limitations induced by industrial wastewaters, Bioresource Technol. 122 (2012), 160–170.

1.39 H. Lin, W. Peng, M. Zhang, J. Chen, H Huachang, Y. Zhang, A review on anaerobic membrane bioreactors: Applications, membrane fouling and future perspectives, Desalination 314 (2013), 169–188.

1.40 I.S. Chang, P.L. Clech, B. Jefferson, S. Judd, Membrane fouling in membrane bioreactors for wastewater treatment, J. Environ. Eng. 128 (2002), 1018–1029.

1.41 M.V.G. Vallero, G. Lettinga, P.N.L. Lens, High rate sulfate reduction in a submerged anaerobic membrane bioreactor (SAMBaR) at high salinity, J. Membr. Sci. 253 (2005), 217–232.

1.42 B.Q. Liao, J.T. Kraemer, D.M. Bagley, Anaerobic membrane bioreactors: Applications and research directions, Crit. Rev. Env. Sci. Tec. 36 (2006), 489–530.

1.43 L. Dvořák, M. Gómez, M. Dvořáková, I. Růžičková, J. Wanner, The impact of different operating conditions on membrane fouling and EPS production, Bioresource Technol. 102 (2011), 6870–6875.

1.44 A. Pollice, A. Brookes, B. Jefferson, S. Judd, Sub–critical flux fouling in membrane bioreactors–a review of recent literature, Desalination 174 (2004), 221–230.

1.45 G. Skouteris, D. Hermosilla, P. López, C. Negro, A. Blanco, Anaerobic membrane bioreactors for wastewater treatment: A review, Chem. Eng. J. 198/199 (2012), 138–148.

1.46 A. Akram, D.C. Stuckey, Flux and performance improvement in a submerged anaerobic membrane bioreactor (SAMBR), using powdered activated carbon (PAC), Process Biochem. 43 (2008), 93–102.

1.47 A. Akram, D.C. Stuckey, Biomass acclimatisation and adaptation during startup of a submerged anaerobic membrane bioreactor (SAMBR), Environ. Technol. 29 (2008), 1053–1065.

1.48 S.F. Aquino, A.Y. Hu, A. Akram, D.C. Stuckey, Characterization of dissolved compounds in submerged anaerobic membrane bioreactors (SAMBRs), J. Chem. Technol. Biotechnol. 81 (2006), 1894–1904.

1.49 J. Bohdziewicz, E. Neczaj, A. Kwarciak, Landfill leachate treatment by means of anaerobic membrane bioreactor, Desalination 221 (2008), 559–565.

1.50 K. Calderón, B. Rodelas, N. Cabirol, J. González–López, A. Noyola, Analysis of microbial communities developed on the fouling layers of a membranecoupled anaerobic bioreactor applied to wastewater treatment, Bioresource Technol. 102 (2011), 4618–4627.

1.51 W.J. Gao, H.J. Lin, K.T. Lin, H. Schraft, B.Q. Liao, Structure of cake layer in submerged anaerobic membrane bioreactor, J. Membr. Sci. 374 (2011), 110–120.

1.52 A.Y. Hu, D.C. Stuckey, Activated carbon addition to a submerged anaerobic membrane bioreactor: effect on performance, transmembrane pressure, and flux, J. Environ. Eng. 133 (2007), 73–80.

1.53 Z. Huang, S.L. Ong, H.Y. Ng, Feasibility of submerged anaerobic membrane bioreactor (SAMBR) for treatment of low–strength wastewater, Water Sci. Technol. 58 (2008), 1925–1931.

1.54 Z. Huang, S.L. Ong, H.Y. Ng, Submerged anaerobic membrane bioreactor for low-strength wastewater treatment: effect of HRT and SRT on treatment performance and membrane fouling, Water Res. 45 (2011) 705–713.

1.55 J. Kim, K. Kim, H. Ye, E. Lee, C. Shin, P.L. McCarty, J. Bae, Anaerobic fluidised bed membrane bioreactor for wastewater treatment, Environ. Sci. Technol. 45 (2011), 576–581.

1.56 E. Kocadagistan, N. Topcu, Treatment investigation of the Erzurum city municipal wastewaters with anaerobic membrane bioreactors, Desalination 216 (2007), 367–376.

1.57 B.Q. Liao, K. Xie, H.J. Lin, D. Bertoldo, Treatment of kraft evaporator condensate using a thermophilic submerged anaerobic membrane bioreactor, Water Sci. Technol. 61 (2010), 2177–2183.

1.58 H.J. Lin, K. Xie, B. Mahendran, D.M. Bagley, K.T. Leung, S.N. Liss, B.Q. Liao, Sludge properties and their effects on membrane fouling in submerged anaerobic membrane bioreactors (SAnMBRs), Water Res. 43 (2009), 3827–3837.

1.59 H.J. Lin, K. Xie, B. Mehendran, D.M. Bagley, K.T. Leung, S.N. Liss, B.Q. Liao, Factors affecting sludge cake formation in a submerged anaerobic membrane bioreactor, J. Membr. Sci. 361 (2010), 126–134.

1.60 H.J. Lin, B.Q. Liao, J. Chen, W. Gao, L. Wang, F. Wang, X. Lu, New insights into membrane fouling in a submerged anaerobic membrane bioreactor based on characterization of cake sludge and bulk sludge, Bioresource Technol. 102 (2011), 2373–2379.

1.61 B. Rezania, J.A. Oleszkiewicz, N. Cicek, Hydrogen–driven de–nitrification of wastewater in an anaerobic submerged membrane bioreactor: potential for water reuse, Water Sci. Technol. 54 (2006), 207–214.

1.62 A. Spagni, S. Casu, N.A. Crispino, R. Farina, D. Mattioli, Filterability in a submerged anaerobic membrane bioreactor, Desalination 250 (2010), 787–792.

1.63 P. Sui, X. Wen, X. Huang, Feasibility of employing ultrasound for on–line membrane fouling control in an anaerobic membrane bioreactor, Desalination 219 (2008), 203–213.

1.64 A.P. Trzcinski, D.C. Stuckey, Treatment of municipal solid waste leachate using a submerged anaerobic membrane bioreactor at mesophilic and psychrophilic temperatures: analysis of recalcitrants in the permeate using GC–MS, Water Res. 44 (2010), 671–680.

1.65 A.P. Trzcinski, D.C. Stuckey, Anaerobic digestion of the organic fraction of municipal solid waste in a two–stage membrane process, Water Sci. Technol. 60 (2009), 1965–1978.

1.66 P.J. Van Zyl, M.C. Wentzel, G.A. Ekama, K.J. Riedel, Design and start–up of a high rate anaerobic membrane bioreactor for the treatment of a low pH, highstrength, dissolved organic wastewater, Water Sci. Technol. 57 (2008), 291–295.

1.67 I. Vyrides, D.C. Stuckey, Saline sewage treatment using a submerged anaerobic membrane reactor (SAMBR): effects of activated carbon addition and biogas sparging time, Water Res. 43 (2009), 933–942.

1.68 T. Wang, H. Zhang, F. Yang, S. Liu, Z. Fu, H. Chen, Start–up of the Anammox process from conventional activated sludge in a membrane bioreactor, Bioresource Technol. 100 (2009), 2501–2506.

1.69 K. Xie, H.J. Lin, B. Mahendran, D.M. Bagley, K.T. Leung, S.N. Liss, B.Q. Liao, Performance and fouling characteristics of a submerged anaerobic membrane bioreactor for kraft evaporator condensate treatment, Environ. Technol. 31 (2010), 511–521.

1.70 M. Xu, X. Wen, Z. Yu, Y. Li, X. Huang, A hybrid anaerobic membrane bioreactor coupled with on–line ultrasonic equipment for digestion of waste activated sludge, Bioresource Technol. 102 (2011), 5617–5625.

1.71 F.G. Meng, S.R. Chae, A. Drews, M. Kraume, H.S. Shin, F.L. Yang, Recent advances in membrane bioreactors (MBRs): membrane fouling and membrane materials, Water Res. 43 (2009), 2405–2415.

1.72 B.Q. Liao, J.T. Kraemer, D.M. Bagley, Anaerobic membrane bioreactors: Applications and research directions, Crit. Rev. Env. Sci. Tec. 36 (2006), 489–530.

1.73 M. Kraume, D. Wedi, J. Schaller, V. Iversen, A. Drews, Fouling in MBR: what use are lab investigations for full scale operation?, Desalination 236 (2009), 94–103.

1.74 H. Choi, K. Zhang, D.D. Dionysiou, D.B. Oerther, G.A. Sorial, Effect of permeate flux and tangential flow on membrane fouling for wastewater treatment, Sep. Purif. Technol. 45 (2005), 68–78.

1.75 P. Le–Clech, B. Jefferson, I.S. Chang, S.J. Judd, Critical flux determination by the flux–step method in a submerged membrane bioreactor, J. Membr. Sci. 227 (2003), 81–93.

1.76 B. Jefferson, A. Brookes, P. Le–Clech, S.J. Judd, Methods for understanding organic fouling in MBRs, Water Sci. Technol. 49 (2004), 237–244.

1.77 A. Brookes, B. Jefferson, G. Guglielmi, S.J. Judd, Sustainable flux fouling in a membrane bioreactor: impact of flux and MLSS, Sep. Sci. Technol. 41 (2006), 1279–1291.

1.78 T. Kornboonraksa, S.H. Lee, Factors affecting the performance of membrane bioreactor for piggery wastewater treatment, Bioresource Technol. 100 (2009), 2926–2932.

1.79 A. Robles, F. Durán, M.V. Ruano, J. Ribes, J. Ferrer, Influence of total solids concentration on membrane permeability in a submerged hollow–fibre anaerobic membrane bioreactor, Water Sci. Technol. 66 (2012), 377–384.

1.80 T. Itonaga, K. Kimura, Y. Watanabe, Influence of suspension viscosity and colloidal particles on permeability of membrane used in membrane bioreactor (MBR), Water Sci. Technol. 50 (2004), 301–309.

1.81 H.C. Flemming, J.Wingender, Relevance of microbial extracellular polymeric substances (EPSs). Part I. Structural and ecological aspects, Water Sci. Technol. 43 (2001), 1–8.

1.82 C.S. Laspidou, B.E. Rittmann, A unified theory for extracellular polymeric substances, soluble microbial products, and active and inert biomass, Water Res. 36 (2002), 2711–2720.

1.83 B. Frølund, R. Palmgren, K. Keiding, P.H. Nielsen, Extraction of extracellular polymers from activated sludge using a cation exchange resin, Water Res. 30 (1996), 1749–1758.

1.84 M. Dubois, K.A. Gilles, J.K. Hamilton, P.A. Rebers, F. Smith, Colorimetric method for determination of sugar and related substances, Anal. Chem. 28 (1956), 350–356.

1.85 O.H. Lowry, N.J. Rosebrough, A.L. Farr, R.J. Randall, Protein measurement with the folin phenol reagent, J. Biol. Chem. 193 (1951), 265–275.

1.86 S. Rosenberger, H. Evenblij, S. te Poele, T. Wintgens, C. Laabs, The importance of liquid phase analyses to understand fouling in membrane assisted activated sludge processes–six case studies of different European research groups, J. Membr. Sci. 263 (2005), 113–126.

1.87 S. Rosenberger, M. Kraume, Filterability of activated sludge in membrane bioreactors, Desalination 151 (2003), 195–200.

1.88 A. Drews, M. Vocks, U. Bracklow, V. Iversen, M. Kraume, Does fouling in MBRs depend on SMP?, Desalination 231 (2008), 141–149.

1.89 E. Iritani, N. Katagiri, T. Sengoku, K.M. Yoo, K. Kawasaki, A. Matsuda, Flux decline behaviors in dead–end microfiltration of activated sludge and its supernatant, J. Membr. Sci. 300 (2007), 36–44.

1.90 S. Lyko, D. Al–Halbouni, T. Wintgens, A. Janot, J. Hollender, W. Dott, T. Melin, Polymeric compounds in activated sludge supernatant–characterisation and retention mechanisms at a full–scale municipal membrane bioreactor, Water Res. 41 (2007), 3894–3902.

1.91 S. Lyko, T. Wintgens, D. Al–Halbouni, S. Baumgarten, D. Tacke, K. Drensla, A. Janot, W. Dott, J. Pinnekamp, T. Melin, Long–term monitoring of a full–scale municipal membrane bioreactor–characterisation of foulants and operational performance. J. Membr. Sci. 317 (2008), 78–87.

1.92 F. Y. Sun, X. Y. Li, Evaluation of the importance of various operating and sludge property parameters to the fouling of membrane bioreactors. Water Sci. Technol. 64 (2011), 1340–1346

1.93 T. Stephenson, S. Judd, B. Jefferson, K. Brindle, Membrane Bioreactors for Wastewater Treatment, IWA Publishing, London, UK, 2000.

1.94 P.R. Bérubé, E.R. Hall, P.M Sutton, Parameters governing permeate flux in an anaerobic membrane bioreactor treating low–strength municipal wastewaters: A literature review, Water Environ. Res. 78 (2006), 887–896.

1.95 J. Zhang, S.I. Padmasiri, M. Fitch, B. Norddahl, L. Raskin, E. Morgenroth, Influence of cleaning frequency and membrane history on fouling in an anaerobic membrane bioreactor, Desalination 207 (2007), 153–166.

1.96 A.L. Smith, L.B. Stadler, N.G. Love, S.J. Skerlos, L. Raskin, Perspectives on anaerobic membrane bioreactor treatment of domestic wastewater: A critical review, Bioresource Technol. 122 (2012), 149–159.

1.97 C. Wen, X. Huang, Y. Qian, Domestic wastewater treatment using an anaerobic bioreactor coupled with membrane filtration, Process Biochem. 35 (1999), 335–340.

1.98 L.B. Chu, F.L. Yang, X.W. Zhang, Anaerobic treatment of domestic wastewater in a membrane-coupled expended granular sludge bed (EGSB) reactor under moderate to low temperature, Process Biochem. 40 (2005), 1063–1070.

1.99 A.Y. Hu, D.C. Stuckey, Treatment of dilute wastewaters using a novel submerged anaerobic membrane bioreactor, J. Environ. Eng.-ASCE 132 (2006), 190–198.

1.100 S.H. Baek, K.R. Pagilla, Aerobic and anaerobic membrane bioreactors for municipal wastewater treatment, Water Environ. Res. 78 (2006), 133–140.

1.101 A. Saddoud, M. Ellouze, A. Dhouib, S. Sayadi, Anaerobic membrane bioreactor treatment of domestic wastewater in Tunisia, Desalination 207 (2007), 205–215.

1.102 J.H. Ho, S.W. Sung, Anaerobic membrane bioreactor treatment of synthetic municipal wastewater at ambient temperature, Water Environ. Res. 81 (2009), 922– 928.

1.103 J.H. Ho, S.W. Sung, Methanogenic activities in anaerobic membrane bioreactors (AnMBR) treating synthetic municipal wastewater, Bioresource Technol. 101 (2010), 2191–2196.

1.104 B. Lew, S. Tarre, M. Beliavski, C. Dosoretz, M. Green, Anaerobic membrane bioreactor (AnMBR) for domestic wastewater treatment, Desalination 243 (2009), 251–257.

1.105 D.W. Gao, T. Zhang, C.Y.Y. Tang, W.M. Wu, C.Y. Wong, Y.H. Lee, D.H. Yeh, C.S. Criddle, Membrane fouling in an anaerobic membrane bioreactor: differences in relative abundance of bacterial species in the membrane foulant layer and in suspension, J. Membr. Sci. 364 (2010), 331–338.

1.106 M.L. Salazar-Pelaez, J.M. Morgan-Sagastume, A. Noyola, Influence of hydraulic retention time on fouling in a UASB coupled with an external ultrafiltration membrane treating synthetic municipal wastewater, Desalination 277 (2011), 164–170.

1.107 A.L. Smith, H. Dorer, N.G. Love, S.J. Skerlos, L. Raskin, Role of membrane biofilm in psychrophilic anaerobic membrane bioreactor for domestic wastewater treatment, In: 84th Annual Water Environment Federation Technical Exhibition and Conference (WEFTEC), Los Angeles, California, October 15–19, 2011.

1.108 T. Jiang, M.D. Kennedy, B.F. Guinzbourg, P.A.Vanrolleghem, J.C. Schippers, Optimising the operation of a MBR pilot plant by quantitative analysis of the membrane fouling mechanism, Water Sci. Technol. 51 (2005), 19–25.

1.109 P. Bacchin, P. Aimar, R.W. Field, Critical and sustainable fluxes: Theory, experiments and applications, J. Membr. Sci. 281(2006), 42–69.

1.110 G. Guglielmi, D. Chiarani, S.J. Judd, G. Andreottola, Flux criticality and sustainability in a hollow fibre submerged membrane bioreactor for municipal wastewater treatment, J. Membr. Sci. 289 (2007), 241–248.

1.111 R.W. Field, D. Wu, J.A. Howell, B.B. Gupta, Critical flux concept for microfiltration fouling, J. Membr. Sci. 100 (1995), 259–272.

1.112 P. Bachin, P. Aimar, V. Sanchez, Model for colloidal fouling of membranes, AIChE J. 41 (1995), 368–377.

1.113 J.A. Howell, Sub–critical flux operation of microfiltration, J. Membr. Sci. 107 (1995), 165–171.

1.114 W. Naessens, T. Maere, I. Nopens, Critical review of membrane bioreactor models–Part 1: Biokinetic and filtration models, Bioresource Technol. 122 (2012), 95–106.

1.115 M. Henze, W. Gujer, T. Mino, M.C.M. van Loosdrecht, Activated Sludge Models: ASM1, ASM2, ASM2d and ASM3, Scientific and Technical Report no. 9, IWA Publishing, London, UK, 2000.

1.116 D.J. Batstone, J. Keller, I. Angelidaki, S.V. Kalyuzhnyi, S.G. Pavlostathis, A. Rozzi, W.T. Sanders, H. Siegrist, V.A. Vavilin, The IWA anaerobic digestion model No. 1 (ADM1), Water Sci. Technol. 45 (2002), 65–73.

1.117 M. de Gracia, P. Grau, E. Huete, J. Gómez, J.L. García-Heras, E. Ayesa, New generic mathematical model for WWTP sludge digesters operating under aerobic and anaerobic conditions: Model building and experimental verification. Water Res. 43 (2009), 4626–4642.

1.118 R. Barat, J. Serralta, M.V. Ruano, E. Jiménez, J. Ribes, A. Seco, J. Ferrer, Biological Nutrient Removal Model Nº 2 (BNRM2): A general model for Wastewater Treatment Plants, Water Sci. Technol. 67 (2013), 1481–1489.

1.119 W. Naessens, T. Maere, N. Ratkovich, S. Vedantam, I. Nopens, Critical review of membrane bioreactor models – Part 2: Hydrodynamic and integrated models, Bioresource Technol. 122 (2012) 107–118.

1.120 M.F.R. Zuthi, H.H. Ngo, W.S. Guo, Modelling bioprocesses and membrane fouling in membrane bioreactor (MBR): A review towards finding an integrated model framework, Bioresource Technol. 122 (2012) 119–129.

1.121 D. Dochain, P.A. Vanrolleghem, Dynamical modelling and estimation in wastewater treatment processes, IWA Publishing, London, UK, 2001.

1.122 A. Broekmann, J. Busch, T. Wintgens, W. Marquardt, Modeling of pore blocking and cake layer formation in membrane filtration for wastewater treatment, Desalination 189 (2006), 97–109.

1.123 J. Busch, A. Cruse, W. Marquardt, Modeling submerged hollow–fiber membrane filtration for wastewater treatment, J. Membr. Sci. 288 (2007), 94–111.

1.124 A. Drews, H. Arellanogarcia, J. Schoneberger, J. Schaller, G. Wozny, M. Kraume, Model–based recognition of fouling mechanisms in membrane bioreactors, Desalination 236 (2009), 224–233.

1.125 S.J. Khan, C. Visvanathan, V. Jegatheesan, Prediction of membrane fouling in MBR systems using empirically estimated specific cake resistance, Bioresource Technol. 100 (2009), 6133–6136.

1.126 X.y. Li, X.m. Wang, Modelling of membrane fouling in a submerged membrane bioreactor, J. Membr. Sci. 278 (2006), 151–161.

1.127 E. Giraldo, M. LeChevallier, Dynamic mathematical modeling of membrane fouling in submerged membrane bioreactors, Proceedings of Water Environment Foundation, WEFTEC (2006), 4895–4913.

1.128 T. Ludwig, D. Gaida, C. Keysers, J. Pinnekamp, M. Bongards, P. Kern, C. Wolf, A.L. Sousa Brito, An advanced simulation model for membrane bioreactors: Development, Calibration and Validation, In: 6th IWA Specialist Conference on Membrane Technology for Water & Wastewater Treatment, 2011.

1.129 M. Sarioglu, G. Insel, D. Orhon, Dynamic in–series resistance modeling and analysis of a submerged membrane bioreactor using a novel filtration mode, Desalination 285 (2012), 285–294.

1.130 J. Ferrer, A. Seco, J. Serralta, J. Ribes, J. Manga, E. Asensi, J.J. Morenilla, F. Llavador, DESASS: a software tool for designing, simulating and optimising WWTPs, Environ. Modell. Softw. 23(2008), 19–26.

1.131 M.V. Ruano García, Desarrollo de un sistema de control basado en la lógica difusa para la optimización del funcionamiento de una EDAR con eliminación biológica de nutrientes, Tesis doctoral, Departamento de Ingeniería Química, Universidad de Valencia, 2009.

1.132 G. Towler, R.K. Sinnott, Chemical Engineering Design: Principles, Practice and Economics of Plant and Process Design, second ed., Elsevier Science, ISBN: 978–0–08–096659–5, 2012.

1.133 W. Pedrycz, Fuzzy Control and Fuzzy Systems, 2nd extended edition, John Wiley & Sons Inc, New York, 1993.

1.134 H.B. Verbruggen, R. Babuška, Fuzzy logic control: advances in applications, World Scientific, 1999.

1.135 E.H. Mamdani, Application of fuzzy algorithm for control of simple dynamic plant, IEEE Proceedings 121 (1974), 1585–1588.

1.136 P.M. Larsen, Industrial application of fuzzy logic control. International Journal of Man–Machine Studies, 12 (1980), 3–10.

1.137 J.M. Mendel, Fuzzy logic systems for engineering: A tutorial, IEEE Proceedings 83 (1995), 345–376.

1.138 B. Verrecht, T. Maere, I. Nopens, C. Brepols, S. Judd, The cost of a large-scale hollow fibre MBR, Water Res. 44 (2010), 5274–5283.

1.139 G. Ferrero, I. Rodriguez–Roda, J. Comas, Automatic control systems for submerged membrane bioreactors: A state–of–the–art review, Water Res. 46 (2012), 3421–3433.

1.140 P. Cote, A. Janson, H. Rabie, M. Singh, Cyclic aeration system for submerged membrane modules, International patent WO 00/21890, 2000.

1.141 B. Mansell, J. Peterson, C.C. Tang, R. Horvath, J. Stahl, Comparison of biofouling control in a membrane bioreactor via two coarse bubble aeration cycles, Proceedings of WEFTEC 2006, 1904–1916.

1.142 N. Adams, J. Cumin, M. Marschall, T.P. Turák, K. Vizvardi, H. Koops, Reducing the Cost of MBR: The Continuous Optimization of GE's ZeeWeed Technology, 6th IWA specialist conference on membrane technology for water and wastewater treatment, Aachen, Germany, 2011.

1.143 M. Dimitriou, J. Krall, D. Rice, V. Yogendran, R. Byrne, K. George, J. Koch, Energy efficient biological treatment system with filtration membrane, U.S. Patent US/2006/0213831, 2006.

1.144 F. Zha, W. Liu, Dynamic control of membrane bioreactor system, International patent WO 2007/038843, 2007.

1.145 F. Zha, R.W. Phelps, A. Sneddon, T. Nguyen, Improved operating strategies in filtration processes, International patent WO 2007/079540, 2007.

1.146 D. Livingston, Efficient MBR operation in wastewater treatment, International Patent WO/2007/053528, 2007.

1.147 O. Lorain, P. Dufaye, W. Bosq, J. Espenan, A new membrane bioreactor generation for wastewater treatment application: strategy of membrane aeration management by sequencing aeration cycles, Desalination 250 (2010), 639–643.

1.148 D. Jeison, J.B. van Lier, On–line cake–layer management by trans–membrane pressure steady state assessment in anaerobic membrane bioreactors for wastewater treatment, BioChem. Eng. J. 29 (2006), 204–209.

1.149 P.J. Smith, S. Vigneswaran, H.H. Ngo, R. Ben–Aim, H. Nguyen, A new approach to backwash initiation in membrane systems, J. Membr. Sci. 278 (2006), 381–389.

1.150 P.J. Smith, S. Vigneswaran, H.H. Ngo, H. Nguyen, R. Ben–Aim, Application of an automation system and a supervisory control and data acquisition (SCADA), system for the optimal operation of a membrane adsorption hybrid system, Water Sci. Technol. 53 (2006), 179–184.

1.151 S. Hong, H. Zhao, R. Dimassimo, Method for controlling fouling of a membrane filter, International patent WO 2008/137908, 2008.

1.152 B. Ginzburg, F. Yacoub, P. Cote, A. Janson, Process control for an immersed membrane system, International Patent WO/ 2007/006153, 2007.

1.153 B. Ginzburg, J. Peeters, J. Pawloski, On–line fouling control for energy reduction in membrane bioreactors, In: Proceedings of: Membrane Technology, WEF, Atlanta, GA, 2008.

1.154 J. Busch, A. Cruse, W. Marquardt, Run–to–run control of membrane filtration processes, American Institute of Chemical Engineers Journal 53 (2007), 2316–2328.

1.155 J. Busch, W. Marquardt, Model–based control of MF/UF filtration processes: pilot plant implementation and results, Water Sci. Technol. 59 (2009), 1713–1720.

1.156 R. Soleimani, N.A. Shoushtari, B. Mirza, A. Salahi, Experimental investigation, modeling and optimization of membrane separation using artificial neural network and multi–objective optimization using genetic algorithm, Chem. Eng. Res. Des. 91 (2013), 883–903.

1.157 A. Drews, H. Arellano–Garcia, J. Scho¨neberger, J. Schaller, G. Wozny, M. Kraume, Model–based recognition of fouling mechanisms in membrane bioreactors, Desalination 236 (2009), 224–233.

1.158 A. Drews, Membrane fouling in membrane bioreactors–characterisation, contradictions, cause and cures, J. Membr. Sci. 363 (2010), 1–28.

1.159 I. Rodriguez–Roda, J. Comas, M. Poch, G. Ferrero, H. Monclús, J. Sipma, P. Clara, J. Canals, S. Rovira, Procedimiento automatizado de control en tiempo real de un biorreactor de membranas y sistema de control correspondiente, Spanish patent ES 2333837, 2010.

1.160 G. Ferrero, H. Monclús, G. Buttiglieri, J. Comas, I. Rodriguez–Roda, Automatic control system for energy optimization in membrane bioreactors, Desalination 268 (2011), 276–280.

1.161 G. Ferrero, H. Monclús, G. Buttiglieri, S. Gabarron, J. Comas, I. Rodriguez–Roda, Development of a control algorithm for air scour reduction in membrane bioreactors for wastewater treatment, J. Chem. Technol. Biot. 86 (2011), 784–789.

1.162 G. Ferrero, H. Monclús, J.M. Garrido, L. Sancho, J. Comas, I. Rodriguez–Roda, A knowledge–based control system for air scour optimization in membrane bioreactors. Water Sci. Technol. 63 (2011), 2025–2031.

1.163 A. Vargas, I. Moreno–Andrade, G. Buitrón, Controlled backwashing in a membrane sequencing batch reactor used for toxic wastewater treatment, J. Membr. Sci. 320 (2008), 185–190.

1.164 E. Brauns, E. Van Hoof, Supervisory control system and method for membrane cleaning, International patent WO 2008/132186, 2008.

1.165 C. Huyskens, E. Brauns, E. Van Hoof, H. De Wever, A new method for the evaluation of the reversible and irreversible fouling propensity of MBR mixed liquor, J. Membr. Sci. 323 (2008), 185–192.

1.166 C. Huyskens, E. Brauns, E. Van Hoof, E. Diels, H. De Wever, Validation of a supervisory control system for energy saving in membrane bioreactors, Water Res. 45 (2011), 1443–1453.

1.167 H–D. Park, Y.H. Lee, H–B. Kim, J. Moon, C–H. Ahn, K–T. Kim, M–S. Kang, Reduction of membrane fouling by simultaneous upward and downward air sparging in a pilot–scale submerged membrane bioreactor treating municipal wastewater, Desalination 251 (2010), 75–82.

1.168 S.R. Weijers, P.A. Vanrolleghem, A procedure for selecting best identifiable parameters in calibrating activated sludge model no. 1 to full–scale plant data, Water Sci. Technol. 36 (1997), 69–79.

1.169 R. Brun, M. Kühni, H. Siegrist, W. Gujer, P. Reichert, Practical identifiability of ASM2d parameters–systematic selection and tuning of parameter subsets, Water Res. 36 (2002), 4113–4127.

1.170 G. Sin, D. De Pauw, S. Weijers., P.A. Vanrolleghem, Developing a framework for continuous use of models in daily management and operation of WWTPs: A life cycle approach. 10th IWA Conference on Design, Operation and Economics of Large Wastewater Treatment Plants September 7–13, 2007, Vienna, Austria.

1.171 M.V. Ruano, J. Ribes, G. Sin, A. Seco, J. Ferrer, A systematic approach for fine–tuning of fuzzy controllers applied to WWTPs, Environ. Modell. Softw. 25 (2010), 670–676.

1.172 M.V. Ruano, J. Ribes, D.J.W. De Pauw, G. Sin, Parameter subset selection for the dynamic calibration of Activated Sludge Models (ASMs): experience versus systems analysis, Water Sci. Technol. 56 (2007), 107–115.

1.173 S.R. Weijers, P.A. Vanrolleghem, A procedure for selecting best identifiable parameters in calibrating activated sludge model no. 1 to full-scale plant data. Water Sci. Technol. 36 (1997), 69–79.

1.174 R. Brun, M. Kühni, H. Siegrist, W. Gujer, P. Reichert, Practical identifiability of ASM2d parameters-systematic selection and tuning of parameter subsets. Water Res. 36 (2002), 4113–4127.

1.175 A. Saltelli, K. Chan, E.M. Scott, Sensitivity Analysis. John Wiley & Sons, New York, 2000.

1.176 R.J. Cukier, H.B. Levine, K.E. Schuler, Nonlinear sensitivity analysis of multiparameter model systems, J. Comput. Phys. 26 (1978), 1–42.

1.177 A. Saltelli, S. Tarantola, K. Chan, A quantitative, model independent method for global sensitivity analysis of model output, Technometrics 41 (1999), 39–56.

1.178 M.D. Morris. Factorial sampling plans for preliminary computational experiments, Technometrics 33(1991), 161–174.

1.179 A. Saltelli, M. Ratto, S. Tarantola, F. Campologno. Sensitivity Analysis for Chemical Models, Chemical Reviews 108 (2005), 2811–2827.

1.180 J. Zádor, I.G. Zsély, T. Turányi, Local and global analysis of complex Chemicals kinetic Systems, Reliability Engineering and System Safety 91 (2006), 1232–1240.

1.181 D. De Pauw, K. Steppe, B. De Baets, Unravelling the output uncertainty of a tree water flow and storage model using several global sensitivity analysis methods, Biosys. Eng. 101(2008), 87–99.

1.182 M.V. Ruano, J. Ribes, J. Ferrer, G. Sin, Application of the Morris method for screening the influential parameters of fuzzy controllers applied to WWTPs. Water Sci. Technol. 63 (2011), 2199–2206.

1.183 M.V. Ruano, J. Ribes, A. Seco, J. Ferrer, An improved sampling strategy based on trajectory design for the application of Morris method to systems with many input factors, Environ. Modell. Softw. 37 (2012), 103–109.

1.184 R.A. Cropp, R.D. Braddock, The New Morris Method: an efficient second-order screening method. Reliability Engineering and System Safety 78 (2002), 77–83.

1.185 A. Saltelli, S. Tarantola, F. Campolongo, M. Ratto, Sensitivity analysis in practice: a guide to assessing scientific models, Chicester: Wiley 2004.

1.186 F. Campolongo, J. Cariboni, A. Saletlli, An effective screening design for sensitivity analysis of large models, Environ. Modell. Softw. 22 (2007), 1509–1518.

CHAPTER 2:

Instrumentation, control, and automation (ICA) for submerged anaerobic membrane bioreactors (SAnMBRs)

Abstract

A submerged anaerobic MBR (SAnMBR) demonstration plant with two commercial hollow-fibre ultrafiltration systems (PURON®, Koch Membrane Systems, PUR-PSH31) was designed and operated for municipal wastewater treatment. A robust instrumentation, control, and automation (ICA) system was designed and implemented for proper process performance. The following operating variables were managed for controlling the biological process: treatment flow-rate, sludge wasting volume, temperature, and gas sparging intensity in the anaerobic reactor. The main variables controlled for the physical separation process were: permeate flow-rate, transmembrane pressure (TMP), sludge flow-rate recycled through the membrane tanks, and gas sparging intensity in the membrane tanks. Several single-input-single-output (SISO) feedback control loops based on conventional on-off and PID algorithms were implemented to control the above-mentioned operating variables. The proposed ICA for the SAnMBR system enables the optimisation of this new technology to be achieved with a high level of process robustness towards perturbations.

Keywords

Demonstration plant; industrial membranes; instrumentation, control and automation (ICA); municipal wastewater treatment; submerged anaerobic MBR.

Highlights

An SAnMBR demonstration plant was designed and operated with domestic wastewater.
A novel and robust ICA system was developed as part of the plant.
The main disturbances that take place in full-scale plants were reproduced.
Key terms related to the use of instrumentation are addressed.
The proposed ICA provides flexibility and process stability towards perturbations.

A. Robles, F. Durán, M.V. Ruano, J. Ribes, A. Rosado, A. Seco, J. Ferrer
Instrumentation, control, and automation (ICA) for submerged anaerobic membrane bioreactors (SAnMBRs)
Submitted to Control Eng. Pract.

2.1 Introduction

Anaerobic treatments of wastewater have the following main advantages when compared to aerobic treatments (See, for instance, Henze *et al*. [2.1]): lower sludge production due to the low anaerobic biomass yield; lower energy consumption because no aeration is required; and the production of biogas that can be used as energy. However, due to the low-growth rate of anaerobic bacteria, considerable biomass concentrations and/or high temperatures are required to achieve suitable organic matter removal rates.

Membrane technology applied to wastewater treatment using membrane bioreactors (MBRs) is a promising alternative for obtaining high biomass and COD concentrations by decoupling both hydraulic retention time (HRT) and solids retention time (SRT) [2.2]. The complete retention of the microorganisms inside the MBR system enables high SRT to be obtained with reduced working volumes – and so submerged anaerobic MBR (SAnMBR) is a promising technology for wastewater treatment [2.3].

Several issues have been recognised elsewhere as potential drawbacks that must be solved before successfully implementing SAnMBR technology for urban wastewater treatment. These drawbacks include: greater complexity than aerobic processes since many different microorganisms are involved with major syntrophic relationships between them; higher sensitivity to process overloads and other disturbances such as pH or organic acid inhibitions; and possible membrane fouling. This final point is a key issue regarding MBR technology since it decreases membrane permeability and increases operating and maintenance costs [2.4]. Therefore, an SAnMBR system could require more sophisticated monitoring equipment, process control systems, and operating conditions than aerobic MBR systems, or other conventional anaerobic systems – such as up-flow anaerobic sludge blanket (UASB); expanded granular sludge blanket (EGSB); or anaerobic filters (AF). Therefore, due to the complexity of anaerobic processes in general, and of SAnMBR systems in particular, the development of an instrumentation, control, and automation (ICA) system is required to successfully start-up, stabilise, and optimise this new technology.

It is well-known that an ICA system is essential in WWTPs to facilitate system management and save manpower and energy [2.5; 2.6; 2.7; 2.8; 2.9]. Robust ICA systems are needed to optimise SAnMBR performance in terms of energy consumption/production (*i.e.*, operating cost vs. methanation) and COD degradation. The required control systems should take into account the main parameters of the process, such as SRT, HRT, transmembrane pressure (TMP), and recycled biogas flow-rate.

To investigate the possible full-scale implementation of SAnMBR technology for treating municipal wastewater, an SAnMBR demonstration plant was designed and operated. A novel and robust ICA system was developed as part of the plant. The SAnMBR plant is being operated with real wastewater from the pre-treatment of the Carraixet WWTP (Valencia, Spain). Thus, the main disturbances that take place in full-scale plants are reproduced. The objective of this paper is to show how the developed ICA system has allowed us to optimise the overall process performance. This implementation will facilitate its subsequent full-scale implementation. Key terms related to the use of instrumentation will be addressed. The proposed ICA system provides valuable insights into the engineering problems and so it will help engineers to handle day-to-day tasks in full-scale plants of this type, *e.g.* process performance and confirming the robustness of plant design.

2.2 Materials

2.2.1 Demonstration plant description

The SAnMBR demonstration plant used in this study was designed to treat a maximum flow of 1200 L h^{-1}, assuming a net flux of 20 L m^{-2} h^{-1} in two membrane tanks, which lead to a minimum HRT of two hours. The plant consists of an anaerobic reactor with a total volume of 1.3 m^3 (0.4 m^3 head-space volume) connected to two membrane tanks each with a total volume of 0.8 m^3 (0.2 m^3 head-space volume). Each membrane tank includes one industrial hollow-fibre ultrafiltration membrane unit (PURON® Koch Membrane Systems (PUR-PSH31), 0.05 μm pores). Each module has 9 HF bundles, 1.8 m long, giving a total membrane surface of 30 m^2 (for further details about the membrane unit visit http://www.kochmembrane.com). A rotofilter with a 0.5 mm screen size was installed as a pre-treatment system. One equalisation tank (0.3 m^3) and one clean-in-place (CIP) tank (0.2 m^3) are also included as main elements of the plant. To control the temperature when necessary, the anaerobic reactor is jacketed and connected to a water heating/cooling system.

Figure 2.1 shows the flow diagram of the SAnMBR demonstration plant. The plant is fed with the effluent from the Carraixet WWTP pre-treatment (screening, degritter, and grease removal). After further pre-treatment in the rotofilter (RF) and homogenisation in the equalisation tank (ET), the wastewater is pumped to the anaerobic reactor (AnR). To improve the stirring conditions of the anaerobic reactor and to favour stripping the produced gases from the liquid phase, a fraction of the produced biogas is recycled to this reactor. The sludge is continuously recycled through the external membrane tanks (MT) where the effluent is obtained by vacuum filtration. Another fraction of the

produced biogas is also recycled to the membrane tanks from the bottom of each fibre bundle to minimise cake layer formation. With the aim of recovering the biogas bubbles extracted with the membrane effluent, a degasification vessel (DV) was installed between the MT and the vacuum pump. This DV consists of a widening pipe-section that is conic-shaped and so favours the accumulation of biogas at the top of this element. The obtained permeate is stored in the clean-in-place (CIP) tank. The two parallel membrane tanks make plant operating very flexible because it can work with one membrane tank or the other or both. Moreover, each tank enables the resulting permeate to be constantly recycled back into the anaerobic reactor, enabling different transmembrane fluxes to be tested without affecting HRT. To control the SRT in the system, a fraction of the sludge is intermittently extracted from the anaerobic reactor throughout the day.

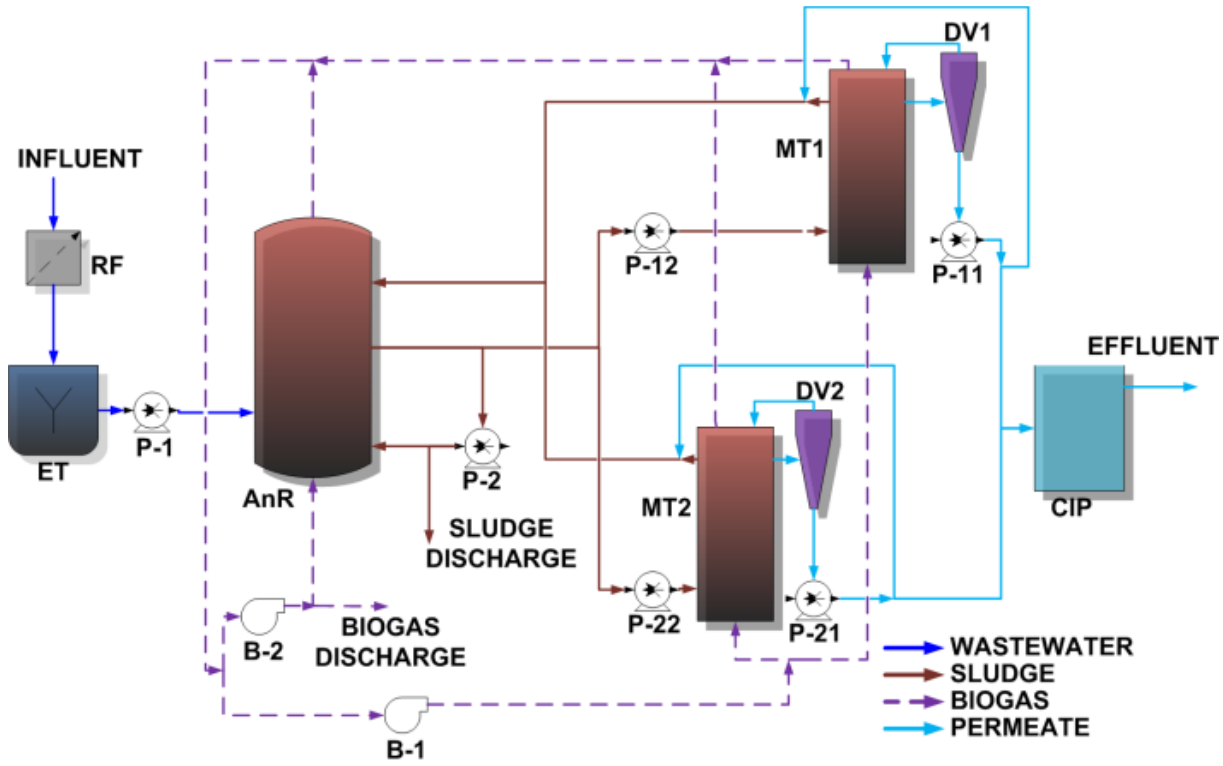

Figure 2.1 Flow diagram of the SAnMBR demonstration plant. Nomenclature: **RF**: rotofilter; **ET**: equalization tank; **AnR**: anaerobic reactor; **MT**: membrane tanks; **DV**: degasification vessel; **CIP**: clean-in-place; **P**: pump; and **B**: blower.

2.2.2 Membrane performance

The membrane operation was automated to enable the study of various relaxation and back-flush frequencies and durations. Membranes are normally operated according to a specific schedule

involving a combination of different individual stages taken from a basic filtration-relaxation (F-R) cycle (see Figure 2.2). In addition to the classical membrane operating stages (filtration, relaxation, and back-flush) the two stages shown below were also considered in the membrane operation:

Degasification: a typical disadvantage of dead-end, hollow-fibre membranes is the accumulation of biogas at the top of the fibres which reduces the effective filtration area. The degasification stage consists of a period of high flow-rate filtration that is carried out to enhance the filtration process efficiency by removing the accumulated biogas.

Ventilation: This stage is similar to back-flush and permeate is pumped to the membrane tank through the degasification vessel instead of through the membrane. The aim of the ventilation stage is to recover the accumulated biogas in the degasification vessel.

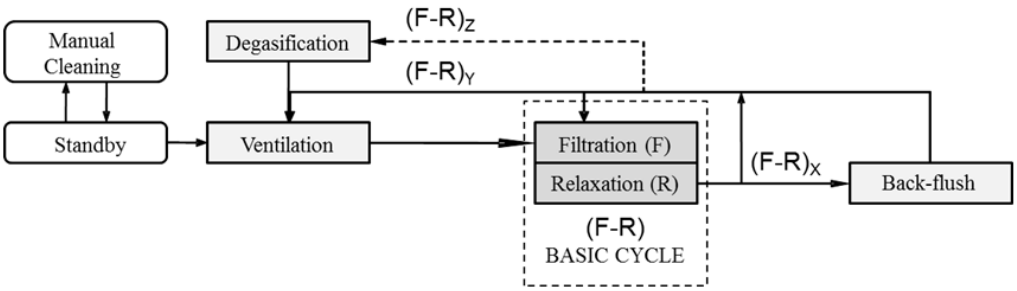

Figure 2.2 Sequence of the individual stages in a normal membrane operating mode

The membrane performance is then established by a correct selection of the membrane operating mode. Figure 2.2 shows the possible membrane operating modes. For instance, the operating mode defined by X=2; Y=10; Z=50 implies that a back-flush is carried out every two F-R cycles; a ventilation is carried out every ten F-R cycles; and a degasification followed by a ventilation is carried out every fifty F-R cycles.

Besides the membrane operating mode, the separation process is also controlled by transmembrane flux (J), TMP, sludge flow-rate recycled through the membrane tanks, and recycled biogas flow-rate.

For further details about this SAnMBR demonstration plant see Giménez *et al*. [2.10].

2.3 Proposed ICA for SAnMBR systems

The main goal of the proposed ICA is not only to facilitate system management and save manpower and energy, but also to allow achieving suitable process performances in terms of methanation and COD degradation. To this aim, the proposed ICA has been developed taking into account the main parameters that affect the performance of an SAnMBR system. These key parameters were determined by using the knowledge gained with the operation of the demonstration plant. The following operating variables were manipulated for controlling the biological process: treatment flow-rate (controlling the HRT), sludge wasting volume (controlling the SRT), temperature, and gas sparging intensity in the anaerobic reactor. The main variables controlled for the physical separation process were: permeate flow-rate, TMP, sludge flow-rate recycled through the membrane tanks, and gas sparging intensity in the membrane tanks.

2.3.1 Demonstration plant instrumentation

Numerous on-line sensors and automatic devices were installed to automate and control the plant operation and provide on-line information about the state of the process. The main characteristics of the installed equipment are as follows: on-line availability of the provided signals; industrial readiness; generally low-cost (with the only exception of the gas composition analyser); resistance to corrosion; long lifespan; low and easy maintenance; and ATEX (explosive atmospheres) protection, which is essential in closed-air reactors containing biogas. In addition, non-corrosive materials are required in systems of this type because of the possible presence of H_2S.

The group of on-line sensors consists of the following: three pH-temperature transmitters (Endress+Hauser model Liquiline M pH-ORP CM42) that are located in the anaerobic reactor and the two membrane tanks (pHT-1, pHT-11 and pHT-21, respectively); one oxidation-reduction potential (ORP) sensor (Endress+Hauser model Liquiline M pH-ORP CM42; ORP-1) that is located in the anaerobic reactor; two solids concentration transmitters that are located in the equalisation tank and anaerobic reactor (Hach Lange model TSS EX1 sc; SIT-0 and SIT-1, respectively); six liquid-flow-rate transmitters (Endress+Hauser model Proline Promag 50; FIT-1, FIT-2, FIT-12, FIT-22, FIT-11 and FIT-21), one for each of the pumps installed (P-1, P-2, P-12, P-22, P-11 and P-21, respectively); two gas-flow-rate transmitters (Iberfluid model VORTEX 84F-U3QS1SSVNE-N; GFIT-1 and GFIT-2), one for each of the installed blowers (B-1 and B-2, respectively); one gas composition analyser (Emerson model X-Stream XEGP) that samples from the gas distribution pipe-system and measures

the CH_4, CO_2, H_2, and H_2S fractions of the produced biogas; one gas meter to quantify the biogas production; five level transmitters (Endress+Hauser model Waterpilot FMX167; LIT-0, LIT-1, LIT-11, LIT-21 and LIT-2) with one for each tank (ET, AnR, MT-1, MT-2 and CIP, respectively); two liquid pressure transmitters (Endress+Hauser model Cerabar M PMC41; PIT-11 and PIT-21) to determine the TMP of each membrane tank (MT-1 and MT-2, respectively); and three gas pressure transmitters (Endress+Hauser model Cerabar M PMC45; PIT-0, PIT-1 and PIT-2) with one for the reactor head-space and one for each blower, respectively.

The group of actuators installed in the SAnMBR demonstration plant consists of the following: eight frequency converters that control the rotating speed of six pumps and two blowers; one regulatory valve to control the biogas discharge according to the pressure in the system; two on-off control valves enabling the continuous recycling of the obtained permeate in the system; and six on-off control valves aimed to control the sludge wastage and the different membrane operating stages (filtration, back-flush, standby, etc.). By including one frequency converter associated with each pump and blower installed, the plant has been designed and automated with a high level of operational flexibility.

2.3.1.1 pH sensors

The use of pH sensors is required since it is necessary to operate the plant within a pH range that is: (1) suitable for anaerobic biomass growth (commonly between 6 and 8 units of pH) since anaerobic organisms are highly dependent on pH (see *e.g.* O'Flaherty *et al*. [2.11]; Hwang *et al*. [2.12]); and (2) able to minimise chemical precipitate formation [2.13; 2.14].

2.3.1.2 ORP sensors

ORP sensors are required since a decrease in the oxidation-reduction potential indicates a possible presence of oxygen in the system. In this respect, it is recommended to maintain an ORP potential below -300 mV (approximately and depending on the wastewater characteristics) in order not to affect anaerobic Methanogenic Archaea activity.

2.3.1.3 Total solids indicator transmitters

Influent total suspended solids (TSS) concentration affects the type and design of the reactor, as well as other operating parameters (depending on the dynamics of the influent load) that must be controlled

– such as the required SRT since the solids hydrolysis is normally the rate-limiting step [2.15]. SRT is a key factor controlling the methanisation process especially in low loaded wastewater treatments. Moreover, it is possible to correlate both influent TSS and COD values, which enables a reduction in the analytical monitoring requirements. In this case, the experimentally determined influent COD concentration (determined according to method 2540 E in Standard Methods [2.16]) showed a linear correlation with the on-line monitored influent TSS (measured by the influent TSS sensor, SIT-0) with a correlation coefficient (R^2) of 0.988 (see Eq. 2.1). It is therefore possible to predict the organic load rate (OLR) using the on-line data from the influent TSS sensor and the flow indicator transmitter associated with the influent pump (P-1). Moreover, the MLTS sensor (SIT-1) installed in the anaerobic reactor facilitates a rigorous SRT control. The sludge wasting volume required to maintain an established SRT can be continuously recalculated using this MLTS sensor.

$$COD_{ESTIMATED} = 1.342 \cdot TSS + 151.2 \ (R^2 = 0.988) \qquad \textbf{Eq. 2.1}$$

2.3.1.4 Biogas meter

On-line monitoring the amount and composition of the produced biogas provides useful information about the biological process performance and facilitates the identification of possible operating problems.

2.3.1.5 Liquid flow indicator transmitters

On-line flow indicator transmitters are needed to establish and/or control different operating variables, such as HRT, SRT, or OLR.

2.3.1.6 TMP indicator transmitters

Pressure indicator transmitters are one of the key sensors in MBR technology since they are used to monitor and control TMP. Depending on the TMP performance, different control strategies [2.17; 2.18; 2.19] can be developed aimed to optimise the filtration task by minimising membrane fouling and operating costs.

2.3.1.7 Gas flow indicator transmitters

Gas flow indicator transmitters enable the gas sparging intensity that keeps the mixed liquor suspended to be maintained and so avoids the formation of death zones. Moreover, gas flow measurement is essential in the membrane tanks to control the gas sparging intensity for membrane scouring. Monitoring this parameter enables quantifying both the specific gas demand with respect to membrane area (SGD_m) and the specific gas demand with respect to permeate volume (SGD_P), both of which are key factors that must be determined to assess the feasibility of SAnMBR technology for treating urban wastewater.

The normalised volumetric gas flow-rate depends on gas composition. The measured volumetric biogas flow (firstly calibrated by measuring air using the off-line rotameter) can be corrected on-line by taking into account the biogas composition provided by the gas composition analyser. The proposed correction is shown in Eq. 2.2.

$$G_{CORRECTED} = G_{MEASURED} \cdot frho \qquad \textbf{Eq. 2.2}$$

where:

- $frho = \sqrt{\dfrac{rho_{AIR}}{\left(rho_{CH4} \cdot \%CH_4 + rho_{CO2} \cdot \%CO_2 + rho_{H2} \cdot \%H_2 + rho_{H2S} \cdot \%H_2S + rho_{N2} \cdot (100 - \%CH_4 - \%CO_2 - \%H_2 - \%H_2S)\right)/100}}$
- rho_{AIR}: volumetric weight of air (1.2930 kg m^{-3})
- rho_{CH4} volumetric weight of CH_4 (0.7168 kg m^{-3})
- rho_{CO2}: volumetric weight of CO_2 (1.9768 kg m^{-3})
- rho_{H2}: volumetric weight of H_2 (0.0449 kg m^{-3})
- rho_{H2S}: volumetric weight of H_2S (1.5195 kg m^{-3})
- rho_{N2}: volumetric weight of N_2 (1.2505 kg m^{-3})

2.3.1.8 Gas pressure indicator transmitters

Gas pressure indicator transmitters are required to control the pressure in the anaerobic reactor head-space. High head-space gas pressures are not recommended since they mean higher partial pressures of each gas, especially of methane (CH_4), and so higher amounts of dissolved methane in the liquid phase in equilibrium with the gas phase. The methane molar fraction in pure water (no data available for wastewater) can be calculated by means of Henry's Law. According to these theoretical considerations, the higher the methane partial pressure, the greater the loss of methane in the effluent.

Further details on the procedure for determining the amount of dissolved methane in the effluent of this SAnMBR system can be found in Giménez *et al*. [2.20].

The pressure indicator transmitters located in the outlet of each blower are useful to quantify the energy consumption of the associated blower. Moreover, these pressure indicator transmitters are useful to theoretically estimate the gas flow entering the tank when a fault in the gas flow indicator transmitters associated with the blower is detected.

2.3.1.9 Level indicator transmitters

Level indicator transmitters are required to obtain a measurement of the total working volume and avoid possible problems related to overloads or low levels in the tanks that can cause various operating problems, such as overpressure or vacuum-pumping. In this respect, maximum and minimum level set-points must be established for each tank. The head-space pressure must be considered to obtain the liquid level of each tank from the level indicator transmitter.

2.3.2 Demonstration plant automation

Due to the complexity of anaerobic processes in general, and SAnMBR systems in particular, a complete network system is required to ensure a high level of system robustness towards perturbations. Therefore, a robust network system based on a high number of sensors-transmitters and actuators, a complete PLC, and an exhaustively designed SCADA was developed. This system enables a high level of process autonomy to be achieved thus minimising human supervision.

2.3.3 Demonstration plant control

Based on the instrumentation installed, the plant includes several lower layer control loops. These lower layer controllers consist of several classical PID and on-off controllers that are programmed to control the main operating variables. Moreover, the SCADA is linked to an OPC (OLE for process control) system, which enables connection to dedicated applications incorporating, for instance, upper layer controllers. These upper layer controllers usually consist of advanced supervisory controllers such as fuzzy-logic-based control systems. The implementation of supervisory controllers enables the various set-points of the before-mentioned operating variables to be automatically established according to information gathered from sensors installed in the plant.

2.3.3.1 Lower layer controllers

Table 2.1 summarises the lower layer controllers implemented in the SAnMBR demonstration plant. Figure 2.3 shows a simplified lay-out of the SAnMBR demonstration plant including the lower layer controllers and their associated instrumentation. The lower layer control group consist of classical PID and on-off controllers designed to control the following operating variables: flow-rates (influent, permeate, sludge recycling and wasting, and recycled biogas through both reactor and membrane tanks); biogas pressure in the system; blower output pressure; transmembrane pressure; reactor temperature; and mixed liquor level.

Table 2.1 Lower layer controllers implemented in the SAnMBR demonstration plant.

Control	Control algorism	Controlled variable	Manipulated variable	Indirectly manipulated variable
1a	PID	P1 flow	P1 rotating speed	---
1b	PID	AnR level	P1 rotating speed	Influent flow
2	PID	P2 flow	P2 rotating speed	---
3-1	PID	P12 flow	P12 rotating speed	---
3-2	PID	P22 flow	P22 rotating speed	---
4a-1	PID	P11 flow	P11 rotating speed	---
4b-1	PID	AnR level	P11 rotating speed	Permeate flow
4c-1	PID	MT1 TMP	P11 rotating speed	Permeate flow
4a-2	PID	P21 flow	P21 rotating speed	---
4b-2	PID	AnR level	P21 rotating speed	Permeate flow
4c-2	PID	MT2 TMP	P21 rotating speed	Permeate flow
5a	PID	B1 output pressure	B1 rotating speed	B1 gas flow
5b	PID	B1 gas flow	B1 rotating speed	B1 output pressure
6a	PID	B2 output pressure	B2 rotating speed	B2 gas flow
6b	PID	B2 gas flow	B2 rotating speed	B2 output pressure
7	PID	AnR pressure	V-2 opening	Biogas discharge
8	ON-OFF	Sludge wasting	V-1 position	---
9	ON-OFF	AnR temperature	V-3 position	Heating/cooling water flow

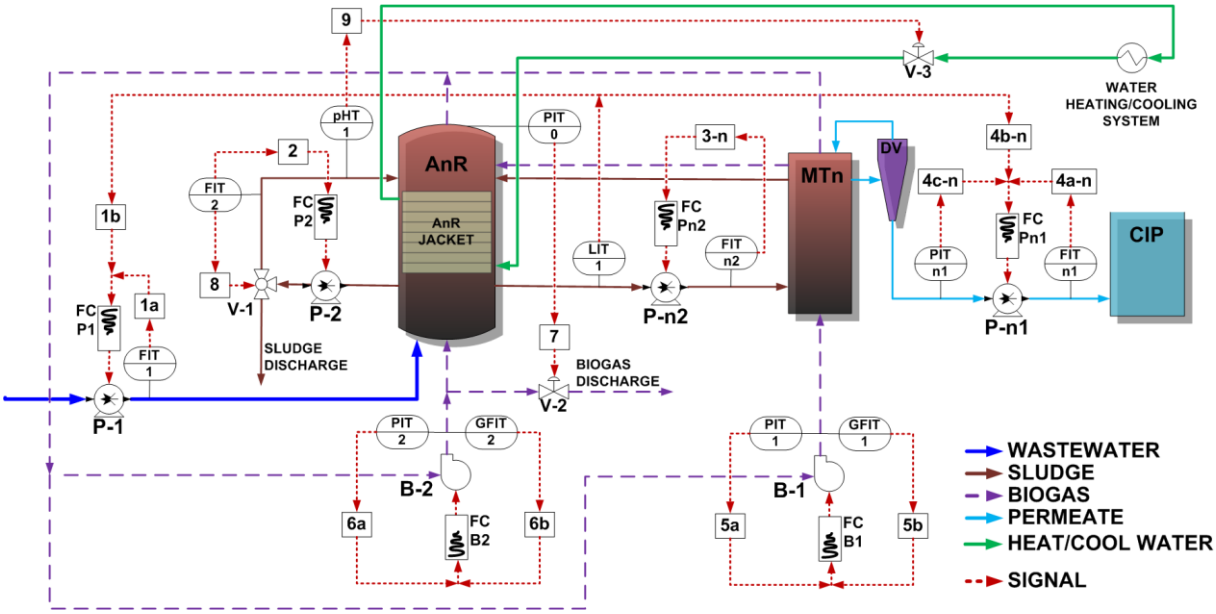

Figure 2.3 Simplified lay-out of the SAnMBR demonstration plant including the lower-layer controllers (n: number of membrane tank). Nomenclature: **AnR**: anaerobic reactor; **MT**: membrane tanks; **DV**: degasification vessel; **CIP**: clean-in-place; **P**: pump; **B**: blower; **V**: valve; **pH-T**: pH-temperature transmitters; **FIT**: liquid-flow-rate transmitters; **GFIT**: gas-flow-rate transmitters; **LIT**: level transmitters; **PIT**: pressure transmitters; and **FC**: frequency converter.

2.3.3.1.1 Wastewater, sludge, and permeate flow control

All the pumps are controlled by frequency converters controlled by traditional PID feedback controllers to maintain the respective measured variables close to their corresponding set-point values. The feed pump (P-1) can be governed by two PID control modes: (1) by maintaining an influent flow set-point using the corresponding flow indicator transmitter (FIT-1) (see Figure 2.3: controller 1a); or (2) by maintaining a level set-point in the AnR using the corresponding level indicator transmitter (LIT-1) (see Figure 2.3: controller 1b). The recirculation pump (P-2) of the reactor and the membrane tank feed pumps (P-12 and P-22) work at the correct frequency to maintain a flow set-point by using the corresponding flow indicator transmitter (FIT-2, FIT-12, and FIT-22, respectively) (see Figure 2.3: controllers 2, 3-1, and 3-2, respectively). The permeate pumps (P-11 and P-21) can be governed by three different PID control modes that manipulate the pump's rotating speed to: (1) maintain the transmembrane flow set-point by using the corresponding flow indicator transmitters (FIT-11 and FIT-21, respectively) (see Figure 2.3: controllers 4a-1 and 4a-2, respectively); (2) maintain a TMP set-point by using the corresponding pressure indicator transmitter (PIT-11 and PIT-21, respectively) (see Figure 2.3: controllers 4c-1 and 4c-2, respectively); or (3) maintain a level set-point in the AnR using the corresponding level indicator transmitter (LIT-1) (see Figure 2.3: controllers 4b-1 and 4b-2,

respectively). Both P-11 and P-21 include a control mode (3) that connects their performance to the influent flow-rate to stabilise the system by maintaining a fixed reactor level.

2.3.3.1.2 Biogas flow and pressure control

The blowers are also controlled by frequency converters that are controlled by traditional PID feedback controllers to maintain the measured variable close to the corresponding set-point value. The blowers (B-1 and B-2) have two PID control modes that manipulate the rotating speed to: (1) maintain the output pressure set-point of the blowers by using their corresponding pressure indicator transmitters (PIT-1 and PIT-2, respectively) (see Figure 2.3: controllers 5a and 6a, respectively); or (2) maintain a biogas flow set-point by using the corresponding flow indicator transmitters (GFIT-1 and GFIT-2, respectively) (see Figure 2.3: controllers 5b and 6b, respectively). Finally, the gas pressure in the anaerobic reactor (measured by PIT-0) is controlled by manipulating the pressure control valve opening (V-2) (see Figure 2.3: controller 7). For security reasons, if a minimum pressure set-point is reached inside the reactor then V-2 is automatically closed.

2.3.3.1.3 SRT control

As in conventional suspended mixed liquor processes, a fraction of the sludge is wasted over time to maintain a specific SRT. To this end, an SRT controller (see Figure 2.3: controller 8) has been developed that manipulates the position of a three-way valve (V-1) depending on the flow-rate established for the recirculation pump (P-2). This on-off controller switches V-1 from the recycling to the waste position to achieve the established sludge waste volume per day. To ensure that the sludge wastage is performed uniformly during the operating day, the inputs to the SRT controller are the total volume of mixed liquor to be wasted and the number of discharges to be conducted per day.

2.3.3.1.4 Temperature control

The anaerobic reactor is jacketed and connected to a water heating/cooling system to control the temperature when necessary. An on-off temperature controller (see Figure 2.3: controller 9) is also programmed in the PLC. The temperature sensor of the anaerobic reactor (pHT-1) is linked to a control valve (V-3) connected to the water heating/cooling system using an on-off control loop. This controller manipulates the valve opening according to an established temperature set-point and hysteresis range.

2.3.3.1.5 Safety layer control

Based on the instrumentation installed, the plant includes several safety layer control rules to guarantee the safe operation of the SAnMBR system, such as the following: safety rules for the operating level of each of the tanks in the plant, which ensure that minimum and maximum operating levels are not surpassed in order to avoid accidents, equipment deterioration, or premature deterioration of the membrane modules; safety operating rules for water and mixed liquor pumps, which prevent the pumps from operating at flow-rates lower than the minimum established avoiding possible operating problems related to obstructions in the pipe system; or safety operating rules for TMP, which prevent minimum and maximum TMP values from being surpassed to avoid premature deterioration of the membrane modules.

2.3.3.2 Upper layer controllers

Various upper layer controllers are generally needed to optimise system performance in terms of organic matter degradation, biogas production, or energy savings related, for instance, to filtration. The following indexes can be used to evaluate the performance of a SAnMBR system: COD removal efficiency; methane yield (Y_{CH4}), which is defined as the amount of produced methane per unit of removed organic matter; and overall energy balance, which accounted for the energy consumption related to the wastewater treatment (heat and power) and the potential energy recovery from biogas.
So far, one dedicated application has been developed to control the organic loading rate (OLR) in this SAnMBR system, which is described in the following section.

2.3.3.2.1 Organic loading rate control

OLR is a key operation parameter affecting the anaerobic process performance. The OLR controller enables the organic matter entering the system to be controlled and it is aimed to optimise the biological process performance in terms of COD removal efficiency and Y_{CH4}. In addition, this controller can be applied when a regulatory tank is available and there is storage capacity for minimising variations derived from influent dynamics.

This upper layer controller consists of a fuzzy-logic-based control system that includes a single-input single-output (SISO) control structure. In this SISO control structure the control parameter is the OLR entering the system and the manipulated variable is the ratio between the duration of the filtration and the relaxation stage (manipulating the net permeate volume). The suitable performance of this

controller was assessed by determining the integral of absolute error (IAE) and the integral of absolute error multiplied per time (ITAE).

The OLR controller was developed to provide the system with a high level of operational flexibility. This upper layer control involves the following control operating modes: (1) controlled OLR mode, where the influent flow entering the SAnMBR system is modified to maintain an established OLR set-point; (2) maximum operating OLR mode, where the influent flow is only controlled when a maximum influent COD concentration is detected; and (3) uncontrolled OLR mode, where the OLR is defined by the non-controlled influent flow entering the system.

The OLR was calculated by means of the COD concentration entering the system (on-line estimated with Eq. 2.1) and the measured net permeate flow-rate. Because the influent is sulphate rich (around 100 mg S L^{-1}), the OLR considered was related to the available COD for Methanogenic *Archaea* (MA) growth: OLR_{MA}. The influent sulphate is reduced to sulphide by sulphate-reducing bacteria (SRB) using organic matter as a carbon source. Since this concentration remained more or less constant throughout the experimental period, OLR_{MA} was calculated using the available COD for MA to grow: COD_{MA}. COD_{MA} was calculated with the influent COD concentration (estimated by Eq. 2.1); while the off-line sulphate influent concentration measurement in terms of COD ($0.67 \cdot SO_4^{3-}$ in Eq. 2.3) was calculated using the stoichiometric ratio, 0.67, which represents the kg of sulphate reduced to sulphide per kg of COD degraded.

$$COD_{MA} = COD - 0.67 \cdot SO_4^{3-} \qquad \textbf{Eq. 2.3}$$

The inputs to this fuzzy-logic-based control system are obtained by means of the OLR_{MA}, which correspond to the error (Eq. 2.4) and the error difference (Eq. 2.5).

$$eOLR_{MA}(t) = OLR_{MA}(t) - OLR_{MA_{SP}} \qquad \textbf{Eq. 2.4}$$

where:

- $eOLR_{MA}(t)$: error of the OLR_{MA} at the sample time
- $OLR_{MA}(t)$: measured OLR_{MA} at the sample time
- $OLR_{MA_{SP}}$: OLR_{MA} set-point

$$\Delta eOLR_{MA}(t) = eOLR_{MA}(t) - \delta \cdot eOLR_{MA}(t - RT) \quad \textbf{Eq. 2.5}$$

where:

- $\Delta eOLR_{MA}(t)$: error difference of the OLR_{MA} at the sample time
- δ: modifying algebraic factor (Eq. 2.6)
- $eOLR_{MA}(t - RT)$: error of the OLR_{MA} at the previous sample time
- *RT* is the response time of the controller, *i.e.* the time interval between two control actions

The OLR_{MA} error difference variable will be negative or positive if the OLR_{MA} tends to the set-point value or not. This OLR_{MA} error difference variable includes a modifying algebraic factor that is defined in Eq. 2.6.

$$\delta = \frac{eOLR_{MA}(t) \cdot eOLR_{MA}(t - RT)}{\left| eOLR_{MA}(t) \cdot eOLR_{MA}(t - RT) \right|} \quad \textbf{Eq. 2.6}$$

This factor has a negative sign when both $eOLR_{MA}(t)$ and $eOLR_{MA}(t - RT)$ have opposite signs. The error difference will be positive when both errors have opposite signs, taking into account that the OLR_{MA} tendency is moving away from the set-point value.

The fuzzy-logic-based controller determines the variation in the set point of the F/R ratio (*i.e.* $\Delta F/R_{SP}$) on the basis of two inputs obtained from the organic loading rate, *i.e.* error (Eq. 2.4) and error difference (Eq. 2.5). The structure of this controller is, therefore, a fuzzy equivalent of the classical PD controller. The output control action is defined by Eq. 2.7:

$$F/R_{SP}(t) = F/R_{SP}(t - RT) + \Delta F/R_{SP}(t) \quad \textbf{Eq. 2.7}$$

where:

- $F/R_{SP}(t)$: F/R set-point at the control time
- $F/R_{SP}(t - RT)$: methane flow-rate set-point at the previous control time
- $\Delta F/R_{SP}(t)$: modification in the F/R ratio set-point at the control time

Table 2.2 shows the calibrated values for the parameters (centre, amplitude, and singleton) defining the membership functions of the fuzzy-logic-based controller. With regard to the *fuzzification* stage, three Gaussian membership functions are considered for the *eOLR* and the $\Delta eOLR$: negative (*N*), zero (*Z*), and positive (*P*). For the *defuzzification* stage, four singleton functions were defined as output linguistic variables: high negative (*HN*), low negative (*LN*), low positive (*LP*), and high positive (*HP*).

Table 2.3 shows the inference rules defined for the proposed fuzzy-logic-based control system. As Table 2.3 shows, each inference rule consists of an if-then fuzzy implication that is built by the fuzzy intersection (AND) of two input fuzzy sets (N, Z, P) from the input variables ($eOLR_{MA}$ and $\Delta eOLR_{MA}$). The selection of the inference rule subset was carried out on the basis of the know-how of the process.

Table 2.2 Inference rules of the control system. Nomenclature: $\boldsymbol{eOLR_{MA}}$ (kg COD d^{-1}): error of OLR_{MA}; $\boldsymbol{\Delta eOLR_{MA}}$ (kg COD d^{-1}): error difference of OLR_{MA}; ***ΔF/R***: output of the controller; ***HN***: high negative; ***N***: negative; ***LN***: low negative; ***Z***: cero; ***LP***: low positive; ***P***: positive; and ***HP***: high positive.

Inference Rules
If $eOLR_{MA}$ is *N* and $\Delta eOLR_{MA}$ is *Z* then $\Delta F/R$ is *HP*
If $eOLR_{MA}$ is *N* and $\Delta eOLR_{MA}$ is *P* then $\Delta F/R$ is *HP*
If $eOLR_{MA}$ is *P* and $\Delta eOLR_{MA}$ is *Z* then $\Delta F/R$ is *HN*
If $eOLR_{MA}$ is *P* and $\Delta eOLR_{MA}$ is *P* then $\Delta F/R$ is *HN*
If $eOLR_{MA}$ is *Z* and $eOLR_{MA} > 0$ and $\Delta eOLR_{MA}$ is *N* then $\Delta F/R$ is *LP*
If $eOLR_{MA}$ is *Z* and $eOLR_{MA} < 0$ and $\Delta eOLR_{MA}$ is *N* then $\Delta F/R$ is *LN*
If $eOLR_{MA}$ is *Z* and $eOLR_{MA} > 0$ and $\Delta eOLR_{MA}$ is *P* then $\Delta F/R$ is *HN*
If $eOLR_{MA}$ is *Z* and $eOLR_{MA} < 0$ and $\Delta eOLR_{MA}$ is *P* then $\Delta F/R$ is *HP*

Table 2.3 Centre and amplitude values of the different membership functions from the *fuzzification* stage and values of the singleton functions from the *defuzzification* stage. Nomenclature: $\boldsymbol{eOLR_{MA}}$ (kg COD d^{-1}): error of OLR_{MA}; $\boldsymbol{\Delta eOLR_{MA}}$ (kg COD d^{-1}): error difference of OLR_{MA}; ***ΔF/R***: output of the controller; ***HN***: high negative; ***N***: negative; ***LN***: low negative; ***Z***: cero; ***LP***: low positive; ***P***: positive; ***HP***: high positive; ***C***: centre; $\boldsymbol{\sigma}$: amplitude; and ***S***: singleton.

INPUT	***N***		***Z***		***P***	
	$\mathbf{C_N}$	$\sigma_{\mathbf{N}}$	$\mathbf{C_Z}$	$\sigma_{\mathbf{Z}}$	$\mathbf{C_P}$	$\sigma_{\mathbf{P}}$
$\boldsymbol{eOLR_{MA}}$	-1	0.35	0	0.35	+1	0.35
$\boldsymbol{\Delta eOLR_{MA}}$	-0.5	0.15	0	0.15	+0.5	0.15
OUTPUT	***HN***		***LN***	***LP***	***HP***	
	$\mathbf{S_{HN}}$		$\mathbf{S_{LN}}$	$\mathbf{S_{LP}}$	$\mathbf{S_{HP}}$	
ΔF/R	-0.1		-0.05	+0.05	+0.1	

The output linguistic variables were obtained using the Larsen's fuzzy inference method [2.21], which includes the Max-Prod operator. The *defuzzification* stage was carried out using the height defuzzifer method [2.22].

To avoid possible operational problems, *i.e.* overloads and/or washouts of soluble compounds, the net permeate flow-rate was only modified in a pre-defined HRT range (Eq. 2.8).

$$HRT_{min} \leq HRT \leq HRT_{max} \quad \textbf{Eq. 2.8}$$

where:

- HRT_{min}: 10 hours, minimum HRT (corresponding to a maximum permeate flow-rate of 5000 L d^{-1}).
- HRT_{max}: 24 hours, maximum HRT (corresponding to a minimum permeate flow-rate of 2000 L d^{-1}).

2.4 Results and discussion

2.4.1 Lower layer control performance

Once the basic lower layer control performance was assessed at the demonstration plant, two critical issues were detected. One key point was the initial frequency oscillation derived from those PID controllers whose normal operating mode means intermittent operation of the associated equipment (*i.e.* permeate pumps). This oscillation critically affects the filtration process performance. Other issue detected was associated with the closed-configuration of this wastewater treatment process, where the mixed liquor volume should be maintained constant to avoid possible process perturbations related to head-space pressure variations.

2.4.1.1 Starting-up correcting action for the PID controllers

To avoid the initial oscillation detected in PID controllers fined-up by trial-error, a starting-up correcting action was programmed in those controllers whose normal operating mode means intermittent operation of the associated equipment (*i.e.* permeate pumps). This correcting action consists of operating at an initial time at fixed frequency (FF) before starting the PID controller. This fixed frequency value is established equal to the average operating frequency resulting from the first quarter of the previous homologous membrane operating stage. Figure 2.4 shows an example of the results obtained using both the single PID controller and FF+PID control combination.

Figure 2.4a shows how the operating frequency of the pump is initially established (for 10 seconds) in a value close to the expected operating value (around 17 Hz). As a result of operating in FF+PID

control mode, a start-up of the PID controller from an initial situation far from the established flow set-point is avoided, which results in a high level of stability around the established flow set-point (400 L h^{-1}) in a short period of time (see Figure 2.4b).

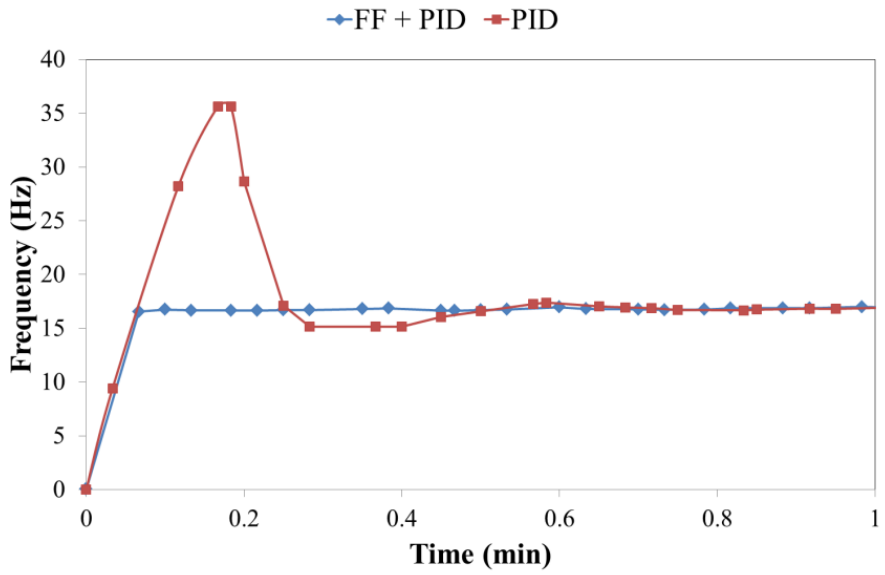

(a)

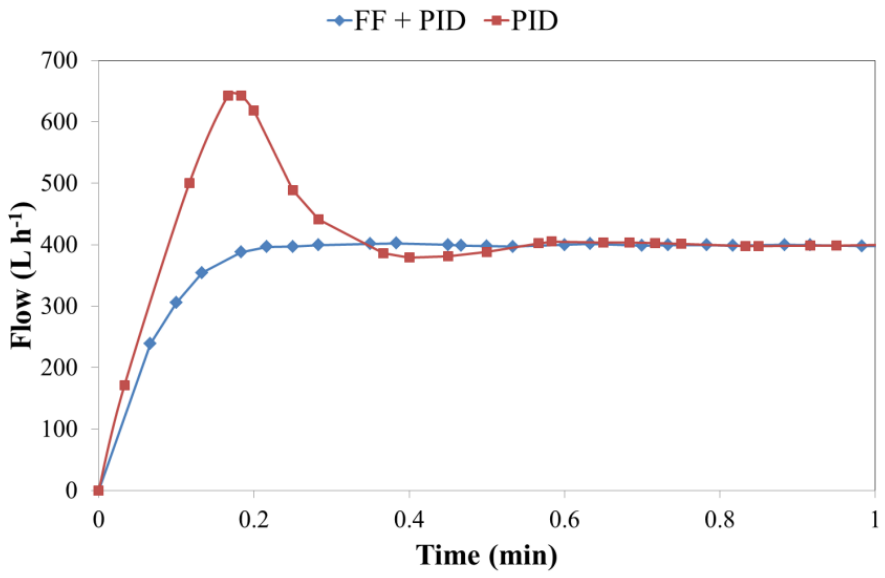

(b)

Figure 2.4 Action of the lower layer controller governing the permeate pump performance. Evolution of: **(a)** pump operating frequency; and **(b)** permeate flow. Nomenclature: **FF**: fixed frequency; and **PID**: proportional-integrative-derivative controller.

Therefore, operating in FF+PID control mode may be required to maintain filtration process working correctly.

2.4.1.2 Mixed liquor level control

Figure 2.5 shows an example of the SAnMBR performance operated at: (1) a constant mixed liquor volume (until hour 2.5 in the figure); and (2) variable mixed liquor volume as a function of the ratio between influent and effluent streams (from hour 2.5 to 6), *i.e.* operating with an effluent flow different to the influent flow. Figure 2.5a depicts the mixed liquor level in the anaerobic reactor and the feed pump frequency. Until hour 2.5, the SAnMBR plant operated at a constant mixed liquor level: a PID controller was programmed to govern the performance of the permeate pump to maintain a level set-point in the anaerobic reactor. Therefore, the proposed control strategy established indirectly a transmembrane flux proportional to the influent flow entering the system. Oppositely, from period 2.5 to 6 hours the controller maintained the effluent flow lower than the influent flow, which resulted in a variation of the mixed liquor level. Therefore, the feed pump operated intermittently between two security level threshold values. The influent pump is stopped when a maximum mixed liquor level is reached. Once the feed pump stops it is not re-started until the mixed liquor level achieves the established 'on' level value. Important to highlight is that variations in the mixed liquor level affects the MLTS concentration (affecting the physical separation process performance); as well as other operating variables such as head-space pressure, blower output pressure, and blower operating frequency.

Figure 2.5b illustrates the effect of a variable mixed liquor level on the above-mentioned variables: SAnMBR head-space pressure; blower output pressure; and blower operating frequency. As Figure 2.5b shows, any variation in the mixed liquor level results in an inversely proportional variation of the blower output pressures, as well as in a proportional variation in the head-space pressure and blower operating frequencies. As regards SAnMBR head-space pressure, an increase and decrease in the mixed liquor level results in an increase and decrease in the SAnMBR head-space pressure, respectively. This behaviour is caused by the corresponding compression and expansion of the biogas in the SAnMBR head-space. These level oscillations cause two effects on blower output pressure: (1) an increase in the level results in an increase in the water column resistance to be overcome by the gas flow entering the corresponding tank; and (2) reductions in the SAnMBR head-space increases the SAnMBR head-pressure, and so increase the total resistance in the output zone of the blowers. Therefore, high energy consumption is required to maintain fixed biogas flow-rates. On the other hand, a decrease in the mixed liquor level can result in an excessive biogas recirculation to the

corresponding tank when operating in fixed pressure control mode. Excessive biogas flows can result in various operating problems such as foaming. Low biogas flows can also result in other operating problems: insufficient gas sparging intensities for membrane scouring, weak mixing intensities in the SAnMBR system, death zones in the anaerobic reactor, and so on.

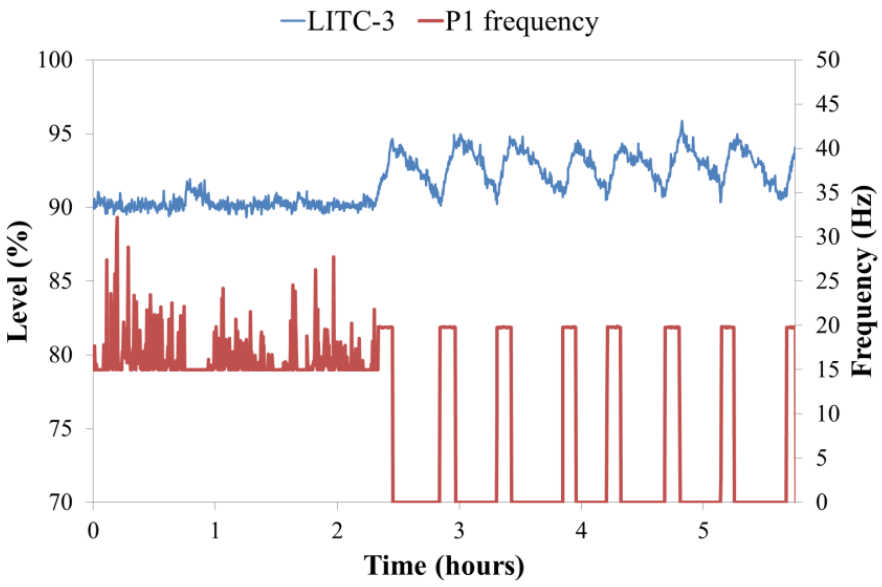

(a)

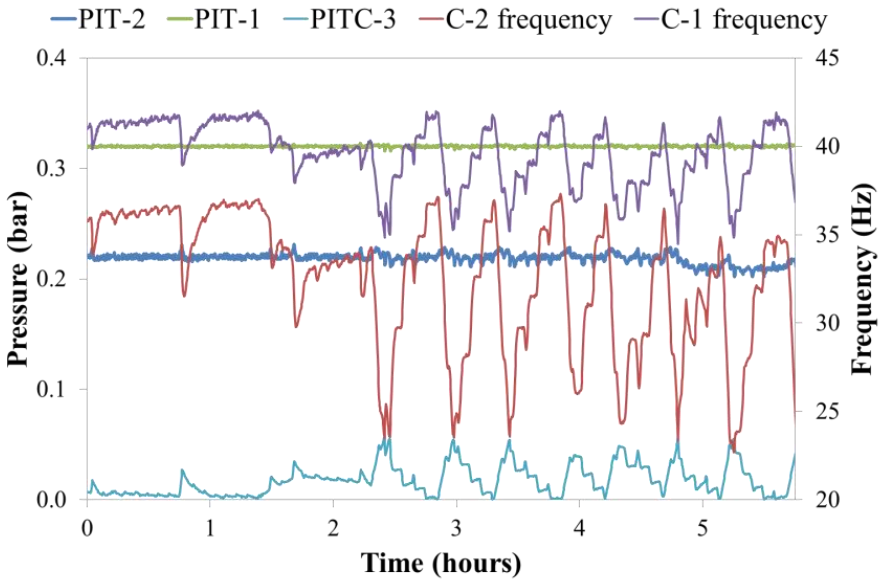

(b)

Figure 2.5 Example of operating at constant (until hour 2.5 in the figure) and variable volume (from hour 2.5 to 6) of the mixed liquor in the system. Evolution of: **(a)** anaerobic reactor level and feed pump operating frequency; and **(b)** SAnMBR head-space pressure, blower output pressures, and blower operating frequencies.

Therefore, a proper control strategy to maintain constant mixed liquor level such as the one shown in Figure 2.5 (until hour 2.5 in the figure) is essential to maintain the SAnMBR system working correctly.

2.4.2 OLR controller performance

Figure 2.6 shows the results of the performance of the OLR control system when operated with the final tuned values of control time *TR* (2 minutes) and *fuzzification*/*defuzzification* parameters (see Table 2.2). The operating mode for the controller was established as controlled OLR, where the influent flow entering the SAnMBR system is modified to maintain an established OLR set-point. The set-point for the OLR_{MA} in this experimental period was set to 1.4 kg COD m^{-3} d^{-1}. Figure 2.6a shows the evolution of the resulting OLR_{MA}, as well as the F/R ratio regulated by the control system. Figure 2.6b shows the evolution of the COD and COD_{MA}, and the resulting permeate flow-rate. As Figure 2.6 illustrates, the control performance maintained the controlled variable at values close to the established set-point when operating in the established HRT range. Figure 2.6b shows that the effluent permeate flow-rate reached its maximum established value during hours 17-19, 32-42, 50-68, and 72-76 (corresponding to 10 hours of HRT at minimum fixed value). In these periods the controller could not increase the influent flow-rate and so the OLR_{MA} decreased (see Figure 2.6a). Moreover, when the HRT remained in the established operating range the controller maintained the OLR_{MA} close to its set-point even when working with high total COD influent oscillations (from 350 to 750 mg COD L^{-1}).

Results from Figure 2.6 show a satisfactory performance of the fuzzy-logic-based controller proposed in this work as the OLR_{MA} resulted in a deviation below 10% of the established set-point (1.4 kg COD m^{-3} d^{-1}) when no interaction of the threshold HRT values was reached (IAE and ITAE resulted in 0.033 and 0.059, respectively). It is important to highlight that this control system was operated under similar conditions to those found in full-scale plants.

The proposed fuzzy-logic-based control system can be applied for biological process performance optimisation since the OLR_{MA} set-point can be established by using a supervisory controller (*i.e.* optimising methane production and/or COD removal). The proposed upper layer controller enables suitable COD removals to be achieved using the on-line equipment available in the pilot plant. The controller is easy to operate and adaptable to new operational requirements.

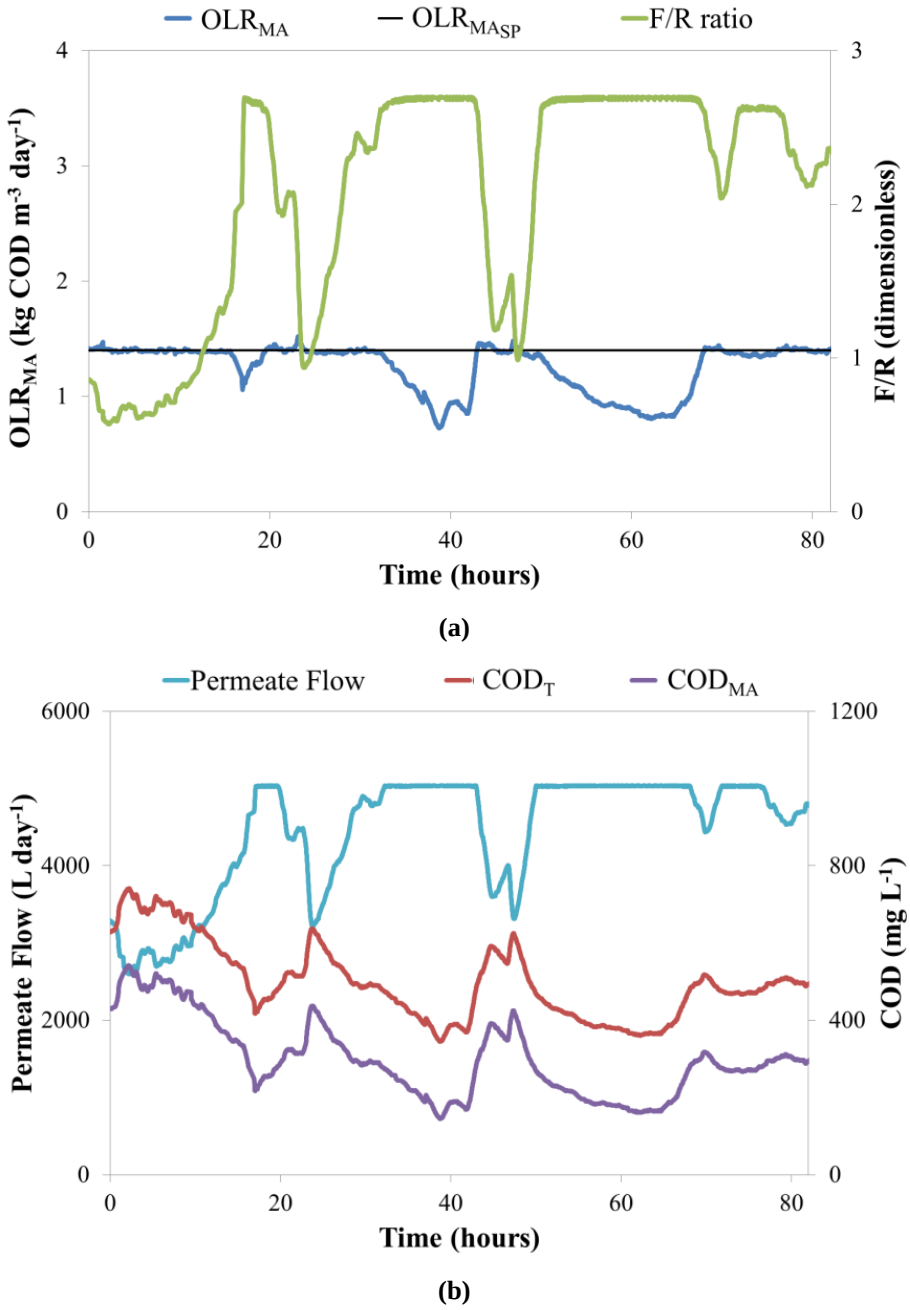

Figure 2.6 Fuzzy-logic-based control system performance. Evolution of: **(a)** organic loading rate and filtration/relaxation duration ratio; and **(b)** permeate flow and COD entering the SAnMBR system. Nomenclature: **OLR**: Organic loading rate; **MA**: Methanogenic Archaea; **SP**: Set-point; **F/R**: Filtration/relaxation duration ratio; $\mathbf{COD_T}$: total COD; and $\mathbf{COD_{MA}}$: available COD for Methanogenic Archaea.

2.4.3 Filtration system performance

Figure 2.7 shows an example of the TMP profile obtained and the membrane operating mode established. The membrane operating conditions were the following: a permeate flux of 20 LMH

(normalised to 20 ºC); a biogas sparging intensity of around 0.1 Nm^3 m^{-2} h^{-1}; and an MLTS in the anaerobic reactor of 10 g L^{-1}. The MLTS in the membrane tank was around 12.5 g L^{-1}, according to the ratio between the sludge flow entering the membrane tank (2500 L h^{-1}) and the permeate flow-rate (600 L h^{-1}).

Figure 2.7 shows a slight TMP recovery after the relaxation stage. Therefore, the short relaxation applied enables a reduction in the increase of TMP over time by applying non-prohibitive downtimes for relaxation of the operating time. However, TMP recovery can only be classified as significant after applying a back-flush stage. Back-flush stage is required to maintain the sustainable long-term operation of membranes. Figure 2.7 also illustrates the results of applying the non-conventional membrane operating stages considered in the membrane operational mode: ventilation and degasification. In terms of membrane recovery, ventilation acts as a relaxation stage since membrane scouring using the same biogas sparging intensity as in the relaxation stage is conducted without filtration. As can be observed in Figure 2.7, since longer periods of ventilation than relaxation are applied, the TMP recovery achieved by ventilation is slightly higher than the TMP recovery achieved by relaxation. Nevertheless, the TMP recovery after ventilation is still lower than the TMP recovery after back-flush. Finally, this figure also shows the effect of applying a degasification stage on membrane performance. Figure 2.7 show that a significant TMP recovery (in comparison with the TMP recovery after back-flush) is achieved after applying the degasification stage. Degasification is applied to remove the accumulated biogas at the top of the dead-end hollow-fibres and this action recovers the total effective filtration area.

It is important to highlight that the membrane control mode must be carefully defined to enable the different operating stages to be applied correctly. Suitable instrumentation and automation equipment is necessary to automatically implement an optimised membrane operating mode. A successful implementation of a robust and suitable ICA system for SAnMBR technology is essential for optimised process performance; and the proposed ICA system is a promising alternative for SAnMBR systems operation.

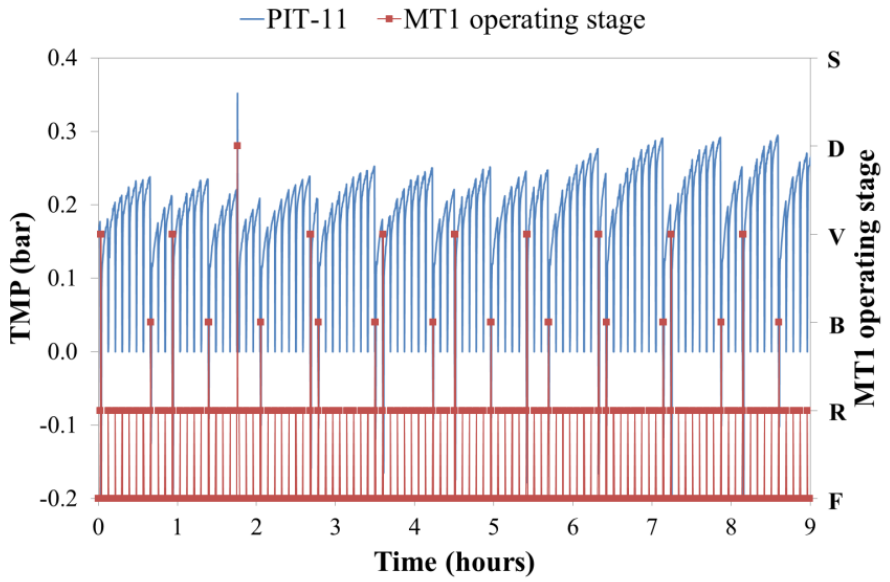

(a)

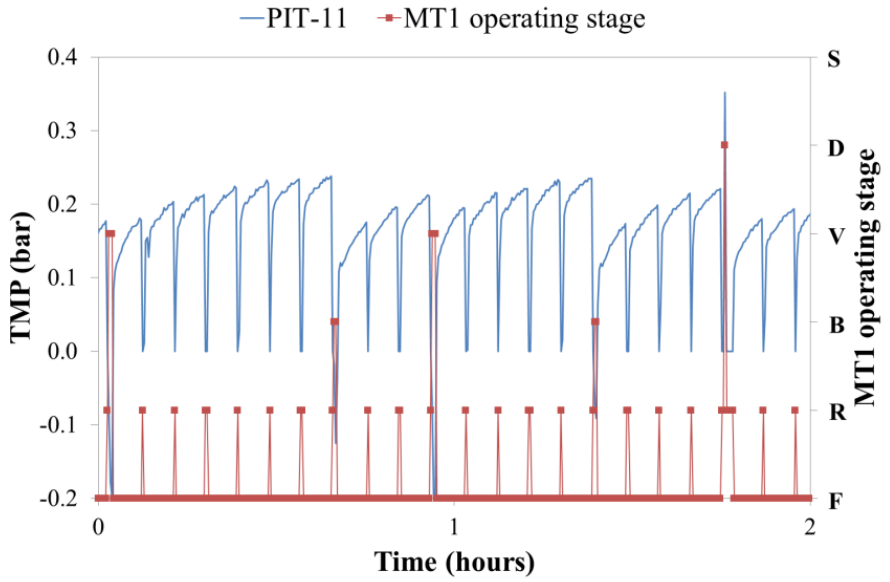

(b)

Figure 2.7 (a) Example of the membrane operating mode: 320-second F-R basic cycles (300 s filtration and 20 s relaxation); 20 seconds of back-flush every 8 F-R cycles; 30 seconds of ventilation every 10 F-R cycles; and 30 seconds of degasification every 50 F-R cycles. **(a)** Zoom to two hours of operation. Nomenclature: **S**: Standby; **D**: Degasification; **V**: Ventilation; **B**: Back Flush; **R**: Relaxation; **F**: Filtration; **PIT**: pressure indicator transmitter; **MT**: membrane tank; and **TMP**: transmembrane pressure.

2.4.4 Overall SAnMBR demonstration plant performance

The SAnMBR demonstration plant has been in operation for more than three years. Throughout the experimental period different operating conditions for both biological and physical processes were easily tested because of the ICA system implemented in the SAnMBR plant. The SAnMBR system was operated at different SRTs (from 20 to 70 days), HRTs (from 5 to 30 hours), organic loading rates (OLR) between 0.5 and 2.0 kg COD m^{-3} d^{-1}, and temperatures (controlled temperatures of 33, 25, and 20, and ambient temperature oscillating from approximately 14 to 31 ºC). The system was operated at different transmembrane fluxes (from 6.6 to 20 LMH) and gas sparging intensities (from 0.1 to 0.5 Nm^3 h^{-1} m^{-2}). Moreover, the SAnMBR was operated in a wide range of MLTS (from approximately 10 to 30 g L^{-1}).

In general, low effluent VFA concentrations (< 30 mg COD L^{-1}), as well as significant methane-rich (up to 70% v/v) biogas productions were observed (around 100 L d^{-1} in average), which evidenced a suitable biological process performance. Overall, high treatment efficiencies in terms of COD removal were achieved (around 85 %). Further details on the biological process performance of the SAnMBR system can be found in Giménez *et al*. [2.10].

Until operating day 810, the membranes have not required chemical cleaning, and this is mainly because they have been operating in sub-critical filtration conditions and within an adequate membrane operating mode. Another factor that has helped avoid the need to clean the membranes was that no fouling problems caused by high pH levels in the mixed liquor arose. For instance, chemical precipitation was not detected because the pH of the mixed liquor was kept at values below 7.2 as a result of recycling the produced biogas for in-situ sparging [2.14]. On the other hand, low biofouling propensities were observed as a result of the low amount of extracellular polymeric substances and soluble microbial products detected in the system [2.23]. Further details on the physical process performance of this SAnMBR system can be found in Robles *et al*. [2.23; 2.24].

The proposed ICA makes plant operating very flexible with suitable and stable biological and physical separation process performances. The know-how acquired after almost three years of plant operation experience has contributed to develop and enhance this ICA for SAnMBR technology. The proposed ICA offers high process stability, which is essential to control the key operating issues of SAnMBR technology, and specially to optimize membranes performance. In this respect, the key operating parameters are: TMP and biogas recycling flow rate to control membrane fouling; membrane operating mode, which provides flexibility to cope with the strong dynamics in the influent flow and

load; mixed liquor level and system pressure to avoid significant pressure oscillations in the system; OLR, required to minimise biological process disturbances; and pH, ORP and temperature, which indicate a suitable anaerobic process performance.

2.5 Conclusions

A robust ICA system for SAnMBR systems is presented in this paper. It has been implemented and tested in an SAnMBR demonstration plant. Several lower layer control loops have been implemented and are described. These control algorithms enable a suitable and stable process performance. Moreover, various modifications to the classical PID controllers were implemented to enhance global process performance. The high level of flexibility provided by the developed ICA system enables various upper layer controllers to be implemented to optimise the performance of the SAnMBR system. The level of automatic control of the proposed ICA system reduces the involvement of operators and laboratory personnel, lowers operational costs, and improves process stability following input disturbances.

2.6 Acknowledgements

This research work has been supported by the Spanish Ministry of Economy and Competitiveness (MINECO, Projects CTM2011-28595-C02-01/02) jointly with the European Regional Development Fund (ERDF), which are gratefully acknowledged. The revision of the English in this paper was funded by the Universitat Politècnica de València, Spain.

2.7 References

2.1 M. Henze, M.C.M. van Loosdrecht, G.A. Ekama, D. Brdjanovic, Biological Wastewater Treatment, Principles, Modelling and Design, IWA Publishing, I.S.B.N.: 978-184-33-9188-3, 2008.

2.2 S. Judd, C. Judd, The MBR Book: Principles and Applications of Membrane Bioreactors in Water and Wastewater Treatment, Second Edition, ELVESIER, ISBN: 978-0-08-096682-3, 2011.

2.3 Z. Huang, S.L. Ong, H.Y. Ng, Submerged anaerobic membrane bioreactors for low-strength wastewater treatment: Effect of HRT and SRT on treatment performance and membrane fouling, Water Res. 45 (2011), 705–713.

2.4 I.S. Chang, P.L. Clech, B. Jefferson, S. Judd, Membrane fouling in membrane bioreactors for wastewater treatment, J. Environ. Eng. 128 (2002), 1018–1029.

2.5 U. Jeppsson, J. Alex, M.N. Pons, H. Spanjers, P.A. Vanrolleghem, Status and future trends of ICA in wastewater treatment–a European perspective, Water Sci. Technol. 45 (2002), 485–494.

2.6 P.A. Vanrolleghem, D.S. Lee, On-line monitoring equipment for wastewater treatment processes: state of the art, Water Sci. Technol. 47 (2003), 1–34.

2.7 G. Olsson, M.K. Nielsen, Z. Yuan, A. Lynggaard-Jensen, J.P. Steyer, Instrumentation, control and automation in wastewater systems, IWA Publishing, 2005.

2.8 H. Haimi, M. Mulas, K. Sahlstedt, R. Vahala, Advanced operation and control methods of municipal wastewater treatment processes in Finland, Water and Wastewater Engineering, Helsinki University of Technology. I.S.B.N.: 978-951-22-9975-1, 2009.

2.9 M.V. Ruano, J. Ribes, A. Seco, J. Ferrer, Low cost-sensors as a real alternative to on-line nitrogen analysers in continuous systems, Water Sci. Technol. 60 (2009), 3261–3268.

2.10 J.B. Giménez, A. Robles, L. Carretero, F. Durán, M.V. Ruano, M.N. Gatti, J. Ribes, J. Ferrer, A. Seco, Experimental study of the anaerobic urban wastewater treatment in a submerged hollow-fibre membrane bioreactor at pilot scale, Bioresource Technol. 102 (2011), 8799–8806.

2.11 V. O'Flaherty, T. Mahony, R. O'Kennedy, E. Colleran, Effect of pH on growth kinetics and sulphide toxicity thresholds of a range of methanogenic, syntrophic and sulphate-reducing bacteria, Process Biochem. 33 (1998), 555–569.

2.12 M.H. Hwang, N.J. Jang, S.H. Hyun, I.S. Kim, Anaerobic bio-hydrogen production from ethanol fermentation: the role of pH, J. Biotechnol. 111 (2004), 297–309.

2.13 L. Pastor, D. Mangin, R. Barat, A. Seco, A pilot-scale study of struvite precipitation in a stirred tank reactor: Conditions influencing the process, Bioresource Technol. 99 (2008), 6285–6291.

2.14 A. Robles, M.V. Ruano, J. Ribes, J. Ferrer, Sub-critical long-term operation of industrial scale hollow-fibre membranes in a submerged anaerobic MBR (HF-SAnMBR) system, Sep. Purif. Technol. 100 (2012), 88–96.

2.15 H. Spanjers, J.B. Lier, Instrumentation in anaerobic treatment–research and practice, Water Sci. Technol. 53 (2006), 63–76.

2.16 American Public Health Association/American Water Works Association/Water Environmental Federation, Standard methods for the Examination of Water and Wastewater, 21st edition, Washington DC, USA, 2005.

2.17 G. Ferrero, H. Monclús, G. Buttiglieri, J. Comas, I. Rodriguez-Roda, Automatic control system for energy optimization in membrane bioreactors, Desalination 268 (2011), 276–280**.**

2.18 C. Huyskens, E. Brauns, E. Van Hoof, L. Diels, H. De Wever, Validation of a supervisory control system for energy savings in membrane bioreactors, Water Res. 45 (2011), 1443–1453.

2.19 G. Ferrero, I. Rodriguez-Roda, J. Comas, Automatic control systems for submerged membrane bioreactors, Water Res. 46 (2012), 3421–3433.

2.20 J.B. Giménez, N. Martí, J. Ferrer, A. Seco, Methane recovery efficiency in a submerged anaerobic membrane bioreactor (SAnMBR) treating sulphate-rich urban wastewater: Evaluation of methane losses with the effluent, Bioresource Technol. 118 (2012), 67–72.

2.21 P.M. Larsen, Industrial application of fuzzy logic control, Int. J. Man-Mach. Stud. 12 (1980), 3–10.

2.22 J.M. Mendel, Fuzzy logic systems for engineering: a tutorial, Proc. IEEE, 83 (1995), 345–375**.**

2.23 A. Robles, M.V. Ruano, J. Ribes, J. Ferrer, Performance of industrial scale hollow-fibre membranes in a submerged anaerobic MBR (HF-SAnMBR) system at mesophilic and psychrophilic conditions, Sep. Purif. Technol. 104 (2012), 290–296.

2.24 A. Robles, M.V. Ruano, J. Ribes, J. Ferrer, Factors that affect the permeability of commercial hollow-fibre membranes in a submerged anaerobic MBR (HF-SAnMBR) system, Water Res. 47 (2012), 1277–1288.

CHAPTER 3:

Sub-critical filtration conditions of commercial hollow-fibre membranes in a submerged anaerobic MBR (HF-SAnMBR) system: the effect of gas sparging intensity

Abstract

A submerged anaerobic MBR demonstration plant with two commercial hollow-fibre ultrafiltration systems (PURON®, Koch Membrane Systems, PUR-PSH31) was operated using municipal wastewater at high levels of mixed liquor total solids (MLTS) (above 22 g L^{-1}). A modified flux-step method was applied to assess the critical flux (J_C) at different gas sparging intensities. The results showed a linear dependency between J_C and the specific gas demand per unit of membrane area (SGDm). J_C ranged from 12 to 19 LMH at SGDm values of between 0.17 and 0.5 $Nm^3\ m^{-2}\ h^{-1}$, which are quite low in comparison to aerobic MBR. Long-term trials showed that the membranes operated steadily at fluxes close to the estimated J_C, which validates the J_C obtained by this method. After operating the membrane for almost two years at sub-critical levels, no irreversible fouling problems were detected, and therefore, no chemical cleaning was conducted.

Keywords

Critical flux; gas sparging; industrial hollow-fibre membranes; modified flux-step method; submerged anaerobic membrane bioreactor.

Highlights

A SAnMBR demonstration plant was operated with urban wastewater at high MLTS.
A modified flux-step method was conducted under different gas sparging intensities.
The J_C ranged from 12 to 19 LMH for SGDm values between 0.17 and 0.5 $Nm^3\ h^{-3}\ m^{-2}$.
A stable operation of the membranes was observed at fluxes close to the obtained JC.
No irreversible fouling problems were detected, even for high MLTS concentrations.

A. Robles, M.V. Ruano, F. García-Usach, J. Ferrer
Sub-critical filtration conditions of commercial hollow-fibre membranes in a submerged anaerobic MBR (HF-SAnMBR) system: The effect of gas sparging intensity
Bioresour. Technol. 114 (2012), 247 – 254

3.1 Introduction

In recent years there has been increased interest in assessing the feasibility of the anaerobic treatment of municipal wastewater at ambient temperature conditions. This interest focusses on the sustainability advantages of anaerobic rather than aerobic processes, *i.e.* low sludge production due to the low anaerobic biomass yield; low energy consumption because no aeration is needed; and the generation of biogas which can be used as an energy resource. The total greenhouse emissions of this technology are, therefore, low because low energy consumption indirectly means low gas emissions. The main challenge of anaerobic biotechnology is to develop treatment systems that prevent biomass loss and enable high sludge retention times (SRT) in order to offset the low growth rates of anaerobic biomass at ambient temperatures [3.1]. In this respect, anaerobic membrane bioreactors (AnMBR) are a promising technology for municipal wastewater treatment. Furthermore, the membrane separation process allows high organic loading to be obtained with municipal wastewater, since low COD levels are remedied by high treatment flow rates in small reaction volumes: something not possible with classical anaerobic systems (UASB and EGSB). However, operating membrane bioreactors with high SRTs may mean operating at high mixed liquor total solid (MLTS) levels: one of the main constraints of using membranes [3.2]. These high MLTS levels contribute to membrane fouling: the key issue of membrane technology. Fouling decreases membrane permeability (K) and increases operating and maintenance costs [3.3]. It is important to emphasise that AnMBR systems enable membranes to operate at MLTS levels higher than in aerobic MBRs because anaerobic MBRs do not have the oxygen transfer constraints that limit MLTS levels in aerobic MBRs [3.4]. In this respect, a considerable reduction in the design operating volume can be achieved in comparison with the volume required in aerobic conditions.

The key operating challenge in AnMBR technology is to optimise membrane operation in order to minimise any kind of membrane fouling and thereby increase the membrane lifespan. The gas sparging intensity in each operating range is a key operating parameter that must be optimized in order to minimise both investment and operating costs in AnMBR systems. Several strategies to control fouling [3.5; 3.6; 3.7] aim to optimise filtration whilst minimising investment and operating costs. One such strategy is based on using membranes in sub-critical filtration conditions. These conditions are limited by the critical flux (J_C): a quantitative filtration parameter defined firstly as "the flux below which no fouling occurs" [3.8], or as "the flux below which a decline of flux with time does not occur; above it, fouling is observed" [3.9]. On the basis of these definitions, two different concepts have developed. In the "strong" concept, critical flux (J_{CS}) is defined as the flux below which membrane performance is equal to its ability to treat clean water under same operating conditions. In the "weak"

concept, critical flux (J_{CW}) is defined as the flux (not necessarily the same as the clean-water flux) below which the transmembrane pressure (TMP) and J are not directly related.

Different methodologies to determine J_C have been reported in literature, the flux-step method being the most common [3.10; 3.11; 3.12]. This method enables J_C to be determined in a wide range of operating conditions, mainly in relation to the level of MLTS or gas sparging intensity, usually measured as specific gas demand per unit of membrane area (SGD_m). MLTS level and gas sparging intensity have both been identified as the factors that affect J_C most. Furthermore, it has been pointed out that the J_C resulting from the flux-step method cannot be used to estimate the critical flux of full-scale systems operated continuously because it is a short-term estimate usually made off line [3.10].

Several published studies provide the J_C of both aerobic and anaerobic MBRs on a laboratory scale [3.13; 3.14; 3.15]. However, further studies are needed in order to determine the J_C of submerged AnMBR (SAnMBR) technology on a semi-industrial scale. Moreover, the effect of the main operating conditions on membrane fouling cannot be evaluated properly at the lab scale because they depend heavily on the membrane size. In hollow-fibre (HF) membranes in particular the HF length is a critical parameter. Therefore, since membrane performance cannot be scaled up directly from laboratory to plant dimensions, especially in the case of HF-based technology, further studies of HF-SAnMBR technology on an industrial scale are needed in order to facilitate its design and implementation in full-scale wastewater treatment plants (WWTP).

To gain more insight into the optimisation of the physical separation process in a SAnMBR system on an industrial scale, our study evaluated the critical filtration conditions of industrial HF membranes. In order to obtain robust results that can be extrapolated to full-scale plants, a SAnMBR system featuring industrial HF membrane units was operated using effluent from the pre-treatment of the Carraixet WWTP (Valencia, Spain). The main objective of this study was to assess the ability of the flux-step method to predict the critical flux in continuous full-scale HF-SAnMBR operations and validate the J_C values obtained during the long-term operating of membranes in sub-critical conditions. Furthermore, the effect of the gas sparging intensity on both membrane performance and J_C was studied whilst operating the membranes with high levels of MLTS.

3.2 Materials and methods

3.2.1 Demonstration plant description

Figure 3.1 shows the HF-SAnMBR demonstration plant used in this study. As previously introduced, it consists of an anaerobic reactor with a total volume of 1.3 m^3 (0.4 m^3 head space) connected to two membrane tanks each with a total volume of 0.8 m^3 (0.2 m^3 head space). Each membrane tank has one industrial HF ultrafiltration membrane unit (PURON®, Koch Membrane Systems (PUR-PSH31) with 0.05 μm pores). Each module has 9 HF bundles, 1.8 m long, giving a total membrane surface of 30 m^2. Normal membrane operation consists of a specific schedule involving a combination of different individual stages taken from a basic filtration-relaxation (F-R) cycle. Besides classical membrane operating stages (filtration, relaxation and back-flush), two additional stages were also considered in membrane operation: degasification and ventilation (see Chapter 2).

Figure 3.1 General view of the SAnMBR demonstration plant.

The HF-SAnMBR demonstration plant is fed with the effluent from the Carraixet WWTP pre-treatment (screening, degritter, and grease removal). After further pre-treatment in the rotofilter (RF) and homogenisation in the equalisation tank (ET), the wastewater is pumped to the anaerobic reactor

(AnR). In order to improve the stirring conditions of the anaerobic reactor and to favour the stripping of the produced gases from the liquid phase, a fraction of the produced biogas is recycled to this reactor. The sludge is continuously recycled through the external membrane tanks (MT) where the effluent is obtained by vacuum filtration. In order to minimise the cake layer formation, another fraction of the produced biogas is also recycled to the membrane tanks from the bottom of each fibre bundle.

For further details about this SAnMBR demonstration plant see Chapter 2 or Giménez *et al*. [3.16].

3.2.2 Demonstration plant monitoring

Numerous on-line sensors and items of automatic equipment were installed in order to automate and control demonstration plant operations and provide on-line information about the state of the process. Specifically, the on-line sensors assigned to each membrane tank consist of: 1 pH-temperature transmitter (Endress+Hauser Orbisint CPS11D Memosens); 1 level indicator transmitter (Endress+Hauser Waterpilot FMX167); 1 flow indicator transmitter for the mixed liquor feed pump (Endress+Hauser Promag 50W); 1 flow indicator transmitter for the permeate pump (Endress+Hauser Promag 50P); and 1 liquid pressure indicator transmitter to control the TMP (Endress+Hauser Cerabar M PMC41). The group of actuators assigned to each membrane tank consists of a group of on/off control valves which determine the direction of the flow in order to control the different membrane operating stages (filtration, back-flush, relaxation…), and 3 frequency converters (Micromaster Siemens 420). Each frequency converter controls the rotational speed of the permeate pump (JUROP VL02 NBR), the mixed liquor feed pump (CompAir NEMO), and the membrane tank blower (FPZ 30HD).

Besides the on-line process monitoring, in order to assess the performance of the biological process, 24-hour composite samples were taken from influent and effluent streams, and grab samples of anaerobic sludge were taken once a day. The following parameters were analysed daily in influent stream: total suspended solids (TSS); volatile suspended solids (VSS); volatile fatty acids (VFA) concentration; carbonate alkalinity (Alk); and nutrients (ammonium (NH_4-N) and orthophosphate (PO_4-P)); the following parameters were analysed daily in effluent stream: VFA concentration; carbonate alkalinity; and nutrients (NH_4-N and PO_4-P); and the following parameters were analysed daily in mixed liquor: total solids (MLTS); volatile solids (MLVS); VFA concentration; carbonate alkalinity; and nutrients (NH_4-N and PO_4-P). The total and soluble chemical oxygen demand (COD_T and COD_S, respectively) were determined once a week in both influent and effluent streams, and

mixed liquor. In addition, the total and soluble biological oxygen demand (BOD_T and BOD_S, respectively) were determined once a week in both influent and effluent streams in order to get an idea of the aerobically biodegradable fraction of organic matter that is anaerobically removed in the system.

3.2.3 Demonstration plant operation

The start-up of the demonstration plant was carried out with biomass inoculum (40% of the working volume) coming from a full-scale anaerobic digester.

The long-term operation of this SAnMBR system was conducted at different SRTs (from 30 to 70 days), hydraulic retention times (HRTs) ranged from 6 to 26 hours, and organic loading rates (OLR) between 0.3 and 1.1 kgCOD m^{-3} d^{-1}. The temperature varied from 33 to 17 ºC. The pH of the mixed sludge throughout this period ranged from 6.5 to 7.1. The MLTS level ranged from around 10 to 30 g L^{-1}. With regard to the physical separation process, J_{20} was varied from 9 to 13.3 LMH, with SGD_m values from around 0.23 to 0.33 Nm^3 h^{-1} m^{-2}. The cross-flow sludge velocity over the membrane surface was set to 3.6 mm s^{-1}, giving a sludge flow rate through the membrane module of 2700 L h^{-1}. The membrane operating mode was: a 300-second basic F-R cycle (250 s filtration and 50 s relaxation), 30 seconds of back-flush every 10 F-R cycles, 40 seconds of ventilation every 10 F-R cycles, and 30 seconds of degasification every 50 F-R cycles.

The specific operating conditions corresponding to the short-term trials were: an SRT of 70 days; controlled temperature of 33 ºC; and a MLTS level in the sludge fed to the membrane tank of 23 g L^{-1}.

Important to highlight is the wide variation in the anaerobic reactor influent loads during the experiment (*i.e.* 186 ± 61 mg L^{-1} of TSS or 388 ± 95 mg L^{-1} of Total COD), reflected by the high standard deviation of each parameter.

3.2.4 Demonstration plant monitoring

3.2.4.1 Analytical monitoring

Total solids, volatile solids, total suspended solids, volatile suspended solids, COD_T and COD_S, BOD_T and BOD_S, NH_4-N, and PO_4-P were determined according to Standard Methods [3.17] and using the

following approaches for each parameter: 2540 B, 2540 E, 2540 D, 2540 E, 5220 B and 5220 D, 5210 B and 5210 C, 4500-NH3 G, and 4500-P E, respectively. Carbonate alkalinity and VFA concentration were determined by titration according to the method proposed by WRC [3.18]. The methane fraction of the biogas was measured using a gas chromatograph equipped with a Flame Ionization Detector (GC-FID, Thermo Scientific). 1 mL of biogas was collected by a gas-tight syringe and injected into a 30 m x 0.319 mm x 25 μm HP-MOLESIEVE column (Agilent Technologies) that was maintained at 40 ºC. The carrier gas was helium at a flow-rate of 40 mL min^{-1}. CH4 pure gas (99.9995%) was used as standard.

3.2.4.2 Modified flux-step method and membrane performance indices

The 20 ºC-normalised membrane permeability (K_{20}) was calculated using a simple filtration model (Eq. 3.1) that takes into account the on-line monitored data of TMP and J. This simple filtration model includes temperature correction (Eq. 3.2) to account for the dependence of permeate viscosity on temperature [3.19], and therefore the normalised flux (J_{20}) was obtained by using Eq. 3.3. Total membrane resistance (R_T) was theoretically represented by the following partial resistances (Eq. 3.4): membrane resistance (R_M); cake layer resistance (R_C); and irreversible layer resistance (R_I).

$$K_{20} = \frac{1}{\mu \cdot R_T} = \frac{J_T f_T}{TMP} \qquad \textbf{Eq. 3.1}$$

$$f_T = e^{-0.0239\,(T-20)} \qquad \textbf{Eq. 3.2}$$

$$J_{20} = J_T \cdot e^{-0.0239\,(T-20)} \qquad \textbf{Eq. 3.3}$$

$$R_T = R_m + R_c + R_I \qquad \textbf{Eq. 3.4}$$

In our study, J_{CW} (critical flux in the weak definition, as stated before) was determined by applying a modified flux-step method based on the method proposed by van der Marel *et al*. [3.12]. This modified method (see Figure 3.2a and Figure 3.2b) establishes successive flux-steps analogous to the common flux-step method. The duration of the filtration stage was set to 15 minutes. The flux-step size was arbitrarily set to a J_{20} of 1.22 LMH, and downward flux-stepping was started when a maximum TMP threshold value was reached (0.4 bars). In order to reduce the effect of reversible fouling on J_{CW} calculations, a relaxation stage of 15 minutes was inserted between each flux-step. The

relaxation stages were conducted using the same SGD_m as in the filtration stages. In this study, five flux-step tests were carried out at an SGD_m of 0.17, 0.23, 0.33, 0.4 and 0.5 $Nm^3\ h^{-1}\ m^{-2}$.

In a way similar to the approach suggested by several authors [3.4; 3.10], the data processing of the results from the flux-step method used the derived parameters shown in Eq. 3.5 to Eq. 3.8. Eq. 3.5 and Eq. 3.6 give the average values of TMP and K_{20} for each flux-step (J^n), respectively. Eq. 3.7 is the difference in TMP at the same J_{20} between upward flux-stepping and downward flux-stepping (see Figure 3.2c). The fouling rate (Eq. 3.8) was calculated as the increase in TMP in individual filtration stages.

$$TMP_{J^n}^{AVE} = \left(\sum_{j=1}^{z} TMP_{J^n}^{j}\right) \Big/ \sum z \qquad \textbf{Eq. 3.5}$$

$$K_{20}{}_{J^n}^{AVE} = \left(\sum_{j=1}^{z} K_{20}{}_{J^n}^{j}\right) \Big/ \sum z \qquad \textbf{Eq. 3.6}$$

$$\Delta TMP_{AVE} = \left(TMP_{J^n}^{AVE}\right)^{DOWNWARD} - \left(TMP_{J^n}^{AVE}\right)^{UPWARD} \qquad \textbf{Eq. 3.7}$$

$$\frac{dTMP}{dt} \approx \frac{\Delta \mathrm{TMP}}{\Delta t} = \frac{TMP_{J^n}^{f} - TMP_{J^n}^{i}}{t_{J^n}^{f} - t_{J^n}^{i}} \qquad \textbf{Eq. 3.8}$$

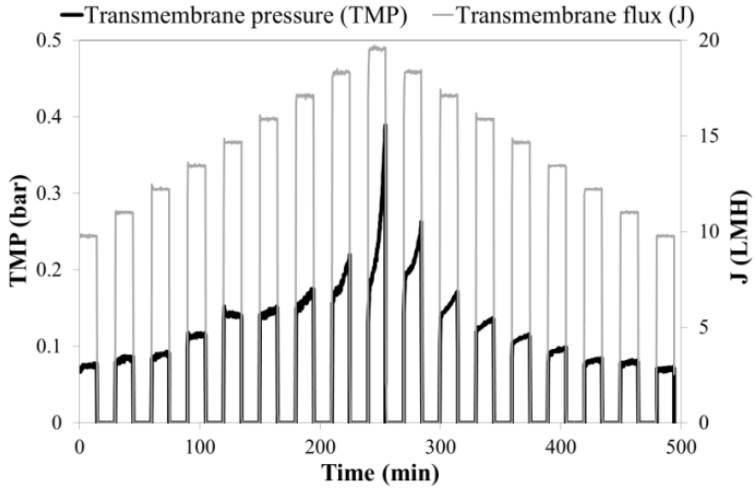

(a)

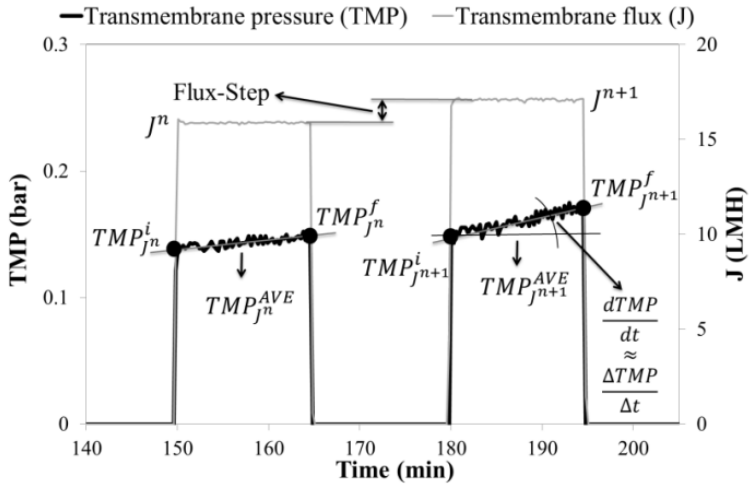

(b)

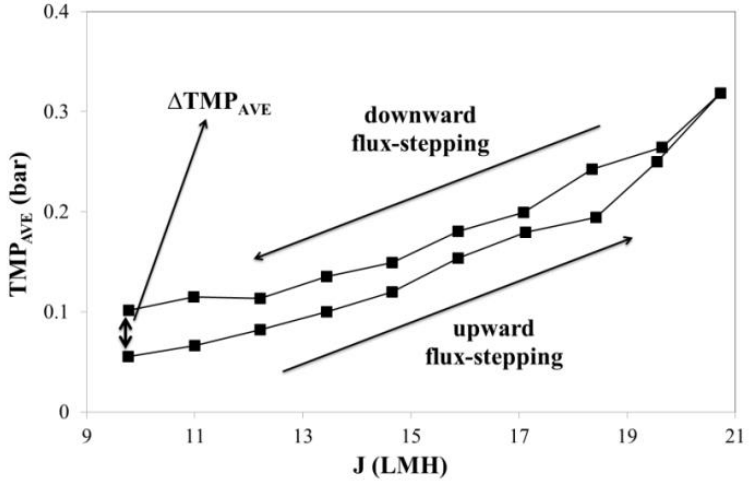

(c)

Figure 3.2 Schematic representation of: **(a)** the modified flux-step method; **(b)** derived parameters; and **(c)** the increase in TMP at the same J between the upward flux-stepping and the downward flux-stepping.

3.3 Results and discussion

This study entailed short-term and long-term trials. In the short-term trials, SGD_m ranged from 0.17 to 0.50 $Nm^3\ h^{-1}\ m^{-2}$, whilst J_{20} varied from around 9.5 to 20.5 LMH. In these short-term trials the MLTS level in the anaerobic sludge entering the membrane tank was 23 $g\ L^{-1}$. It must be emphasised that the MLTS level in the membrane tank increased according to the ratio between the membrane tank sludge intake and the net permeate flow rate (the MLTS level in the membrane tank was around 26 $g\ L^{-1}$).

3.3.1 Short-term trials: Effect of SGD_m on membrane performance

Figure 3.3 shows the results of the short-term trials of both TMP_{AVE} and $K_{AVE,20}$ obtained by applying Eq. 3.5 and Eq. 3.6, respectively. As Figure 3.3a shows, the effect of J_{20} on TMP_{AVE} becomes evident at levels of above 13 LMH, there being no obvious relationship below this level. This behaviour highlights the need to optimise the physical separation process at every operating range, since considerable energy savings could be achieved. For instance, Figure 3.3a shows that it is theoretically possible to operate the membranes at SGD_m of 0.17 $Nm^3\ h^{-1}\ m^{-2}$ when operating at a J_{20} of less than 13 LMH: a value far lower than the lower threshold in the typical operating range for aerobic processes suggested by the membrane supplier (0.3 $Nm^3\ h^{-1}\ m^{-2}$). This figure shows that the higher the J_{20}, the greater the effect of SGD_m on TMP_{AVE}. When J_{20} is higher than 13 LMH, an increase in SGD_m from 0.17 to 0.33 $Nm^3\ h^{-1}\ m^{-2}$ affects TMP_{AVE} considerably but a further increase to 0.5 $Nm^3\ h^{-1}\ m^{-2}$ has no significant effect at J_{20} values lower than 15.8 LMH. Thus, an SGD_m of 0.5 $Nm^3\ h^{-1}\ m^{-2}$ would only be needed at J_{20} values of more than 18 LMH. It must be said that the maximum SGD_m studied (0.5 $Nm^3\ h^{-1}\ m^{-2}$) is lower than the upper threshold in the typical operating range for aerobic processes suggested by the membrane supplier (0.7 $Nm^3\ h^{-1}\ m^{-2}$).

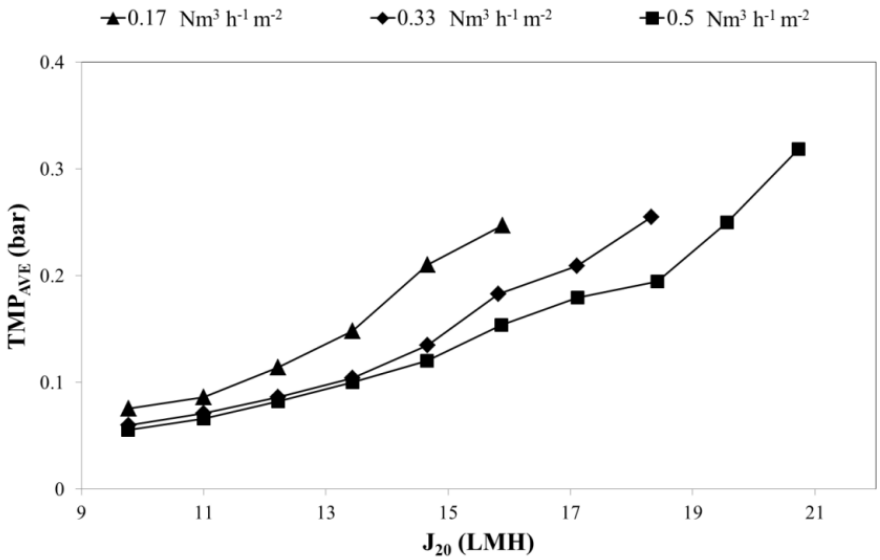

(a)

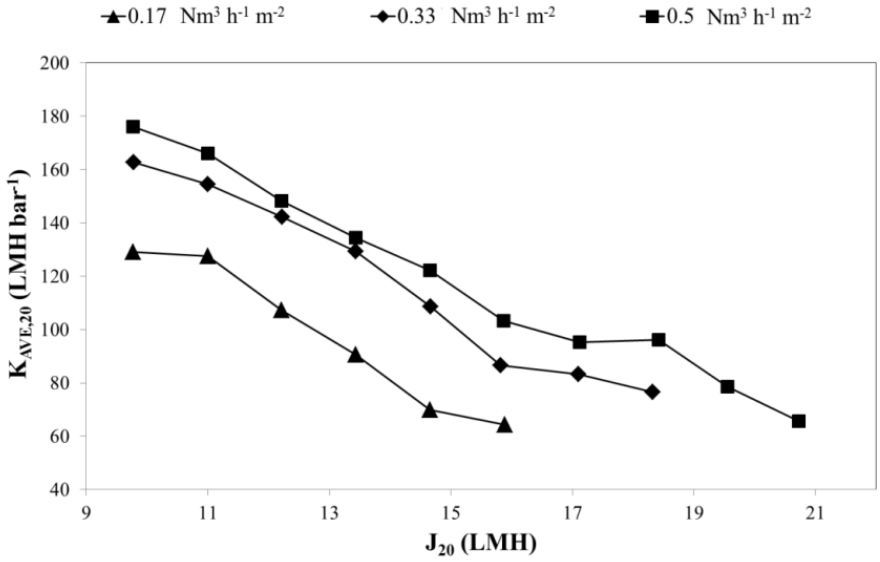

(b)

Figure 3.3 Results of short-term trials with an SGD_m of 0.17, 0.33, and 0.5 $Nm^3\ h^{-1}\ m^{-2}$: **(a)** effect of J_{20} on TMP_{AVE}; and **(b)** effect of J_{20} on K_{AVE20}.

Figure 3.3b shows how at similar J_{20} values the resulting $K_{AVE,20}$ decreases as SGD_m decreases. A flux of J_{20} = 15.8 LMH, for instance, resulted in a $K_{AVE,20}$ of 70, 90, and 110 LMH bar^{-1} at an SGD_m of 0.17, 0.33 and 0.5 $Nm^3\ h^{-1}\ m^{-2}$, respectively. It must be said that the K_{20} values predicted by these short-term trials are quite high taking into account the relatively high J_{20} applied and the low SGD_m applied. For instance, the K_{20} values of full-scale aerobic MBR plants treating domestic wastewater are generally between 150 and 250 LMH bar^{-1}, whilst the applied SGD_m is usually higher when

operating at similar J_{20} values [3.2]. On the other hand, it is well known that K_{20} depends considerably on the applied SGD_m. This dependency is related mainly to the contribution of the reversible fouling component (related to R_C) to the R_T. In this respect, the higher K_{20} obtained in the series of experiments conducted with an SGD_m level of 0.5 $Nm^3\ h^{-1}\ m^{-2}$ was related to the lowest cake layer formation rate. It must be said that according to the conceptual filtration model, two different effects determine R_C: the cake layer formation rate (due to the filtration process) and the cake layer removal rate (due mainly to biogas sparging). Thus, at an established MLTS concentration the cake layer removal efficiency decreases as SGD_m decreases. In this respect, long-term operating with a considerable amount of cake layer on the membrane surface throughout successive filtration stages could result in a higher propensity to irreversible fouling (related to R_I), due to greater cake layer formation and consolidation on the membrane surface.

3.3.2 Short-term trials: Effect of SGD_m on J_{CW}

Figure 3.4a shows the fouling rates (calculated using Eq. 3.8) during the short-term trials carried out at a MLTS of 23 g L^{-1} and different SGD_m levels. This figure shows the effect of the gas sparging intensity upon the membrane fouling rate at different values of J_{20}. It can be seen that there is a minimum J_{20} value (around 13 LMH) below which the fouling rate seems to be independent of both J_{20} and SGD_m. However, when J_{20} was above 13 LMH then the effect of J_{20} on the fouling rate declined when SGD_m increased. For instance, at a J_{20} of 12 LMH it is theoretically possible to operate membranes sub-critically with a gas sparging intensity of 0.17 $Nm^3\ h^{-1}\ m^{-2}$, a value that has to be increased to 0.5 $Nm^3\ h^{-1}\ m^{-2}$ in order to achieve a J_{20} of 19 LMH. These results predict that it is theoretically possible to maintain sub-critical filtration conditions (*i.e.* to operate at sustainable J_{20} values) when operating membranes at quite high MLTS levels, without applying a prohibitive SGD_m.

As mentioned before, these results confirm that the optimisation of the physical separation process in every operating range will result in significant energy savings in HF-SAnMBR systems. On the other hand, Figure 3.4b shows J_{CW} to be directly related to SGD_m at the selected operating conditions. This relationship predicts that it is theoretically possible to operate membranes sub-critically when J_{20} is between 12 and 19 LMH, and when SGD_m ranges from 0.17 to 0.50 $Nm^3\ h^{-1}\ m^{-2}$. Thus, a considerable increase in J_{20} can be achieved in sub-critical filtrations conditions by increasing SGD_m just slightly.

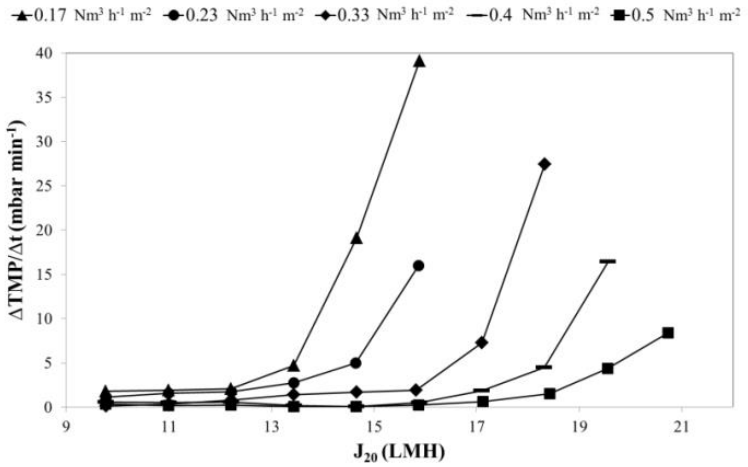

(a)

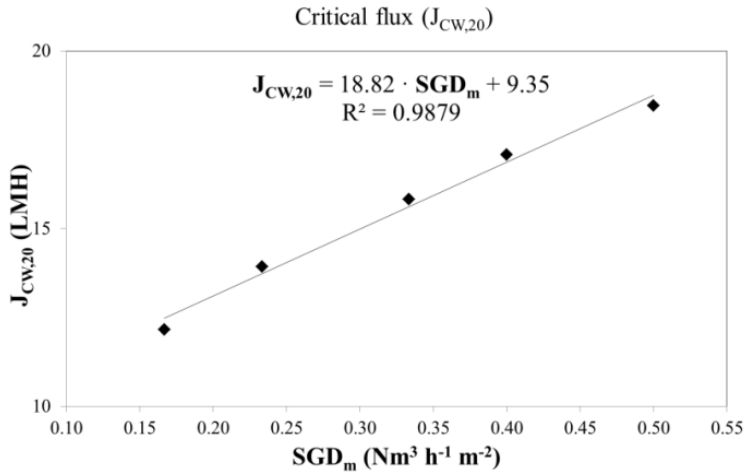

(b)

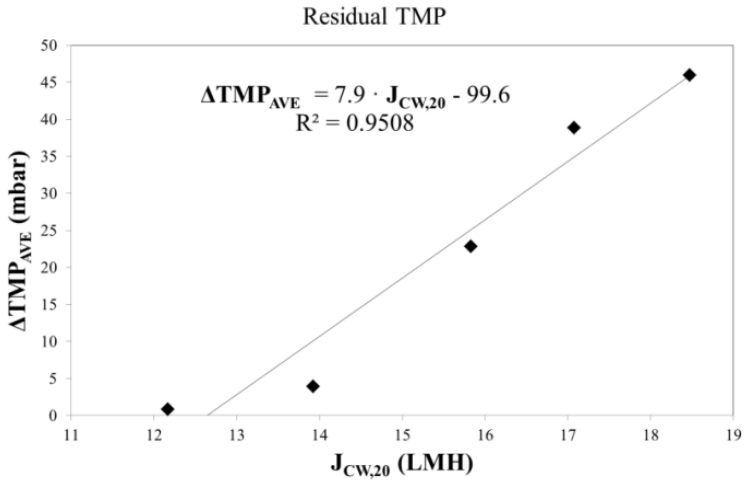

(c)

Figure 3.4 Results of short-term trials: **(a)** effect of J_{20} on membrane fouling rate with an SGD_m of 0.17, 0.23, 0.33, 0.4 and 0.5 $Nm^3\ h^{-1}\ m^{-2}$; **(b)** effect of SGD_m on J_{CW20}; and **(c)** effect of J_{CW20} on ΔTMP_{AVE}.

Table 3.1 summarises some of the J_C values found in literature under different operating conditions: membrane type and pore size, wastewater feed, MBR system, operating MLTS level, and air/gas sparging intensity. In contrast with other publications, results from our study revealed J_C to be closely related to SGD_m, as shown by the linear regression in Figure 3.4b. The high pseudoplastic behaviour of the sludge at high MLTS levels must be mentioned. In this respect, a considerable decrease in sludge viscosity was recorded by a rotation viscometer (from about 8000 to 400 cp) when the velocity gradient was increased (from 0.1 to 5 s^{-1}, respectively). This non-Newtonian behaviour of sludge may explain the significant increase in J_C when SGD_m increased. Guglielmi *et al*. [3.11] observed a slight dependency under aerobic conditions for MLTS concentrations of 10 g L^{-1}. The J_C values obtained by these authors were higher than those obtained in this study due to the lower operating MLTS level and the higher SGD_m applied. These results tally well with the behaviour observed in this study, which showed that above a certain SGD_m value the fouling rate becomes independent of J_{20} at a specific MLTS level. Howell *et al*. [3.20] obtained critical flux values ranging from 10 to 20 LMH (aerobic MBR, MLTS of 20 g L^{-1}, and upward airflow velocity (U_G) between 25 and 200 mm s^{-1}). These results are in agreement with the J_C values obtained in our study (carried out under similar conditions). Nevertheless, it is important to highlight that the results in Table 3.1 were obtained in laboratories and cannot, therefore, be automatically applied directly to full-scale plants since the effect of gas sparging upon membrane fouling depends considerably on fibre length and hydrodynamic conditions in membrane tanks.

These results confirm the need to optimise the gas sparging intensity for both every operating range and every membrane operating mode. As mentioned before, this enables not only considerable energy savings but also adequate long-term operating since it is possible to minimise the onset of irreversible fouling problems. In this respect, the main operating factors affecting membrane fouling should be also assessed: frequency and duration of the physical cleaning stages (back-flush and relaxation); treatment flow rate (which affects the J and thus the sub-critical filtration conditions); MLTS levels, which also affect the sub-critical conditions considerably; and cross-flow sludge velocity, which affects not only the removal of the cake layer but also the MLTS level in the membrane tank. Hence, it is essential to control the gas sparging to ensure adequate membrane scouring and thereby optimise the economic feasibility of HF membranes in SAnMBR systems.

Table 3.1 Critical flux: some experimental values found in literature. (Nomenclature: **FS**: Flat-Sheet; **HF**: Hollow-Fibre; MLTS: mixed liquor total solids level; $\mathbf{J_{C,20}}$: 20 ºC-normalised critical flux; $\mathbf{U_G}$: upward gas/airflow velocity; **(A/G)R**: air/gas rate; and $\mathbf{S(A/G)D_m}$: specific air/gas demand per m^2 of membrane area).

Membrane (type)	Pore (μm)	Influent (type)	MBR (type)	MLTS (g L^{-1})	$J_{C,20}$ (LMH)	U_G (mm s^{-1})	(A/G)R (Nm^3 h^{-1})	$S(A/G)D_m$ (Nm^3 m^{-2} h^{-1})	Reference
FS	0.22	Synthetic	UASB	< 0.55	30 - 50	--	--	--	[3.21]
FS	0.4	Synthetic	Aerobic	20	10 - 22	25 - 200	--	--	[3.20]
FS	0.4	Municipal	Aerobic	8	17.5	--	1.5	8.6	[3.22]
FS	0.8	Municipal	Aerobic	8	29.5	--	1.5	8.6	[3.22]
FS	0.2	Municipal	Aerobic	8	41.5	--	1.5	8.6	[3.22]
FS	0.45	Synthetic	Aerobic	10	25	300 - 600	--	--	[3.23]
FS	0.37	Municipal	Aerobic	14	5	--	0.18	--	[3.24]
FS	0.1	Municipal	Aerobic	10	50	--	0.4	--	[3.12]
Tubular	0.2	Synthetic	Aerobic	3	10	--	0.36	1.9	[3.10]
Tubular	0.2	Municipal	Aerobic	3	10	--	0.36	1.9	[3.10]
Tubular	0.2	Synthetic	Anaerobic	25	16 - 22	97 - 195	--	--	[3.13]
Tubular	0.2	Synthetic	Anaerobic	35	3 - 6	55 - 195	--	--	[3.25]
HF	0.1	Domestic	Aerobic	12 - 19	19	--	--	--	[3.26]
HF	0.4	Domestic	Aerobic	10 - 18	20	--	--	--	[3.26]
HF	0.04	Municipal	Aerobic	10	25 - 31	--	20.9 - 69.6	0.3 - 1.0	[3.4]
HF	0.04	Municipal	Aerobic	10	28	--	37.8	0.35	[3.11]
HF	0.05	Municipal	Anaerobic	23	12 - 19	50 - 160	5 - 15	0.17 - 0.5	Our study

3.3.3 Short-term trials: Effect of SGD_m on residual TMP

It has been observed by other authors that an increase in the average TMP (ΔTMP_{AVE}) at identical J_{20} can be obtained, between upward flux-stepping and downward flux-stepping (see Figure 3.2c). This increase could be related to "how much gas scouring is able to mechanically limit the extent of irreversible fouling due to the overcoming of the critical flux" [3.15]. Despite non-clear dependencies having been observed in our study between both ΔTMP_{AVE} and J_{20} in each flux-step, a direct dependency between the final ΔTMP_{AVE} and the J_{CW20} obtained in each short-term trial was observed (see Figure 3.4c). As shown in this figure, the higher the J_{CW20} obtained, the higher the residual TMP at the end of the short-term trial. This dependency reveals that SGD_m values higher than those resulting from the flux-step method are needed in order to minimise the possibility of membranes being irreversibly fouled during long-term operating. In this respect, membranes operating continuously at J_{20} levels similar to the theoretical J_{CW20} values calculated for the flux-step method could result in the incomplete removal of the cake layer from the membrane surface. This incomplete

removal increases the propensity of the cake layer to consolidate on the membrane surface, thus irreversible fouling may tend to increase. Hence, a higher SGD_m might be necessary when membranes are operated under near-critical conditions. For this reason, a critical flux security factor (ζ_{CF}) for long-term operation is recommended in our study. The ζ_{CF} values range from 0 to 1 (0.75 to 0.95 is the range recommended in our study). This factor multiplies the J_{CW20} value obtained in experiments, setting an operating J_{20} lower than the critical value predicted by the flux-step method. Hence, the main aim of this ζ_{CF} is to operate membranes sub-critically in order to minimise the possibility of irreversible fouling problems.

3.3.4 Long-term trials: Assessment of sub-critical filtration conditions

As mentioned before, it has been pointed out by several authors that the J_C resulting from the flux-step method cannot be used to estimate the critical flux in continuously operated full-scale systems because it is usually determined during a short-term experiment normally carried out off-line. However, this limitation was reduced in our study because the flux-step method was carried out with industrial membranes operating with real municipal wastewater and, therefore, with a biomass population and mixed liquor properties similar to those expected during long-term membrane operation. In addition, the following limiting factors related to the membrane size have been overcome: (1) membrane length, which is well-known to affect not only shear conditions and gas sparging efficiency, but also the TMP needed due to the axial pressure differential; (2) packaging density, which affects the hydrodynamics of the membrane tank considerably, and specifically the space inside the membrane package structure; and (3) the grade of lateral movement, which is affected considerably by the membrane module length and contributes to removing the cake layer. Thus, differences between the theoretical J_C values (calculated using the flux-step method) and those observed in long-term experiments have been reduced in this study. Hence, the membranes were seen to operate steadily at fluxes close to the theoretical J_C value.

Different long-term trials were carried out in order to assess the performance of membranes at specific sub-critical conditions similar to those expected in full-scale plants (*i.e.* variations in MLTS levels, variations in influent loads, etc). Figure 3.5 shows the K_{20} obtained in the long-term trials carried out with a J_{20} value of 10 LMH (Figure 3.5a) and 13.3 LMH (Figure 3.5b). The SGD_m in these long-term trials was 0.23 and 0.33 $Nm^3\ h^{-1}\ m^{-2}$ respectively. The J_{CW20} of these SGD_m and MLTS of 23 g L^{-1} resulted in 13 and 15 LMH, respectively. This figure also includes the MLTS level of the sludge fed to the membrane tank throughout the experimental periods. As mentioned before, this MLTS level increased in the membrane tank (up to 5 g L^{-1}) according to the ratio between the sludge flow-rate

entering the membrane tank and the net permeate flow rate. It is important to note the considerable variation in MLTS levels (from around 22 to 30 g L^{-1}) in the SAnMBR system throughout the long-term trials, due to considerable fluctuations in the influent concentration (*i.e.* 186 ± 61 mg L^{-1} of TSS). This figure shows the considerable effect of MLTS levels on K_{20} during the two experimental periods using different J_{20}. Every variation in the MLTS level was inversely reflected in the K_{20}. Nevertheless, even with high MLTS levels (up to 25 g L^{-1}), K_{20} remained at sustainable values (above 100 LMH bar^{-1}). This figure also shows that stable MLTS concentrations give quite stable K_{20} values. The stability of K_{20} could be attributed to the low TMP achieved during this period (around 0.1 bars), which illustrates low membrane and cake layer compression, resulting in a stable R_M value and an R_C value that only depends on the thickness of the cake layer, respectively. Moreover, the K_{20} improved when the MLTS decreased (see Figure 3.5b), which indicates the absence of an irreversible fouling component (related to R_I) on R_T. Therefore, only the dynamic component R_C was detected in this experimental period.

The results of this study suggest that sub-critical filtration conditions together with an adequate schedule of the different physical cleaning stages of membranes (relaxation and back-flush) enable long-term membrane operation and minimise the possibility of irreversible fouling problems. On the other hand, operating membranes with a suitable ζ_{CF} value could minimise the appearance of filtration problems. In this study, a ζ_{CF} ranging from around 80 to 90% was established for both 10 and 13.3 LMH long-term trials. It is a well-known fact that working with a ζ_{CF} could cause the design of MBR plants to be overdimensioned since a higher total filtration area is required for a specific J_{20}. However, this larger filtration area causes an increase in the membrane lifespan. Hence, a reduction in replacement and maintenance costs can be achieved. In this respect, after almost two years of operating the membranes at sub-critical levels, no irreversible fouling problems were detected, even at high MLTS levels.

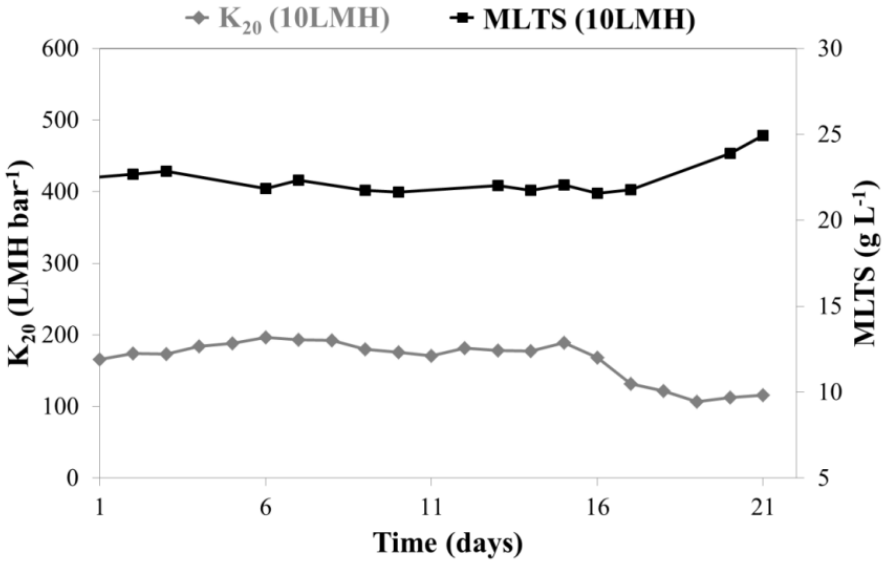

(a)

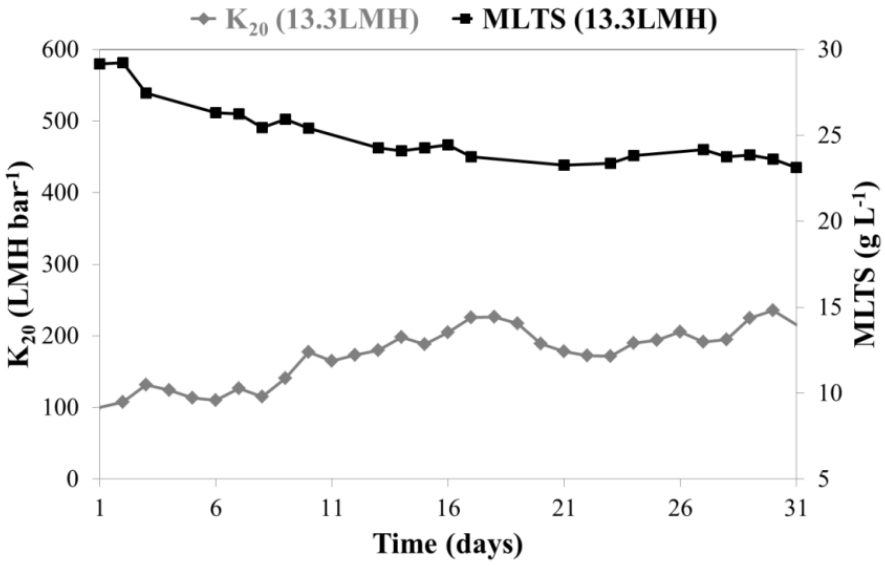

(b)

Figure 3.5 Long-term operating in sub-critical filtration conditions: **(a)** J_{20} of 10 LMH and SGD_m of 0.23 Nm^3 h^{-1} m^{-2}; and **(b)** J_{20} of 13.3 LMH and SGD_m of 0.33 Nm^3 h^{-1} m^{-2}.

Figure 3.6 shows the TMP profile obtained during the long-term operating period, as well as the MLTS level in the anaerobic sludge fed to the membrane tank. Both TMP and MLTS level are referred to its daily average value. This figure illustrates how the TMP was maintained at low values (around 0.1 bars) even for high MLTS levels (up to 25 g L^{-1}). Above this value, the TMP showed a sharp increase when the critical filtration conditions were exceeded. In fact, the TMP reached considerable high values (above 0.3 bars) for MLTS levels around 30 g L^{-1}. It is important to

emphasise that it was possible to operate membranes at low TMP with relatively low SGD_m values (around 0.23 $Nm^3\ h^{-1}\ m^{-2}$), even at high MLTS levels (up to 25 $g\ L^{-1}$).

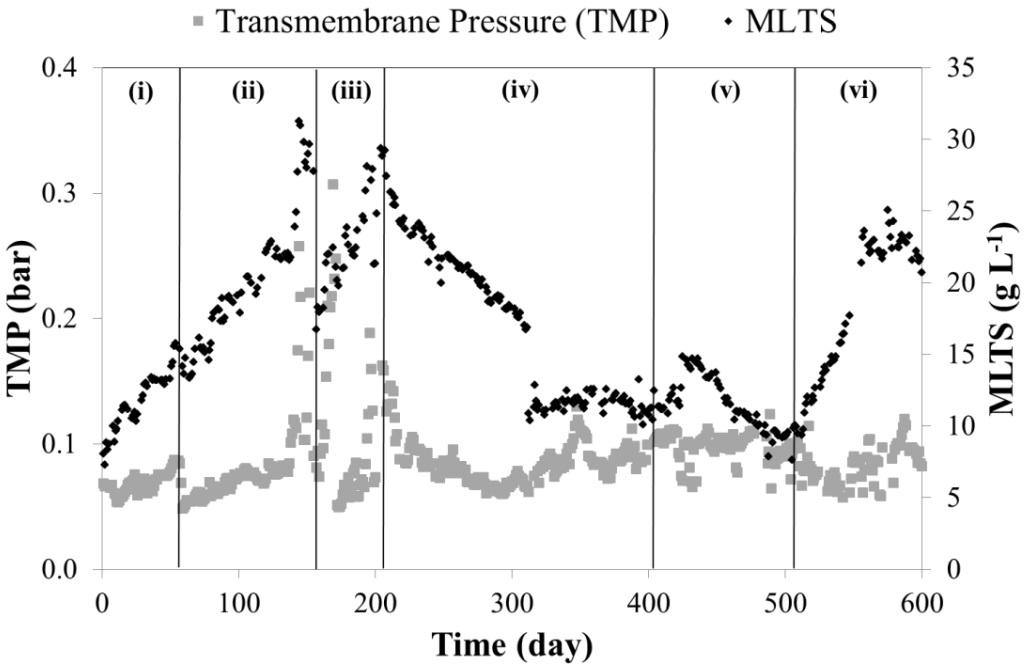

Figure 3.6 Long-term operation: evolution during the operating period of TMP and MLTS. (Experimental period: **(i)** J_{20} of 13.3 LMH and temperature of 33 ºC; **(ii)** J_{20} of 10 LMH and temperature of 33 ºC; **(iii)** J_{20} of 12 LMH and temperature of 25 ºC; **(iv)** J_{20} of 13.3 LMH and temperature of 20 ºC; and **(v)** J_{20} of 11 LMH and ambient temperature (spring and summer season, from 20 to 30 ºC); and **(vi)** J_{20} of 9 LMH and ambient temperature (autumn and winter seasons, from 30 to 15 ºC)).

The membranes therefore required non-chemical cleaning, mainly due to both operating in sub-critical filtration conditions and establishing an adequate membrane operating mode. However, further research is needed in order to gather more information about different operating conditions, information which will be necessary in order to carry out an exhaustive economic analysis of the proposed technology in comparison with existing technologies.

Finally, with regard to the biological process performance, in general low effluent VFA concentrations (< 30 mg COD L^{-1}), as well as significant methane-rich (over 70% v/v) biogas productions were observed (around 100 L d^{-1} in average), which evidenced a suitable biological process performance. Overall, high treatment efficiencies in term of COD removal were achieved (around 85 %). Further details on the biological process performance of this SAnMBR system can be found in Giménez *et al*. [3.16].

3.4 Conclusions

The results of this study suggest that HF-SAnMBR technology is promising for municipal wastewater treatment since it can consume less energy than aerobic MBRs. A linear dependency between the J_C and the SGD_m was observed. At MLTS above 22 g L^{-1}, J_C ranged from 12 to 19 LMH at quite low SGD_m values compared to aerobic MBRs (between 0.17 and 0.5 $Nm^3\ h^{-1}\ m^{-2}$, respectively). Long-term trials suggested that operating in sub-critical filtration conditions and an adequate operating mode can result in adequate and sustainable membrane performance.

3.5 Acknowledgements

This research work has been supported by the Spanish Research Foundation (CICYT Projects CTM2008-06809-C02-01 and CTM2008-06809-C02-02, and MICINN FPI grant BES-2009-023712) and Generalitat Valenciana (Projects GVA-ACOMP2010/130 and GVA-ACOMP2011/182), which are gratefully acknowledged.

3.6 References

3.1 H.J. Lin, K. Xie, B. Mahendran, D.M. Bagley, K.T. Leung, S.N. Liss, B.Q. Liao, Factors affecting sludge cake formation in a submerged anaerobic membrane bioreactor, J. Membr. Sci. 36 (2010), 126–134.

3.2 S. Judd, C. Judd, The MBR Book: Principles and Applications of Membrane Bioreactors in Water and Wastewater Treatment, Second Edition, ELVESIER, ISBN: 978-0-08-096682-3, 2011.

3.3 I.S. Chang, P.L. Clech, B. Jefferson, S. Judd, Membrane fouling in membrane bioreactors for wastewater treatment, J. Environ. Eng. 128 (2002), 1018–1029.

3.4 T. Stephenson, S. Judd, B. Jefferson, K. Brindle, Membrane Bioreactors for Wastewater Treatment, IWA publishing, London, UK, 2000.

3.5 B.Q. Liao, J.T. Kraemer, D.M. Bagley, Anaerobic membrane bioreactors: Applications and research directions, Crit. Rev. Env. Sci. Tec. 36 (2006), 489–530.

3.6 M.V.G. Vallero, G. Lettinga, P.N.L. Lens, High rate sulfate reduction in a submerged anaerobic membrane bioreactor (SAMBaR) at high salinity, J. Membr. Sci. 253 (2005), 217–232.

3.7 L. Dvořák, M. Gómez, M. Dvořáková, I. Růžičková, J. Wanner, The impact of different operating conditions on membrane fouling and EPS production, Bioresource Technol. 102 (2011), 6870–6875.

3.8 P. Bachin, P. Aimar, V. Sanchez, Model for colloidal fouling of membranes, AIChE J. 41 (1995), 368–377.

3.9 R.W. Field, D. Wu, J.A. Howell, B.B. Gupta, Critical flux concept for microfiltration fouling, J. Membr. Sci. 100 (1995), 259–272.

3.10 P. Le-Clech, B. Jefferson, I.S. Chang, S. Judd, Critical flux determination by the flux-step method in a submerged membrane bioreactor, J. Membr. Sci. 227 (2003), 81–93.

3.11 G. Guglielmi, D.P. Saroj, D. Chiarani, G. Andreottola, Sub-critical fouling in a membrane bioreactor for municipal wastewater treatment: Experimental investigation and mathematical modelling, Water Res. 41 (2007), 3903–3914.

3.12 P. van der Marel, A. Zwijnenburg, A. Kemperman, M. Wessling, H. Temmink, W. van der Meer, An improved flux-step method to determinate the critical flux and the critical flux for irreversibility in a membrane bioreactor, J. Membr. Sci. 332 (2009), 24–29.

3.13 G. Guglielmi, D. Chiarani, S.J. Judd, G. Andreottola, Flux criticality and sustainability in a hollow fibre submerged membrane bioreactor for municipal wastewater treatment, J. Membr. Sci. 289 (2006), 241–248.

3.14 D. Jeison, J.B. van Lier, Cake layer formation in anaerobic submerged membrane bioreactors (AnSMBR) for wastewater treatment, J. Membr. Sci. 284 (2006), 227–236.

3.15 S. Delgado, R. Villaroel, E. González, Effect of shear intensity on fouling in submerged membrane bioreactor for wastewater treatment, J. Membr. Sci. 311 (2008), 173–181.

3.16 J.B. Giménez, A. Robles, L. Carretero, F. Durán, M.V. Ruano, M.N. Gatti, J. Ribes, J. Ferrer, A. Seco, Experimental study of the anaerobic urban wastewater treatment in a submerged hollow-fibre membrane bioreactor at pilot scale, Bioresource Technol. 102 (2011), 8799–8806.

3.17 American Public Health Association/American Water Works Association/Water Environmental Federation, Standard methods for the Examination of Water and Wastewater, 21st edition, Washington DC, USA, 2005.

3.18 WRC, Simple titration procedures to determine H2CO3* alkalinity and short-chain fatty acids in aqueous solutions containing known concentrations of ammonium, phosphate and sulphide weak acid/bases, Report No. TT 57/92, Water Res. Commission, University of Cape Town, Pretoria, Republic of South Africa, 1992.

3.19 S. Rosenberger, C. Laabs, B. Lesjean, R. Gnirss, G. Amy, M. Jekel, J.C. Schrotter, Impact of colloidal and soluble organic material on membrane performance in membrane bioreactors for municipal wastewater treatment, Water Res. 40 (2006), 710–720.

3.20 J.A. Howell, H.C. Chua, T.C. Arnot, In situ manipulation of critical flux in a submerged membrane bioreactor using variable rates, and effects of membrane history, J. Membr. Sci. 242 (2004), 13–19.

3.21 B.D. Cho, A.G. Fane, Fouling transients in nominally sub-critical flux operation of a membrane bioreactor, J. Membr. Sci. 209 (2002), 391–403.

3.22 Z. Wu, Z. Wang, S. Huang, S. Mai, C. Yang, X. Wang, Z. Zhou, Effects of various factors on critical flux in submerged membrane bioreactors for municipal wastewater treatment, Sep. Purif. Technol. 62 (2008), 56–63.

3.23 W.S. Guo, S. Vigneswaran, H.H. Ngo, W. Xing, Comparison of membrane bioreactor systems in wastewater treatment, Desalination 231 (2008), 61–70.

3.24 A. Bottino, G. Capannelli, A. Comite, R. Margano, Critical flux in submerged membrane bioreactors for municipal wastewater treatment, Desalination 245 (2009), 748–753.

3.25 D. Jeison, J.B. van Lier, Cake formation and consolidation: Main factors governing the applicable flux in anaerobic submerged membrane bioreactors (AnSMBR) treating acidified wastewaters, Sep. Purif. Technol. 56 (2007), 71–78.

3.26 G. Guglielmi, Membrane bioreactors for municipal wastewater treatment, Ph.D. thesis, Universita' di Trento, Italy, 2002.

CHAPTER 4:

Factors that affect the permeability of commercial hollow-fibre membranes in a submerged anaerobic MBR (HF-SAnMBR) system

Abstract

A demonstration plant with two commercial HF ultrafiltration membrane modules (PURON®, Koch Membrane Systems, PUR-PSH31) was operated with urban wastewater. The effect of the main operating variables on membrane performance at sub-critical and supra-critical filtration conditions was tested. The physical operating variables that affected membrane performance most were gas sparging intensity and back-flush (BF) frequency. Indeed, low gas sparging intensities (around 0.23 $Nm^3\ m^{-2}\ h^{-1}$) and low BF frequencies (30 second back-flush for every 10 basic filtration-relaxation cycles) were enough to enable membranes to be operated sub-critically even when levels of mixed liquor total solids were high (up to 25 $g\ L^{-1}$). On the other hand, significant gas sparging intensities and BF frequencies were required in order to maintain long-term operating at supra-critical filtration conditions. After operating for more than two years at sub-critical conditions (transmembrane flux between 9 and 13.3 LMH at gas sparging intensities of around 0.23 $Nm^3\ m^{-2}\ h^{-1}$ and MLTS levels from around 10 to 30 $g\ L^{-1}$) no significant irreversible/irrecoverable fouling problems were detected (membrane permeability remained above 100 LMH bar^{-1} and total filtration resistance remained below $10^{13}\ m^{-1}$), therefore no chemical cleaning was conducted. Membrane performance was similar to the aerobic HF membranes operated in full-scale MBR plants.

Keywords

Critical flux; gas sparging; industrial hollow-fibre membranes; modified flux-step method; submerged anaerobic membrane bioreactor.

Highlights

Membrane performance in SAnMBR treating urban wastewater was similar to aerobic MBRs.
The main variables affecting K_{20} under sub/supra-critical conditions were tested.
SGD_m and BF are the physical variables that affect membrane performance most.
No chemical cleaning was needed after two years operating sub-critically.
K_{20} remained above 100 LMH bar^{-1} and RT below $10^{13}\ m^{-1}$.

A. Robles, M.V. Ruano, J. Ribes, J. Ferrer
Factors that affect the permeability of commercial hollow-fibre membranes in a submerged anaerobic MBR (HF-SAnMBR) system
Water Res. 47 (2013), 1277 – 1288

4.1 Introduction

4.1.1 Anaerobic treatment of urban wastewater using MBR technology

As previously introduced, in recent years there has been increased interest in assessing the feasibility of the anaerobic treatment of urban wastewater at ambient temperatures. This interest focuses on the sustainable advantages of anaerobic rather than aerobic processes, *i.e.* anaerobic processes generate little sludge due to the low anaerobic biomass yield; consume little energy because no aeration is needed; and generate biogas that can be used as an energy resource. The total greenhouse gas emissions of this technology are, therefore, low because low energy consumption indirectly means low gas emissions. The main challenge of anaerobic biotechnology is to develop treatment systems that prevent biomass loss and enable high sludge retention times (SRTs) in order to offset the low growth rates of anaerobic biomass at ambient temperatures [4.1]. In this respect, submerged anaerobic membrane bioreactors (SAnMBRs) are a promising technology for urban wastewater treatment. However, operating membrane bioreactors with high SRTs may lead to high mixed liquor total solids (MLTS) at a specific reacting volume. This is one of the main constraints of using membranes [4.2] since it can result in high membrane fouling propensities.

4.1.2 Membrane fouling in SAnMBRs

The key challenge in SAnMBR technology is how to optimise membrane operation in order to minimise any kind of membrane fouling, especially the irrecoverable/permanent component that cannot be eliminated by chemical cleaning. The extent of irrecoverable/permanent fouling is what ultimately determines the membrane lifespan [4.3; 4.4; 4.5]. Several strategies to control fouling (see, for example, Liao *et al*. [4.6]) aim to optimise filtration whilst minimising investment and operating costs. In this respect, the SAnMBR design strategy must be carefully selected. Depending on the design strategy, different design criteria can be adopted. One such criterion is based on operating membranes in sub-critical filtration conditions that are limited by the so-called critical flux (J_C) [4.7; 4.8]. Operating membranes sub-critically gives membranes long lifespans, which reduces replacement and maintenance costs (by minimising physical cleaning costs, *i.e.* membrane scouring or back-flush). In this respect, MLTS has been widely identified as one of the factors that affect J_C most. Thus, an investment compromise between operating reactor volume and filtration area should be selected in order to keep MLTS at sub-critical levels for a given transmembrane flux (J). Another design criterion is based on operating membranes at critical or supra-critical filtration conditions. This reduces initial

investment costs because it requires lower operating volumes and/or lower membrane surfaces than when operating membranes at sub-critical filtration conditions, however, replacement, maintenance and operating costs are probably higher.

Regardless of the design criterion adopted, it is necessary to determine which filtration conditions [4.9] are most suitable in order to optimise the membrane module design and configuration. An exhaustive analysis in the different potential operating conditions is, therefore, necessary in order to optimise both membrane lifespan (*i.e.* membrane replacement cost) and operating and maintenance costs (*i.e.* the cleaning mechanism). In this respect, it is necessary to assess the impact of the main operating variables upon membrane performance, *i.e.* frequency and duration of the physical cleaning stages (back-flush and relaxation); gas sparging intensity; cross-flow sludge velocity over the membrane surface (for cross-flow membrane configurations); up-flow sludge velocity in the membrane tank (submerged membrane configurations) which determines the sludge concentration factor when the membranes are located in external tanks; and maximum operating transmembrane pressure (TMP).

4.1.3 Full-scale implementation of SAnMBRs

Membrane technology has been used increasingly to treat wastewater over the last decade [4.10] even in large urban WWTPs. The treatment capacity of urban MBR WWTP has significantly increased (to maximum design flow rates of more than 150000 m^3 day^{-1}) in just a few years [4.11]. As regards membrane configuration, flat sheet (FS) membranes are used mostly in small plants (< 5000 m^3 d^{-1}), whilst hollow fibre (HF) membranes are used for the entire flow range and prevail in large plants (> 10000 m^3 d^{-1}) and account for about 75% of all total MBR installed capacity [4.12].

Nevertheless, it is important to highlight that all these urban MBR WWTPs are aerobic wastewater treatments. Although MBR technology has not yet been applied to full-scale anaerobic urban wastewater treatment, the scientific community is showing increasing interest in the feasibility of its full-scale implementation because of the above-mentioned advantages. Indeed, several studies which assess the feasibility of using SAnMBR technology to treat urban wastewater at the laboratory scale have been published [4.13; 4.14; 4.15]. However, the impact of the main operating conditions upon membrane fouling cannot be determined exactly at the lab scale because they depend heavily on the membrane size. In HF membranes in particular, HF length is a key performance parameter. In this respect, there is still a lack of thorough knowledge about fouling mechanisms, mainly as regards hydraulic performance and membrane permeability [4.16; 4.17; 4.18]. In addition, it is expected that

membrane fouling will be affected to a considerable degree by the different characteristics of aerobic and anaerobic mixed liquors, such as particle size distribution, extracellular polymeric substances (EPS), soluble microbiological products (SMP), biomass concentration, inorganic and organic compounds [4.19], or pH values affecting both biofouling [4.20] and formation of chemical precipitates.

Therefore, since membrane performance cannot be scaled up directly from laboratory to plant dimensions, especially in the case of HF-based technology [4.6], further studies of HF-SAnMBR technology on an industrial scale are needed in order to facilitate its design and implementation in full-scale wastewater treatment plants (WWTPs).

To gain more insight into the optimisation of the physical separation process in a SAnMBR system at the industrial scale, this paper shows the impact of the main operating variables upon the performance of industrial HF membranes. Gas sparging intensity, up-flow sludge velocity in the membrane tank, duration and frequency of the different physical cleaning stages (relaxation and back-flush), and length of filtration stage were evaluated in an SAnMBR system featuring commercial HF membrane modules. The effect of these variables at two different membrane operating conditions (sub-critical and critical/supra-critical filtration conditions) was assessed. The plant was operated using Carraixet WWTP pre-treatment effluent (Valencia, Spain). On the basis of the results obtained this study aims to provide guidelines for the sub-critical and critical operation of commercial HF membranes in an SAnMBR system.

4.2 Materials and methods

4.2.1 Demonstration plant description

This study was conducted in the HF-SAnMBR demonstration plant already described in Chapter 2. It consists mainly of an anaerobic reactor with a total volume of 1.3 m^3 connected to two membrane tanks each with a total volume of 0.8 m^3. Each membrane tank has one industrial HF ultrafiltration membrane unit (PURON®, Koch Membrane Systems (PUR-PSH31) with 0.05 μm pores). Each module has 9 HF bundles, 1.8 m long, giving a total membrane surface of 30 m^2. Normal membrane operation entails a specific schedule involving a combination of different individual stages taken from a basic filtration-relaxation (F-R) cycle. In addition to traditional membrane operating stages (filtration, relaxation and back-flush), another two stages of membrane operation were considered:

degasification and ventilation. For further details of this SAnMBR demonstration plant see Giménez *et al*. [4.21] and Robles *et al*. [4.22].

4.2.2 Operating conditions

The demonstration plant was fed with effluent from pre-treatment of a full-scale WWTP (screening, degritter, and grease removal), which main component is domestic type. It is important to emphasise the great variation in the characteristics of the anaerobic reactor influent (*e.g.* 186 ± 61 mg L^{-1} of TSS and 388 ± 95 mg L^{-1} of total COD), which is reflected by the high standard deviation of each parameter. The plant was operated using an SRT of 70 days on operating days 1 to 445, and an SRT of 40 days on operating days 446 to 600. Hydraulic retention times (HRTs) ranged from 5 to 24 hours. The temperature varied from around 33 to 15 ºC. The pH of the mixed sludge ranged from 6.5 to 7.1, and carbonate alkalinity remained at values of around 600 mg$CaCO_3$ L^{-1}.

We studied how membranes operate in both short-term trials and in the long term. In the latter instance, the membrane underwent 300-second basic F-R cycles (250 s filtration and 50 s relaxation) with 30 seconds of back-flush every 10 cycles, 40 seconds of ventilation every 10 cycles, and 30 seconds of degasification every 50 cycles. In addition, six different J_{20} and temperature conditions were tested: 13.3, 10, 12, 13.3, 11 and 9 LMH, at controlled temperatures of 33, 33, 25, and 20 ºC, spring and summer ambient temperatures (from approx. 20 to 30 ºC), and autumn and winter ambient temperatures (from approx. 30 to 14 ºC), respectively. Hence, the overall operating period was divided into six experimental periods (periods i, ii, iii, iv, v and vi) taking into account both J_{20} and temperature. The average specific gas demand per membrane area (SGD_m) was 0.23 Nm^3 h^{-1} m^{-2}. A maximum TMP safety value of 0.4 bars was set. The flow of sludge through the membrane tank was set to 2700 L h^{-1}, giving an up-flow sludge velocity of 2.7 mm s^{-1}.

In order to evaluate the critical filtration conditions throughout the long-term membrane performance, different short-term trials (flux-step type, see Robles *et al*. [4.28]) were carried out. For instance, on day 125 and day 590 (operating with MLTS of 23 g L^{-1} and SGD_m of 0.23 Nm^3 h^{-1} m^{-2}), the critical flux resulted in 14 and 10.5 LMH, respectively. Therefore, the critical flux remained generally at values over 10.5 – 14 LMH during the operating period since SGD_m was maintained at 0.23 Nm^3 h^{-1} m^{-2} and MLTS remained mostly below 23 g L^{-1}. Hence, the long-term operating shown in this study was mainly carried out at sub-critical filtration conditions (J_{20} was varied from 9 to 13.3 LMH).

In addition, several short-term trials were conducted at sub-critical and supra-critical filtration conditions with varying gas sparging intensities, up-flow sludge velocities in the membrane tank, durations and frequencies of the different physical cleaning stages (relaxation and back-flush), and lengths of filtration. Normally, the membrane was operated with 300-second basic F-R cycles (250 s filtration and 50 s relaxation), 30 seconds of back-flush every 10 cycles, 40 seconds of ventilation every 10 cycles, and 30 seconds of degasification every 50 cycles, whilst the operating J_{20} was 10 LMH, the average SGD_m was 0.23 $Nm^3\ h^{-1}\ m^{-2}$, and the up-flow sludge velocity was 2.7 mm s^{-1}. Table 4.1 summarises the values of the operating variables studied in each short-term trial. In each trial, the sub-critical and supra-critical conditions were determined by the different levels of MLTS. The J_{20} in these short-term trials was set to 10 LMH, whilst the other operating variables of the membrane operating mode were established in the same way as the general, long-term operating conditions mentioned above.

Table 4.1 Short-term trials operating conditions (Nomenclature: **MLTS**: mixed liquor total solid; **SGD_m**: specific gas demand per membrane area; **BF**: back-flush; and **F-R**: filtration-relaxation)

Trial	Variable studied	Sub-critical conditions		Supra-critical/Critical conditions	
		Value	**MLTS ($g\ L^{-1}$)**	**Value**	**MLTS ($g\ L^{-1}$)**
1	SGD_m ($Nm^3\ h^{-1}\ m^{-2}$)	0.17, 0.23, 0.3, 0.4	20	0.17	30
				0.23	28, 31.5
2	Up-flow sludge velocity (mm s^{-1})	1.3	18	1.0, 2.2, 2.7	28
3	BF frequency (BF:F-R)	1:10, 1:30	24	1:10, 1:30	28, 31.5
4	Relaxation stage duration (seconds)	30, 50	25	30, 50	28
5	Filtration stage duration (seconds)	250, 350, 450 (1BF:10F-R)	23	250 (1BF:10F-R)	31.5
		250, 350, 450 (1BF:30F-R)		250 (1BF:30F-R)	

4.2.3 Analytical methods

4.2.3.1 Analytical monitoring

In addition to the on-line process monitoring, the performance of the biological process was assessed by taking 24-hour composite samples of the influent and effluent streams, and taking grab samples of anaerobic sludge once a day. The following parameters were analysed daily: total solids (TS); total suspended solids (TSS); volatile suspended solids (VSS); carbonate alkalinity; and nutrients (ammonium (NH_4-N) and orthophosphate (PO_4-P)). The total and soluble chemical oxygen demand (COD_T and COD_S, respectively) were determined once a week.

Solids, COD, and nutrients were determined according to Standard Methods [4.23]. Carbonate alkalinity was determined by titration according to the method proposed by WRC [4.24].

4.2.3.2 Membrane performance indices

The 20 ºC-normalised membrane permeability (K_{20}) was calculated using a simple filtration model (Eq. 4.1) that takes into account the TMP and J data monitored online. This simple filtration model includes temperature correction (Eq. 4.2) to account for the dependence of permeate viscosity on temperature [4.25], and therefore the 20 ºC-normalised transmembrane flux (J_{20}) was calculated by applying Eq. 4.3. Relative membrane permeability (K_0) was used to assess the effect of the different operating factors on membrane performance. This relative permeability was defined as shown in Eq. 4.4. Total membrane resistance (R_T) was theoretically represented by the following partial resistances (Eq. 4.5): membrane resistance (R_M); cake layer resistance (R_C); irreversible layer resistance (R_I); and irrecoverable layer resistance (R_{IC}).

$$K_{20} = \frac{J_T f_T}{TMP} \qquad \textbf{Eq. 4.1}$$

$$f_T = \exp\left(-0.0239\,(T-20)\right) \qquad \textbf{Eq. 4.2}$$

$$J_{20} = J_T \cdot \exp\left(-0.0239\,(T-20)\right) \qquad \textbf{Eq. 4.3}$$

$$K_0(t) = \frac{K_{20}(t)}{K_{20}(t=0)} \qquad \textbf{Eq. 4.4}$$

$$R_T = R_M + R_C + R_I + R_{IC} \quad \textbf{Eq. 4.5}$$

Moreover, J_C was determined by applying a modified flux-step method based on the method proposed by van der Marel *et al*. [4.26]. J_C was calculated according to its weak concept: the flux below which TMP and J are not directly related. When applying this method, the duration of both filtration and relaxation stages was set to 15 min. Flux-stepping was arbitrarily set to 1.22 LMH of J_{20} (equivalent to a permeate flow rate of 50 L h^{-1}). The relaxation stages were conducted using the same SGD_m as in the filtration stages. For further details about the applied flux-step method, see Robles *et al*. [4.22].

4.3 Results and discussion

4.3.1 Long-term performance

Figure 4.1 depicts the average daily K_{20} (Figure 4.1a) and the average daily R_T (Figure 4.1b) obtained during the operating period, and the average daily MLTS in the anaerobic sludge entering the membrane tank. It must be said that the MLTS level in the membrane tank increased by up to 5 g L^{-1}, depending on the ratio between the net permeate flow rate and the sludge flow rate entering the membrane tank. The results shown in Figure 4.1 can be divided in two different long-term operating periods according to the irreversible/ irrecoverable fouling component observed: (1) days 1 to 300; and (2) days 300 to 600. It is important to note that since no chemical cleaning was conducted throughout the operating period, it was not possible to determine the single contribution to R_T of both R_I and R_{IC}.

Up to operating day 300, no significant irreversible/irrecoverable fouling was observed, since K_{20} and R_T recovered to values very close to the values obtained at the beginning of the long-term operation as MLTS decreased. This behaviour indicated that throughout this operating period, R_T was mainly related to R_C (R_I was negligible), whilst a relatively constant contribution of about $5 \cdot 10^{11}$ m^{-1} (at 650 LMH bar^{-1} of K_{20} treating clean water in similar operating conditions) was attributed to R_M. This behaviour means that the MLTS level is a key factor as regards membrane permeability in this HF-SAnMBR system [4.27]. In this respect, Figure 4.1a illustrates how every variation in MLTS was inversely reflected by K_{20}. Nevertheless, it is important to note that even at high MLTS levels (up to 25 g L^{-1}) and relatively low SGD_m values (around 0.23 Nm^3 h^{-1} m^{-2}), K_{20} and R_T remained at sustainable values, above 100 LMH bar^{-1} and below $3 \cdot 10^{12}$ m^{-1}, respectively. At MLTS of more than 25 g L^{-1}, K_{20} showed fell sharply because the 20 ºC-normalised J_C was exceeded: 10 and 13 LMH when operating at 0.23 Nm^3 h^{-1} m^{-2} of SGD_m and MLTS levels of 28 and 23 g L^{-1}, respectively (close

to the operating membrane fluxes). Thus, at MLTS levels higher than 25 g L^{-1}, an SGD_m of 0.23 Nm^3 h^{-1} m^{-2} was not enough to maintain sub-critical filtration conditions.

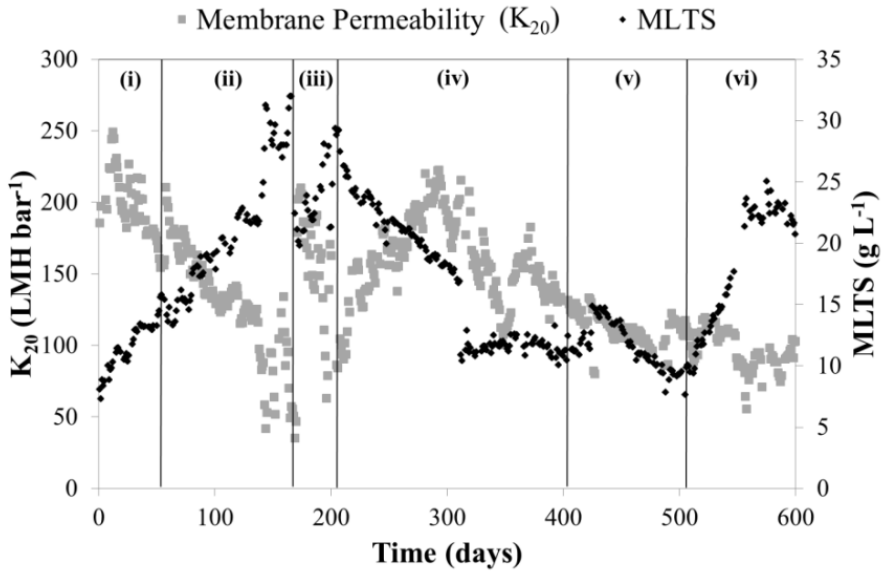

(a)

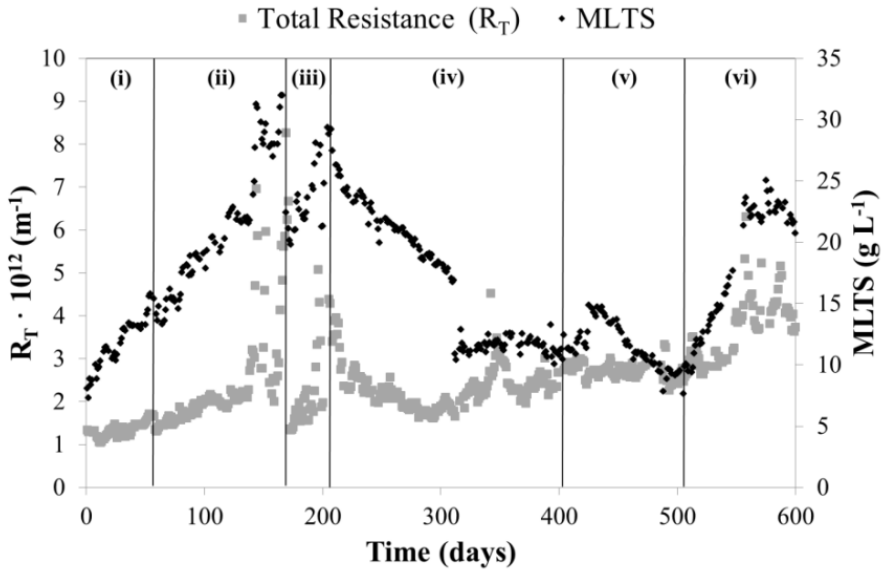

(b)

Figure 4.1 Long-term operation: evolution of **(a)** K_{20} and MLTS; and **(b)** R_T and MLTS. Experimental periods: **(i)** J_{20} of 13.3 LMH and temperature of 33 ºC; **(ii)** J_{20} = 10 LMH and T= 33 ºC; **(iii)** J_{20} = 12 LMH and T= 25 ºC; **(iv)** J_{20} = 13.3 LMH and T= 20 ºC; and **(v)** J_{20} = 11 LMH and ambient temperature (spring and summer, from about 20 to 30 ºC); and **(vi)** J_{20} = 9 LMH and ambient temperature (autumn and winter, from about 30 to 15 ºC).

After operating day 300, a slight downward trend in K_{20} and a slight upward trend in R_T were observed even when operating at a more or less stable MLTS level (see period day 300 to 400). This behaviour revealed a progressive accumulation of irreversible/irrecoverable fouling over the membrane surface after one year of operation and R_I/R_{IC} was detected along this period. Nevertheless, it must be emphasised that the membranes did not require any chemical cleaning after more than two years of operation, even with high MLTS and temperature shocks affecting the biomass population and the derived compounds. These results revealed that reversible fouling was successfully removed from the membrane surface and that irreversible fouling was low, mainly due to applying physical cleaning mechanisms (relaxation, back-flush and shear intensity gas sparging) and operating membranes under sub-critical filtration conditions.

These results suggested that operating membranes under sub-critical filtration conditions during long-term operation minimises the likelihood of membranes being irreversibly fouled. However, it is well known that operating membranes under sub-critical rather than critical levels implies a higher total filtration area at a given J_{20}. Nevertheless, this larger filtration area will probably increase the membrane lifespan whilst decreasing maintaining necessities. Hence, a reduction in replacement, maintenance and operating costs can be achieved.

4.3.2 Short-term trials: main factors affecting membrane performance

4.3.2.1 Effect of gas sparging intensity

Different sub-critical short-term trials were carried out at 0.17, 0.23, 0.33 and 0.40 $Nm^3\ h^{-1}\ m^{-2}$ of SGD_m and MLTS of 20 g L^{-1}. An almost stable K_0 close to 1 (*i.e.* K_{20} (t) remained very close to K_{20} (t=0)) was achieved in all trials. Thus, low fouling rates were observed (lower than 10 mbar min^{-1}). Membrane permeability recovered to the initial value of the short-term trial, indicating that no irreversible fouling component was detected. These results reveal that a SGD_m of 0.17 $Nm^3\ h^{-1}\ m^{-2}$ (equal to 5 cm s^{-1} *i.e.* the minimum value supplied by the blower) was enough to completely remove the reversible fouling from the membrane surface.

4.3.2.1.1 Major role of gas sparging intensity when operating supra-critically

Figure 4.2 shows the resulting K_0 at different SGD_m when the membranes were operated with high MLTS, and thereby at supra-critical filtration conditions. The SGD_m was set to 0.23 $Nm^3\ h^{-1}\ m^{-2}$ when the MLTS level fed to the membrane tank was 28 and 31.5 g L^{-1}, whilst the SGD_m was set to 0.17 Nm^3

h^{-1} m^{-2} when operating at an MLTS of 30 g L^{-1}. As it can be observed in Figure 4.2, even operating at similar MLTS levels, the two short-term trials carried out at MLTS of 28 and 30 g L^{-1} and different SGD_m resulted in quite different behaviours. A sharp decrease in K_0 was detected in the short-term trial conducted at the lowest SGD_m (0.17 Nm^3 h^{-1} m^{-2}). In these operating conditions, a considerable increase of the reversible fouling rate was observed throughout the trial (up to 80 mbar min^{-1}). In this case, the SGD_m applied was not enough to fulfil the membrane scouring necessities, and the filtration process was stopped because the maximum TMP (safety value set to 0.4 bars) was reached. On the other hand, in the trial carried out at 0.23 Nm^3 h^{-1} m^{-2} (equal to 7 cm s^{-1}) and an MLTS of 28 g L^{-1}, K_0 did not reach unsustainable values (the reversible fouling rate remained at values lower than 25 mbar min^{-1}.). However, K_0 decreased continuously throughout the trial as the reversible fouling was accumulated over the membrane. This accumulation could lead to a high irreversible/irrecoverable fouling propensity.

It is important to highlight that the SGD_m applied in these short-term trials (0.23 Nm^3 h^{-1} m^{-2}) was quite low compared to the typical operating range the supplier proposed for aerobic processes (from 0.3 to 0.7 Nm^3 h^{-1} m^{-2}).

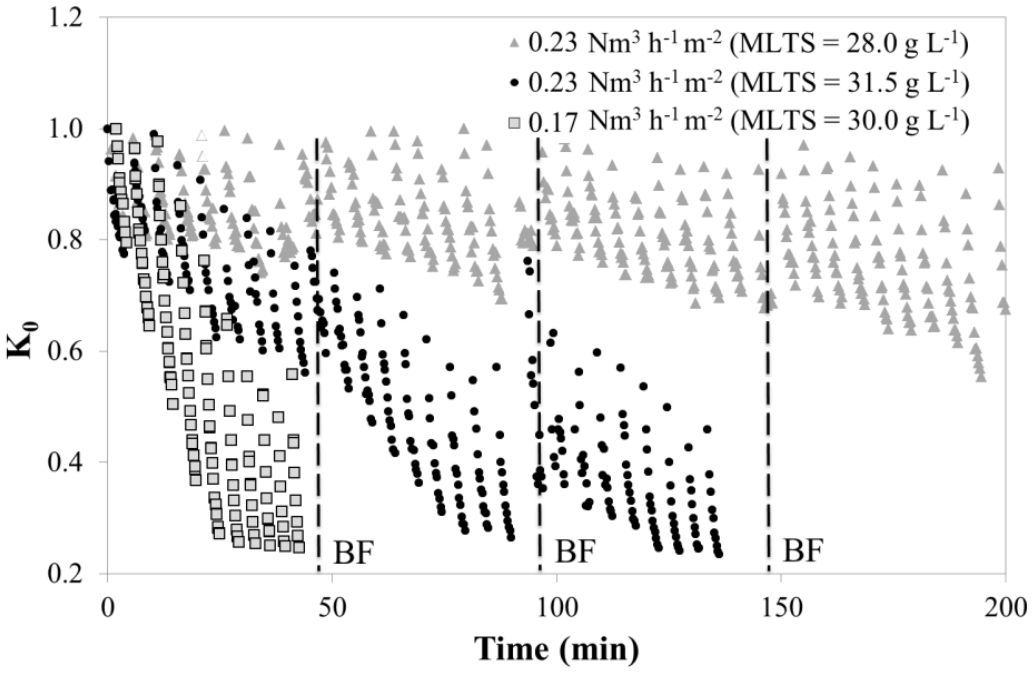

Figure 4.2 . Short-term trial 1: Effect of gas sparging intensity on membrane permeability at MLTS level of 28, 30 and 31.5 g L^{-1}. Nomenclature: **MLTS**: mixed liquor total solids; **K_0**: unit-normalised membrane permeability; **BF**: back-flush.

As Figure 4.2 shows, an increase in MLTS from 28 to 31.5 g L^{-1} at the same SGD_m (0.23 Nm^3 h^{-1} m^{-2}) resulted in a significant decrease of K_0. In the trial with an MLTS of 31.5 g L^{-1}, an increase in the membrane reversible fouling rate of up to 80 mbar min^{-1} was observed. The maximum TMP value was reached after 140 minutes and the trial was stopped. Hence, as a result of operating under critical filtration conditions, small variations in the MLTS concentration affected membrane performance considerably. Nevertheless, previous studies (flux-step type, see Robles *et al*. [4.22]) showed that it is theoretically possible to operate sub-critically at 10 LMH of J_{20} and MLTS of 28 g L^{-1} when SGD_m is about 0.25 Nm^3 h^{-1} m^{-2}. Therefore, it is assumed that gas sparging intensities around 0.3 – 0.5 Nm^3 h^{-1} m^{-2} may keep K_0 at proper values when operating at MLTS levels around 30 – 31.5 g L^{-1}.

The results shown in Figure 4.2 suggest that when membranes are operated supra-critically at low specific SGD_m the duration and/or frequency of the physical cleaning stages (relaxation and back-flush) must be increased considerably. On the other hand, in order to operate the membranes sub-critically at 13.3 LMH of J_{20} and MLTS levels of 23 and 28 g L^{-1}, the theoretical SGD_m required is approx. 0.23 and 0.45 Nm^3 h^{-1} m^{-2} (both calculated using the flux-step method), respectively. In contrast, SGD_m values lower than 0.1 Nm^3 h^{-1} m^{-2} are theoretically needed when operating sub-critically at 13.3 LMH of J_{20} and MLTS levels of 11.5 g L^{-1}, which are quite low when compared with aerobic MBR technology operating in similar conditions.

4.3.2.1.2 Gas sparging intensity as a key operating parameter for optimising SAnMBRs at the industrial scale

The results obtained confirm the need to optimise the gas sparging intensity in all membrane operating conditions. The gas sparging intensity poses a major challenge since it must be minimised in order to maximise energy savings. It is important to emphasise that aeration energy can account for up to 50 - 75% of all the energy consumed by aerobic MBR technology [4.29]. Not only can considerable energy savings be achieved but also appropriate long-term operating because the onset of irreversible/irrecoverable fouling problems can be minimised.

Hence, controlling gas sparging to ensure appropriate membrane scouring is mandatory in order to optimise the economic feasibility of operating HF membranes in full-scale SAnMBR systems. In this respect, several recently-published studies assess different monitoring strategies designed to save energy in aerobic MBR technology (see, for instance, Huyskens *et al*. [4.30]; Ferrero *et al*. [4.31]). Nevertheless, the applicability of these control strategies for saving energy in SAnMBR technology on an industrial scale has yet to be evaluated.

4.3.2.2 Effect of up-flow sludge velocity in the membrane tank

Figure 4.3 illustrates how the up-flow sludge velocity in the membrane tank affects membrane performance. This operating variable is related to the sludge concentration factor resulting from the ratio between the sludge flow entering the membrane tank and the net permeate flow. For instance, Eq. 4.6, Eq. 4.7 and Eq. 4.8 show the expected MLTS level in the membrane tank as a function of the MLTS level in the sludge fed to the membrane tank when the up-flow sludge velocity is set to 1.0, 2.2 and 2.7 mm s^{-1}, respectively. This expected MLTS was calculated on the basis of a mass balance according to the above-mentioned ratio between the sludge flow entering the membrane tank and the net permeate flow (*i.e.* according to the applied up-flow sludge velocity in the membrane tank). The permeate flow rate was set to a constant value of 300 L h^{-1} (J_{20} of 10 LMH). As indicated by Eq. 4.6, Eq. 4.7 and Eq. 4.8, MLTS could theoretically rise to 43, 16 and 12% when the up-flow sludge velocity is set to 1.0, 2.2 and 2.7 mm s^{-1}, respectively. Hence, the MLTS in the membrane tank could reach prohibitive values when the concentration in the sludge entering the membrane tank has considerably high values. For instance, when the MLTS entering the membrane tank is 25 g L^{-1} and the up-flow sludge velocity is 2.7 mm s^{-1} (the maximum studied value), the MLTS recycled to the anaerobic reactor is expected to be around 28 g L^{-1}.

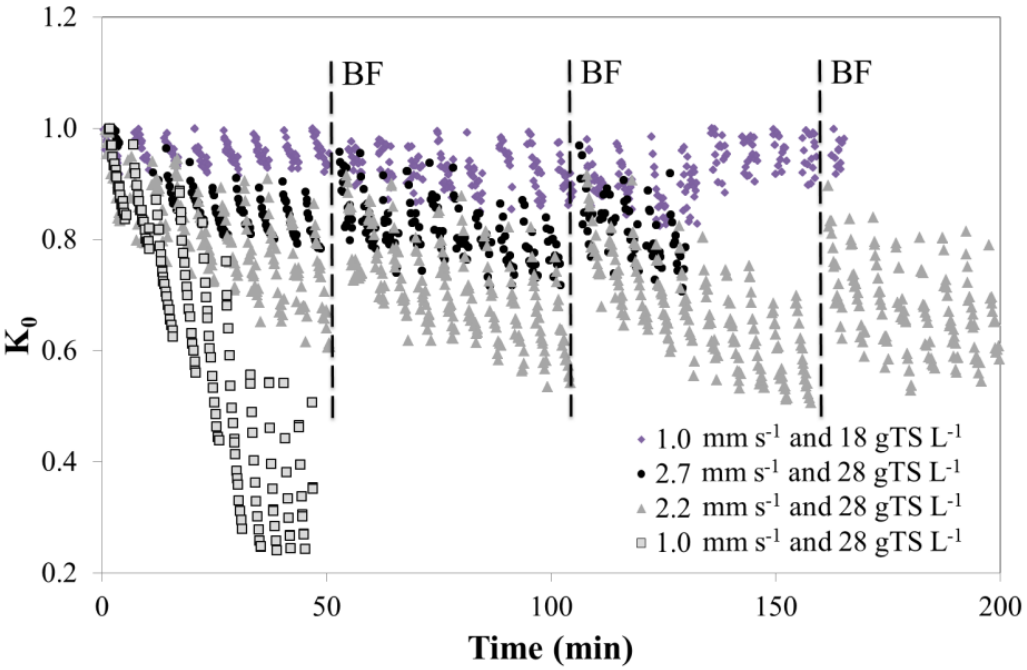

Figure 4.3 Short-term trial 2: Effect of up-flow sludge velocity on membrane permeability at MLTS levels of 18 and 28 g L^{-1}, and up-flow sludge velocity of 1.0, 2.2, and 2.7 mm s^{-1}. Nomenclature: **MLTS**: mixed liquor total solids; **TS**: total solids; $\mathbf{K_0}$: unit-normalised membrane permeability; **BF**: back-flush.

$$Theoretical\ MLTS_{Outlet} = 1.43 \cdot\ MLTS_{Inlet} \quad \textbf{Eq. 4.6}$$

$$Theoretical\ MLTS_{Outlet} = 1.16 \cdot\ MLTS_{Inlet} \quad \textbf{Eq. 4.7}$$

$$Theoretical\ MLTS_{Outlet} = 1.12 \cdot\ MLTS_{Inlet} \quad \textbf{Eq. 4.8}$$

Figure 4.3 shows the short-term trials carried out with MLTS of 18 g L^{-1} and an up-flow sludge velocity of 1 mm s^{-1} (*i.e.* sub-critical conditions), and MLTS of 28 g L^{-1} and an up-flow sludge velocity of 1, 2.2 and 2.7 mm s^{-1} (*i.e.* critical/supra-critical conditions). Figure 4.3 shows that K_0 remained at values close to 1 when operating membranes sub-critically. In this respect, the reversible fouling rate remained at values lower than 10 mbar min^{-1}. Up-flow sludge velocities of less than 1 mm s^{-1} when operating with MLTS of 18 g L^{-1} resulted in critical filtration conditions (data not shown) as a result of the corresponding increase in MLTS in the membrane tank. On the other hand, this figure illustrates that the up-flow sludge velocity had a significant effect on K_0 when the membranes were operated at high MLTS levels (around 28 g L^{-1}, *i.e.* critical/supra-critical filtration conditions). For instance, at an up-flow sludge velocity of 1 mm s^{-1}, the maximum TMP value was reached at minute 50, so the filtration process was promptly stopped. In this case, a maximum reversible fouling rate of about 90 mbar min^{-1} was observed. On the other hand, when the up-flow sludge velocity was set to 2.7 and 2.2 mm s^{-1} a maximum reversible fouling rate of around 10 and 20 mbar min^{-1} was achieved, respectively. In both cases, K_0 recovered to values lower than 10 mbar min^{-1} after back-flushing. Hence, it was possible to keep the filtration process operating at appropriate TMP values.

These results show that in order to keep the filtration process working properly, the operating up-flow sludge velocity must be selected carefully depending on the operating conditions. When the membranes are operated at high MLTS levels, the up-flow sludge velocity in the membrane tank has to be high enough not only to keep MLTS at suitable levels, but also to minimise the energy consumption needed to keep J_{20} at sub-critical levels (*e.g.* required SGD_m). Nonetheless, up-flow sludge velocity must be minimised in order to maximise energy savings since pumping energy accounts for up to 15 – 20% of all the energy consumed by aerobic MBR technology [4.29]. Hence, it is advisable for the up-flow sludge velocity to be regulated in order to optimise the economic feasibility of HF membranes in full-scale SAnMBR systems.

Another aspect that must be taken into account is whether or not the up-flow sludge is well distributed over the filtration area. A sludge flow distributed evenly across the membrane tank helps remedy any death zones and minimises the likelihood of clogging. Consequently, a minimum up-flow sludge

velocity is required to ensure that the sludge is adequately distributed over the filtration area. The configuration of the membrane tank is important in this respect.

4.3.2.3 Effect of back-flush frequency

Several short-term trials were carried out in order to assess the effect of the duration and frequency of the different physical cleaning stages (relaxation and back-flush) on membrane performance. Figure 4.4 shows the effect of back-flush frequency on membrane permeability with MLTS of 24, 28 and 31.5 g L^{-1}. Two different back-flush frequencies were tested: 30 seconds of back-flush every 10 F-R basic cycles (1:10) and 30 seconds of back-flush every 30 F-R basic cycles (1:30) (Figure 4.4a and Figure 4.4b, respectively).

Figure 4.4 shows that at MLTS levels of less than 24 g L^{-1}, the K_0 performance was independent of the back-flush frequency, at the selected operating conditions. In these short-term trials, the reversible fouling rate remained less than 5 mbar min^{-1}, and no residual fouling component was observed. Hence, a complete recovery of K_0 was achieved after each relaxation stage. At MLTS levels above 24 g L^{-1}, a significant decrease in K_0 was detected, making it necessary to increase the back-flush frequency from 1:30 to 1:10 in order to keep the filtration process working below the TMP safety value mentioned earlier. In this respect, when the back-flush frequency was set to 1:30, the maximum reversible fouling rate reached was around 25 and 80 mbar min^{-1}, at MLTS levels of 28 and 31.5 g L^{-1}, respectively. On the other hand, when the back-flush frequency was increased to 1:10, the maximum reversible fouling rate at an MLTS level of 28 g L^{-1} decreased to values around 20 mbar min^{-1}. However, this higher back-flush frequency had no noticeable effect on membrane performance when the MLTS level was 31.5 g L^{-1}, *i.e.* K_0 quickly returned to its previous values after back-flushing.

Hence, these results showed that values of MLTS above 30 g L^{-1} are not advisable since increasing the back-flush frequency from 1:30 to 1:10 did not improve the membrane performance. However, at MLTS levels lower than 28 g L^{-1}, it was possible to improve membrane performance considerably without significantly increasing the back-flush frequency.

It is a well-known fact that back-flush frequency affects the economic feasibility of the process not only because of the pumping cost but also due to the resulting decrease in the net J_{20}. Hence, it is essential to control the back-flush frequency to ensure that the membrane is physically cleaned correctly and thereby maximise the J_{20} at minimum operating costs.

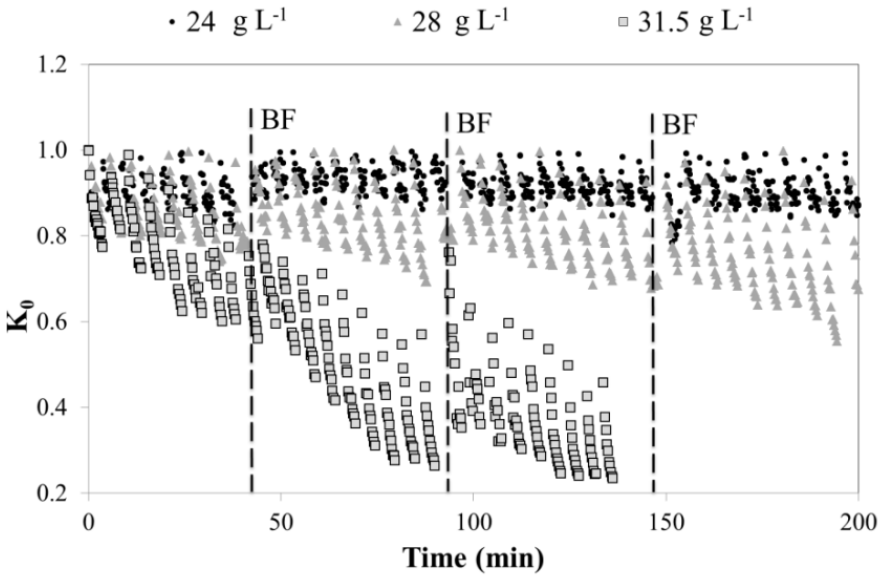

(a)

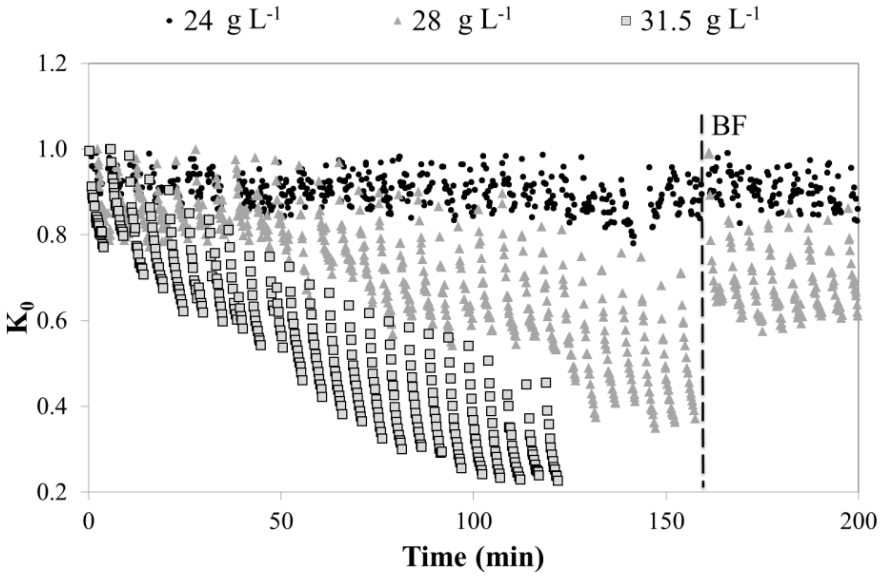

(b)

Figure 4.4 Short-term trial 3: Effect of back-flush frequency on membrane permeability at MLTS of 24, 28 and 31.5 g L^{-1} and **(a)** 30 seconds of back-flush every 10 F-R cycles; and **(b)** 30 seconds of back-flush every 30 F-R cycles. Nomenclature: $\mathbf{K_0}$: unit-normalised membrane permeability; **BF**: back-flush.

4.3.2.4 Effect of relaxation stage duration

Different sub-critical short-term trials were carried out to assess how the duration of the relaxation stage affects membrane performance. Relaxation stages of 50 and 30 seconds were tested when operating at MLTS of 25 g L^{-1} and sub-critical filtration conditions, and at MLTS of 28 g L^{-1} and

supra-critical filtration conditions. An almost complete recovery of K_0 was achieved when the MLTS level was 25 g L^{-1}. Hence, it was observed that membrane performance was not critically affected by relaxation stages of between 30 and 50 seconds at the selected operating conditions when operating at MLTS levels below 25 g L^{-1}. In this case, reversible fouling rates lower than 5 mbar min^{-1} were achieved. On the other hand decreasing the relaxation stage duration from 50 to 30 seconds at MLTS levels of 28 g L^{-1} slightly affected membrane performance, *i.e.* a slight increase in the reversible fouling component that accumulated on the membrane surface was observed (see Figure 4.5). In this case, the reversible fouling rate reached values of around 10 mbar min^{-1}. However, the TMP recovered to values lower than 0.1 bars after back-flushing.

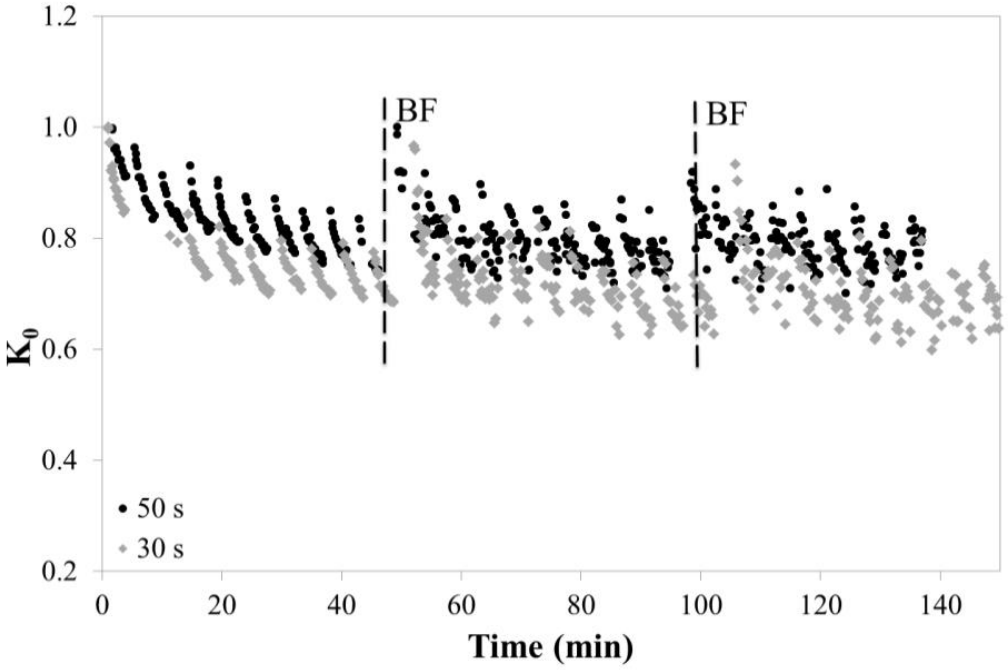

Figure 4.5 Short-term trial 4: Effect of relaxation stage duration on membrane permeability at MLTS level of 28 g L^{-1}. Nomenclature: $\mathbf{K_0}$: unit-normalised membrane permeability; **BF**: back-flush.

These results showed that combining relaxation stages with an appropriate back-flush frequency keep TMP stable at quite low values. However, the prolonged accumulation of reversible fouling components upon over the membrane surface could lead to an increased likelihood of irreversible fouling. For that reason, reducing the relaxation stage from 50 to 30 seconds when membranes are operated at MLTS levels higher than 25 g L^{-1} is not recommendable, if the other operating conditions are kept constant (250-second filtration stage, 30 seconds of back-flush every 10 F-R cycles, 10 LMH of J_{20}, and SGD_m at 0.23 Nm^3 h^{-1} m^{-2}).

Relaxation stage duration affects the economic feasibility of the process because of the resulting decrease in the net J_{20}. Hence, it is advisable to control the length of the relaxation stage in order to ensure that the membrane is correctly cleaned physically and thereby minimise the decrease in the net transmembrane flux whilst minimising the operating cost per unit of treated water (*e.g.* reducing the specific gas demand per volume of permeate).

4.3.2.5 Effect of filtration stage duration

Figure 4.6 shows an example of the short-term trials carried out in order to assess the effect of filtration stage duration on membrane performance. Duration was set to 250, 350 and 450 seconds. In this case, the MLTS level in the sludge fed to the membrane tank was 23 and 31.5 g L^{-1} and the back-flush frequency was set to 30 seconds of back-flushing every 10 F-R basic cycles (Figure 4.6a), and 30 seconds of back-flushing every 30 F-R basic cycles (Figure 4.6b).

Figure 4.6 shows that with MLTS of 31.5 g L^{-1}, increasing the back-flush frequency from 1:30 to 1:10 did not improve membrane performance. It was not possible to test filtration lasting more than 250 seconds because the maximum TMP value was reached in both 250-second trials.

In the short-term trials carried out with MLTS of 23 g L^{-1}, an increase in the filtration stage duration from 250 to 450 seconds resulted in the incomplete removal of the reversible fouling component from the membrane surface. Despite no high reversible fouling rates having been reached, a slight and continuous decrease of K_0 over time was observed when the filtration stage duration was set to 450 seconds: an effect that was slightly accentuated when the back-flush frequency was reduced from 1:10 to 1:30.

Increasing the duration of the filtration stage causes an increase in net J_{20}. However, as observed in this trial, it is essential to strike a balance between maximising net J_{20} and minimising maintenance and operating costs.

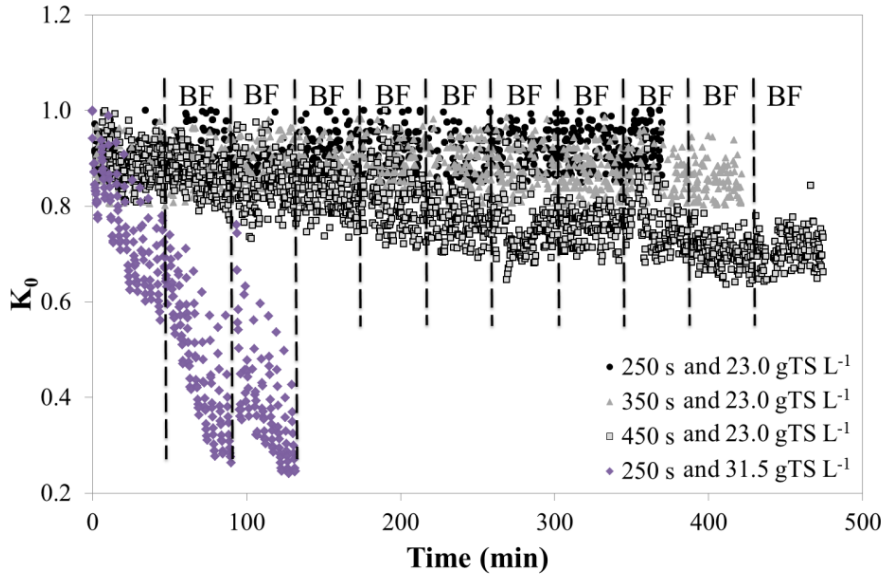

(a)

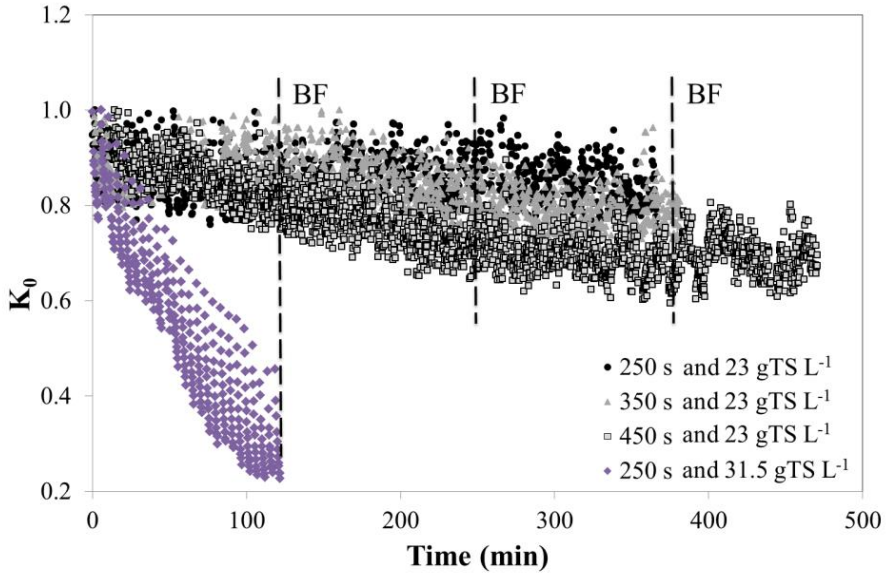

(b)

Figure 4.6 Short-term trial 5: Effect of filtration stage duration on membrane permeability at **(a)** MLTS levels of 23 and 31.5 g L^{-1} and back-flush frequency of 1 back-flush every 10 F-R cycles; and **(b)** MLTS levels of 23 and 31.5 g L^{-1} and back-flush frequency of 1 back-flush every 30 F-R cycles. Nomenclature: $\mathbf{K_0}$: unit-normalised membrane permeability; **BF**: back-flush.

4.3.2.6 Overall effect of MLTS and sustainable operating MLTS level

On the basis of the results shown in this study, we established a critical value for long-term membrane operation of around 20 – 25 g L^{-1}. Since several operating variables considerably affect the appearance

of reversible fouling at short-term, this maximum operating MLTS was established for the following scenario: 300-second basic F-R cycles (250 s filtration and 30-50 s relaxation) with 30 seconds of back-flush every 10 cycles; J_{20} of about 10 LMH; SGD_m of 0.23 $Nm^3\ h^{-1}\ m^{-2}$; and up-flow sludge velocity of 2.7 mm s^{-1}. For this specific scenario, increasing the filtration stage duration over 250 s will lead to a progressively reduction in K_0 over time, being this effect greater when the back-flush frequency is decreased to 1 back-flush every 30 F-R cycles (see Figure 4.6). On the other hand, back-flushing can be decreased from a frequency of 1 back-flush every 10 F-R cycles to 1 back-flush every 30 F-R cycles when membranes are operated at MLTS levels lower that 24 g L^{-1}, whilst the same increase considerably affects K_0 when the MLTS is around 28 g L^{-1} (see Figure 4.4). As regards gas sparging intensity, an SGD_m of around 0.17 – 0.23 $Nm^3\ h^{-1}\ m^{-2}$ allows maintaining proper long-term operation when the MLTS entering the membrane tank is around 20 g L^{-1}, whilst this value is not enough to properly operate at MLTS levels around 28 g L^{-1} (see Figure 4.2). Finally, reducing the up-flow sludge velocity from 2.7 to 2.2 mm s^{-1} may lead to a considerable decrease in K_0, due to a significant increase in the MLTS level when its concentration entering the membrane tank is around 28 g L^{-1} (see Figure 4.3).

Functioning with similar operating modes may allow reducing the offset of irreversible/irrecoverable fouling at long-term operation since the accumulation of reversible fouling component over the membrane surface can be minimised.

4.3.3 Overall membrane operation compared to full-scale aerobic MBR plant

On the basis of the long-term results obtained in this work, MLTS levels above 25 g L^{-1} are not recommended for commercial HF membranes because J_C drops to less than 10 LMH, making the filtration process unnecessarily expensive. On the basis of the short-term results, two opposite design strategies could be applied depending on the operating regime adopted. If the design strategy is based on sub-critical operating, the installed filtration area must be increased – which increases the initial investment. On the other hand, if the design strategy selected is based on supra-critical operating, then high back-flush frequencies and/or unsustainable SGD_m are required – which increases operating and maintenance/replacement costs. This may result in low process efficiency per unit of treated water (*i.e.* a decrease in net J_{20}) or high energy consumption, respectively.

The long-term membrane performance shown in this study, demonstrates that working at sub-critical filtration conditions is an adequate operating strategy for SAnMBR technology because no considerable irreversible/irrecoverable fouling component was detected after operating for almost two

years. Indeed, membranes did not required chemical cleaning. Nevertheless, an exhaustive economic analysis is needed to accurately demonstrate the feasibility of working at sub-critical or critical/supra-critical levels in an specific scenario. However, in order to shed more light upon the economic feasibility of SAnMBR technology for treating urban wastewater, the long-term operating strategy proposed in our study is compared in Table 4.2 and Table 4.3 with some available data related to full-scale aerobic MBR operations.

4.3.3.1 Average operating values for transmembrane flux, membrane permeability and specific gas demand

Table 4.2 shows a summary of data for full-scale aerobic plants treating both urban and industrial wastewater with submerged MBR (extracted from Judd and Judd [4.2]) and the average values obtained throughout the long-term operation of our study.

Table 4.2 Summary of full-scale plant data for urban wastewater treatment: Average data for submerged MBRs (adapted from Judd and Judd [4.2]). Nomenclature: **FS**: Flat-sheet; **HF**: hollow-fibre; **WW**: wastewater; **J**: transmembrane flux; **K**: membrane permeability; **$S(A/G)D_m$**: specific air/gas demand per membrane area; **$S(A/G)D_P$**: specific air/gas demand per permeate volume.

Technology	Treatment	J (LMH)	K (LMH bar^{-1})	$S(A/G)D_m$ ($Nm^3\ h^{-1}\ m^{-2}$)	$S(A/G)D_P$
FS	Aerobic; Urban WW	19.4	261	0.57	27.5
FS	Aerobic; Industrial WW	13.4	--	0.80	91.9
HF	Aerobic; Urban WW	19.5	104	0.30	15.4
HF	Aerobic; Industrial WW	15.4	47	0.23	16.5
This study (HF)	Anaerobic; Urban WW	11.1	135	0.23	20.7

Using FS membranes in urban wastewater treatment enables higher transmembrane fluxes (19.4 LMH) and membrane permeability (261 LMH bar^{-1}) in comparison with the results obtained in our work: transmembrane fluxes of around 11 LMH, resulting in membrane permeability of 135 LMH bar^{-1} in average. However, higher SGD_m and higher specific gas demand with respect to permeate volume (SGD_P) are commonly required in FS technology (see Table 4.2). It is well known that HF technology allows some degree of lateral movement which enables greater cake layer detachment at lower gas sparging intensities than in FS technology. On the other hand, when using FS membranes to treat industrial wastewater, commonly operating at high MLTS levels, the transmembrane fluxes and

membrane permeability are similar to those obtained in our study. However, considerably higher SGD_m and SGD_P are reported when using FS membranes.

As regards HF technology, the results from full-scale aerobic operation are similar to the results obtained in our study. Both aerobic and anaerobic operation result in reasonably adequate transmembrane fluxes and membrane permeability by applying low air/gas demands. In this respect, even though the resulting J_{20} was lower in the case of anaerobic HF membranes (around 11 LMH vs. approx. 17 LMH), higher K_{20} levels were obtained (around 135 LMH bar^{-1} vs. approx. 75 LMH bar^{-1}) whilst applying similar SGD_m (around 0.25 $Nm^3 h^{-1} m^{-2}$) in both anaerobic and aerobic HF. Moreover, SGD_P remained in a similar range (from approx. 15.5 to approx. 20.5) in both cases. Some studies suggested that the cake layer formed with aerobic and anaerobic sludge might have different removability (see, for instance, Meng *et al*. [4.32]). Nevertheless, based on comparable results for the aerobic and anaerobic operation of HF membranes, it can be assumed in this study that differences between anaerobic and aerobic sludge properties (*i.e.* particle size distribution, EPS, SMP and biomass concentration, etc.) did not critically determine the removability of the cake layer from the membrane surface. In this respect, HF technology is a promising, competitive technology for the anaerobic treatment of urban wastewater.

4.3.3.2 Physical and chemical cleaning requirements

A summary of the physical cleaning protocols for full-scale aerobic MBRs treating urban wastewater (extracted from Judd and Judd [4.2]) and the average values applied throughout the long-term operation of our study are shown in Table 4.3. Full-scale results from aerobic MBR technology reveal a relaxation downtime of around 10% of the operating time in both FS and HF configurations. This value is significantly lower than the resulting relaxation downtime obtained in our study (around 16.7% of the operating time). However, the relaxation stage duration applied in our work can be considered as a quite conservative value – selected in order to avoid possible problems when operating at large MLTS concentrations – since the results from the short-term trials showed that it is possible to reduce this parameter to a value of 30 seconds with a minimum impact on membrane performance when operating at MLTS levels below 25 g L^{-1}. This decrease in the duration of the relaxation stage results in a downtime of around 10% of operating time, which is similar to the average downtime shown in Table 4.3 for full-scale aerobic MBRs. On the other hand, a back-flush downtime of around 6 – 9% of operating time was reported by Judd and Judd [4.2] in the aerobic treatment of urban wastewater in full-scale MBRs. In this respect, only an additional downtime of around 1% of the operating period was obtained in our study (carried out with a back-flush frequency of 0.5 min every

10 F-R cycles). This gives a total average downtime for physical cleaning of 17.7% of operating time throughout the long-term operation of HF membranes shown in our study (instead of an average downtime of around 16 – 19% when using HF technology to treat urban wastewater aerobically). Moreover, it is important to emphasise that the membranes in our study did not require chemical cleaning after operating for more than two years – despite operating at high MLTS levels and with temperature shocks that affected mixed sludge properties – which is a considerably longer than the periods usually employed in aerobic MBR technology.

Table 4.3 Summary of full-scale urban physical cleaning protocols. Average data on submerged MBRs (adapted from Judd and Judd [4.2]). Nomenclature: **FS**: Flat-sheet; **HF**: hollow-fibre; **WW**: wastewater; **F**: Filtration stage duration; **R**: Relaxation stage duration; **BF**: Back-flush stage duration.

Technology	**Treatment**	**F (min)**	**R (min)**	**BF (min)**
FS	Aerobic; Urban WW	22.0	2.2	---
HF	Aerobic; Urban WW	10.0	1.0	0.43
This study (HF)	Anaerobic; Urban WW	4.2	0.8	0.50

Hence, the results of our study predict that HF membranes will result in a sustainable approach for SAnMBR technology compared to the full-scale results reported for aerobic MBR technology.

4.4 Conclusions

The membrane performance demonstrated that HF-SAnMBR may be a promising technology for urban wastewater treatment since low maintenance and operating costs related to membrane separation process can be achieved. According to the results, gas sparging intensity and back-flush frequency are the physical variables that affect membrane performance most. In our study, low gas sparging intensities (around 0.23 $Nm^3\ h^{-1}\ m^{-2}$) and low BF frequencies (30 seconds of BF every 10 basic F-R cycle) were enough to operate membranes sub-critically even at high levels of MLTS (up to 25 $g\ L^{-1}$). On the other hand, operating at critical filtration conditions involves significant physical cleaning (gas sparging intensity and BF frequency) to ensure that membranes operate correctly. The results of our study show that establishing a suitable physical cleaning schedule (relaxation, back-flush and gas sparging intensity) enhances the removal of the reversible fouling component accumulated on the membrane surface, and thus minimises the irreversible fouling propensity. After more than two years of sub-critical operation (transmembrane flux between 9 and 13.3 LMH at gas sparging intensities of around 0.23 $Nm^3\ h^{-1}\ m^{-2}$ and MLTS levels in the mixed liquor entering the membrane tank of around

10 to 30 g L^{-1}) no significant irreversible/irrecoverable fouling problems were detected (membrane permeability remained above 100 LMH bar^{-1} and total filtration resistance remained below 10^{13} m^{-1}), thus no chemical cleaning was conducted. Membrane performance was similar to the aerobic HF membranes operated in full-scale MBR plants. On the basis of the different experiments carried out, different control strategies will be developed with a view to optimising membrane performance in both sub-critical and critical/supra-critical operating. Nevertheless, an exhaustive economic analysis is needed to make the best choice between the two different operating regimes in a specific scenario: working at sub-critical levels or critical/supra-critical levels.

4.5 Acknowledgements

This research work has been supported by the Spanish Research Foundation (MICINN Projects CTM2008-06809-C02-01 and CTM2008-06809-C02-02, and MICINN FPI grant BES-2009-023712) and Generalitat Valenciana (Projects GVA-ACOMP2010/130 and GVA-ACOMP2011/182), which are gratefully acknowledged.

4.6 References

4.1 H.J. Lin, K. Xie, B. Mahendran, D.M. Bagley, K.T. Leung, S.N. Liss, B.Q. Liao, Factors affecting sludge cake formation in a submerged anaerobic membrane bioreactor, J. Membr. Sci. 361 (2010), 126–134.

4.2 S. Judd, C. Judd, The MBR Book: Principles and Applications of Membrane Bioreactors in Water and Wastewater Treatment, Second Edition, ELVESIER, ISBN: 978-0-08-096682-3, 2011.

4.3 A. Drews, Membrane fouling in membrane bioreactors–Characterization, contradictions, causes and cures, J. Membr. Sci. 253 (2010), 1–28.

4.4 S. Judd, The status of membrane bioreactor technology, Trends Biotechnol. 26 (2008), 109–116.

4.5 S.I. Patsios, A.J. Karabelas, An investigation of the long-term filtration performance of a membrane bioreactor (MBR): The role of specific organic fractions, J. Membr. Sci. 253 (2011), 102–115.

4.6 B.Q. Liao, J.T. Kraemer, D.M. Bagley, Anaerobic membrane bioreactors: Applications and research directions, Crit. Rev. Env. Sci. Tec. 36 (2006), 489–530.

4.7 P. Bachin, P. Aimar, V. Sanchez, Model for colloidal fouling of membranes, AIChE J. 41 (1995), 368–377.

4.8 R.W. Field, D. Wu, J.A. Howell, B.B. Gupta, Critical flux concept for microfiltration fouling, J. Membr. Sci. 100 (1995), 259–272.

4.9 A. Drews, H. Prieske, E.L. Meyer, G. Senger, M. Kraume, Advantageous and detrimental effects of air sparging in membrane filtration: Bubble movement, exerted shear and particle classification, Desalination 250 (2010), 1083–1086.

4.10 B. Lesjean, E.H. Huisjes, Survey of European MBR market, trends and perspectives. Proceedings of the IWA 4th International Membrane Technologies Conference, 15 - 17 May 2007, Harrogate, UK.

4.11 E.H. Huisjes, K. Colombel, B. Lesjean, The European MBR market: Specificities and future trends. Proceedings of the Final MBR-Network Workshop. Berlin, 31 March–1 April 2009. Germany.

4.12 P. Cote, Z. Alam, J. Penny, Hollow fibre membrane life in membrane bioreactors (MBR), Desalination 288 (2012), 145–151.

4.13 D. Jeison, J.B. van Lier, Cake formation and consolidation: Main factors governing the applicable flux in anaerobic submerged membrane bioreactors (AnSMBR) treating acidified wastewaters, Sep. Purif. Technol. 56 (2007), 71–78.

4.14 Z. Huang, S.L. Ong, H.Y. Ng, Feasibility of submerged anaerobic membrane bioreactor (SAMBR) for treatment of low-strength wastewater, Water Sci. Technol. 58 (2008), 1925–1931.

4.15 B. Lew, S. Tarre, M. Beliavski, C. Dosoretz, M. Green, Anaerobic membrane bioreactor (AnMBR) for domestic wastewater treatment, Desalination 243 (2009), 251–257.

4.16 G. Guglielmi, D.P. Saroj, D. Chiarani, G. Andreottola, Sub-critical fouling in a membrane bioreactor for municipal wastewater treatment: Experimental investigation and mathematical modelling, Water Res. 41 (2007), 3903–3914.

4.17 G. Di Bella, F. Durante, M. Torregrossa, G. Viviani, Start-up with or without inoculum? Analysis of an SMBR pilot plant, Desalination 260 (2010), 79–90.

4.18 G. Mannina, G. Di Bella, G. Viviani, An integrated model for biological and physical process simulation in membrane bioreactors (MBRs), J. Membr. Sci. 376 (2011), 56–69.

4.19 H.J. Lin, K. Xie, B. Mahendran, D.M. Bagley, K.T. Leung, S.N. Liss, B.Q. Liao, Sludge properties and their effects on membrane fouling in submerged anaerobic membrane bioreactors (SAnMBRs), Water Res. 43 (2009), 3827–3837.

4.20 A. Sweity, W. Ying, S. Belfer, G. Oron, M. Herzberg, pH effects on the adherence and fouling propensity of extracellular polymeric substances in a membrane bioreactor, J. Membr. Sci. 378 (2011), 186–193.

4.21 J.B. Giménez, A. Robles, L. Carretero, F. Durán, M.V. Ruano, M.N. Gatti, J. Ribes, J. Ferrer, A. Seco, Experimental study of the anaerobic urban wastewater treatment in a submerged hollow-fibre membrane bioreactor at pilot scale, Bioresource Technol. 102 (2011), 8799–8806.

4.22 A. Robles, M.V. Ruano, F. García-Usach, J. Ferrer, Sub-critical filtration conditions of commercial hollow-fibre membranes in a submerged anaerobic MBR (HF-SAnMBR) system: The effect of gas sparging intensity, Bioresource Technol. 114 (2012), 247–254.

4.23 American Public Health Association/American Water Works Association/Water Environmental Federation, Standard methods for the Examination of Water and Wastewater, 21st edition, Washington DC, USA, 2005.

4.24 WRC, Simple titration procedures to determine H2CO3* alkalinity and short-chain fatty acids in aqueous solutions containing known concentrations of ammonium, phosphate and sulphide weak acid/bases, Report No. TT 57/92, Water Res. Commission, University of Cape Town, Pretoria, Republic of South Africa, 1992.

4.25 S. Rosenberger, C. Laabs, B. Lesjean, R. Gnirss, G. Amy, M. Jekel, J.C. Schrotter, Impact of colloidal and soluble organic material on membrane performance in membrane bioreactors for municipal wastewater treatment, Water Res. 40 (2006), 710–720.

4.26 P. van der Marel, A. Zwijnenburg, A. Kemperman, M. Wessling, H. Temmink, W. van der Meer, An improved flux-step method to determinate the critical flux and the critical flux for irreversibility in a membrane bioreactor, J. Membr. Sci. 332 (2009), 24–29.

4.27 A. Robles, M.V. Ruano, J. Ribes, J. Ferrer, Performance of industrial hollow–fibre membranes in a submerged anaerobic MBR (HF–SAnMBR), system under mesophilic and psychrophilic conditions, Sep. Purif. Technol. 104 (2013), 290–296.

4.28 A. Robles, M.V. Ruano, J. Ribes, J. Ferrer, Sub-critical long-term operation of industrial scale hollow-fibre membranes in a submerged anaerobic MBR (HF-SAnMBR) system, Sep. Purif. Technol. 100 (2012), 88–96.

4.29 B. Verrecht, T. Maere, I. Nopens, C. Brepols, S. Judd, The cost of a large-scale hollow fibre MBR, Water Res. 44 (2010), 5274–5283.

4.30 C. Huyskens, E. Brauns, E. Van Hoof, E. Diels, H. De Wever, Validation of a supervisory control system for energy saving in membrane bioreactors, Water Res. 45 (2011), 1443–1453.

4.31 G. Ferrero, I. Rodriguez–Roda, J. Comas, Automatic control systems for submerged membrane bioreactors: A state–of–the–art review, Water Res. 46 (2012), 3421–3433.

4.32 F. Meng, S.R. Chae, A. Drews, M. Kraume, H.S. Shin, F. Yang, Recent advances in membrane bioreactors (MBRs): Membrane fouling and membrane material, Water Res. 43 (2009), 1489–1512.

CHAPTER 5:

Sub-critical long-term operation of industrial scale hollow-fibre membranes in a submerged anaerobic MBR (HF-SAnMBR) system

Abstract

The aim of this study was to evaluate the long-term performance of hollow-fibre (HF) membranes used to treat urban wastewater in a Submerged Anaerobic MBR when operating sub-critically. To this end, a demonstration plant with two industrial scale HF ultrafiltration membrane modules was operated under different conditions. The main factor affecting membrane performance was the concentration of mixed liquor total solids (MLTS). The reversible fouling rate remained low even when MLTS levels (about 25 g L^{-1}) in the membrane tank were high. No chemical cleaning was conducted whilst operating the plant for more than one year because no irreversible fouling problems were detected. The almost complete absence of irreversible fouling was mainly attributed to: operating at sub-critical filtration conditions; establishing a proper membrane operating mode; and to the characteristics of the anaerobic environment. No chemical precipitation problems were observed in the membranes due to the relatively low operating pH (always below 7) of the sludge. The biogas sparging encouraged high levels of dissolved CO_2 in the sludge, resulting in pH levels below 7 and alkalinity values around 600 mg $CaCO_2$ L^{-1}.

Keywords

Filtering resistance; industrial scale hollow-fibre membranes; long-term operation; sub-critical filtration; submerged anaerobic MBR.

Highlights

MLTS level was the main factor affecting membrane performance.
Low fouling rates were achieved, even for high MLTS levels (25 g L^{-1}).
No chemical precipitation problems were observed as a result of the low sludge pH.
After more than one year of operation no chemical cleaning was required.

A. Robles, M.V. Ruano, J. Ribes, J. Ferrer
Sub-critical long-term operation of industrial scale hollow-fibre membranes in a submerged anaerobic MBR (HF-SAnMBR) system
Sep. Purif. Technol. 100 (2012), 88 – 96

5.1 Introduction

Because of an increased interest in sustainability within wastewater management, there has been growing attention in recent years in the study of anaerobic urban wastewater treatment at ambient temperatures. Interest has focused on the greater sustainability advantages of anaerobic processes over aerobic processes, *i.e.* low sludge production due to low anaerobic biomass yield; low energy consumption because no aeration is required; the production of biogas that can be used as energy; and low greenhouse gases emissions when methane is recovered from both biogas and effluent streams. The main challenge posed by anaerobic biotechnology is how to develop treatment systems that prevent biomass loss whilst enabling high sludge retention times (SRTs) in order to compensate for the low growth rates of anaerobic biomass at ambient temperatures [5.1]. Against the well-established Up-flow Anaerobic Sludge Blanket (UASB) and Expanded Granular Sludge Blanket (EGSB) reactor configurations, anaerobic membrane bioreactors (AnMBRs) allow meeting longer SRTs, which is the main requirement necessary for high-rate anaerobic treatment. These longer SRTs are possible since complete physical retention of solids and almost all microorganisms can be achieved in membrane separation processes. Hence, AnMBRs provide an alternative strategy for urban wastewater treatment at ambient temperatures with the potential for a high quality effluent [5.2].

However, operating membrane bioreactors with long SRTs commonly means working with high MLTS levels, which is precisely one of the main operating drawbacks of membranes [5.3]. These high MLTS levels contribute to membrane fouling: the key issue of membrane technology. Membrane fouling decreases membrane permeability (K) and increases operating and maintenance costs [5.4]. Therefore, the need to work with high SRTs during the anaerobic treatment of low strength wastewaters could lead to high MLTS levels, in which case higher reactor volume might be required in order to operate at lower MLTS levels. In this respect, in order to design this technology adequately, the effect of MLTS on membrane fouling must be assessed.

In addition to MLTS level, other sludge properties have been identified elsewhere as key factors affecting membrane performance [5.5], such as pH and chemical precipitation. For instance, aerobic MBRs usually have high pH values probably because of the considerable CO_2 stripped from the liquid phase by the air sparging used in both membrane scouring and aeration. In this respect, the solubility of chemical precipitates is directly related to the pH when a representative amount of salts is present in the mixed liquor. For instance, Martí *et al*. [5.6] found that the amount of fixed phosphorous (mainly in the form of struvite) increases at pH values above 7.1.

In order to minimise any kind of membrane fouling (reversible, irreversible, or irrecoverable) and thereby increase membrane lifespan, the main operating challenge for AnMBRs is to optimise membrane operation and configuration. Several fouling control strategies can be applied [5.7; 5.8; 5.9], which must be able to optimise the filtration process with minimum operating and investment cost. The main points of these control strategies as regards membrane operation are: optimising the frequency and duration of the physical cleaning stages (back-flush and relaxation); optimising different operating variables such as gas sparging intensity or permeate/influent flow rate ratios; and operating membranes under the sub-critical filtration conditions bounded by critical flux (J_C) [5.10; 5.11]. As for membrane configuration, hollow fibre (HF) membranes are used for the entire flow range and account for about 75% of all total MBR installed capacity [5.12]. HF membranes require little energy due mainly to the low transmembrane pressure (TMP) required for filtration. Moreover, HF membranes are situated in the mixed liquor itself (out-in filtration) and some of the biogas produced can be recycled to the bottom of the membrane tank for in-situ sparging [5.1].

Therefore, the key challenge in AnMBR technology is how to achieve suitable long-term membrane performances at competitive transmembrane fluxes (J) whilst reducing membrane fouling propensity. Martinez-Sosa *et al*. [5.13] achieved considerable low fouling rates at J of 7 LMH when operating under psychrophilic temperature conditions in a range of total suspended solids (TSS) from approx. 9.5 to 17.5 g L^{-1}. However, stable membrane operation was achieved neither at 12 nor at 10 LMH and TSS of around 13 – 14 g L^{-1}. Under mesophilic temperature conditions, Martinez-Sosa *et al*. [5.14] reported a stable membrane operation at J of 7 LMH and TSS from approx. 15 to 20 g L^{-1}. Nevertheless, under psychrophilic temperature conditions, considerable high fouling rates were observed operating at 7 LMH when TSS was over 17 g L^{-1}. Akram *et al*. [5.15] operated at J of 10 LMH resulting in low TMP values around 0.1 bars, whilst Yoo *et al*. [5.16] achieved stable long-term membrane operation (TMP values generally lower than 0.1 bars) at J of up to 11 – 12 LMH. However, these higher J values were possible because of the scouring effect on membrane surface of the fluidised activated carbon introduced to the system.

Several studies have been published about the feasibility of submerged anaerobic MBRs (SAnMBRs) for treating urban wastewater on a laboratory scale [5.17; 5.18; 5.19; 5.20; 5.21], but few about the use of SAnMBR technology with commercial membranes on an industrial scale. Moreover, the impact of the main operating conditions on membrane fouling has not been adequately evaluated on the lab scale because it depends to a large extent on the membrane size. In HF membranes in particular, the HF length is a key design parameter, which means that they cannot be directly scaled up from the laboratory scale to full scale. Therefore, further studies are needed on HF membranes at the industrial

scale in order to facilitate the design and implementation of SAnMBR technology in full-scale WWTPs.

In order to shed more light on the optimisation of the physical separation process in SAnMBRs systems on an industrial scale, this paper now analyses the long-term performance of commercial HF membranes. In order to obtain accurate results that could be extrapolated to the design and operation of full-scale plants, an SAnMBR system featuring industrial scale HF membrane modules was operated with effluent from the pre-treatment of the Carraixet WWTP (Valencia, Spain). Several parameters that affect the physical separation process in SAnMBR technology were studied, *i.e.* 20 ºC-normalised transmembrane flux (J_{20}), MLTS level, pH, carbonate alkalinity (Alk) and chemical precipitation propensity. The novelty of this study lies in analysing the feasibility of the physical separation process featured in this technology under specific conditions that are similar to the ones expected at full-scale plants.

5.2 Materials and methods

5.2.1 Demonstration plant description

The same SAnMBR plant described in Chapter 2 was used to conduct this study, using also the same industrial scale ultrafiltration membrane units (PURON®, Koch Membrane Systems (PUR-PSH31) with 0.05 μm pores). The membrane unit consists of braided HF membranes (polyethersulfone (PES)) for outside-in operation. Each module has 9 HF bundles, 1.8 m long, giving a total membrane surface of 30 m^2.

Each membrane tank (MT1 and MT2) allows recycling continuously the obtained permeate to the anaerobic reactor. The obtained permeate from MT1 (see Figure 2.1) was continuously recycled to the system in order to test different J_{20} without affecting the hydraulic retention time (HRT) of the process. On the other hand, the biological process was operated by using MT2 (see Figure 2.1), which worked without recycling the obtained permeate. The biological process was operated at different HRTs tested by means of setting different operating filtration modes in MT2. As a result the MLTS level in the anaerobic sludge varied throughout the experimental period. In this work, the filtration process results that are presented correspond to the experimental data obtained from MT1.

5.2.2 Demonstration plant operation

The demonstration plant was operated at an SRT of 70 days. During the experimental period of our study, the usual membrane operating mode was as follows: a 300-second basic F-R cycle (250 s filtration and 50 s relaxation), 30 seconds of back-flush every 10 F-R cycles, 40 seconds of ventilation every 10 F-R cycles, and 30 seconds of degasification every 50 F-R cycles. Four gross J_{20} were tested in this work: 13.3, 10, 12 and 13.3 LMH, at controlled temperatures of 33, 33, 25, and 20 ºC, respectively. Hence, the operating period was divided in four experimental periods (Period i, ii, iii and iv) taking into account both J_{20} (13.3, 10, 12, and 13.3 LMH, respectively) and temperature (33, 33, 25 and 20 ºC, respectively). The long-term operation was carried out under sub-critical filtration conditions. To this end, the average specific gas demand per membrane area (SGD_m) was set to 0.23 $Nm^3\ h^{-1}\ m^{-2}$, taking into account the expected MLTS level. The maximum security value for the TMP was set to 0.4 bars. The cross-flow sludge velocity over the membrane surface was set to 2.7 mm s^{-1}.

Important to highlight is the wide variation in the anaerobic reactor influent loads during the experimental period (*e.g.* 186 ± 61 mg L^{-1} of TSS or 388 ± 95 mg L^{-1} of COD), reflected by the high standard deviation of each parameter. The uncertainty associated with each value includes both the standard deviation of the different samples analysed throughout the experiment and the variation coefficient associated with the analytical methods. The plant was fed with effluent from pre-treatment of a full-scale WWTP (screening, degritter, and grease removal), which main component is domestic type. No significant levels of process inhibitors were detected (*i.e.* oil, grease, heavy metals, conductivity, etc.).

5.2.3 Analytical methods

5.2.3.1 Analytical monitoring

In addition to monitoring the process on-line, the performance of the biological process was assessed by taking 24-hour composite samples from influent and effluent streams, and taking grab samples of biogas and anaerobic sludge once a day. The following parameters were analysed: total solids (TS); TSS; COD; carbonate alkalinity (Alk); sulphate (SO_4-S); sulphide (HS^-); nitrite (NO_2-N) and nitrate (NO_3-N); and nutrients (ammonium (NH_4-N) and orthophosphate (PO_4-P)). In addition, the following ion concentrations were analysed: chlorine (Cl^-); magnesium (Mg^{2+}); calcium (Ca^{2+}); potassium (K^+); and sodium (Na^+).

Solids, COD, sulphate, sulphide, nitrite and nitrate, nutrients, and ions were determined according to Standard Methods [5.22]. Carbonate alkalinity was determined by titration according to the method proposed by WRC [5.23].

5.2.3.2 Membrane performance indices

A classical resistance model (Eq. 5.1) was used in order to quantify the total membrane resistance (R_T), which was theoretically represented by the following partial resistances: membrane resistance (R_M); cake layer resistance (R_C); and irreversible layer resistance (R_I). J_T was corrected (Eq. 5.2) to 20 ºC (J_{20}) to account for the dependence of permeate viscosity (μ) on temperature (T). The fouling rate was calculated using a classical regression model (Eq. 5.3) that takes into account the total number of data monitored (n) during the filtration time (t) in order to minimise any possible noise from the pressure indicator transmitter.

$$R_T = R_M + R_C + R_I = \frac{TMP}{\mu \cdot J_T} \qquad \textbf{Eq. 5.1}$$

$$J_{20} = J_T \cdot e^{-0.0239\,(T-20)} \qquad \textbf{Eq. 5.2}$$

$$\frac{\partial TMP}{\partial t} = \frac{n \cdot \sum_1^n (TMP_i \cdot t_i) + \sum_1^n TMP_i \cdot \sum_1^n t_i}{n \cdot \sum_1^n TMP_i^2 - \left(\sum_1^n TMP_i\right)^2} \qquad \textbf{Eq. 5.3}$$

In addition, a modified flux-step method based on the method proposed by van der Marel *et al*. [5.24] was carried out in order to determinate the J_C of each operating interval. Each J_C was calculated according to the weak definition of this concept (J_{CW}), *i.e.* the flux above which the relationship between J and TMP becomes non-linear. When applying this method, the duration of both filtration and relaxation stages was set to 15 min. The step size was arbitrarily set to 1.22 LMH of J_{20} (equivalent to a permeate flow-rate of 50 L h^{-1}). The relaxation stages were conducted using the same SGD_m as in the filtration stages.

5.3 Results and discussion

5.3.1 Long-term SAnMBR performance

5.3.1.1 Evolution of the filtering resistance

Figure 5.1 shows the average daily R_T (calculated using Eq. 5.1) obtained during the operating period, and the average daily MLTS level in the anaerobic sludge entering the membrane tank. It must be said that the MLTS level in the membrane tank increased (up to 5 g L^{-1}) as per the ratio between the net permeate flow rate and the sludge flow rate entering the membrane tank. As mentioned before, the MLTS variation in the anaerobic sludge was the result of the different HRTs studied by means of the remaining parallel membrane tank (MT2), which was operated according to the biological process.

Figure 5.1 shows how any variation in the MLTS level affects R_T. Nevertheless, even at high MLTS levels (up to 25 g L^{-1}), R_T remained at adequate values (below $3 \cdot 10^{12}$ m^{-1}). Above this value a sudden increase in R_T was observed. This behaviour can be explained by the following: 1) the low TMP (below 0.1 bars) achieved throughout the experimental period minimised membrane compression and gave a stable R_M value; 2) R_T dropped back to previous values when MLTS level fell, thereby indicating that no significant irreversible fouling component (related to R_I) contributed to R_T; and 3) when the critical filtration conditions were exceeded (on days 135 to 170, and on days 190 to 220), a sharp increase on R_T was observed due to a higher cake layer formation rate (*i.e.* the accumulation of more reversible fouling on the membrane surface). It must be said that R_C is caused by two different effects: the cake layer formation rate (due to the filtration process) and the cake layer removal rate (due mainly to biogas sparging). It is a well-known fact that at an established SGD_m the cake layer removal efficiency decreases as the MLTS level increases. As can be concluded from this figure, on days 135 to 170 and days 190 to 220, the SGD_m applied to the membrane tank was not enough to meet the membrane requirements necessary to maintain sub-critical filtration conditions because of the high MLTS levels reached.

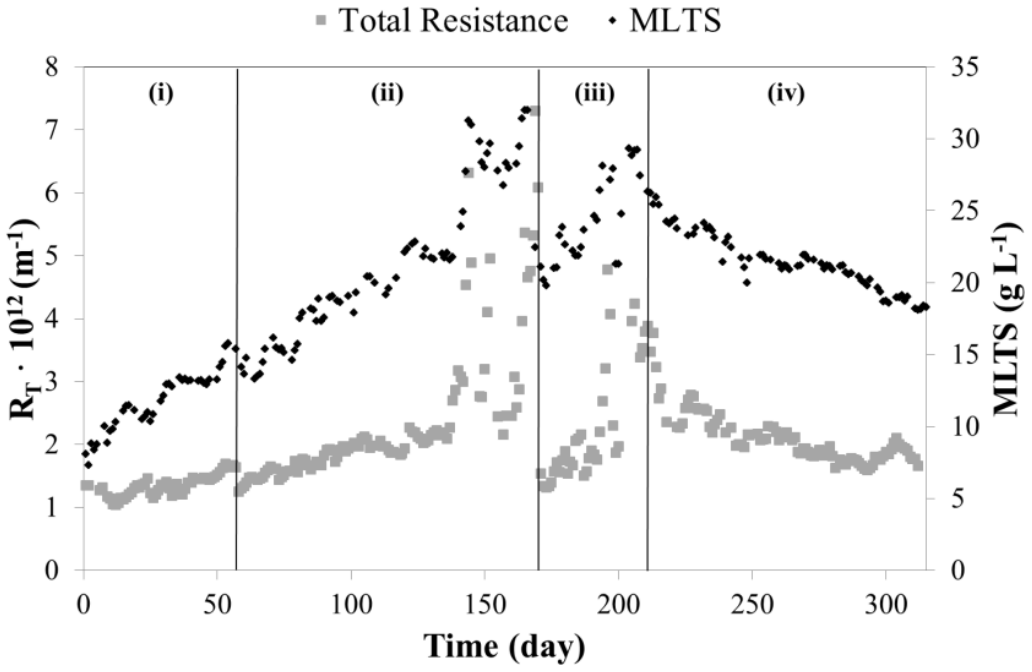

Figure 5.1 Evolution of R_T and MLTS during experimental periods: **(i)** J_{20} at 13.3 LMH and 33 ºC; **(ii)** J_{20} at 10 LMH and 33 ºC; **(iii)** J_{20} at 12 LMH and 25 ºC; and **(iv)** J_{20} at 13.3 LMH and 20 ºC.

Hence, according to our study, where R_I component was observed to be negligible, the component making the main contribution to R_T was R_C (between $8 \cdot 10^{11}$ and $16 \cdot 10^{11}$ m^{-1}, approx. 60 - 75% R_C/R_T, calculated as the difference between R_T and R_M), whilst a constant contribution of about $5 \cdot 10^{11}$ m^{-1} (calculated from the original K_{20} treating clean water in similar operating conditions: approx. 650 LMH bar^{-1}) was attributed to R_M (25 - 40% R_M/R_T). It must be emphasised that the R_T values obtained in this work were considerably lower than the results given in other studies on submerged MBR systems. For instance, Botino *et al*. [5.25] determined by means of the flux-step method R_T values from $1.56 \cdot 10^{12}$ to $4.82 \cdot 10^{12}$ m^{-1} for aerobic sub-critical filtration (MLTS levels from 3 to 14 g L^{-1} and J_C values from 4.9 to 14.7 LMH); Lin *et al*. [5.5] obtained R_T values of $8.47 \cdot 10^{13}$ and $1.72 \cdot 10^{13}$ m^{-1} at fluxes around 2.4 and 7.2 LMH treating kraft evaporator condensate under thermophilic and mesophilic temperature conditions, respectively; and Martinez-Sosa *et al*. [5.13; 5.14] observed R_T values from approx. $4.0 \cdot 10^{12}$ to $1.4 \cdot 10^{13}$ m^{-1} treating urban wastewater at 7 LMH of J_{20} and TSS (from approx. 9.5 to 20 g L^{-1}). Nevertheless, no stable operation of membranes was possible at J_{20} over 10 LMH.

The low R_T values obtained in our study can be attributed to the low cake layer formation throughout the operating period (the average TMP was around 0.1 bars), resulting in a low R_C contribution to R_T. Hence, the contribution of R_M to R_T became significant as a result of the low R_C achieved. It must be

emphasised that the membranes were operated sub-critically during almost the whole operating period. Only when the critical filtration conditions were exceeded (on days 135 to 170, and days 190 to 220) did R_C became the only major contribution to R_T, reaching values of around $5.5 \cdot 10^{12}$ m^{-1} (*i.e.* about 90% R_C/R_T). Even in supra-critical filtration conditions R_T remained under $1 \cdot 10^{13}$ m^{-1}. Since low R_T values directly mean low energy consumptions related to permeation, the results shown in Figure 5.1 highlight the necessity of optimising the physical separation process in SAnMBR systems in order to maximise the economic feasibility of this technology.

5.3.1.2 Evolution of the fouling rate

Figure 5.2 shows the fouling rate profile (calculated with Eq. 5.3) obtained during the operating period, as well as the MLTS level in the anaerobic sludge fed to the membrane tank. The fouling rate and MLTS level are both daily averages. As can be observed in Figure 5.2, the fouling rate remained at low values (below 10 mbar min^{-1}) until the MLTS raised the above-mentioned threshold concentration (around 25 g L^{-1}). Above this value, the fouling rate showed a sharp increase due to exceeding the critical filtration conditions. In fact, the fouling rate reached unsustainable values (around 100 mbar min^{-1}) at quite large MLTS levels (around 30 g L^{-1}). For instance, at an SGD_m of 0.23 Nm^3 h^{-1} m^{-2} and a MLTS level of 28 and 23 g L^{-1}, the 20 ºC-normalised J_{CW} ($J_{CW,20}$) calculated by the flux-step method resulted in approx. 10 and 13 LMH, respectively (see Figure 5.3). It must be emphasised that since the flux-step method was conducted using industrial scale membranes, the differences between the theoretical and the observed values were reduced [5.26]. The fouling rate profile in Figure 5.2 shows that the filtration process remained sub-critical until day 135. As mentioned before, in the periods from days 135 to 170 (period ii) and days 190 to 220 (period iii), supra-critical filtration conditions were reached, as shown by the significant fouling rate obtained, due to the high MLTS levels reached. Nevertheless, it was possible to operate the membranes at low fouling rates (below 20 mbar min^{-1}) even when operating at high MLTS levels (up to 25 g L^{-1}) without applying unsustainable SGD_m values (SGD_m was always under 0.25 Nm^3 h^{-1} m^{-2}). Finally, from days 210 to 315 (period iv) the fouling rate decreased because of the decrease in the MLTS level.

The results shown in Figure 5.1 and Figure 5.2 highlight the possibility of operating membranes anaerobically at higher MLTS levels (up to 25 g L^{-1}) than aerobically, since no oxygen for organic matter removal is required. MLTS levels in aerobic MBRs are limited due to oxygen transfer limitation problems [5.27]. In this respect, the operating volume envisaged originally can be reduced considerably in comparison with the volume required under aerobic conditions. Moreover, these results confirm that the MLTS level is a key factor governing membrane fouling in this HF-SAnMBR

system, since membrane permeability was restored to previous values when the MLTS level fell. Nevertheless, the effect of other factors mainly related to sludge characteristics (*i.e.* biomass, SMP and EPS concentrations) on membrane fouling should be considered.

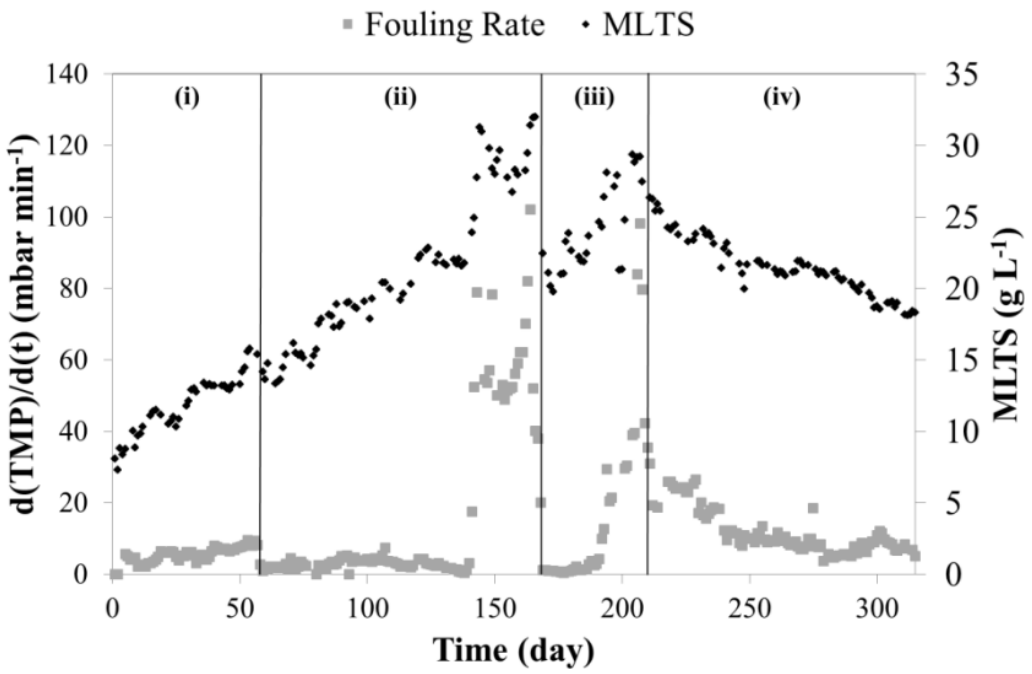

Figure 5.2 Evolution of reversible fouling rate and MLTS during experimental periods: **(i)** J_{20} at 13.3 LMH and 33 ºC; **(ii)** J_{20} at 10 LMH and 33 ºC; **(iii)** J_{20} at 12 LMH and 25 ºC; and **(iv)** J_{20} at 13.3 LMH and 20 ºC.

5.3.2 Sub-critical filtration conditions

Figure 5.3 shows $J_{CW,20}$ to be directly related to SGD_m when operating at high MLTS levels (at 23 and 28 g L^{-1}). This relationship predicts that it is theoretically possible to operate membranes sub-critically at high MLTS levels without applying prohibitive SGD_m levels (from 0.17 to 0.50 Nm^3 h^{-1} m^{-2}) when working at J_{20} between 10 and 15 LMH. For instance, as Figure 5.3 shows, it is theoretically possible to operate membranes sub-critically at a J_{20} of 14 LMH by applying an SGD_m of approx. 0.25 Nm^3 h^{-1} m^{-2} at 23 g L^{-1} of MLTS, whilst SGD_m has to be set to 0.50 Nm^3 h^{-1} m^{-2} for MLTS levels of around 28 g L^{-1}. On the other hand, when operating at constant SGD_m a decline in $J_{CW,20}$ of up to 4 LMH could be reached when MLTS increases from 23 to 28 g L^{-1}. Therefore, MLTS levels above 28 g L^{-1} are not advisable because this would cause $J_{CW,20}$ values to drop below 10 LMH (for SGD_m of 0.23 Nm^3 h^{-1} m^{-2}) and would make the filtration process unnecessarily expensive when operating sub-critically.

Important to note is the competitive $J_{CW,20}$ values obtained in our study (taking into account the operating solids concentration) in comparison with other J_C values found in recent MBR literature. Botino *et al*. [5.25] obtained JC values from 4.9 to 14.7 LMH in an aerobic HF-MBR at TSS levels from 3 to 14 g L^{-1}; Monclús *et al*. [5.28] identified J_C of 14.5 LMH in an aerobic HF-MBR operated at TSS of 8 g L^{-1} and SGD_m of 0.24 Nm^3 h^{-1} m^{-2}; Martin-Garcia *et al*. [5.29] obtained J_C values from approx. 2 to 5 LMH in a HF-SAnMBR operated at TSS of 7.7 g L^{-1} and SGD_m from 0.19 to 1.16 Nm^3 h^{-1} m^{-2}, whilst the same authors obtained J_C values from approx. 3 to 14 LMH in aerobic HF-MBR operated at TSS of 8.7 g L^{-1} and SGD_m from 0.19 to 1.16 Nm^3 h^{-1} m^{-2}; and Tiranuntakul *et al*. [5.30] reported J_C values from 9 to 16 LMH calculated by different methods in an aerobic MBR operated at TSS around 6 – 7 g L^{-1} and SGD_m of 0.36 Nm^3 h^{-1} m^{-2}. The results obtained in our study predict that it is theoretically possible to maintain sub-critical filtration conditions meanwhile operating at sustainable J_{20} values when operating membranes at quite high MLTS levels (up to around 25 g L^{-1}), without applying a prohibitive SGD_m. As mentioned before, these results confirm that the optimisation of the physical separation process in every operating range will result in significant energy savings in HF-SAnMBR systems.

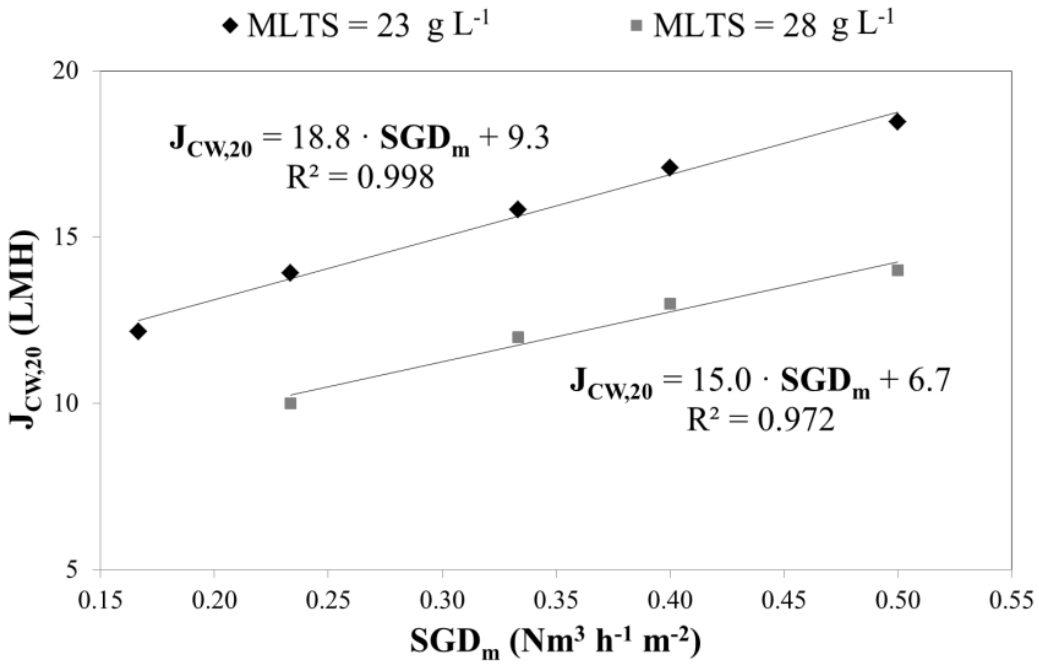

Figure 5.3 Effect of SGD_m on J_{CW20} at MLTS levels of 23 and 28 g L^{-1}.

5.3.3 Membrane operating mode

Figure 5.4a shows the TMP profile at the end of the second experimental period (day 135) and also the membrane operating mode. In this case, the MLTS in the anaerobic reactor was 22 g L^{-1}, whilst the MLTS in the membrane tank was estimated to be approximately 24.5 g L^{-1} according to the ratio between the net permeate flow rate and the sludge flow rate entering the membrane tank. As stated before, the critical flux (normalised at 20 ºC) under these conditions was calculated to be approximately 13 LMH. Hence, the membranes were operated at sub-critical filtration conditions. Figure 5.4a shows the total TMP recovery after the relaxation stage, which confirms that no irreversible fouling was detected throughout the operating period. The maximum TMP was 0.08 bars, which is very low compared to both the maximum value recommended by the supplier (0.6 bars) and the normal values in aerobic membrane bioreactors (approximately 0.1 to 0.3 bars).

Figure 5.4b enlarges a 45-minute operating period taken from Figure 5.4a, as well as a 45-minute operating period taken from days 195 and 250 (third and fourth experimental period, respectively). The MLTS in the anaerobic reactor was 25 g L^{-1} on day 195 and 22 g L^{-1} on day 250, whilst the MLTS in the membrane tank was estimated to be approximately 28.5 and 25.5 g L^{-1}, respectively. The maximum TMP on days 195 and 250 was 0.15 and 0.11 bars, respectively. Figure 5.4b shows that the TMP remained practically constant during the filtration periods at 10 LMH of J_{20} and MLTS of 22 g L^{-1} (day 135). On the other hand, a slight increase in TMP was observed when membranes were operated at 12 LMH of J_{20} and MLTS of 25 g L^{-1} (day 195), and at 13.3 LMH of J_{20} and MLTS of 22 g L^{-1} (day 250). The higher fouling rate values observed on days 195 and 250 indicated that membranes were operated critically. Nevertheless, continuous increase on TMP through consecutive filtration stages was observed neither on day 195 nor on day 250. Moreover, as stated before, the total filtration resistance observed in this study was mainly related to the reversible fouling component. Therefore, the physical cleaning mechanisms (relaxation, back-flush and shear intensity of gas sparging) were enough to completely remove the physical fouling from the membrane surface. This fouling removal also highlights the importance of establishing both an adequate membrane configuration and an adequate membrane operating mode in order to minimise filtration problems such as clogging and irreversible/irrecoverable fouling.

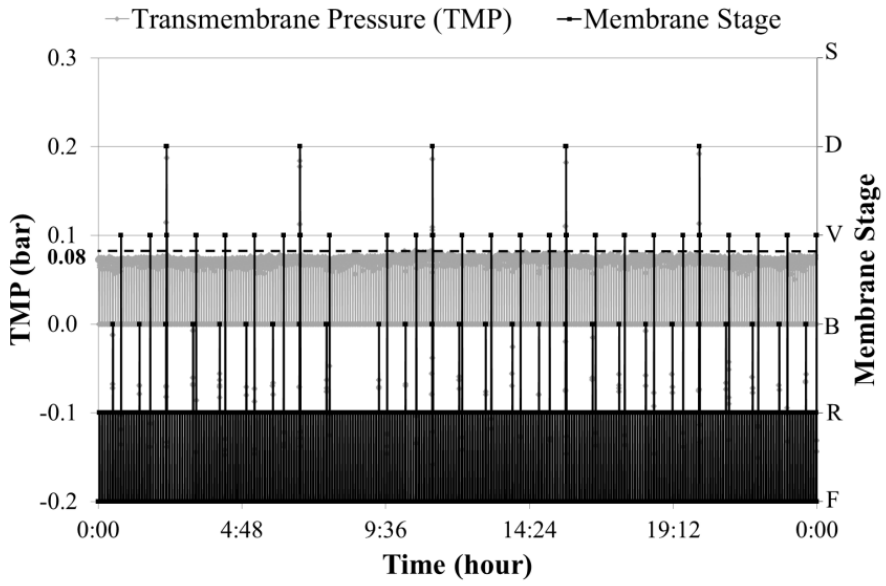

(a)

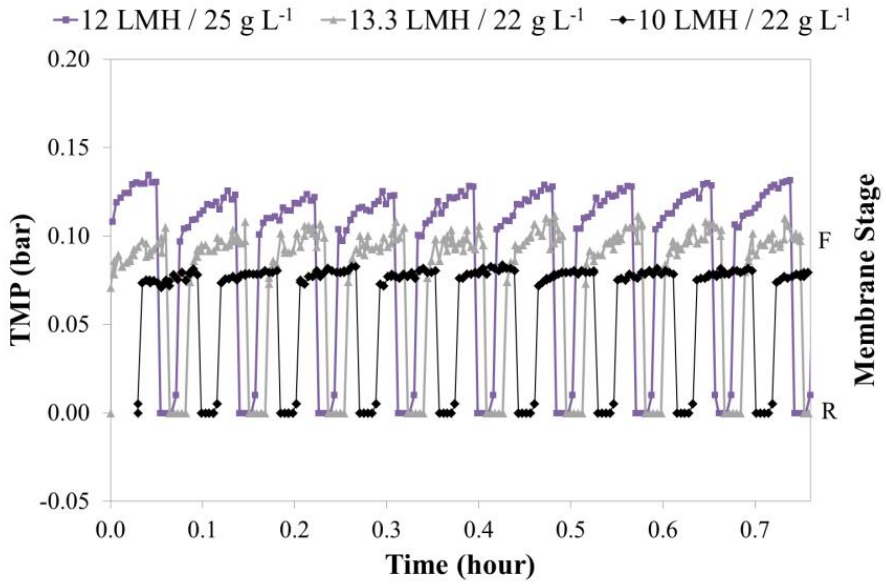

(b)

Figure 5.4 (a) TMP performance on day 135 of operation (period ii, MLTS of 22 g L^{-1} and J_{20} at 10 LMH). **(b)** Detail of 45-minute period of operation on days 135 (period ii, MLTS of 22 g L^{-1} and J_{20} at 10 LMH), 195 (period iii, MLTS of 25 g L^{-1} and J_{20} at 12 LMH) and 250 (period iv, MLTS of 22 g L^{-1} and J_{20} at 13.3 LMH). Nomenclature: **R**: Relaxation; and **F**: Filtration.

Hence, proper membrane configuration and operating mode may allow for establishing competitive transmembrane fluxes in order to increase the economic feasibility of full-scale anaerobic MBRs compared to full-scale aerobic MBRs, which commonly operate at J_{20} from 10 to 25 LMH [5.31]. In our work, membranes were operated at gross J_{20} values from 10 to 13.3 LMH, resulting in low fouling

rate values. Recent literature on anaerobic MBRs has also shown the potential of SAnMBR technology for urban wastewater treatment. For instance, Martinez-Sosa *et al*. [5.32] achieved proper long-term operation of membranes (resulting in low fouling rates) at J values of up to 10 LMH and TSS levels of up to 15 g L^{-1}. However, above these J values a considerable increase in fouling rate was observed since the critical flux was established at 7 LMH for similar TSS. In contrast, our study showed lower TMP and fouling rates at higher J_{20} than the above-mentioned study, whilst operating at similar gas sparging intensities. This behaviour can be mainly attributed to the membrane scale. Membrane length is a key design parameter that not only affects the shear conditions and gas sparging efficiency, but also the grade of lateral movement, which also contributes to partially-removing the cake layer. Moreover, the transmembrane fluxes used in our work are higher than the fluxes applied in SAnMBR systems treating industrial wastewater, which are commonly operated at transmembrane fluxes below 10 LMH whilst operating at TSS levels around 10 g L^{-1} [5.33]. Hence, the results presented in our work highlight the potential of SAnMBR technology for urban wastewater treatment at full-scale.

5.3.4 Chemical factors minimising the onset of irreversible fouling problems

Apart from operating at sub-critical filtration conditions and establishing an adequate membrane operating mode, other factors were identified as key parameters minimising possible irreversible/irrecoverable fouling problems in this HF-SAnMBR system, such as the relatively low operating pH (around 6.7), which reduces the chemical precipitation propensity.

Throughout the operating period shown in Figure 5.1 and Figure 5.2, the pH of the mixed liquor remained relatively stable around 6.7. This behaviour highlights the importance in SAnMBR systems of carrying out membrane scouring with a fraction of the produced biogas. In these systems it is possible to assume that equilibrium conditions between liquid and gas phases are achieved, *i.e.* the effluent CO_2 concentration will be similar to the CO_2 solubility concentration. Thus, most of the CO_2 produced remained in the mixed liquor working as a pH tampon factor. This can be confirmed by the high Alk values of the mixed liquor (around 6 mmol$CaCO_3$ L^{-1} during the operating period), in comparison with the influent Alk (around 3.1 mg$CaCO_3$ L^{-1}). It is important to highlight that chemical precipitates, which are usually produced at pH values greater than 7, increase the irreversible fouling propensity due to increasing both superficial and internal fouling. Since the pH was mainly under 7, the possible fouling problems related to chemical precipitation were reduced.

The equilibrium speciation programme MINTEQA2 [5.34] was used to estimate the expected concentrations for the biologically induced precipitates most likely in this SAnMBR system: amorphous calcium phosphate one, two, and β (ACP 1, ACP 2 and ACP β, respectively), hydroxyapatite (HAP), struvite (MAP) and calcite. This programme calculates the saturation index (SI) of the selected precipitates, thereby establishing the stability order of precipitation or dissolution. Indeed, if SI is positive the solution is oversaturated and there is possibility of chemical precipitation. On the other hand, if SI is negative the solution is undersaturated and no chemical precipitation is expected. The value of 13.3 – as proposed by Pastor *et al*. [5.35] – was selected for the struvite solubility product (pK_{SMAP}). Table 5.1 shows the compound concentrations used for evaluating the chemical precipitation propensities, which were obtained from the average experimental values of the mixed liquor. Table 5.2 shows the estimated SI values for the selected precipitates calculated at different pH levels (6.5, 6.75, 7 and 7.25) and temperature (20, 25 and 33 ºC).

Table 5.1 Mean concentrations entered in the MINTEQA2 programme to estimate the chemical precipitation propensity of the system.

Parameter	**Value (mmol L^{-1})**
NO_2^-	0.0398
NO_3^-	0.0418
NH_4^+	3.1000
PO_4^{3-}	0.1711
SO_4^{2-}	0.0938
HS^-	2.9844
Cl^-	4.5275
Mg^{2+}	2.1564
Ca^{2+}	4.9150
K^+	0.5578
Na^+	8.6336
CO_3^{2-}	6.1651

As Table 5.2 shows, the results obtained from MINTEQA2 indicated that the induced formation of the selected precipitates is low when working at pH values of less than 7, although chemical precipitation propensity increases as pH increases. For pH values lower than 6.75 only the SI of HAP was significantly positive as regards its precipitation. However, this precipitate is formed from its precursors (ACP 1, ACP 2 and ACP β) which present SI values lower than or close to zero. It is

important to highlight that no significant amount of struvite is expected even at pH values of around 7.5.

Besides chemical precipitation propensity, recent literature has demonstrated that pH affects the anaerobic sludge properties thus affecting the biofouling propensity. In this respect, Jane Gao *et al*. [5.36] observed that elevated pH shocks induced the dispersion of sludge flocs resulting in sub-products generation (colloids and solutes or biopolymers). On the other hand, Sweity *et al*. [5.37] studied how pH affects on the adherence and fouling propensity of EPS over ultrafiltration (UF) membranes. These authors observed that the fouling rate of UF membranes operated at similar EPS concentrations was significantly lower at pH value of 6.3 than at pH value of 8.3.

Therefore, further research is needed in order to assess the actual effect of pH on membrane fouling.

Table 5.2 Estimated SI values for the main chemical precipitates expected in the system at different operating temperatures and pH.

pH	T	ACP 1	ACP 2	ACP β	HAP	MAP	Calcite
6.50	20	-3.998	-1.227	-0.136	5.698	-2.217	-0.063
	25	-3.646	-0.896	-0.226	5.804	-2.193	0.001
	33	-3.107	-0.389	0.365	5.963	-2.159	0.100
6.75	20	-3.215	-0.444	0.647	7.124	-1.827	0.172
	25	-2.869	-0.119	0.551	7.219	-1.806	0.235
	33	-2.341	0.377	0.401	7.362	-1.777	0.332
7.00	20	-2.504	0.267	1.358	8.440	-1.472	0.404
	25	-2.165	0.585	1.255	8.526	-1.455	0.466
	33	-1.648	1.070	1.095	8.652	-1.432	0.562
7.25	20	-1.861	0.910	2.001	9.654	-1.152	0.634
	25	-1.528	1.222	1.892	9.730	-1.138	0.696
	33	-1.022	1.696	1.721	9.841	-1.121	0.792

5.4 Conclusions

The membrane performance demonstrated that HF-SAnMBR is a promising technology for urban wastewater treatment. MLTS was identified as the main factor affecting membrane performance. Nevertheless, R_T remained at sustainable values even when operating membranes at MLTS levels of approx. 25 g L^{-1}. Beneath this level, the fouling rate remained low (less than 20 mbar min^{-1}) and

suddenly increased when this threshold value was exceeded. After almost one year of operation no irreversible fouling problems (usually related to chemical precipitation in the membranes) were detected, and low fouling rates were observed even when MLTS was high. This was mainly attributed to: operating at sub-critical filtration conditions; establishing an adequate membrane operating mode; and working at pH values of less than 7 as a result of some of the biogas produced being recycled for in-situ sparging

5.5 Acknowledgements

This research work has been supported by the Spanish Research Foundation (CICYT Projects CTM2008-06809-C02-01 and CTM2008-06809-C02-02, and MICINN FPI grant BES-2009-023712) and Generalitat Valenciana (Projects GVA-ACOMP2010/130 and GVA-ACOMP2011/182), which are gratefully acknowledged.

5.6 References

5.1 H.J. Lin, K. Xie, B. Mahendran, D.M. Bagley, K.T. Leung, S.N. Liss, B.Q. Liao, Factors affecting sludge cake formation in a submerged anaerobic membrane bioreactor, J. Membr. Sci. 361 (2010) 126–134.

5.2 A.L. Smith, L.B. Stadler, N.G. Love, S.J. Skerlos, L. Raskin, Perspectives on anaerobic membrane bioreactor treatment of domestic wastewater: A critical review, Bioresource Technol. 122 (2012), 149–159.

5.3 S. Judd, C. Judd, The MBR Book: Principles and Applications of Membrane Bioreactors for Water and Wastewater Treatment, 2nd edition, Elsevier, ISBN: 978-0-08-096682-3, 2011.

5.4 I.S. Chang, P.L. Clech, B. Jefferson, S. Judd, Membrane fouling in membrane bioreactors for wastewater treatment, J. Environ. Eng. 128 (2002) 1018–1029.

5.5 H.J. Lin, K. Xie, B. Mahendran, D.M. Bagley, K.T. Leung, S.N. Liss, B.Q. Liao, Sludge properties and their effects on membrane fouling in submerged anaerobic membrane bioreactors (SAnMBRs), Water Res. 43 (2009) 3827–3837.

5.6 N. Martí, A. Bouzas, A. Seco, J. Ferrer, Struvite precipitation assessment in anaerobic digestion processes, Chem. Eng. J. 141 (2008) 67–74.

5.7 B.Q. Liao, J.T. Kraemer, D.M.Bagley, Anaerobic membrane bioreactors: Applications and research directions, Crit. Rev. Env. Sci. Tec. 36 (2006) 489–530.

5.8 M.V.G. Vallero, G. Lettinga, P.N.L. Lens, High rate sulfate reduction in a submerged anaerobic membrane bioreactor (SAMBaR) at high salinity, J. Membr. Sci. 253 (2005) 217–232.

5.9 L. Dvořák, M. Gómez, M. Dvořáková, I. Růžičková, J. Wanner, The impact of different operating conditions on membrane fouling and EPS production, J. Membr. Sci. 102 (2011) 6870–6875.

5.10 P. Bachin, P. Aimar, V. Sanchez, Model for colloidal fouling of membranes. AIChE J. 41 (1995) 368–377.

5.11 Field R.W., Wu D., Howell J.A., and Gupta B.B. (1995) Critical flux concept for microfiltration fouling, J. Membr. Sci. 100 (3), 259–272.

5.12 P. Cote, Z. Alam, J. Penny, Hollow fibre membrane life in membrane bioreactors (MBR), Desalination 288 (2012) 145–151.

5.13 D. Martinez-Sosa, B. Helmreich, H. Horn, Anaerobic submerged membrane bioreactor (AnSMBR) treating low-strength wastewater under psychrophilic temperature conditions, Process Biochem. 47 (2012) 792–798.

5.14 D. Martinez-Sosa, B. Helmreich, T. Netter, S. Paris, F. Bischof, H. Horn, Anaerobic submerged membrane bioreactor (AnSMBR) for municipal wastewater treatment under mesophilic and psychrophilic temperature conditions, Bioresource Technol. 102 (2011) 10377–10385.

5.15 A. Akram, D.C. Stuckey, Flux and performance improvement in a submerged anaerobic membrane bioreactor (SAMBR) using powdered activated carbon (PAC), Process Biochem. 43 (2008) 93–102.

5.16 R. Yoo, J. Kim, P.L. McCarty, J. Bae, Anaerobic treatment of municipal wastewater with a staged anaerobicfluidized membrane bioreactor (SAF-MBR) system, . Bioresource Technol. 120 (2012) 133–139.

5.17 A.Y. Hu, D.C. Stuckey, Treatment of Dilute Wastewaters Using a Novel Submerged Anaerobic Membrane Bioreactor, J. Environ. Eng. 132 (2006) 190–198.

5.18 F. Fawehinmi, B. Jefferson, C. Tak, F. Rogalla, Submerged Anaerobic Membrane Bioreactors (SAnMBR): Ready for the Big Ball?, Proceedings of the Water Environment Federation, WEFTEC 2007 (2007) 6393–6401.

5.19 D. Jeison, J.B. van Lier, Cake formation and consolidation: Main factors governing the applicable flux in anaerobic submerged membrane bioreactors (AnSMBR) treating acidified wastewaters, Sep. Purif. Technol. 56 (2007) 71–78.

5.20 Z. Huang, S.L. Ong, H.Y. Ng, Feasibility of submerged anaerobic membrane bioreactor (SAMBR) for treatment of low-strength wastewater, Water Sci. Technol. 58 (2008) 1925–1931.

5.21 B. Lew, S. Tarre, M. Beliavski, C. Dosoretz, M. Green, Anaerobic membrane bioreactor (AnMBR) for domestic wastewater treatment, Desalination 243 (2009) 251–257.

5.22 American Public Health Association/American Water Works Association/Water Environmental Federation, Standard methods for the Examination of Water and Wastewater, 21st edition, Washington DC, USA, 2005.

5.23 Water Res. Commission, University of Cape Town, Simple titration procedures to determine H2CO3* alkalinity and short-chain fatty acids in aqueous solutions containing known concentrations of ammonium, phosphate and sulphide weak acid/bases, Report No. TT 57/92, Pretoria, Republic of South Africa, 1992.

5.24 P. van der Marel, A. Zwijnenburg, A. Kemperman, M. Wessling, H. Temmink, W. van der Meer, An improved flux-step method to determine the critical flux and the critical flux for irreversibility in a membrane bioreactor, J. Membr. Sci. 332 (2009) 24–29.

5.25 A. Bottino, G. Capannelli, A. Comite, R. Mangano, Critical flux in submerged membrane bioreactors for municipal wastewater treatment, Desalination 245 (2009) 748–753.

5.26 A. Robles, M.V. Ruano, F. García-Usach, J. Ferrer, Sub-critical filtration conditions of commercial hollow-fibre membranes in a submerged anaerobic MBR (HF-SAnMBR) system: The effect of gas sparging intensity, Bioresource Technol. 114 (2012) 247–254.

5.27 T. Stephenson, S. Judd, B. Jefferson, K. Brindle, Membrane Bioreactors for Wastewater Treatment, IWA publishing, London, UK, 2000.

5.28 H. Monclus, S. Zacharias, A. Santos, M. Pidou, S. Judd, Criticality of Flux and Aeration for a Hollow Fiber Membrane Bioreactor, Sep. Sci. Technol. 45 (2010) 956–961.

5.29 I. Martin-Garcia, V. Monsalvo, M. Pidou, P. Le-Clech, S.J. Judd, E.J. McAdam, B. Jefferson, Impact of membrane configuration on fouling in anaerobic membrane bioreactors, J. Membr. Sci. 382 (2012) 41–49.

5.30 M. Tiranuntakul, P.A. Schneider, V. Jegatheesan, Assessments of critical flux in a pilot-scale membrane bioreactor, Bioresource Technol. 102 (2011) 5370–5374.

5.31 T. Zsirai, P. Buzatu, P. Aerts, S. Judd, Efficacy of relaxation, backflushing, chemical cleaning and clogging removal for an immersed hollow fibre membrane bioreactor, Water Res. 46 (2012) 4499–4507.

5.32 D. Martinez-Sosa, B. Helmreich, T. Netter, S. Paris, F. Bischof, H. Horn, Pilot-scale anaerobic submerged membrane bioreactor (AnSMBR) treating municipal wastewater: the fouling phenomenon and long-term operation, Water Sci. Technol. 64 (2011) 1804–1811.

5.33 R.K. Dereli, M.E. Ersahin, H. Ozgun, I. Ozturk, D. Jeison, F. van der Zee, J.B. van Lier, Potentials of anaerobic membrane bioreactors to overcome treatment limitations induced by industrial wastewaters, Bioresource Technol. 122 (2012), 160–170.

5.34 J.D. Allison, D.S. Brown, K.J. Novo-Gradak, MINTEQA2/PRODEFA2, A Geochemical Assessment Model for Environmental Systems: Version 3.0, EPA/600/3-91/021, USEPA, Washington DC, USA, 1991.

5.35 L. Pastor, D. Mangin, R. Barat, A. Seco, A pilot-scale study of struvite precipitation in a stirred tank reactor: Conditions influencing the process, Bioresource Technol. 99 (2008) 6285–6291.

5.36 W.J. Jane Gao, H.J. Lin, K.T. Leunga, B.Q. Liao, Influence of elevated pH shocks on the performance of a submerged anaerobic membrane bioreactor, Process Biochem. 45 (2010) 1279–1287.

5.37 A. Sweity, W. Ying, S.a Belfer, G. Oron, M. Herzberg, pH effects on the adherence and fouling propensity of extracellular polymeric substances in a membrane bioreactor, J. Membr. Sci. 378 (2011) 186–193.

CHAPTER 6:

Performance of industrial scale hollow-fibre membranes in a submerged anaerobic MBR (HF-SAnMBR) system at mesophilic and psychrophilic conditions

Abstract

The aim of this work was to evaluate the effect of temperature on the performance of industrial hollow-fibre (HF) membranes treating urban wastewater in a submerged anaerobic MBR system (SAnMBR). To this end, a demonstration plant with two commercial HF ultrafiltration membrane modules (PURON®, Koch Membrane Systems, PUR-PSH31) was operated at 20, 25 and 33 ºC. The mixed liquor total solid (MLTS) level was a key factor affecting membrane permeability (K). K was higher under psychrophilic than mesophilic conditions when operating at similar transmembrane fluxes and MLTS, because the biomass activity of the psychrophilic mixed liquor was lower than the mesophilic mixed liquor. Thus, lower extracellular polymeric substances (EPS) and soluble microbial products (SMP) levels were observed at psychrophilic conditions, which affected not only the three-dimensional floc matrix, but also the fouling propensity. However, no chemical cleaning was needed during the experimental period (almost one year) because no irreversible fouling problems were detected.

Keywords

Extracellular polymeric substances (EPS); industrial hollow-fibre membranes; membrane permeability; mesophilic and psychrophilic anaerobic conditions; soluble microbial products (SMP).

Highlights

MLTS level was a key factor affecting membrane permeability.
K was lower under mesophilic than psychrophilic conditions, at similar J and MLTS.
Lower EPS and SMP were observed under mesophilic than psychrophilic conditions.
EPS and SMP affected the three-dimensional floc matrix and the fouling propensity.
No chemical cleaning was needed during the experimental period (almost one year).

A. Robles, M.V. Ruano, J. Ribes, J. Ferrer
Performance of industrial scale hollow-fibre membranes in a submerged anaerobic MBR (HF-SAnMBR) system at mesophilic and psychrophilic conditions
Sep. Purif. Technol. 104 (2013), 290 – 296

6.1 Introduction

Aerobic membrane bioreactors (MBR) have recently become not only a legitimate alternative to conventional activated sludge processes, but also the preferred choice for urban wastewater treatment because of their reliability and efficiency [6.1]. The quality of the effluent is very good but the operating costs of aeration and sludge handling remain the biggest drawbacks of aerobic MBR technology [6.2]. High energy demand and high waste generation are both at odds with sustainability principles.

In this respect, in recent years there has been increasing interest in the study of anaerobic urban wastewater treatment at ambient temperatures, mainly focused on the sustainability benefits of anaerobic processes as opposed to aerobic processes (lower sludge production, lower energy demands, and energy recovery from methane production). The main challenge of anaerobic biotechnology is to develop treatment systems, such as anaerobic membrane bioreactors (AnMBR) that prevent biomass loss and enable high sludge retention times (SRTs) in order to compensate for the low growth rates of anaerobic microorganisms at ambient temperatures [6.3]. However, operating membrane bioreactors at high SRTs may imply operating at high MLTS levels. This is considered to be one of the main constraints on membrane operation [6.4] because it can result in a higher membrane fouling propensity.

Besides MLTS levels, several sludge properties have been identified elsewhere as key factors that affect membrane performance (because they can lead to the onset of either irreversible or irrecoverable fouling), *i.e.* particle size distribution, extracellular polymeric substances (EPS), soluble microbiological products (SMP), and biomass concentration [6.5]. Moreover, the limitations of anaerobic metabolism at ambient temperatures can cause non-complete organic matter degradation, leading to an increase in colloidal and soluble components that increase the fouling propensity of membranes [6.6]. Threshold EPS have been reported not only as the major sludge component keeping the floc in a three-dimensional matrix, but also as a key membrane foulant in MBR systems [6.7; 6.8; 6.9]. On the other hand, it is widely accepted that EPSs and SMPs are identical concepts [6.1], and that SMPs easily accumulate in MBRs because they are absorbed on the membrane surface where they block membrane pores and reduce membrane permeability [6.10]. Moreover, SMPs influence the structure and porosity of the cake layer formed on membrane surface [6.11]. Both EPSs and SMPs have been directly related to the biomass concentration of the mixed liquor [6.12], as well as to operating SRT [6.13]: a key factor in anaerobic biomass growth at ambient temperatures.

Several published studies have evaluated the effect of different sludge properties on membrane fouling in SAnMBR technology on a laboratory scale [6.3; 6.4; 6.14; 6.15]. However, there is still a lack of knowledge about the assessment of the different fouling mechanisms in SAnMBR technology treating low-strength wastewaters on an industrial scale. Moreover, the effect of the main operating conditions on membrane fouling has not been adequately evaluated on a laboratory scale because it depends considerably on the membrane size, especially in the case of hollow-fibre (HF) membranes. Therefore, further research is needed on HF-SAnMBR technology with industrial scale membranes in order to facilitate the design and implementation of this technology in full-scale WWTPs.

The main objective of this paper was to study the effect of temperature on the performance of industrial hollow-fibre membranes. This study is innovative because it studies membrane performance under specific conditions similar to those expected in full-scale plants located in warm climate regions (*e.g.* Mediterranean ones). In this respect, this study shows the long-term performance of industrial HF membranes at mesophilic and psychrophilic conditions in an SAnMBR demonstration plant treating effluent from a pre-treatment WWTP. The SAnMBR plant is located in Valencia (Spain), where the average daily ambient temperature ranges from 15 and 35 ºC approx. during the year. The assessment of the impact of temperature upon membrane performance will shed more light on the possible applications of this technology in the treatment of urban wastewater at ambient temperatures.

6.2 Materials and methods

6.2.1 Demonstration plant description

The previously described SAnMBR demonstration plant entailing industrial-scale HF membranes (see Chapter 2) was used to conduct this study. In this study, the obtained permeate from MT1 (see Figure 2.1) was continuously recycled to the system in order to test different J_{20} without affecting the hydraulic retention time (HRT) of the process. On the other hand, the obtained permeate from MT2 was fed to the CIP tank and corresponds to the effluent wastewater of the system (see Figure 2.1). Hence, different operating filtration modes were set in MT2 to achieve the different HRTs that were programmed to assess the biological process performance.

6.2.2 Demonstration plant operation

The SAnMBR demonstration plant was operated at a constant SRT of 70 days and three different temperatures (20, 25 and 33 ºC). The pH of the mixed liquor remained relatively stable at around 6.75 (the pH ranged from 6.5 to 7), and the alkalinity of the mixed liquor remained at values of approximately 600 mg$CaCO_3$ L^{-1}. During the experimental period, the usual membrane operating mode was as follows: a 300-second basic F-R cycle (250 s filtration and 50 s relaxation), 30 seconds of back-flush every 10 F-R cycles, 40 seconds of ventilation every 10 F-R cycles, and 30 seconds of degasification every 50 F-R cycles. The up-flow sludge velocity in the membrane surface was set to 2.7 mm s^{-1}; and the average specific gas demand per square metre of membrane (SGD_m) was 0.23 Nm^3 m^{-2} h^{-1} (corresponding to a gas sparging velocity of around 7 mm s^{-1}) . The operating period shown in this work was divided into four experimental periods taking into account both the 20 ºC-normalised transmembrane flux (J_{20}) and the controlled temperature values studied. Table 6.1 summarises the average values for J_{20}, 20 ºC-normalised critical flux ($J_{C,20}$), temperature and HRT in each experimental period. As mentioned before, the J_{20} values were set by using MT1, whilst the HRT values were set by using MT2.

Table 6.1 Average values for the 20 ºC-normalised transmembrane flux (J_{20}), 20 ºC-normalised critical flux ($J_{C,20}$), controlled temperature (T), and hydraulic retention time (HRT) in each operating period. J_{20} was studied in MT1 and HRT in the system was controlled with MT2. $J_{C,20}$ determined in MT1 at MLTS of 23 g L^{-1} and SGD_m of 0.23 Nm^3 h^{-1} m^{-2}. N.D.: not determined.

Variable	**Period i** (days 1 to 58)	**Period ii** (days 59 to 170)	**Period iii** (days 171 to 206)	**Period iv** (days 207 to 310)
J_{20} in MT1 (LMH)	13.3	10	12	13.3
$J_{C,20}$ in MT1 (LMH)	N.D.	14	13.5	14
Controlled T (ºC)	33	33	25	20
HRT (h)	16.5	5.5, 9.5, 12	5.5	24.5

Table 6.2 shows the average wastewater characteristics of the influent entering the anaerobic reactor. This table highlights the significant influent sulphate levels, and also the wide variation in the influent loads, reflected by the high standard deviation of each parameter. The uncertainty associated with each value includes both the standard deviation of the different samples analysed throughout the experiment and the variation coefficient associated with the analytical methods.

Table 6.2 Average influent wastewater characteristics.

Parameter	Unit	Mean ± SD
TSS	mgTSS L^{-1}	242 ± 189
VSS	mgVSS L^{-1}	199 ± 148
Total COD	mgCOD L^{-1}	459 ± 263
Soluble COD	mgCOD L^{-1}	81 ± 23
VFA	mgCOD L^{-1}	7 ± 6
SO_4-S	mgS L^{-1}	107 ± 28
NH_4-N	mgN L^{-1}	28.6 ± 9.0
PO_4-P	mgP L^{-1}	3.1 ± 1.3
Alk	mg$CaCO_3$ L^{-1}	309.7 ± 44.8

6.2.3 Analytical methods

6.2.3.1 Water quality analysis

In addition to monitoring the process on-line, the performance of the biological process was assessed by taking 24-hour composite samples from influent and effluent streams, and taking grab samples of biogas and anaerobic sludge once a day. The following parameters were analysed in influent, effluent and anaerobic sludge: total solids (TS); volatile solids (VS); total suspended solids (TSS); volatile suspended solids (VSS); volatile fatty acids (VFA); carbonate alkalinity (Alk); sulphate (SO_4-S); total sulphide (measured as HS^-); nutrients (ammonium (NH_4-N) and orthophosphate (PO_4-P)); and total and soluble chemical oxygen demand (COD_T and COD_S, respectively). Particle size distribution, and EPS and SMP levels were measured twice a month. Furthermore, a sludge sample was fixed for microbiological analysis once a week.

Solids, COD, sulphate, sulphide and nutrients were determined according to Standard Methods [6.16]. Alk and VFA levels were determined by titration according to the method proposed by WRC [6.17].

6.2.3.2 Floc structure and particle size distribution

Particle size distribution was measured twice a month using a MASTERSIZER2000 coupled to Hydro 2000SM (A) with a detection range of 0.02 to 2000 μm. The sludge floc was examined by light microscopy and the images were captured with a microscope Leica DM2500 and a Leica DFC420c digital camera.

6.2.3.3 Microbiological analysis

Microbiological analysis was performed once a week by using the FISH (fluorescent in situ hybridization) technique [6.18] to identify the different species of sulphate reducing bacteria (SRB) and methanogenic archaea (MA). Hybridized cells were enumerated by capturing images with a Leica DM2500 epifluorescence microscope and a Leica DFC420c digital camera and using automated bacteria quantification software [6.19] programmed in Matlab®. Further details about the microbiological analysis approach can be found in Giménez *et al*. [6.20].

6.2.3.4 EPS and SMP extraction and measurement

EPS and SMP extraction and measurement were carried out twice a month. Mixed liquor was collected from the membrane tank and a sample of 150 mL was centrifuged at 2000xG for 15 min at 4 ºC (Eppendorf Centrifuge 5804R). The supernatant was filtered with a 1.2 μm filter and the SMP levels (SMP_C and SMP_P, related to carbohydrates and proteins, respectively) were measured. The EPS extraction was based on the Cation Exchange Resin (CER) method proposed by Frølund *et al*. [6.21]. The sludge pellets were resuspended to their original volume using a buffer consisting of 2 mM Na_3PO_4, 4 mM NaH_2PO_4, 9 mM NaCl and 1 mM KCl at pH 7. The EPS extraction was performed as follows: 100 mL of the suspension was transferred to an extraction container and 70 g/g MLVS of CER were added; the suspension was stirred at the selected intensity (900 rpm) and extraction time (20 hours) at 4 ºC. The extracted EPS was harvested by centrifuging the CER/sludge suspension for 15 min at 12000xG and 4 ºC to remove the CER and MLTS. The supernatant was taken and filtered with a 1.2 μm filter and the extracted EPS levels ($eEPS_C$ and $eEPS_P$, related to carbohydrates and proteins, respectively) were measured. The carbohydrates and proteins of both SMP and eEPS were determined by colorimetry according to the methodology proposed by Dubois *et al*. [6.22] and Lowry *et al*. [6.23], respectively. Bovine serum albumin (BSA) and glucose were used as protein and carbohydrate standards, respectively.

6.2.3.5 Membrane performance indices

The 20 ºC-normalised membrane permeability (K_{20}) was calculated using a simple filtration model (Eq. 6.1) that takes into account the TMP and J values monitored on line. This simple filtration model includes a temperature correction (Eq. 6.2) to take into account the dependence of permeate viscosity on temperature. The same temperature correction was used for J (Eq. 6.3). The total membrane

resistance (R_T) was represented theoretically by the following partial resistances (Eq. 6.4): membrane resistance (R_M); cake layer resistance (R_C); and irreversible layer resistance (R_I).

$$K_{20} = \frac{J_T f_T}{TMP} \quad \textbf{Eq. 6.1}$$

$$f_T = e^{-0.0239\,(T-20)} \quad \textbf{Eq. 6.2}$$

$$J_{20} = J_T \cdot e^{-0.0239\,(T-20)} \quad \textbf{Eq. 6.3}$$

$$R_T = R_M + R_C + R_I \quad \textbf{Eq. 6.4}$$

Moreover, a modified flux-step method [6.24] was carried out in order to determinate the $J_{C,20}$ of each operating interval. Each $J_{C,20}$ was calculated according to the weak definition of this concept, *i.e.* the flux above which the relationship between J_{20} and TMP becomes non-linear. Table 6.1 shows the obtained results for $J_{C,20}$ in each experimental period. These values were obtained at 23 g L^{-1} of MLTS and SGD_m of 0.23 $Nm^3\ h^{-1}\ m^{-2}$.

6.3 Results and discussion

6.3.1 Long-term membrane performance at mesophilic and psychrophilic conditions

Table 6.1 shows the obtained results for $J_{C,20}$ in each experimental period (determined at 23 g L^{-1} of MLTS and SGD_m of 0.23 $Nm^3\ h^{-1}\ m^{-2}$). For instance, on day 125 and day 240, $J_{C,20}$ resulted in 14 LMH in both trials. Therefore, the critical flux remained generally at values over 14 LMH during the operating period since SGD_m was maintained at 0.23 $Nm^3\ h^{-1}\ m^{-2}$ and MLTS remained generally below 23 g L^{-1} (see days 1-125 and 240-310). Hence, the long-term operating shown in this study was mainly carried out at sub-critical filtration conditions since J_{20} was varied from 10 to 13.3 LMH [6.25].

Figure 6.1 shows the average daily K_{20} (calculated with Eq. 6.1 and Eq. 6.2) obtained during the operating period, and the average daily MLTS level in the anaerobic sludge entering the membrane tank. Notice that the MLTS level in the membrane tank increases in proportion to the ratio between the net permeate flow rate and the sludge flow rate entering the membrane tank. Therefore, the operating MLTS in the membrane tank was actually higher (up to 5 g L^{-1}) than the ones shown in this work, since the data presented correspond to the MLTS level entering the membrane tank.

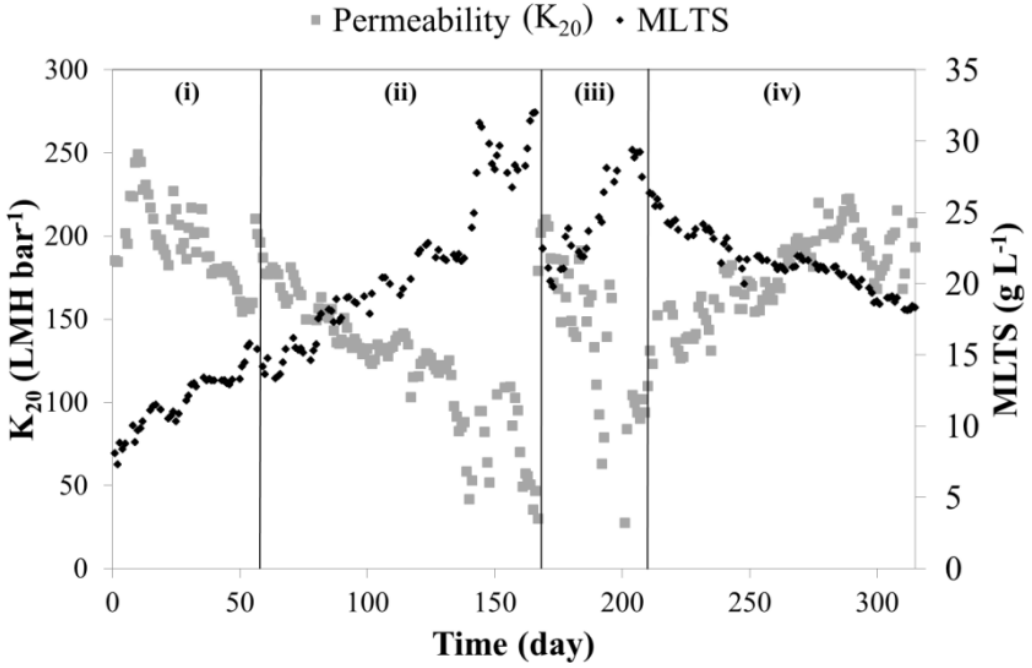

Figure 6.1 Evolution of membrane permeability and MLTS during the operating period. Experimental period: **(i)** J_{20} at 13.3 LMH and 33 ºC; **(ii)** J_{20} at 10 LMH and 33 ºC; **(iii)** J_{20} at 12 LMH and 25 ºC; and **(iv)** J_{20} at 13.3 LMH and 20 ºC.

Figure 6.1 shows the considerable extent to which the MLTS level affects K_{20} in the four experimental periods in this study (the MLTS decrease observed on day 170 was caused by a problem in the sludge wasting system). Every variation of the MLTS level was inversely reflected on K_{20}. It is important to note that even at high MLTS levels (up to 25 g L^{-1}), K_{20} remained at sustainable values. As can be seen in period ii, K_{20} remained at values above 100 LMH bar^{-1} until a MLTS level of around 25 g L^{-1} was reached. Similar behaviour was observed in period iii. This figure also shows that at relatively stable MLTS levels (see days 90 - 110 or days 120 - 135), K_{20} remained quite stable. This K_{20} stability could be due to the low TMP achieved during this period (below 0.1 bars), which minimises membrane compression and causes a stable R_M. Moreover, as can be observed in period iv, K_{20} improved when MLTS decreased, which indicates the absence of irreversible fouling components on R_T. Hence, the higher K_{20} obtained during the first months of operation was related to a lower cake layer formation rate due to lower MLTS levels. It is important to highlight the two different effects that determine R_C: the cake layer formation rate (due to the filtration process) and the cake layer removal rate (due mainly to biogas sparging). It is well known that at a given SGD_m the cake layer removal efficiency decreases when the MLTS level increases. Therefore, in our study, which was carried out at a constant SGD_m, the decrease in K_{20} caused by a higher MLTS level was mainly due to an increase in the cake layer

formation rate. However, no irreversible fouling was detected, mainly as a result of both working at sub-critical filtration conditions and establishing an adequate membrane operating mode.

Figure 6.1 shows the different membrane performances in period i (mesophilic conditions) and period iv (psychrophilic conditions), which were conducted at identical J_{20}. Similar K_{20} values were achieved even though membranes operated at higher MLTS levels in period iv than in period i. This behaviour can be observed better in Figure 6.2.

6.3.2 Sludge properties affecting membrane performance at mesophilic and psychrophilic conditions

6.3.2.1 Effect of MLTS on membrane performance

Figure 6.2 shows how the MLTS level affects K_{20} in three of the four series carried out during different operating periods. As can be observed in this figure, under the selected operating conditions (0.23 $Nm^3\ h^{-1}\ m^{-2}$ of SGD_m), a linear dependency of K_{20} on MLTS was observed for each J_{20}. Any increase in the MLTS level caused a proportional decrease in K_{20}. As this figure illustrates, the behaviour in the two experimental series carried out at 33 ºC (13.3 and 10 LMH of J_{20}) is similar since both series were carried out at the same mesophilic operating conditions. Despite observing no clear differences between the two series conducted at mesophilic conditions, it can be concluded that at similar MLTS levels the higher the J_{20} applied the lower the K_{20} obtained. This difference can also be observed in the slope of the linear regression between the MLTS level and K_{20}. This slope was slightly higher with a J_{20} of 13.3 LMH than of 10 LMH, which indicated a higher reversible fouling propensity at higher fluxes. Moreover, both mathematical equations seem to indicate that the dependency of K_{20} on MLTS starts becoming independent of J_{20} when the MLTS level tends to zero since both intercept terms present similar values. On the contrary, the impact of J_{20} on K_{20} gets higher as MLTS increases. This behaviour tallies well with the classical definition of membrane permeability treating pure water. On the other hand, Figure 6.2 shows clear differences in the resulting K_{20} between both mesophilic and psychrophilic conditions. In this respect, K_{20} is considerably higher when the system is operated at psychrophilic than at mesophilic conditions. For instance, as can be deduced from the slope of the linear regressions resulting from the experimental series conducted at 13.3 LMH, K_{20} is more sensitive to changes in MLTS when operating at 20 ºC than at 33 ºC. Figure 6.2 illustrates that the differences in K_{20} observed between mesophilic and psychrophilic conditions are higher when the MLTS level decreases. In contrast, when the MLTS level increases, this parameter becomes a key factor affecting

membrane performance in the operating conditions studied. Hence, it is possible to state that the influence of MLTS on K_{20} under mesophilic and psychrophilic operating conditions is also conditioned by other operating factors.

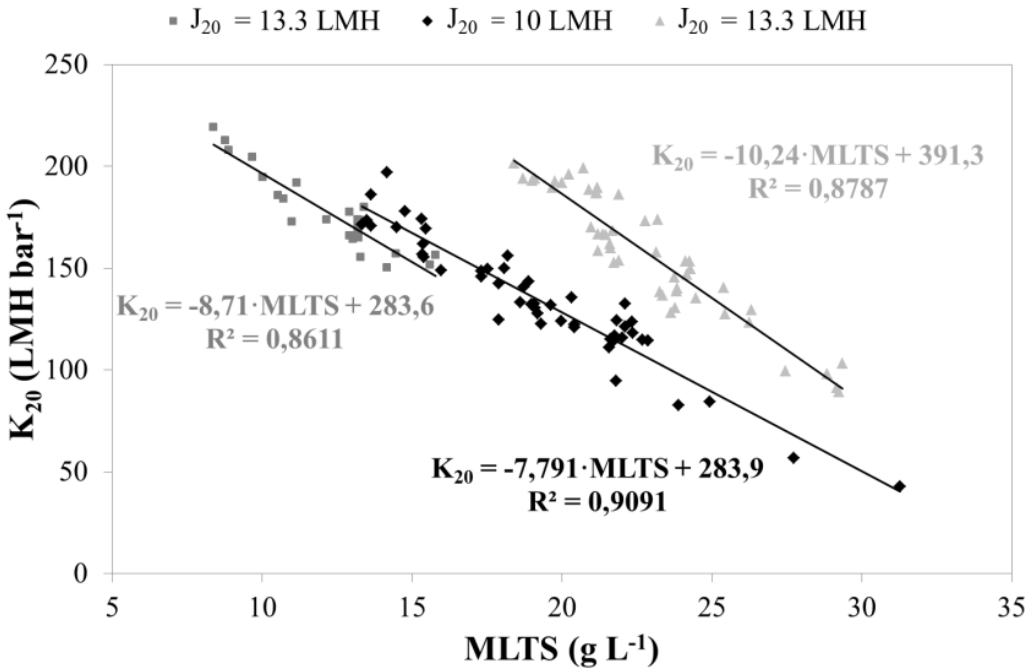

Figure 6.2 Linear dependence of K_{20} upon MLTS and mathematical equation for three of the four experimental series: J_{20} at 13.3 LMH and 33 ºC; J_{20} at 10 LMH and 33 ºC; and J_{20} at 13.3 LMH and 20ºC.

6.3.2.2 Effect of particle size distribution on membrane performance

Figure 6.3 shows the distribution of the average particle size in the mixed liquor corresponding to the three temperatures studied. For each temperature period, only one distribution is shown since the mean particle size throughout each temperature period depicted the same distribution shape. As can be seen in this figure, a unimodal floc size distribution was observed in every experimental period, which indicates that only one population of aggregates was present in the sludge. As ascertained by other authors [6.4], the single-peak distribution was demonstrated by microscopic observations of the flocs in the mixed liquor (see Figure 6.4). In these microscopic observations, a large amount of fine flocs in the mixed liquor was not observed. Thus, a low membrane fouling propensity, *i.e.* a low probability of permeability decrease, was expected [6.4; 6.26]. However, a slight decrease in the average value of these unimodal floc size distributions was detected when the temperature was reduced. These results were corroborated by examining the flocs in the mixed liquor by light microscopy. The mean floc sizes observed under psychrophilic conditions were smaller than those observed at mesophilic ones.

Therefore, at psychrophilic conditions lower cake layer porosities may be reached as a result of the small average particle sizes. Moreover, as a result of the operating pressure, lower cake layer porosities may lead to higher cake layer tortuosity, which implies a higher specific cake layer resistance [6.27]. Nevertheless, Figure 6.3 shows that no particles smaller than 0.3 μm were detected. Hence, considering that the mean pore size of the membranes is 0.05 μm, these results predict that, for our case study, this decrease of the particle sizes due to the decrease of temperature could only affect the cake layer formation and/or consolidation over the membrane surface, but no other membrane filtration resistances related to MLTS, such as the one related to the internal fouling due to the blockage of pore channels.

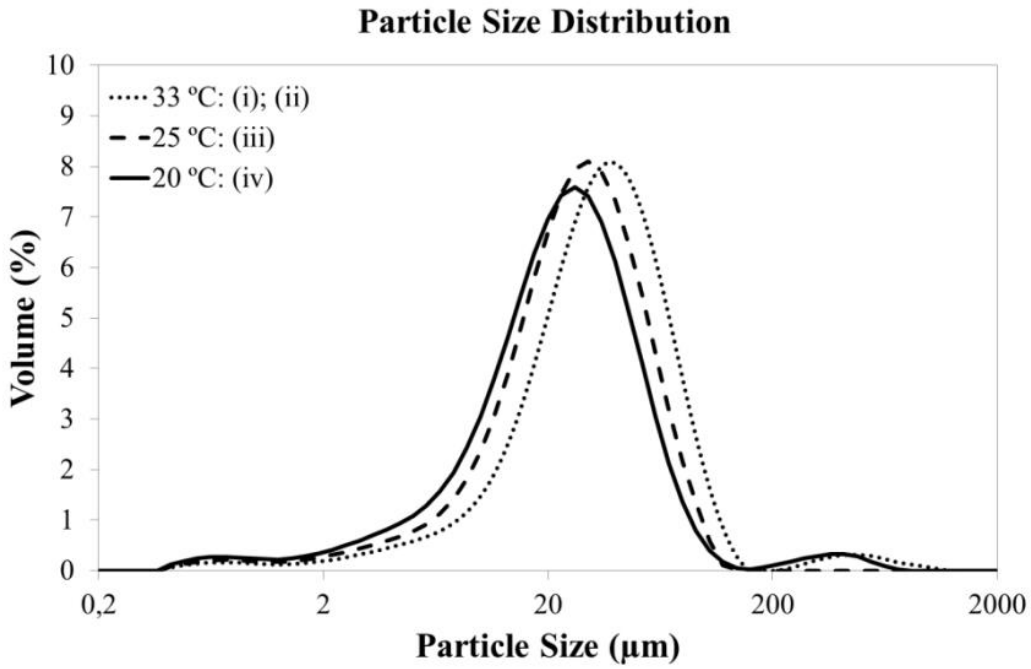

Figure 6.3 Distribution of mean particle size during the experimental period: **(i)** J_{20} at 13.3 LMH and 33 ºC; **(ii)** J_{20} at 10 LMH and 33 ºC; **(iii)** J_{20} at 12 LMH and 25 ºC; and **(iv)** J_{20} at 13.3 LMH and 20 ºC.

6.3.2.3 Effect of biomass population, and EPS and SMP compounds on membrane performance

Figure 6.4 shows a sample of the microscopic observations of floc size and structure in the mixed liquor under mesophilic (Figure 6.4a) and psychrophilic (Figure 6.4b) conditions. This figure illustrates that the mean floc size in the mixed liquor was lower under psychrophilic conditions (approx. from 25 to 100 μm) than under mesophilic conditions (approx. from 50 to 200 μm). This reduction in floc size can be attributed to the impact of temperature upon the anaerobic biomass

growth rate. Since the SRT was set constant to 70 days throughout the operating period, biomass activity declined sharply when the temperature was decreased. Thus, lower biomass concentrations were detected under psychrophilic conditions (see Table 6.3), which resulted in a lower enzymatic activity that could affect the sludge conglomeration.

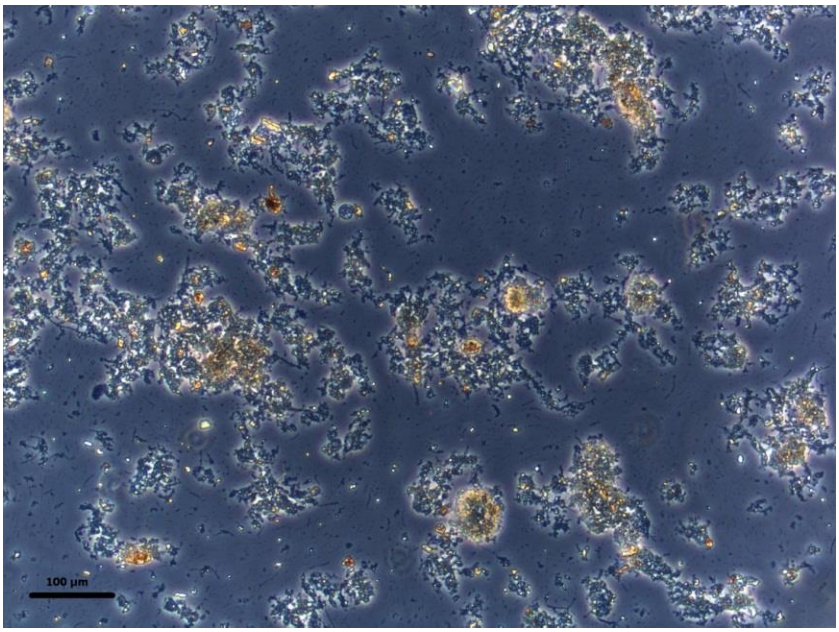

(a)

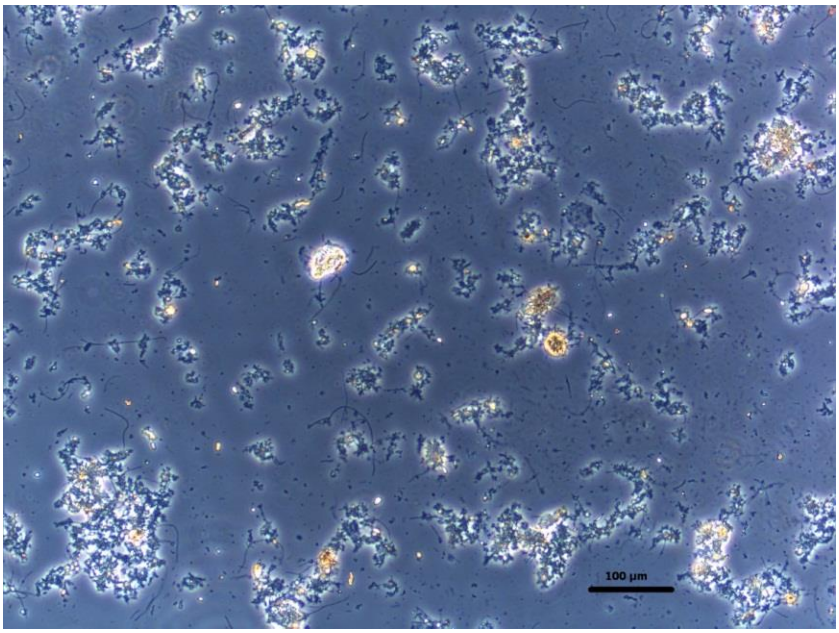

(b)

Figure 6.4 Microscopic observation of mixed liquor at **(a)** mesophilic and **(b)** psychrophilic conditions (bar = 100μm).

Table 6.3 shows the average values derived from the anaerobic biomass activity in both mesophilic and psychrophilic operating periods. The uncertainty associated with each value includes both the standard deviation of the different samples analysed throughout the experimental period and the coefficient of variation associated with the analytical methods. This table shows a lower biomass concentration (referred to SRB and MA) at psychrophilic conditions than at mesophilic ones. This lower biomass concentration resulted in a considerably lower concentration of EPS in the mixed liquor, and also a lower SMP production. It is important to note that the EPS level is considered to be one of the main sludge components that keeps the floc in a three-dimensional matrix. This fact was also observed in Figure 6.4, *i.e.* the average sizes of the psychrophilic flocs were lower than the mesophilic flocs, probably as a result of the lower EPS levels shown in Table 6.3.

Table 6.3 Average sludge characteristics. Nomenclature: **SRB**: sulphate reducing bacteria; **MA**: methanogenic archaea; **SMP**: soluble microbial products; **EPS**: extracellular polymeric substances; **C**: carbohydrates; and **P**: proteins.

Parameter	**Unit**	**Mean ± SD**	
		Mesophilic (33 ºC)	**Psychrophilic (20 ºC)**
SRB	%	6 ± 2	3 ± 1
MA	%	4 ± 2	2 ± 1
SRB + MA	%	10 ± 4	5 ± 2
Specific SMP_C	mg g^{-1}MLVS	5 ± 1	2 ± 1
Specific SMP_P	mg g^{-1}MLVS	82 ± 3	14 ± 5
SMP-P/C ratio	mgSMP_P $mg^{-1}SMP_C$	16.4	7.0
$eEPS_C$	mg g^{-1}MLVS	34 ± 4	24 ± 6
$eEPS_P$	mg g^{-1}MLVS	121 ± 9	74 ± 13
eEPS-P/C ratio	mgEPS_P $mg^{-1}EPS_C$	16.4	7.0

Table 6.3 shows a considerably higher fraction of proteins than carbohydrates in both eEPS and SMP. The protein (P)/carbohydrate (C) ratio of SMP was 16.4 and 7.0 for mesophilic and psychrophilic sludge, respectively. The P/C ratio of eEPS was 3.6 and 3.1 for mesophilic and the psychrophilic sludge, respectively. Liao *et al*. [6.28] observed that an increase in the P/C ratio resulted in an increase of the hydrophobicity of the floc, thus increasing the cake layer formation propensity. Since no clear differences were observed in the eEPS-P/C ratios, it was assumed that this parameter made no critical contribution to the differences observed in this study concerning the consolidation of the cake layer upon the membrane surface under mesophilic and psychrophilic conditions. A considerable difference was, however, observed between both SMP-P/C ratios under mesophilic and psychrophilic conditions

(more than double). Therefore, the SMP level (and SMP_P particularly) was identified as one key factor affecting K_{20} in this work. Pollice *et al*. [6.12] established that there is proportionality between biomass concentration and SMP production due to the increased release of organic material from cell lysis. In this sense, results from Table 6.3 show both higher biomass concentrations and higher SMP and eEPS levels under mesophilic conditions than under psychrophilic conditions. It is well known that the amount of SMP and EPS in mixed liquor directly affects membrane permeability. This effect was also observed in our study because lower values of K_{20} were reached when the SMP and eEP_C levels in the mixed liquor were higher, *i.e.* at higher temperatures. Moreover, Huang *et al*. [6.10] observed that the SMP could induce inter-particle pore blocking when they pass through the cake layer, resulting in a higher cake layer formation rate. In this respect, a given gas sparging intensity could be less effective in detaching the cake layer from the membrane surface when there is a higher SMP level in the system, as a result of a higher propensity of cake layer formation and consolidation upon the membrane surface [6.7]. In addition, some studies have shown that when membranes are operated at sub-critical filtration conditions (as in our study), SMP and EPS are the main factors affecting membrane fouling since these compounds are accumulated in the system [6.12].

Hence, the differences observed in this study between K_{20} under mesophilic and psychrophilic operating conditions can be explained by a higher fouling propensity at mesophilic than psychrophilic conditions due to a higher biomass concentration resulting in higher SMP and eEPS levels in the mixed liquor. In either case, since the level of EPS and SMP in the mixed liquor influences the structure and porosity of the cake layer created over the membrane surface [6.11], this higher fouling propensity was related to the reversible cake layer resistance. This hypothesis was strengthened because the K_{20} returned to its previous values when the MLTS level decreased.

6.3.2.4 Other factors minimising the onset of irreversible fouling problems

As it has been mentioned before K_{20} returned to initial values when the MLTS concentration decreased (see Figure 6.1). The recovery of K_{20} was achieved without any chemical cleaning of the membrane. Hence, after almost one year of operation, no irreversible fouling problems were detected, even with high MLTS and temperature shocks affecting biomass population and its derived compounds. Moreover, it is important to highlight that the total filtering resistance remained at similar values throughout the whole operating period, when operating at similar MLTS levels. The total filtering resistance was $1.5 \cdot 10^{12}$ m^{-1} in average. Further details on the absence of irreversible fouling in this system can be found in Robles *et al*. [6.25].

Apart from operating at sub-critical filtration conditions and establishing an adequate membrane operating mode, no chemical cleaning was necessary probably because of the pH of the mixed liquor, which was always kept at values below 7 by recycling the biogas produced for in-situ sparging purposes (*i.e.* the CO_2 remained in the mixed liquor, resulting in alkalinity values of approx. 600 $mgCaCO_3\ L^{-1}$). pH values below 7 may result in a negligible formation of chemical precipitates (*e.g.* struvite), which favours the absence of chemical fouling problems [6.25]. Low pH indirectly means low fouling propensity due to low dispersion of sludge flocs resulting in sub-products generation directly related to biofouling, *i.e.* colloids and solutes or biopolymers [6.29]. Moreover, it has been observed that low pH levels result in a low adherence and fouling propensity of EPS [6.30]. Nevertheless, further research is needed in order to assess the actual effect of pH on membrane fouling in anaerobic systems.

6.3.3 Overall biological process performance

The SAnMBR plant was operated at a SRT of 70 days and the HRT was ranged from approx. 5 to 24 hours. As regards the COD removal efficiency no significant differences were observed under both mesophilic and psychrophilic operating conditions, taking also into account the considerable dynamics in the influent load. COD removal efficiencies of around 85 % and low effluent COD concentrations (< 100 mg L^{-1}) were achieved. No significant differences were observed throughout the period, mainly due to the high retention of solids achieved by the physical process and the significant operating SRT. On the other hand, the decrease in the temperature resulted in an increase in the average sludge production (approx. 30%): from about 0.16 to 0.23 kg VS kg^{-1} $COD_{REMOVED}$. This increase was attributed to the decline of the biomass activity observed when the temperature was reduced, particularly due to a decrease in the hydrolysis rate. This decrease in the hydrolysis rate resulted in an accumulation of solids in the system. Nevertheless, the sludge production at psychrophilic temperature conditions was still lower than the common values observed in aerobic treatment of urban wastewaters (≈ 0.5 kg VS kg^{-1} $COD_{REMOVED}$). Concerning the biogas production, the decrease in the temperature resulted in a decrease in the methane production (approx. 20%), which was also related to the decrease in the hydrolysis rate. Nevertheless, a significant average biogas production (around 100 L d^{-1}) was observed throughout the whole experimental period, which evidenced a suitable biological process performance under both mesophilic and psychrophilic operating conditions. Regarding the sulphate reducing activity, influent sulphate was almost completely reduced to sulphide for the whole operating period (around 95%). It resulted in a concentration of hydrogen sulphide in the biogas of 1.3% in average.

6.4 Conclusions

MLTS was identified as one of the key factors that affects K_{20}. Nevertheless, K_{20} remained at sustainable values even at high MLTS (up to 25 g L^{-1}). The floc analysis showed a smaller mean floc size under psychrophilic than under mesophilic conditions, mainly due to a lower biomass activity, and thus lower EPS levels. Higher membrane fouling propensities were observed under mesophilic than under psychrophilic conditions due to higher SMP production. Nevertheless, after almost one year of operating, no irreversible fouling problems were detected. The long-term membrane performance demonstrated that HF-SAnMBR is a promising technology for urban wastewater treatment.

6.5 Acknowledgements

This research work has been supported by the Spanish Research Foundation (CICYT Projects CTM2008-06809-C02-01 and CTM2008-06809-C02-02, and MICINN FPI grant BES-2009-023712) and Generalitat Valenciana (Projects GVA-ACOMP2010/130 and GVA-ACOMP2011/182), which are gratefully acknowledged.

6.6 References

6.1 P. Le-Clech, V. Chen, T.A.G. Fane, Fouling in membrane bioreactors used in wastewater treatment, J. Membr. Sci. 284 (2006) 17–53.

6.2 D. Martinez-Sosa, B. Helmreich, T. Netter, S. Paris, F. Bischof, H. Horn, Anaerobic submerged membrane bioreactor (AnSMBR) for municipal wastewater treatment under mesophilic and psychrophilic temperature conditions, Bioresource Technol. 102 (2011) 10377–10385.

6.3 H.J. Lin, K. Xie, B. Mahendran, D.M. Bagley, K.T. Leung, S.N. Liss, B.Q. Liao, Factors affecting sludge cake formation in a submerged anaerobic membrane bioreactor, J. Membr. Sci. 361 (2010) 126–134.

6.4 S. Judd, C. Judd, The MBR Book: Principles and Applications of Membrane Bioreactors for Water and Wastewater Treatment, 2nd edition, Elsevier, ISBN: 978-0-08-096682-3, 2011.

6.5 H.J. Lin, K. Xie, B. Mahendran, D.M. Bagley, K.T. Leung, S.N. Liss, B.Q. Liao, Sludge properties and their effects on membrane fouling in submerged anaerobic membrane bioreactors (SAnMBRs), Water Res. 43 (2009), 3827–3837.

6.6 M. Herrera-Robledo, D.M. Cid-León, J.M. Morgan-Sagastume, A. Noyola, Biofouling in an anaerobic membrane bioreactor treating municipal sewage, Sep. Purif. Technol. 81 (2011) 49–55.

6.7 S. Tsuneda, H. Aikawa, H. Hayashi, A. Yuasa, A. Hirata, Extracellular polymeric substances responsible for bacterial adhesion onto solid surface, FEMS Microbiology Letters 223 (2003) 287–292.

6.8 S. Lyko, D. Al-Halbouni, T. Wintgens, A. Janot, J. Hollender, W. Dott, T. Melin, Polymeric compounds in activated sludge supernatant–Characterisation and retention mechanisms at a full-scale municipal membrane bioreactor, Water Res. 41 (2007) 3894–3902.

6.9 F.G. Meng, S.R. Chae, A. Drews, M. Kraume, H.S. Shin, F.L. Yang, Recent advances in membrane bioreactors (MBRs): membrane fouling and membrane materials, Water Res. 43 (2009) 2405–2415.

6.10 Z. Huang, S.L. Ong, H.Y. Ng, Feasibility of submerged anaerobic membrane bioreactor (SAMBR) for treatment of low-strength wastewater, Water Sci. Technol. 58 (2008) 1925–1931.

6.11 L. Dvořák, M. Gómez, M. Dvořáková, I. Růžičková, J. Wanner, The impact of different operating conditions on membrane fouling and EPS production, Bioresource Technol. 102 (2011) 6870–6875.

6.12 A. Pollice, A. Brookes, B. Jefferson, S. Judd, Sub-critical flux fouling in membrane bioreactors–a review of recent literature, Desalination 174 (2005) 221–230.

6.13 Y. Lee, C. Jinwoo, Y. Seo, J.W. Lee, K.H. Ahn, Modeling of submerged membrane bioreactor process for wastewater treatment, Desalination 146 (2002) 451–457.

6.14 Z. Huang, S.L. Ong, H.Y. Ng, Submerged anaerobic membrane bioreactors for low-strength wastewater treatment: Effect of HRT and SRT on treatment performance and membrane fouling, Water Res. 45 (2011) 705–713.

6.15 H. Lin, B.Q. Liao, J. Chen, W. Gao, L. Wang, F. Wang, X. Lu, New insights into membrane fouling in a submerged anaerobic membrane bioreactor based on characterization of cake sludge and bulk sludge, Bioresource Technol. 102 (2011), 2373–2379.

6.16 American Public Health Association/American Water Works Association/Water Environmental Federation, Standard methods for the Examination of Water and Wastewater, 21st edition, Washington DC, USA, 2005.

6.17 Water Res. Commission, University of Cape Town, Simple titration procedures to determine H2CO3* alkalinity and short-chain fatty acids in aqueous solutions containing known concentrations of ammonium, phosphate and sulphide weak acid/bases, Report No. TT 57/92, Pretoria, Republic of South Africa, 1992.

6.18 R. Amann, B.J. Binder, R.J. Olson, S.W. Chisholm, R., Deveroux, D.A. Stahl, Combination of 16s Ribosomal-RNA-Targeted Oligonucleotide Probes with Flow-Cytometry for Analyzing Mixed Microbial-Populations, App. Environ. Microbiol. 56 (1990), 1919–1925.

6.19 L. Borrás, Microbiological techniques applied to the identification and quantification of microorganisms that are present in EBPR systems (Técnicas microbiológicas aplicadas a la identificación y cuantificación de microorganismos presentes en sistemas EBPR), 2008, PhD Thesis, Departamento de Ingeniería Hidráulica y Medio Ambiente, Universidad Politécnica de Valencia, Spain.

6.20 J.B. Giménez, L. Carretero, M.N. Gatti, N. Martí, L. Borras, J. Ribes, A. Seco, Reliable method for assessing the COD mass balance of a submerged anaerobic membrane bioreactor (SAMBR) treating sulphate-rich municipal wastewater, Water Sci. Technol. 66 (2012) 494–502.

6.21 B. Frølund, R. Palmgren, K. Keiding, P.H. Nielsen, Extraction of extracellular polymers from activated sludge using a cation exchange resin, Water Res. 30 (1996) 1749–1758.

6.22 M. Dubois, K.A. Gilles, J.K. Hamilton, P.A. Rebers, F. Smith, Colorimetric method for determination of sugar and related substances, Anal. Chem. 28 (1956) 350–356.

6.23 O.H. Lowry, N.J. Rosebrough, A.L. Farr, R.J. Randall, Protein measurement with the folin phenol reagent, J. Biol. Chem. 193 (1951) 265–275.

6.24 A. Robles, M.V. Ruano, F. García-Usach, J. Ferrer, Sub-critical filtration conditions of commercial hollow-fibre membranes in a submerged anaerobic MBR (HF-SAnMBR) system: The effect of gas sparging intensity, Bioresource Technol. 114 (2012) 247–254.

6.25 A. Robles, M.V. Ruano, F. García-Usach, J. Ferrer, Sub-critical long-term operation of industrial scale hollow-fibre membranes in a submerged anaerobic MBR (HF-SAnMBR) system, Sep. Purif. Technol. 100 (2012) 88–96.

6.26 H.Y. Ng, S.W. Hermanowicz, Specific resistance to filtration of biomass from membrane bioreactor reactor and activated sludge: effects of exocellular polymeric substances and dispersed microorganisms, Water Environ. Res. 77 (2005) 187–192.

6.27 A.A. Merdaw, A.O. Sharif, G.A.W. Derwish, Mass transfer in pressure-driven membrane separation processes, Part I, Chem. Eng. J. 77 (2011) 215–228.

6.28 B.Q. Liao, D.G. Allen, I.G. Droppo, G.G. Leppard, S.N. Liss, Surface properties of sludge and their role in bioflocculation and settleability, Water Res. 35 (2001) 339–350.

6.29 W.J. Jane Gao, H.J.Lin, K.T. Leunga, B.Q. Liao, Influence of elevated pH shocks on the performance of a submerged anaerobic membrane bioreactor, Process Biochem. 45 (2010) 1279–1287.

6.30 A. Sweity, W. Ying, S. Belfer, G. Oron, M. Herzberg, pH effects on the adherence and fouling propensity of extracellular polymeric substances in a membrane bioreactor, J. Membr. Sci. 378 (2011) 186–193.

CHAPTER 7:

A filtration model applied to submerged anaerobic MBRs (SAnMBRs)

Abstract

The aim of this study was to develop a model able to correctly reproduce the filtration process of submerged anaerobic MBRs (SAnMBRs). The proposed model was calibrated and validated in a SAnMBR demonstration plant fitted with industrial-scale hollow-fibre membranes. Three suspended components were contemplated in the model: total solids concentration; dry mass of cake on the membrane surface; and dry mass of irreversible fouling on the membrane surface. The model addressed the following physical processes: the build-up and compression of the cake layer during filtration; cake layer removal using biogas sparging to scour the membrane; cake layer removal during back-flushing; and the consolidation of irreversible fouling. The short- and long-term validation of the model resulted in correlation coefficients (R^2) of 0.962 and 0.929, respectively.

Keywords

Industrial-scale hollow-fibre membranes; resistance-in-series-based; filtration model; submerged anaerobic MBR.

Highlights

A model for filtration in SAnMBRs has been developed.
This model (based on the resistance-in-series model) can easily be used with any biological model.
The model was calibrated and validated using industrial-scale hollow-fibre membranes.
Short- and long-term validation resulted in R^2 of 0.962 and 0.929, respectively.

A. Robles, M.V. Ruano, J. Ribes, A. Seco, J. Ferrer
A filtration model applied to submerged anaerobic MBRs (SAnMBRs)
Submitted to J. Membrane Sci. 444 (2013), 139 – 147

7.1 Introduction

In recent years, membrane bioreactors (MBRs), particularly submerged versions [7.1], have attracted a lot of attention in the realm of wastewater treatment. Rather than aerobic MBRs, submerged anaerobic MBRs (SAnMBR) have emerged as a promising technology for municipal wastewater treatment because not only do they feature the main advantages of MBRs (*i.e.* clarified and partially disinfected effluent and a smaller environmental footprint for WWTPs) but they also offer the greater sustainability of anaerobic rather than aerobic processes, *i.e.* low sludge production (due to low anaerobic biomass yield), low energy consumption (no aeration required) and, finally, the biogas generated can be used as an energy resource.

However, further study of membrane technology is needed in order to gain more insight into how to optimise their efficiency. One key operating challenge of SAnMBR technology in particular concerns how membrane performance can be optimised whilst minimising membrane fouling. In this respect, mathematical modelling of MBR technology may help provide an insight into the factors that play a key role in membrane fouling [7.1], whilst providing invaluable data for the design, forecast and control of membrane technology [7.2].

The biological processes involved in MBR systems can be successfully modelled by using either classical models [7.3; 7.4] or plant-wide models [7.5; 7.6].

As for the modelling of the physical processes (in addition to the modelling of integrated processes, *i.e.* biological + physical processes), several empirical/semi-empirical models have been proposed [7.7; 7.8; 7.9] to express the relationship between sludge characteristics and/or operating conditions, and membrane fouling. Broekmann *et al*. [7.10] modelled the pore blocking and cake formation in membrane filtration taking into account the adhesive forces between the particles and the membrane surface, and also the impact of the particle and membrane pore size distributions. Duclos-Orsello *et al*. [7.11] proposed a model for the decrease in flux during microfiltration (as a function of the bulk solids concentration) using three classical fouling mechanisms: pore blockage, pore constriction and cake formation. Li and Wang [7.12] proposed a "comprehensive mathematical model for membrane fouling in a submerged MBR" that includes the impact of shear intensity on membrane scouring. Busch *et al*. [7.13] created a model of submerged hollow-fibre (HF) membrane filtration that incorporated the geometry and hydrodynamics of the system. Zarragoitia-González *et al*. [7.14] developed a mathematical model for simulating the filtration process and impact of aeration in submerged MBRs, including biological kinetics and the dynamics of sludge build-up on membranes and its removal by

the formation and degradation of soluble microbial products (SMP). Mannina *et al*. [7.1] proposed an advanced model for MBR systems that takes into account the exchange of mixed liquor total solids (MLTS) and SMP between mixed liquor and membrane surface. Wu *et al*. [7.15] modelled membrane fouling in a submerged MBR by considering the role of MLTS, soluble and colloidal components, activated sludge floc distribution and aeration intensity.

Most of the above-mentioned modelling approaches can reproduce the way in which sludge affects membrane performance. However, these models usually rely on parameters that cannot be measured on line and require specific laboratory equipment (*e.g.* SMP). Moreover, some of them cannot reproduce the impact of the different membrane module operating stages (relaxation, back-flushing…) or cannot easily be used together with a given biological model. In this respect, some authors are currently developing simple new filtration models that can easily be used in conjunction with biological processes in an attempt to reproduce the impact of the most critical fouling variables, *i.e.* membrane tank shear intensity and MLTS. For instance, Ludwig *et al*. [7.16] proposed a dynamic model for simulating submerged membranes on the basis of the standard parameters usually measured in filtration processes (MLTS and cross flow aeration); whilst Sarioglu *et al*. [7.17] proposed a "resistance-in-series" membrane filtration model that considers overall membrane resistance in terms of three distinct components: intrinsic membrane resistance, accumulated solids resistance and membrane fouling resistance.

The main objective of our study, based on said resistance-in-series filtration model, is to propose a filtration model able to correctly reproduce the filtration performance of SAnMBR technology. On the basis of the experimental results obtained whilst operating a SAnMBR plant fitted with industrial-scale HF membranes, we developed, calibrated and validated a filtration model (based on the resistance-in-series model) that can easily be used in conjunction with a biological model. The model proposed takes into account the effect of the shear intensity in the membrane tank caused by the flow of recycled biogas. This makes it possible to reproduce the membrane scouring process occurring during the different membrane module operating stages (filtration, relaxation…). The physical processes contemplated in our model are: cake layer build-up and compression during filtration; cake layer removal using biogas sparging to scour the membrane; cake layer removal during back-flushing; and the consolidation of irreversible fouling.

7.2 Materials and methods

7.2.1 SAnMBR plant description

The filtration model proposed in our study was calibrated and validated using data obtained from the previously described demonstration-scale SAnMBR system (see Chapter 2). The plant consists of an anaerobic reactor with a total volume of 1.3 m^3 (0.4 m^3 head space for biogas) connected to two membrane tanks each with a total volume of 0.8 m^3 (0.2 m^3 head space for biogas). Each membrane tank (MT) has one industrial HF ultrafiltration membrane unit (PURON®, Koch Membrane Systems (PUR-PSH31) with 0.05 μm pores). Each module has a total membrane surface of 30 m^2. To recover the bubbles of biogas in the permeate leaving the membrane tank, two degasification vessels (DV) were installed: one between each MT and the respective vacuum pump. The funnel-shaped section of conduit makes the biogas accumulate at the top of the DV. The resulting permeate is stored in the CIP tank.

Complete stirring conditions are assumed in the anaerobic reactor and the MTs. To provide proper stirring conditions in the anaerobic reactor, a portion of the sludge is continuously pumped from bottom to top. In addition, a fraction of the produced biogas is recycled from its bottom to improve the stirring conditions. On the other hand, the sludge is continuously recycled from the anaerobic reactor through the external MTs. Another fraction of the produced biogas is also recycled to the MTs from the bottom of each fibre bundle, which improves the stirring conditions.

The membrane operating schedule included not only the classic membrane operating stages (filtration, relaxation and back-flushing) but also a ventilation stage. In the ventilation stage, permeate is pumped into the membrane tank through the degasification vessel instead of through the membrane. The aim of ventilation is to recover the biogas that accumulates in the degasification vessel. As regards membrane cleaning, ventilation acts as relaxation since no transmembrane flux is applied whilst maintaining a given gas sparging intensity.

For further details of this SAnMBR system, see Chapter 2 or Robles *et al*. [7.18].

7.2.2 Monitoring system

Many on-line sensors and automatic devices were installed in order to automate and control plant operations and provide on-line information about the state of the process. The on-line sensors used in this study were: 1 solids concentration sensor located in the anaerobic reactor; 1 flow indicator transmitter for the permeate pump; 1 flow indicator transmitter for the membrane tank blower; 1 pH-temperature sensor located in the membrane tank; and 1 liquid pressure indicator transmitter to monitor the transmembrane pressure (TMP). The actuators used in this study were: 1 group of on/off flow-direction valves to control the different membrane operating stages (filtration, back-flushing, ventilation…), and 2 frequency converters to control the rotating speed of the permeate pump and the membrane tank blower.

In addition to being monitored on line, grab samples of anaerobic sludge were taken once a day to assess filtration performance. MLTS was determined according to Standard Methods [7.19] using procedure 2540 B. Influent COD was also daily determined by Standard Methods [7.19].

7.3 Description of model

Our proposed model was developed on the basis of the resistance-in-series model using the experimental results obtained from operating a SAnMBR plant fitted with industrial-scale HF membranes. Our model contemplates two parameters usually measured in filtration processes: MLTS and biogas recycling flow. Although MLTS is an elementary parameter in comparison with the complexity of the model, MLTS was defined as model input because it can be directly linked with the existing biological models and it is easy to measure. This model reproduces the main processes that occur during filtration in SAnMBRs: cake layer build-up and consolidation during filtration; membrane scouring by biogas sparging; removal of cake layer by back-flushing; and irreversible fouling consolidation. MLTS and biogas recycling flow were identified as the key model parameters related to cake layer build-up and membrane scouring by biogas sparging. In this regard, MLTS and biogas recycling flow finally determine the dry mass of cake on the membrane surface. This was established on the basis of the experimental results obtained from different flux-step trials conducted throughout the whole operating period of the plant. On the other hand, the irreversible fouling consolidation process was considered as a function not only of the dry mass of solids forming the cake-layer but also function of an irreversible fouling rate constant. This irreversible fouling rate constant indirectly reflects the possible effect of the different bulk characteristics affecting the

physiological state of the biomass thus affecting the irreversible fouling phenomenon, such as, for instance, EPSs and SMPs composition.

7.3.1 Conceptual modelling

Resistance-in-series model

The proposed filtration model is based on the resistance-in-series model. The resistance-in-series model (Eq. 7.1) describes the flux through each in-series medium area (A) using Darcy's law: the permeate volume (V_P, m^3) is driven through each medium by a difference in transmembrane hydraulic pressure and the total filtration resistance (R_T, m^{-1}) is assumed to be the sum of the different assumed partial resistances.

$$J = \frac{1}{A}\frac{dV_P}{dt} = \frac{TMP}{\mu \cdot R_T} \qquad \textbf{Eq. 7.1}$$

Like other authors [7.16, 7.17], our model contemplates the following three partial resistances (Eq. 7.2): cake layer resistance (R_C, m^{-1}); irreversible fouling resistance (R_I, m^{-1}); and intrinsic membrane resistance (R_M, m^{-1}). Taking into account the membrane operating mode, cake build-up was considered to be the main fouling mechanism in the short-term, and irreversible fouling, the main fouling mechanism in the long-term. Therefore, the model must be calibrated correctly not only in the short term but also in the long term.

$$R_T = R_C + R_I + R_M \qquad \textbf{Eq. 7.2}$$

As regards R_C, Sarioglu *et al*. [7.17] assumed the cake layer to be homogenous, making it possible to calculate the cake layer thickness (δ_C) using Eq. 7.3.

$$\delta_C = \frac{m_c}{\rho_c \cdot (1-\varepsilon) \cdot A} \qquad \textbf{Eq. 7.3}$$

where:

- m_c is the dry mass of cake layer (kg).
- ρ_c is the cake density (kg m^{-3}).
- A is the area of the medium (m^2).
- ε is the porosity (dimensionless) $= \frac{Total\ pores\ volume}{Total\ porous\ media\ volume}$

Defining the coefficient m_c/A as ω_C (the mass of cake deposited per membrane area, kg m^{-2}), redefines the cake layer thickness thus (Eq. 7.4):

$$\delta_C = \frac{\omega_C}{\rho_c \cdot (1-\varepsilon)} \qquad \textbf{Eq. 7.4}$$

On the other hand, R_C can be calculated by combining the cake layer thickness equation and the Carman-Kozeny equation for flow through porous passages as follows [7.17]:

$$R_C = 180\frac{(1-\varepsilon)\cdot \omega_C}{\varepsilon^3 \cdot d_p^2 \cdot \rho_c} \qquad \textbf{Eq. 7.5}$$

where:

- d_p is the pore diameter (m^2).

From Eq. 7.5 we define the average specific cake resistance (α_C, m kg^{-1}) as shown in Eq. 7.6 and R_C can be expressed as shown in Eq. 7.7.

$$\alpha_C = \frac{180 \cdot (1-\varepsilon)}{\varepsilon^3 \cdot d_p^2 \cdot \rho_c} \qquad \textbf{Eq. 7.6}$$

$$R_C = \omega_C \cdot \alpha_C \qquad \textbf{Eq. 7.7}$$

Concerning R_I, the same approach than the one used for defining α_C and ω_C was considered for defining the average specific irreversible fouling resistance (α_I, m kg^{-1}) and the mass of irreversible fouling per membrane area (ω_I, kg m^{-2}). Therefore, assuming R_M to be constant over time, the resistance-in-series model shown in Eq. 7.1 can be assumed to represent the dynamic evolution of TMP as shown in Eq. 7.8.

$$TMP\,(t) = J \cdot \mu \cdot (\omega_C \cdot \alpha_C + \omega_I \cdot \alpha_I + R_M) \qquad \textbf{Eq. 7.8}$$

Defining the average specific resistances allows reducing a great deal of effort related to correctly determine specific characteristics of the filter medium that Carman-Kozeny equation requires. It is, therefore, advisable to minimise the number of parameters to be included in the model.

The value of α_C was assumed to be time and TMP dependent (its calibration protocol is shown in following sections).

7.3.2 Cake layer compression and sub-critical fouling

As per the methodology proposed by Bugge *et al*. [7.20] and Jørgensen *et al*. [7.21], a linear relationship was assumed between the specific resistance of the cake and TMP (see Eq. 7.9).

$$\alpha_{C,TMP} = \alpha_{C,0} \cdot \left(1 + \frac{TMP}{TMP_a}\right) \quad \textbf{Eq. 7.9}$$

where:

- $\alpha_{C,TMP}$ is the specific resistance of the cake at the operating TMP (kg m^{-2}).
- $\alpha_{C,0}$ is the specific resistance of the cake at zero pressure (kg m^{-2}).
- TMP_a is the pressure needed to double the specific resistance (Pa).

On the other hand, cake compression caused by a drop in pressure is time dependent due to both the deformation of soft sludge flocs and the structural rearrangement of particles [7.22]. The increase in the specific resistance of the cake as a result of the pressure drop over time is described in Eq. 7.10.

$$\frac{d\alpha_C}{dt} = k_t \cdot \left(\alpha_{C,TMP} - \alpha_C\right) \quad \textbf{Eq. 7.10}$$

where:

- $\frac{d\alpha_C}{dt}$ is the change in α_C (kg m^{-2}).
- dt is the time step (s).
- k_t is the time constant (s^{-1}).
- α_C is the specific resistance of the cake (kg m^{-2}).

Eq. 7.11 shows the Euler solution (using the Backward Euler Method) to Eq. 7.10.

$$\alpha_C(t) = \alpha_C(t - \Delta t) + k_t \cdot \left(\alpha_{C,TMP} - \alpha_C\,(t - \Delta t)\right) \cdot \Delta t \quad \textbf{Eq. 7.11}$$

where:

- $\alpha_C(t)$ is the specific resistance of the cake at time t (kg m^{-2}).
- $\alpha_C(t - \Delta t)$ is the specific resistance of the cake at a previous moment in time (kg m^{-2}).
- Δt is the time step (s).

In our study, setting the maximum time step size to 10 seconds was enough to minimise the numerical error. Moreover, the time step must be maintained at low levels to properly reproduce the effect of the different operating stages (*i.e.* filtration, back-flushing, etc.) on membrane performance.

On the other hand, the overall filtration resistance was seen to increase (even when operating sub-critically) during extended filtration periods. This was attributed mainly to increasing partial resistances, not contemplated in the model, associated with specific fouling mechanisms such as colloidal matter absorption. In this respect, Hughes and Field [7.23] observed that colloidal matter absorption increases the specific resistance of cake-like deposits, as a result of which their impact is greater than it would be without such absorption. Therefore, we incorporated an additional single dependence of α_C on time (see Eq. 7.12).

$$\alpha_C(t) = \alpha_C(t - \Delta t) + k_{SF} \cdot \Delta t \qquad \textbf{Eq. 7.12}$$

where:

- k_{SF} is the sub-critical fouling parameter (kg m^{-2} s^{-1}).

In our model, we propose that Eq. 7.11 (dependence of cake compression on TMP and time) be combined with Eq. 7.12 (dependence of sub-critical fouling on time) to give the final variation in α_C (see Eq. 7.13). Therefore, when the maximum α_C related to the structural rearrangement of particles is reached at a given TMP, it is possible to account for the increase in α_C due to the absorption of colloids.

$$\alpha_C(t) = \alpha_C(t - \Delta t) + \max\left(k_{SF}, k_t \cdot \left(\alpha_{C,TMP} - \alpha_C\,(t - \Delta t)\right)\right) \cdot \Delta t \qquad \textbf{Eq. 7.13}$$

7.3.3 Modelling approach

We propose a black-box approach to describe the most important physical interactions occurring in fouling: the attachment of solids to the membrane surface; the removal of solids from the membrane surface; and the irreversible fouling of the membrane. Stirring is considered to be complete, therefore uniform MLTS and shear conditions are assumed. The notation used in this modelling approach complies with the nomenclature proposed by Corominas *et al.* [7.24] and the Petersen/Gujer matrix structure.

The model contemplates 3 suspended components:

- X_{TS} (kg TS m^{-3}) is the MLTS concentration (this component can be obtained from the biological model).
- X_{m_C} (kg TS) is the dry mass of cake on the membrane surface.
- X_{m_I} (kg TS) is the dry mass of irreversible fouling on the membrane surface.

The model we developed contemplates a total of four kinetically governed physical processes: (1) cake layer build-up during filtration; (2) cake layer removal using biogas sparging to scour the membrane; (3) cake layer removal during back-flushing; and (4) irreversible fouling consolidation. Table 7.1 shows the stoichiometry of these four processes. The model does not consider diffusive back transport as this process is thought to be less significant than the other processes considered [7.16].

Table 7.1 Stoichiometry of the kinetic processes contemplated in the model.

Component i / **j Process**	X_{TS} **(kg TS m^{-3})**	X_{m_C} **(kg TS)**	X_{m_I} **(kg TS)**
1. Cake layer formation	-1	1	
2. Membrane scouring by biogas sparging	1	-1	
3. Cake layer detachment during back-flushing	1	-1	
4. Irreversible fouling consolidation		-1	1

Table 7.2 shows the conversion factors to be applied to the elements of the model in the continuity equations. Since no biological processes are contemplated in relation to the cake layer, a value of 1 was assigned to the yield of X_{m_I} generated from X_{m_C}. However, this parameter could be calculated by taking into account the actual content of the bulk foulants that contribute to irreversible fouling (*i.e.* $i_{TS\_X_{m_I}}$ in Table 7.2).

Table 7.2 Conversion factors to be applied in the continuity equations of the mass of the model.

Component i / **Conservation for**	X_{TS} **(kg TS)**	X_{m_C} **(kg TS)**	X_{m_I} **(kg TS)**
Mass (kg TS) i_{TS_i}	-1	1	1

Table 7.3 shows the kinetic expressions of the processes included in the model. Process 1 (cake layer build-up) is the convective transport of foulants (X_{TS} in the model) to the membrane, which is a

function of the permeate flow-rate (Q_{20P}) and the bulk concentration (X_{TS}). Process 2 (membrane scouring by biogas sparging) is the impact of the hydrodynamic conditions in the membrane tank caused by biogas sparging (measured as BRF_V: biogas recycling flow per bulk volume in the membrane tank). In our study, a maximum membrane scouring velocity ($q_{MS,Max}$) was defined for process 2. In process 3, the back-flushing removal rate is defined as a function of the back-flushing flow rate (Q_{20BF}) and X_{m_C}. Like Sarioglu *et al*. [7.17], we defined a maximum back-flushing removal velocity ($q_{BF,Max}$) for process 3.

Table 7.3 Kinetic expressions of the processes included in the model.

j Process	*Kinetic expression*
1. Cake layer formation	$Q_{20P} \cdot X_{TS}$
2. Membrane scouring by biogas sparging	$q_{MS,Max} \cdot M_{X_{m_C}} \cdot I_{MS} \cdot BRF_V \cdot X_{m_C}$
3. Cake layer detachment during back-flushing	$q_{BF,Max} \cdot Q_{20BF} \cdot M_{X_{m_C}} \cdot X_{m_C}$
4. Irreversible fouling consolidation	$q_{IF,Max} \cdot X_{m_C}$

One half-saturation switching function (M_{Xm_C}, Eq. 7.14) for both membrane scouring (process 2) and back-flushing (process 3) was used to vary the removal of solids smoothly as the cake layer disappeared [7.17].

$$M_{X_{m_C}} = \frac{X_{m_C}}{K_{S,\,X_{m_C}} + X_{m_C}} \qquad \textbf{Eq. 7.14}$$

where:

- K_{S,Xm_C} is the half-saturation coefficient for the mass of cake solids during membrane scouring and back-flushing (kg TS).

On the basis of the results obtained from different flux-step trials conducted in accordance with Robles *et al*. [7.25], a fouling rate (FR) model was defined as a function of BRF_V and MLTS (see Eq. 7.15).

$$FR = K_F \cdot e^{(J_{20} \cdot (\beta_1 \cdot BRF_V + \beta_2 \cdot MLTS + \gamma))} \qquad \textbf{Eq. 7.15}$$

where:

- K_F is the adjustment parameter representing the fouling rate when the gross 20 ºC-normalised transmembrane flux (J_{20}) tends to zero (Pa s^{-1}).

- β_1 (s^2 m^{-1}), β_2 (s m^2 kg^{-1}), γ (s m^{-1}) are the model parameters.

Eq. 7.15 predicts that when the membranes are operated sub-critically at given operating conditions (BRF_V and MLTS), the value of FR remain low, which implies operating at maximum membrane scouring velocity ($q_{MS,Max}$). On the other hand, a considerable increase in FR is observed when operating supra-critically, which implies a reduction in the membrane scouring rate (q_{MS}). Therefore, one sigmoid inhibition function (I_{MS}, Eq. 7.16) was defined and used in process 2 to model the impact of filtering at conditions above or below critical levels.

$$I_{MS} = \frac{1}{1 + FR} = \frac{1}{1 + K_F \cdot e^{(J_{20} \cdot (\beta_1 \cdot BRF_V + \beta_2 \cdot MLTS + \gamma))}} \quad \textbf{Eq. 7.16}$$

Moreover, on the basis of long-term experimental results, the value of γ was defined as a function of R_I to account for the reduction over time in the filtering capacity of the membranes due to the onset of irreversible fouling. This dependence on irreversible fouling can be expressed as:

$$\gamma_t = \gamma_0 - \left(R_{I_t} - R_{I_0}\right) \cdot k_{RI} \quad \textbf{Eq. 7.17}$$

where:

- γ_t is the value of γ at time t (s m^{-1}).
- γ_0 is the value of γ at the initial time (s m^{-1}).
- R_{I_t} is the irreversible fouling resistance at time t (m^{-1}).
- R_{I_0} is the irreversible fouling resistance at the initial time (m^{-1}).
- k_{RI} is the proportional constant (s).

Finally, the irreversible fouling (process 4) is represented in the proposed model as a direct function of X_{m_C} and a maximum irreversible fouling kinetic constant ($q_{IF,Max}$). As mentioned before, this irreversible fouling rate constant indirectly reflects the possible effect of the different bulk characteristics affecting the physiological state of the biomass thus affecting the irreversible fouling phenomenon, such as, for instance, EPSs and SMPs composition. In this regard, EPSs and SMPs seem to be the main factors affecting irreversible fouling in MBRs [7.26], which are directly dependent on both T [7.27] and SRT [7.28]. Commonly, SMP and EPS composition decrease as SRT increases, whilst SMP and EPS increase as T increases due to a higher microbial activity. Therefore, $q_{IF,Max}$ is expected to be function of T and SRT. Nevertheless, further research is required to assess the real

dependence of $q_{IF,Max}$ on T and SRT and maybe to find proper link variables between biological and filtration models besides the MLTS used in this model.

7.4 Calibration of model

On the basis of the data available for estimating the parameter (dynamic measurements of TMP, MLTS and biogas recycling flow) we decided to divide the calibration procedure into the following parameter estimation subsets: off-line calibration using short-term data, dynamic calibration using short-term data, parameter estimation from experimental data, and dynamic calibration using long-term data. On the other hand, based on expert knowledge, we assigned default values to those parameters that could not be estimated from the available data.

7.4.1 Off-line calibration in the short-term

The following parameters for membrane scouring by biogas sparging were calibrated by using the short-term filtration data obtained from different flux-step trials according to Robles *et al*. [7.25]: K_F, β_1, β_2 and γ_0. The FR results from the flux-step trials were adjusted to Eq. 7.15 using the GRG non-linear method included in the Solver complement of MS Excel. Figure 7.1 shows the FR results obtained in the flux-step trials conducted at three BRF_V (0.0023, 0.0032 and 0.0046 $Nm^3\ h^{-1}\ m^{-3}$, equivalent to BRFs of 5, 7 and 10 $Nm^3\ h^{-1}$, respectively) and MLTS of 18.5 (Figure 7.1a), 22.5 (Figure 7.1b) and 28.5 g L^{-1} (Figure 7.1c).

Figure 7.1 illustrates the different values estimated for the parameters of Eq. 7.15. As Figure 7.1 shows, it was possible to adjust K_F, β_1, β_2 and γ_0 to identical values for the different MLTS operating levels (18.5, 22.5 and 28.5 g L^{-1}). This clearly demonstrates that critical flux is dependant not only on BRF_V [7.25] but also on MLTS.

The calibrated values of parameters K_F, β_1, β_2 and γ_0 included in the model are shown in Table 7.4.

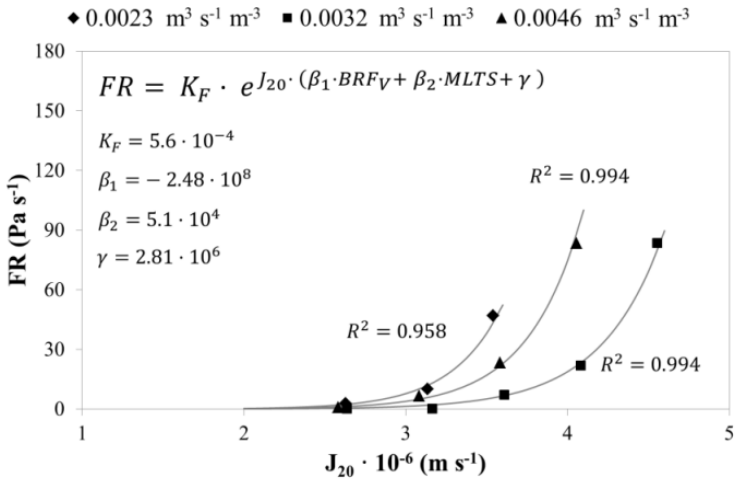

(a)

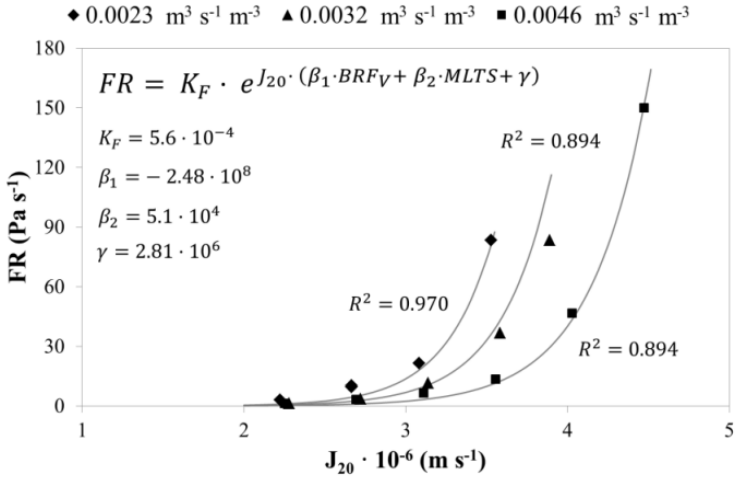

(b)

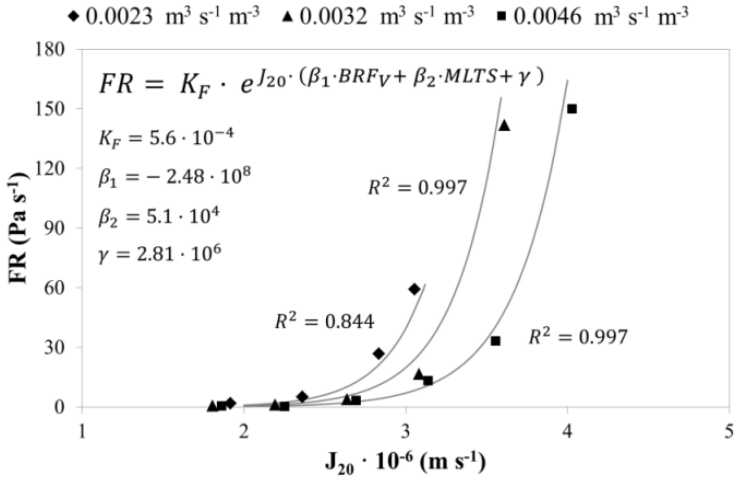

(c)

Figure 7.1 Effect of J_{20} on FR when operating at BRF_V of 0.0023, 0.0032 and 0.0046 $Nm^3\ h^{-1}\ m^{-3}$, and MLTS of **(a)** 18.5, **(b)** 22.5, and **(c)** 28.5 $g\ L^{-1}$.

Table 7.4 Values assumed for the different parameters included in the proposed filtration model.

Parameter	Unit	Value	SD	Calculation method
$q_{MS,Max}$		6.31	0.37	Dynamically calibrated
$q_{BF,Max}$	m^{-3}	1		Default value
$q_{IF,Max}$	s^{-1}	$3 \cdot 10^{-07}$		Calculated from experimental data
$K_{S,XmC}$	kg SST	0.2		Calculated from experimental data
$\alpha_{C,0}$	m kg^{-1}	$1.02 \cdot 10^{13}$	$0.07 \cdot 10^{13}$	Dynamically calibrated
TMP_a	kPa	18.9	0.4	Dynamically calibrated
k_t	s^{-1}	1		Default value
k_{SF}	m kg^{-1} s^{-1}	$4.09 \cdot 10^{10}$	$0.08 \cdot 10^{10}$	Dynamically calibrated
K_F	Pa s^{-1}	$5.6 \cdot 10^{-4}$		Experimentally calibrated
β_1	s^2 m^{-1}	$-2.48 \cdot 10^{8}$		Experimentally calibrated
β_2	s m^2 kg^{-1}	$5.1 \cdot 10^{4}$		Experimentally calibrated
γ_0	s m^{-1}	$2.81 \cdot 10^{6}$		Experimentally calibrated
k_{RI}	s	$1.6 \cdot 10^{-07}$		Calculated from experimental data
α_I	m kg^{-1}	$1 \cdot 10^{14}$		Default value

7.4.2 Dynamic calibration in the short-term

Similar to Bugge *et al*. [7.20] and Jørgensen *et al*. [7.21], this dynamic calibration was carried out using data obtained from different flux-step trials conducted at different BRFs (5, 7 and 10 Nm^3 h^{-1}) and MLTS levels (18.5, 22.5 and 28.5 g L^{-1}). Parameters k_{SF}, $\alpha_{C,0}$, TMP_a, and $q_{MS,Max}$ related to cake build-up and compression (process 1) and membrane scouring by biogas sparging (process 2) were calibrated. The dynamic calibration consisted of adjusting the simulated TMP (TMP_{SIM}) to the experimental TMP (TMP_{EXP}). This non-linear parameter was calculated using the least squares method together with the subspace trust region method [7.29], based on the interior-reflective Newton method (implemented in MATLAB® LSQNONLIN), and the Runge-Kutta method (MATLAB® ode45 function). The minimising objective function (*OF*) applied is shown in Eq. 7.18.

$$OF = \sum \sqrt{(TMP_{SIM} - TMP_{EXP})^2} \qquad \textbf{Eq. 7.18}$$

In this dynamic calibration, the values used for the other parameters contemplated in the proposed model are shown in Table 7.4 together with the values estimated for $q_{MS,Max}$, k_{SF}, $\alpha_{C,0}$ and TMP_a. It is

important to emphasise that the values obtained for α_C and TMP_a were similar to the ones observed by Jørgensen *et al*. [7.21] in aerobic MBRs.

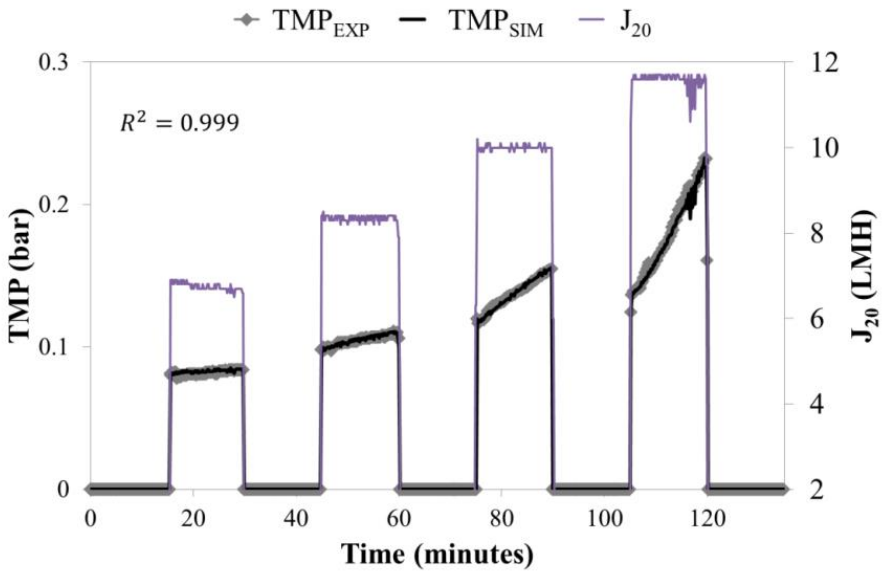

(a)

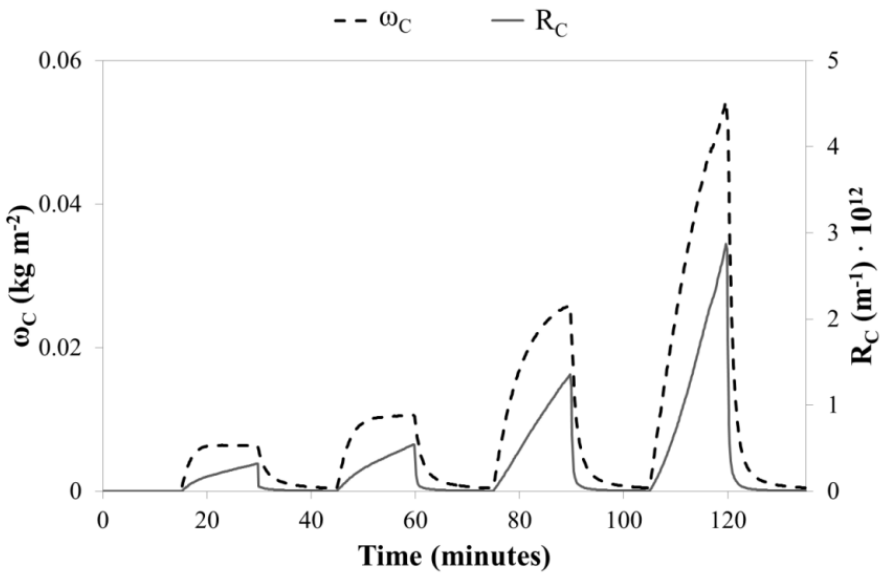

(b)

Figure 7.2 Results of the dynamic calibration of $q_{MS,Max}$, k_{SF}, $\alpha_{C,0}$, and TMP_a. Flux-step experiment conducted at a MLTS of 28.5 g L^{-1} and a BRF of 7 Nm^3 h^{-1}. Evolution of **(a)** TMP_{EXP}, TMP_{SIM} and J_{20} and **(b)** ω_C and R_C.

Figure 7.2 shows how the model evolved in comparison with the experimental data. Figure 7.2a shows the applied J_{20}, the measured TMP and the modelled TMP in a flux-step trial conducted at a BRF of 7 Nm^3 h^{-1} (which corresponds to a BRF_V of 0.0032 Nm^3 h^{-1} m^{-3}) and a MLTS of 28.5 g L^{-1}. Figure 7.2b

shows the modelling results for ω_C and R_C in the same trial. The results obtained (see Figure 7.2a) indicated that the results predicted by the model (TMP_{SIM}) accurately reproduced the corresponding experimental data (TMP_{EXP}): an accurate correlation coefficient (R^2) of 0.999 was obtained for the flux-step trial shown. Moreover, it was possible to simulate ω_C and R_C in the short term (see Figure 7.2b). As Figure 7.2b shows, ω_C increased sharply when J_{20} climbed above 8 LMH, *i.e.* ω_C increased from approx. 0.01 to 0.03 kg m^{-2} when J_{20} increased from approx. 8 to 10 LMH. Moreover, ω_C climbed to 0.06 kg m^{-2} when operating at a J_{20} of approx. 12 LMH, an indication that the critical flux had been exceeded. Figure 7.2b also shows that R_C increased as J_{20} increased. This is the result of not only the effect of J_{20} on ω_C (a direct increase in J_{20} means an increase in ω_C at given operating conditions), but also the effect of TMP on α_C (increasing TMP results in an increase in α_C, see Eq. 7.9 and Eq. 7.10).

It is important to emphasise that modelling ω_C and R_C performance may allow the overall performance of membranes in SAnMBR technology to be optimised. In this respect, operating and control strategies aimed to minimise the formation of a cake layer should be tested and developed.

7.4.3 Parameter estimations using experimental data and long-term dynamic calibration

The parameters $K_{S,\mathrm{Xm_C}}$, k_{RI}, and $q_{\mathrm{IF,Max}}$ were estimated using experimental data and then validated dynamically using long-term data.

The half-saturation coefficient for the mass of cake solids during membrane scouring and back-flushing ($K_{S,\mathrm{Xm_C}}$) was estimated using experimental data obtained from different short-term trials [7.18]. The estimated value is shown in Table 7.4.

The parameter k_{RI} was calculated using data from flux-step trials carried out at different operating times. These flux-step trials resulted in different γ_t values. On the other hand, the R_I of each operating time was estimated using data from back-flushing stages (considering R_M to be constant) as shown in Robles *et al*. [7.30]. Finally, k_{RI} was calculated, the result being $1.6 \cdot 10^{-07}$ (see Table 7.4).

As regards the maximum irreversible fouling rate, since the operating temperature during the operating period was 20 ºC (commonly assumed to be the benchmark temperature when calibrating model parameters) $q_{\mathrm{IF,Max}}$ was directly set as the inverse of the operating SRT (38.5 days in this period):

$3 \cdot 10^{-07}$ s^{-1} (see Table 7.4). Nevertheless, further study of the long-term data is required in order to determine the actual dependence of $q_{IF,Max}$ on T and SRT.

7.4.4 Default values

Due to the lack of data, a default value was set for $q_{BF,Max}$, k_t and α_I (see Table 7.4). As regards $q_{BF,Max}$ and k_t, no significant differences were observed in the dynamic calibration when modifying the established default value. Nevertheless, these parameters were included in the model proposed by Sarioglu *et al*. [7.17] and Bugge *et al*. [7.20]. As regards α_I, it may be necessary to calibrate α_I using the experimental data of R_I and ω_I.

7.5 Validation of model

The model was validated in both the short and the long term. The short-term validation consisted of 24 hours of continuous operation. The long-term validation consisted of a 3-month operating period.

7.5.1 Short-term validation

Figure 7.3 and Figure 7.4 provide an example of the results obtained from the short-term validation (recorded on operating day 167 in Figure 7.5). This validation was carried out using experimental data obtained by applying different J_{20} and BRF values. The results shown in Figures 3 and 4 were obtained when operating with a MLTS concentration of 21 g L^{-1}. The gas sparging intensity ranged from approx. 4 to 12 Nm^3 h^{-1}. The gross J_{20} ranged from approx. 4 to 12 LMH.

Figure 7.3a shows the evolution of the experimental J_{20} and BRF. Figure 7.3b shows the evolution of TMP_{SIM} and TMP_{EXP}, and the membrane operating stage. Like Figure 7.2, Figure 7.3b shows that although considerably high variations were applied to J_{20} and BRF (see Figure 7.3a), the results predicted by the model (TMP_{SIM}) accurately reproduced the corresponding experimental data (TMP_{EXP}) giving a R^2 coefficient of 0.962. On the other hand, Figure 7.3b shows that the model is capable of reproducing the reduction in TMP caused by ventilation or back-flushing (see, for example, minutes 285 and 515, respectively). This model is able to reproduce this reduction in TMP because it takes into account not only the cake build-up, membrane scouring and back-flushing processes, but also the cake compression process. In this respect, a recovery of α_C after each decompression (*i.e.* relaxation and back-flushing) is achieved. Therefore, a considerable decrease in TMP is observed (see

minutes 285 and 515 in Figure 7.3b) even when operating at low ω_C levels (see minutes 200 to 600 in Figure 7.4a).

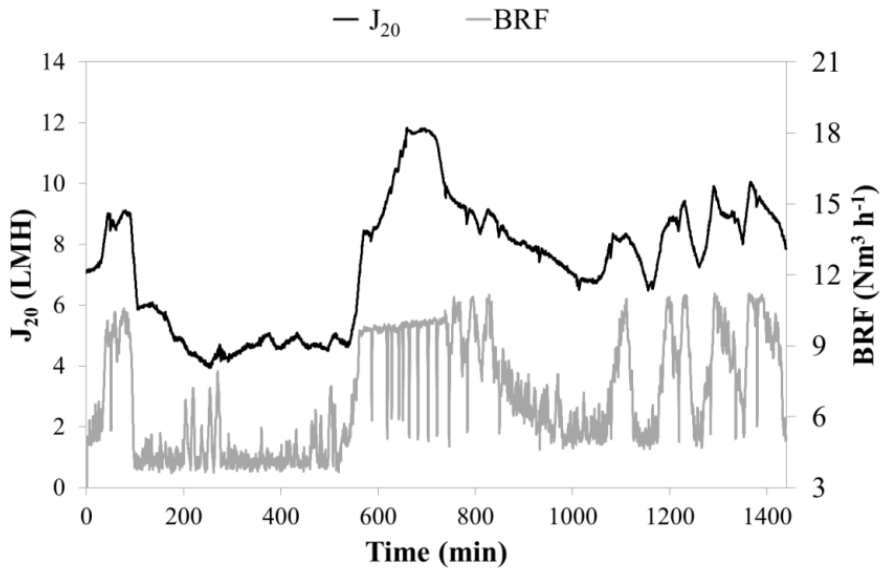

(a)

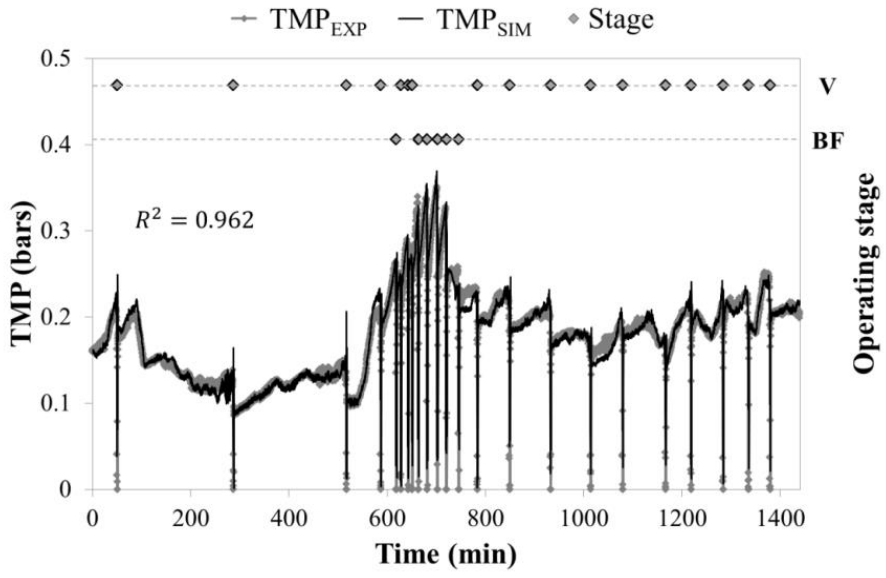

(b)

Figure 7.3 Short-term model validation: results from operating day 167 (see Figure 7.5). Evolution of **(a)** J_{20} and BRF and **(b)** TMP_{EXP}, TMP_{SIM} and membrane operating stage (**V**: Ventilation; **BF**: Back-Flushing).

Figure 7.4 shows the evolution of the simulated ω_C and R_C (Figures 4a and 5b, respectively). As Figure 7.4 shows, a sharp increase in both ω_C and R_C was observed when operating at fluxes close to the critical flux recorded in experiments. Previous trials revealed critical fluxes around operating day

167 of about 8 LMH when operating at a MLTS of 21 g L^{-1} and a BRF of 10 Nm^3 h^{-1}. These results are in line with the results shown in Figure 7.4, where a sharp increase in ω_C was observed (see minutes 600 to 800) when operating at fluxes close to the critical flux.

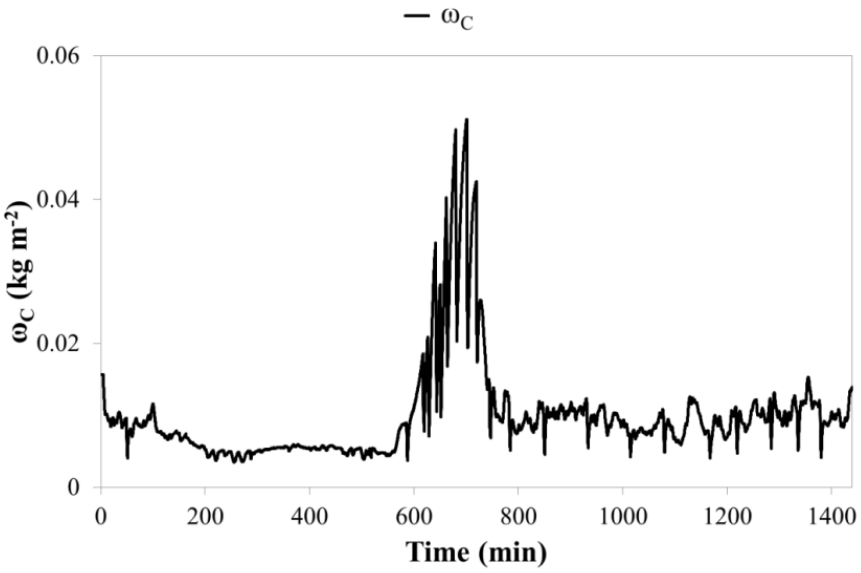

(a)

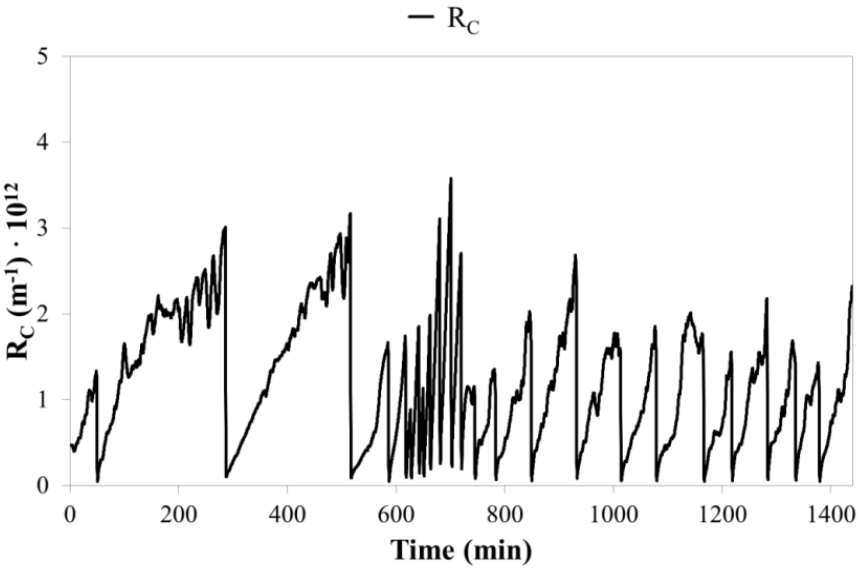

(b)

Figure 7.4 Short-term model validation: results from operating day 167 (see Figure 7.5). Evolution of **(a)** ω_C and **(b)** R_C.

Figure 7.4a also shows a minimum amount of ω_C of about 0.005 kg m^{-2} remaining over time. This performance (modelled mainly by applying the half-saturation switching function represented by Eq.

7.14) is the result of the drop in the effectiveness of the membrane scouring due to the reduction in the membrane area that is reversibly fouled. This remaining ω_C was assumed in our study to be one of the main factors that finally determines the propensity of membranes to foul irreversibly. Therefore, in accordance with the sub-critical filtration theory, higher ω_C values resulting from operating at a high J_{20} will result in a greater propensity to foul irreversibly than when operating at a low J_{20}.

On the other hand, sub-critical fouling has been modelled by the increase in the α_C value resulting from applying Eq. 7.12. In this regard, Figure 7.4b shows how R_C increases during sub-critical filtration (see, for example, minutes 200 to 600) due to increasing α_C. Nevertheless, as mentioned before, α_C returns to its default value when there is no compression of the cake layer, and therefore R_C decreases (see, for example, minutes 285 and 515 in Figure 7.4b). In our study, a constant sub-critical fouling velocity (k_{SF} in Eq. 7.12) was established for simulating the sub-critical fouling processes related to specific mechanisms not contemplated in the model. However, this parameter might be established in accordance with the operating value of J_{20} because sub-critical fouling also depends on J_{20}.

7.5.2 Long-term validation

The proposed model was validated using the long-term data of the following average daily operating conditions: MLTS levels from approx. 15 – 25 g L^{-1}, BRF from 6 to 12 Nm^3 h^{-1} and net 20 ºC-normalised transmembrane fluxes (J_{20net}) from 2.5 to 9 LMH.

Figure 7.5 shows the results from the long-term model validation carried out using data from three months of continuous operation. Figure 7.5a shows the average daily values for J_{20net}, BRF, and MLTS. It is important to note that the model was calibrated and validated using highly fouled membranes, which resulted in very low operating J_{20net} values. Figure 7.5b shows the average daily TMP_{SIM} and TMP_{EXP}. As Figure 7.5 shows, even when operating at different MLTS, J_{20net} and BRF levels (see Figure 7.5a), the model was able to accurately predict the membrane performance in the long term (see Figure 7.5b): a high R^2 coefficient was obtained (0.929).

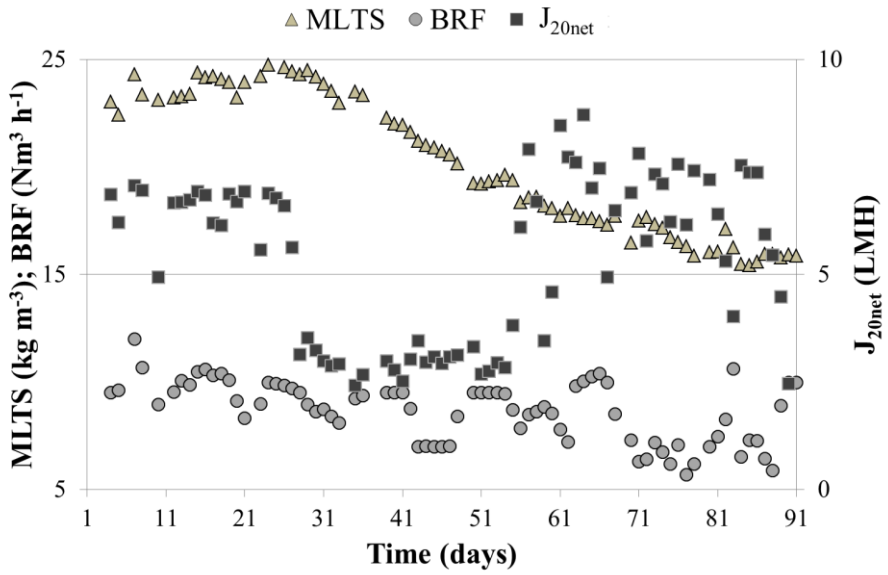

(a)

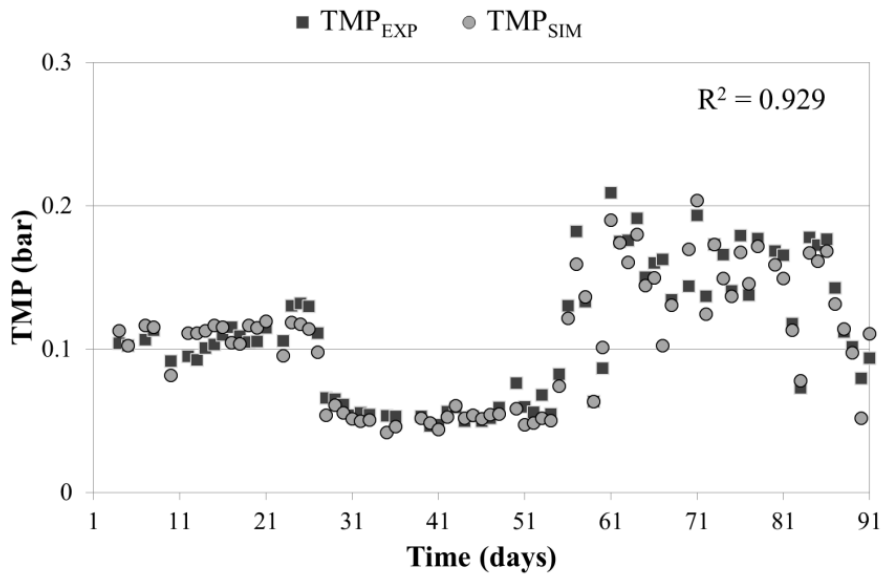

(b)

Figure 7.5 Long-term model validation. Average daily values of **(a)** MLTS, J_{20} and BRF and **(b)** TMP_{EXP} and TMP_{SIM}.

7.5.3 Model applicability and future perspectives

The model validation shown in this study illustrates that the proposed model was able to properly reproduce the filtration performance of an SAnMBR system in the short- and long-term. Moreover, a sensitivity analysis based on the Morris method [7.31] revealed that most of the suggested model parameters were identified as influential (data not shown). This was mainly the result of building the

model on the basis of experimental results. Therefore, most of the proposed model parameters are required to represent in a general way all possible membrane performances in systems of this type. The less influential parameters were: $K_{S,XmC}$, $q_{IF,Max}$, α_I, $q_{BF,Max}$ and k_t, which implies that these parameters could be set to a default value in order to simplify the model calibration.

It is worth to point out that some estimations/measurements (*e.g.* cake and irreversible fouling thickness and specific resistance) would further improve process validation for accurately validating not only the modelling approach but also the calibrated values for the different model parameters. Therefore, further research would be required on this area.

On the other hand, further research must be accomplished in order to extend the applicability of the proposed filtration model to other MBR applications (*e.g.* aerobic operation, flat-sheet membrane modules, industrial wastewater treatment, and so on.). To this aim, it is expected that the re-calibration of the model parameters would be necessary. In this regard, recent literature reveals differences on membrane performance in MBR technology not only due to changes on the physiological state of the mixed liquor but also due to changes on membrane operating mode and configuration [7.18]. Nevertheless, it is important to highlight the wide range of operating conditions in which the model has been validated in this work: influent COD concentration from approx. 200 to 900 mgCOD L^{-1}, MLTS levels from approx. 15 – 25 g L^{-1}, BRF from 6 to 12 Nm^3 h^{-1} and J_{20net} from 2.5 to 9 LMH.

In the future, it is planned to validate this model at a wider range of operating conditions, mainly regarding membrane operating mode and mixed liquor characteristics. Moreover, it is planned to verify the applicability of the model for other membrane module configurations such as flat-sheet type. Then, the corresponding model modifications will be made if necessary, in order to verify and/or extend the applicability of the proposed model, which will facilitate the design and simulation of membrane technology in WWTPs.

Other aspect on filtration process to be considered is that biological modelling on anaerobic filtration-based systems is quite recent, which makes it difficult to obtain reliable information about the interaction between biological and filtration processes. In this respect, enhancing biological modelling of anaerobic processes of this type may allow improving the quality of the proposed filtration model since a greater amount of reliable data related to different fouling mechanisms (*e.g.* EPS, SMP, colloidal matter, etc.) would be available.

Finally, it must be highlighted that the proposed filtration model (in conjunction with a biological model) can be applied for different reasons: to design and upgrade SAnMBR systems, or to develop, operate and control strategies designed to optimise process performance – not only in the short term, but also in the long term.

7.6 Conclusions

The short- and long-term validation of the filtration model proposed in this study resulted in satisfactory correlation coefficients (R^2) of 0.962 and 0.929 respectively. Thus, this model was able to accurately reproduce the filtration process in a SAnMBR demonstration plant fitted with industrial-scale hollow-fibre membranes. This model can be used to develop operating and control strategies intended to optimise filtration in SAnMBRs since the weighted average distribution of overall filtration resistance can be modelled. Further research will be done in order to extend the applicability of the proposed filtration model to a wider range of operating conditions and other MBR applications.

7.7 Acknowledgements

This research has been supported by the Spanish Ministry of Economy and Competitiveness (MINECO Project CTM2011-28595-C02-01/02) jointly with the European Regional Development Fund (ERDF), which are gratefully acknowledged.

7.8 References

7.1 G. Mannina, G. Di Bella, G. Viviani, An integrated model for biological and physical process simulation in membrane bioreactors (MBRs), J. Membr. Sci. 376 (2011), 56–69.

7.2 A.N.L. Ng, A.S. Kim, A mini-review of modeling studies on membrane bioreactor (MBR) treatment for municipal wastewaters, Desalination 212 (2007), 261–281.

7.3 M. Henze, W. Gujer, T. Mino, M.C.M. van Loosdrecht, Activated Sludge Models: ASM1, ASM2, ASM2d and ASM3, Scientific and Technical Report no. 9, IWA Publishing, London, UK, 2000.

7.4 D.J. Batstone, J. Keller, I. Angelidaki, S.V. Kalyuzhnyi, S.G. Pavlostathis, A. Rozzi, W.T. Sanders, H. Siegrist, V.A. Vavilin, The IWA anaerobic digestion model No. 1 (ADM1), Water Sci. Technol. 45 (2002), 65–73.

7.5 M. de Gracia, P. Grau, E. Huete, J. Gómez, J.L. García-Heras, E. Ayesa, New generic mathematical model for WWTP sludge digesters operating under aerobic and anaerobic conditions: Model building and experimental verification. Water Res. 43 (2009), 4626–4642.

7.6 R. Barat, J. Serralta, M.V. Ruano, E. Jiménez, J. Ribes, A. Seco, J. Ferrer, Biological Nutrient Removal Model Nº 2 (BNRM2): A general model for Wastewater Treatment Plants, Water Sci. Technol. 67 (2013), 1481–1489.

7.7 W. Naessens, T. Maere, I. Nopens, Critical review of membrane bioreactor models–Part 1: Biokinetic and filtration models, Bioresource Technol. 122 (2012) 95–106.

7.8 W. Naessens, T. Maere, N. Ratkovich, S. Vedantam, I. Nopens, Critical review of membrane bioreactor models–Part 2: Hydrodynamic and integrated models, Bioresource Technol. 122 (2012) 107–118.

7.9 M.F.R. Zuthi, H.H. Ngo, W.S. Guo, Modelling bioprocesses and membrane fouling in membrane bioreactor (MBR): A review towards finding an integrated model framework, Bioresource Technol. 122 (2012) 119–129.

7.10 A. Broekmann, J. Busch, T. Wintgens, W. Marquardt, Modeling of pore blocking and cake layer formation in membrane filtration for wastewater treatment, Desalination 189 (2006), 97–109.

7.11 C. Duclos-Orsello, W. Li, C.C. Ho, A three mechanism model to describe fouling of microfiltration membranes, J. Membr. Sci. 280 (2006), 856–866.

7.12 X.y. Li, X.m. Wang, Modelling of membrane fouling in a submerged membrane bioreactor, J. Membr. Sci. 278 (2006), 151–161.

7.13 J. Busch, A. Cruse, W. Marquardt, Modeling submerged hollow-fiber membrane filtration for wastewater treatment, J. Membr. Sci. 288 (2007), 94–111.

7.14 A. Zarragoitia-Gonzalez, S. Schetrite, M. Alliet, U. Jauregui-Haza, C. Albasi, Modelling of submerged membrane bioreactor: Conceptual study about link between activated sludge biokinetics, aeration and fouling process, J. Membr. Sci. 325 (2008), 612–624.

7.15 J. Wu, C. He, Y. Zhang, Modeling membrane fouling in a submerged membrane bioreactor by considering the role of solid, colloidal and soluble components, J. Membr. Sci. 397/ 398 (2012), 102– 111.

7.16 T. Ludwig, D. Gaida, C. Keysers, J. Pinnekamp, M. Bongards, P. Kern, C. Wolf, A.L. Sousa Brito, An advanced simulation model for membrane bioreactors: Development, Calibration and Validation, In: 6th IWA Specialist Conference on Membrane Technology for Water & Wastewater Treatment, 2011.

7.17 M. Sarioglu, G. Insel, D. Orhon, Dynamic in-series resistance modeling and analysis of a submerged membrane bioreactor using a novel filtration mode, Desalination 285 (2012), 285–294.

7.18 A. Robles, M.V. Ruano, J. Ribes, J. Ferrer, Factors that affect the permeability of commercial hollow-fibre membranes in a submerged anaerobic MBR (HF-SAnMBR) system, Water Res. 47 (2013), 1277–1288.

7.19 American Public Health Association/American Water Works Association/Water Environmental Federation, Standard methods for the Examination of Water and Wastewater, 21st edition, Washington DC, USA, 2005.

7.20 T.V. Bugge, M.K. Jørgensen, M.L. Christensen, K. Keiding, Modeling cake buildup under TMP-step filtration in a membrane bioreactor: Cake compressibility is significant, Water Res. 46 (2012), 4330–4338.

7.21 M.K. Jørgensen, T.V. Bugge, M.L. Christensen, K. Keiding, Modeling approach to determine cake buildup and compression in a high-shear membrane bioreactor, J. Membr. Sci. 409/410 (2012), 335–345.

7.22 M.L. Christensen, The Effect of Filter Cake Viscoelasticity on Filtration: a Study of Activated Sludge Dewatering, PhD thesis, Aalborg University, Department of Biotechnology, Chemistry and Environmental Engineering, Aalborg, Denmark, 2006.

7.23 LD. Hughes, R.W. Field, Crossflow filtration of washed and unwashed yeast suspensions at constant shear under nominally sub-critical conditions, J. Membr. Sci. 280 (2006), 89–98.

7.24 L. Corominas, L. Rieger, I. Takács, G. Ekama, H. Hauduc, P.A. Vanrolleghem, A. Oehmen, K.V. Gernaey, M.C.M. van Loosdrecht, Y. Comeau, New framework for standardized notation in wastewater treatment modelling, Water Sci. Technol. 61 (2010), 841–857.

7.25 A. Robles, M.V. Ruano, F. García-Usach, J. Ferrer, Sub-critical filtration conditions of commercial hollow-fibre membranes in a submerged anaerobic MBR (HF-SAnMBR) system: The effect of gas sparging intensity, Bioresource Technol. 114 (2012), 247–254.

7.26 P. Le-Clech, V. Chen, T.A.G. Fane, Fouling in membrane bioreactors used in wastewater treatment, J. Membr. Sci. 284 (2006), 17–53.

7.27 A. Robles, M.V. Ruano, J. Ribes, J. Ferrer, Performance of industrial scale hollow-fibre membranes in a submerged anaerobic MBR (HF-SAnMBR) system at mesophilic and psychrophilic conditions, Sep. Purif. Technol. 104 (2013), 290–296.

7.28 F.G. Meng, S.R. Chae, A. Drews, M. Kraume, H.S. Shin, F.L. Yang, Recent advances in membrane bioreactors (MBRs): membrane fouling and membrane materials, Water Res. 43 (2009), 2405–2415.

7.29 T.F. Coleman, Y. Li, An interior, trust region approach for nonlinear minimization subject to bounds. SIAM J. Optim. 6 (1996), 418–445.

7.30 A. Robles, M.V. Ruano, J. Ribes, J. Ferrer, Advanced control system for optimal filtration in submerged anaerobic MBRs (SAnMBRs), J. Membr. Sci. 430 (2013), 330–341.

7.31 M. Morris, Factorial sampling plans for preliminary computational experiments, Technometrics. 33 (1991), 239–245.

CHAPTER 8:

Mathematical modelling of filtration in submerged anaerobic MBRs (SAnMBRs): long-term validation

Abstract

The aim of this study was the long-term validation of a model capable of reproducing the filtration process occurring in a submerged anaerobic membrane bioreactor (SAnMBR) system. The proposed model was validated using data obtained from a SAnMBR demonstration plant fitted with industrial-scale hollow-fibre membranes. The validation was carried out using both lightly and heavily fouled membranes operating at different bulk concentrations, gas sparging intensities and transmembrane fluxes. Across a broad spectrum of operating conditions, the model correctly forecast the respective experimental data in the long term. The simulation results revealed the importance of controlling irreversible fouling in order to ensure sustainable long-term membrane performance.

Keywords

Industrial-scale hollow fibre modules; long-term validation; resistance in series; filtration model; submerged anaerobic membrane bioreactor.

Highlights

A filtration model for SAnMBRs has been validated using long-term data.
The model was validated for lightly and heavily fouled full-scale HF membranes.
Different MLTS levels, gas sparging intensities and permeate fluxes were applied.
The model reproduced the experimental data accurately.

A. Robles, M.V. Ruano, J. Ribes, A. Seco, J. Ferrer
Mathematical modelling of filtration in submerged anaerobic MBRs (SAnMBRs): long-term validation
J. Membrane Sci. 446 (2013), 303 – 309.

8.1 Introduction

Understanding and optimising a complex system such as a membrane bioreactor (MBR) is a difficult and time-consuming process mainly because of the large number of sub-processes taking place simultaneously, which generally are highly dependent upon each other. In this regard, mathematical modelling is a powerful tool for studying such complex systems [8.1].

Certain models have been found to be useful for different objectives related to wastewater treatment plants (WWTPs) such as the research and development of wastewater treatment processes, the design and upgrading of WWTPs, and development of operating and control strategies designed to optimise process performance [8.2; 8.3; 8.4]. Computerised models make it possible to perform many virtual experiments in a short space of time. Therefore the mathematical modelling of filtration in submerged anaerobic MBRs (SAnMBRs) may help gain insights into the key factors in membrane fouling [8.5], and are also invaluable for the design, prediction and control of membrane technology used for treating wastewater [8.6]. In this regard, good modelling practices must guarantee adequate calibration/validation results not only in the short term but also in the long term.

One key issue as regards the long-term validation of a SAnMBR filtration model is the lack of data gathered from full-scale facilities, especially those treating urban wastewater. Specifically, there is still a lack of knowledge about irreversible membrane fouling mechanisms in the long term. Thus, there is a need for further research into the long-term performance of industrial-scale membranes in SAnMBRs dealing with urban wastewater in order to accurately validate a filtration model applied to this technology.

In a previous study, on the basis of the experimental results obtained whilst operating a SAnMBR plant fitted with industrial-scale hollow-fibre (HF) membranes, we developed a mathematical model capable of reproducing filtration in SAnMBRs [8.7]. This filtration model is based on the resistance-in-series modelling concept and can easily be linked to biological models. The proposed model takes into account the effect of the shear intensity in the membrane tank caused by the biogas recycling flow. Thus, the membrane scouring process occurring during the different membrane module operating stages (filtration, relaxation…) can be reproduced. The physical processes considered in this model are: cake layer build-up and compression during filtration; cake layer removal using biogas sparging to scour the membrane; cake layer removal during back-flushing; and the consolidation of irreversible fouling.

The aim of the present study was to validate the above-mentioned filtration model in the long-term under different operating conditions. Once validated, the possibilities of applying this model to the development of different operating and control strategies designed to optimise membrane performance and lifespan were assessed. In order to obtain robust results that could be extrapolated to full-scale applications, the model was validated using long-term data from a SAnMBR plant fitted with industrial-scale HF membranes.

8.2 Materials and methods

8.2.1 SAnMBR plant description

The model was validated in the long term using data from a demonstration-scale SAnMBR system. The plant consists of an anaerobic reactor with a total volume of 1.3 m^3 connected to two membrane tanks each with a total volume of 0.8 m^3. Each membrane tank has one industrial HF ultrafiltration membrane unit (PURON®, Koch Membrane Systems (PUR-PSH31) with 0.05 μm pores). Each module has a total membrane surface of 30 m^2. For further details of this SAnMBR system, see Robles *et al*. [8.8] and Chapter 2.

8.2.2 On-line and analytical monitoring

To account for the dependence of permeate viscosity on temperature (T), the gross 20 ºC-normalised transmembrane flux (J_{20}) was calculated from the on-line monitored temperature and gross transmembrane flux (J_T) using Eq. 8.1.

$$J_{20} = J_T \cdot e^{-0.0239(T-20)} \qquad \textbf{Eq. 8.1}$$

In addition to being monitored on line (Hach Lange model TSS EX1 sc), a grab sample of anaerobic sludge was taken once a day to determine the mixed liquor total solids (MLTS) concentration according to Standard Methods [8.9]. The mixed liquor volatile solids (MLVS) of the anaerobic sludge was also analysed each day. Extracellular polymeric substances (EPS) and soluble microbial products (SMP) were measured as introduced in Chapter 6.

8.2.3 Model description

The filtration model used in this study aims at reproducing the main processes that occur during filtration in SAnMBRs: cake layer build-up and compression; sub-critical fouling; membrane scouring by biogas sparging; removal of cake layer by back-flushing; and irreversible fouling consolidation. To this aim, the model, which is based on the resistance-in-series modelling concept, was developed using the experimental results obtained from a SAnMBR plant fitted with industrial-scale HF membranes. The cake layer compression process during filtration is reproduced by considering that the average specific cake resistance, α_C (m kg^{-1}), is time and TMP dependent. Moreover, the model tries to reproduce the specific fouling mechanisms related to sub-critical fouling (*e.g.* colloidal matter absorption) by increasing α_C over time. On the other hand, a black-box approach was proposed for describing the following physical interactions occurring in fouling (reversible and irreversible): attachment of solids to the membrane surface during filtration; removal of solids from the membrane surface due to membrane scouring and back-flushing; and irreversible fouling of the membrane.

8.2.3.1 Resistance-in-series model

The proposed model represents the dynamic evolution of the transmembrane pressure (TMP) by applying Eq. 8.2 and Eq. 8.3.

$$TMP(t) = J \cdot \mu \cdot R_T \qquad \textbf{Eq. 8.2}$$

where:

- J is the transmembrane flux (m s^{-1})
- μ is the permeate dynamic viscosity (kg m^{-1} s)
- TMP (t) is the TMP at time t (Pa)
- R_T is the total filtration resistance (m^{-1})

$$R_T = R_M + R_C + R_I = R_M + \omega_C \cdot \alpha_C + \omega_I \cdot \alpha_I \qquad \textbf{Eq. 8.3}$$

where:

- R_M is the intrinsic membrane resistance (m^{-1})
- R_C is the cake layer resistance (m^{-1})
- R_I is the irreversible fouling resistance (m^{-1})
- ω_C is the mass of cake deposited per membrane area (kg m^{-2})
- ω_I is the mass of irreversible fouling per membrane area (kg m^{-2})
- α_I is the average specific irreversible fouling resistance (m kg^{-1})

8.2.3.2 Cake layer compression and sub-critical fouling

To account for the cake layer compression process, α_C was defined as both time and TMP dependent (see second term in the max function of Eq. 8.4), as per Bugge *et al*. [8.10] and Jørgensen *et al*. [8.11]. It allowed accounting for the cake compression due to both the deformation of soft sludge flocs and the structural rearrangement of particles [8.12]. In addition, to account for sub-critical fouling, an additional dependence of α_C on time was considered in the model [8.7] (as expressed by the first term in the max function of Eq. 8.4). It allowed accounting for colloidal matter absorption increasing the specific resistance of cake-like deposits [8.13]. In our model, we propose that when the maximum α_C related to the structural rearrangement of particles is reached at a given TMP (see second term in the max function of Eq. 8.4), it is possible to account for the increase in α_C due to the absorption of colloids (first term in the max function of Eq. 8.4), as expressed by Eq. 8.4 below. For further details of the application of Eq. 8.4 see Robles *et al*. [8.7].

$$\alpha_C(t) = \alpha_C(t-\Delta t) + \max\left(k_{SF}, k_t \cdot \left(\alpha_{C,0} \cdot \left(1 + \frac{TMP}{TMP_a}\right) - \alpha_C(t-\Delta t)\right)\right) \cdot \Delta t \qquad \textbf{Eq. 8.4}$$

where:

- $\alpha_C(t)$ is the specific resistance of the cake at time *t* (kg m^{-2}).
- $\alpha_C(t-\Delta t)$ is the specific resistance of the cake at a previous moment in time (kg m^{-2}).
- k_{SF} is the parameter related to sub-critical fouling (kg m^{-2} s^{-1}).
- $\alpha_{C,0}$ is the specific resistance of the cake at zero pressure (kg m^{-2})
- TMP_a is the pressure needed to double the specific resistance (Pa)
- k_t is the time constant (s^{-1}).
- Δt is the time step (s).

8.2.3.3 Black-box approach

For describing the above-mentioned physical interactions affecting TMP (cake layer build-up; removal of solids from the membrane surface due to membrane scouring and back-flushing; and irreversible fouling of the membrane), the variations on ω_C and ω_I must be considered. A black-box approach for modelling the dynamics of ω_C and ω_I is proposed in the model. The black-box approach considers 3 suspended components: MLTS concentration, X_{TS} (kg m^{-3}); dry mass of cake over the membrane surface, X_{m_C} (kg); and dry mass of irreversible fouling over the membrane surface, X_{m_I} (kg).

This model considers a total of four kinetic physical processes: (1) cake layer build-up during filtration; (2) cake layer removal using biogas sparging to scour the membrane; (3) cake layer removal during back-flushing; and (4) irreversible fouling consolidation. The model does not consider diffusive back transport as this process is thought to be less significant than the other processes considered [8.14]. Table 7.3 shows the stoichiometry and the kinetic expressions of the four processes considered in the model. The parameters used in this filtration model were calibrated in a previous study by off-line and dynamic calibration methods using short-term and long-term data (see Robles *et al*. [8.7]). Table 7.4 shows the previously calibrated values, which have been used in this study with no further adjustment. For further details of this filtration model see Chapter 7.

8.2.4 Long-term model validation

The filtration model used in this study was previously calibrated using both short- and long-term data obtained from the SAnMBR plant mentioned earlier [8.7]. As commented above, the calibrated values of the different parameters included in the model are shown in Table 7.4. In this study we have validated the model in the long-term using both heavily-fouled and lightly-fouled membranes. The data needed to validate the model was also obtained from said SAnMBR plant. The long-term validation using heavily-fouled membranes comprised an operating period of 180 days, whilst the long-term validation using lightly-fouled membranes comprised an operating period of 140 days. Both validations aimed to demonstrate the capability of the proposed model to reproduce filtration in SAnMBRs even when operating under quite different dynamic operating conditions (*i.e.* using heavily-fouled and lightly-fouled membranes).

The average daily operating conditions applied during the long-term model validation using heavily-fouled membranes were as follows: sludge retention time (SRT) of 38.5 days, average operating temperature of 20 ºC, MLTS levels from 15 to 25 g L^{-1}, specific gas demand per square metre of membrane (SGD_m) from 0.13 to 0.46 $Nm^3\ h^{-1}\ m^{-2}$ and net 20 ºC-normalised transmembrane flux (J_{20net}) from 2.5 to 12 LMH. The average daily operating conditions applied during the long-term model validation using lightly-fouled membranes were as follows: SRT of 71.5 days, average operating temperature of 33 ºC, MLTS levels from 7 to 25 g L^{-1}, SGD_m controlled at 0.23 $Nm^3\ h^{-1}\ m^{-2}$ and J_{20net} of approx. 8 and 11 LMH.

It must be emphasised that both long-term validations were conducted at different SRT and T, therefore different propensities to irreversible fouling were expected. However, the value of $q_{IF,Max}$ remained the same in both instances, resulting in acceptable results. This was mainly attributed to the

presence of similar amounts of SMP and EPS in the mixed liquor (around 150 – 180 mg g^{-1} MLVS and 60 – 80 mg g^{-1} MLVS, respectively). In this regard, SMP and EPS seem to be the main factors affecting irreversible fouling in MBRs [8.16], which are directly dependent on T [8.17] and SRT [8.18]. Usually, SMP and EPS decrease as SRT increases, whilst SMP and EPS increase as the temperature increases due to greater microbial activity. Therefore, $q_{IF,Max}$ may be assumed to be a function of both T and SRT. In our study, since the operating period spanning the highest SRT (71.5 days) was conducted at the highest temperature (33 ºC) and the period spanning the lowest SRT (38.5 days) was conducted at the lowest temperature (20 ºC), it was expected that the impact of both SRT and T upon irreversible fouling would offset each other. For this reason, the same $q_{IF,Max}$ value was applied in both operating periods.

8.3 Results and discussion

8.3.1 Model validation using heavily-fouled membranes

As commented before, heavily-fouled membranes were used for validating the model when operating at SRT of 38.5 days and 20 ºC. Figure 8.1a shows the daily average values for J_{20net} (ranging from 2.5 to 12 LMH) and SGD_m (ranging from 0.13 to 0.46 $Nm^3\ h^{-1}\ m^{-2}$). Since, as we have already said, model validation was conducted using heavily-fouled membranes, the operating J_{20net} was very low.

Figure 8.1b shows the average daily values of the simulated and experimental TMP (TMP_{SIM} and TMP_{EXP}, respectively). As this figure shows, even when operating with variable J_{20net} and SGD_m (see Figure 8.1a), the model was able to reproduce membrane performance correctly in the long term (see Figure 8.1b), resulting in an adequate Pearson Product-Moment correlation coefficient (r) between TMP_{EXP} and TMP_{SIM} of 0.893. Nevertheless, a slight deviation of TMP_{SIM} from TMP_{EXP} was observed on operating days 67 – 73. This deviation was attributed to the fact that no data was gathered on those days from the on-line biogas composition analyser needed to normalise the volumetric biogas recycling flow (the on-line biogas composition analyser was not available due to maintenance). To account for the dependence of volumetric biogas flow on biogas composition, SGD_m was normalised using Eq. 8.5. On operating days 67 – 73, the on-line biogas composition analyser was not available due to maintenance requirements. Therefore, the correction was not applied and lower SGD_m values than the ones resulting from applying Eq. 8.5 were recorded (a reduction in the SGD_m values on operating days 67 – 73 can be seen in Figure 8.1a). In this regard, the model would probably have predicted lower TMP_{SIM} values than the ones shown on operating days 67 – 73 (see Figure 8.1b) if the

correctly corrected SGD_m had been recorded (decreasing SGD_m means increasing the amount of solids deposited on the membrane surface, which increases TMP).

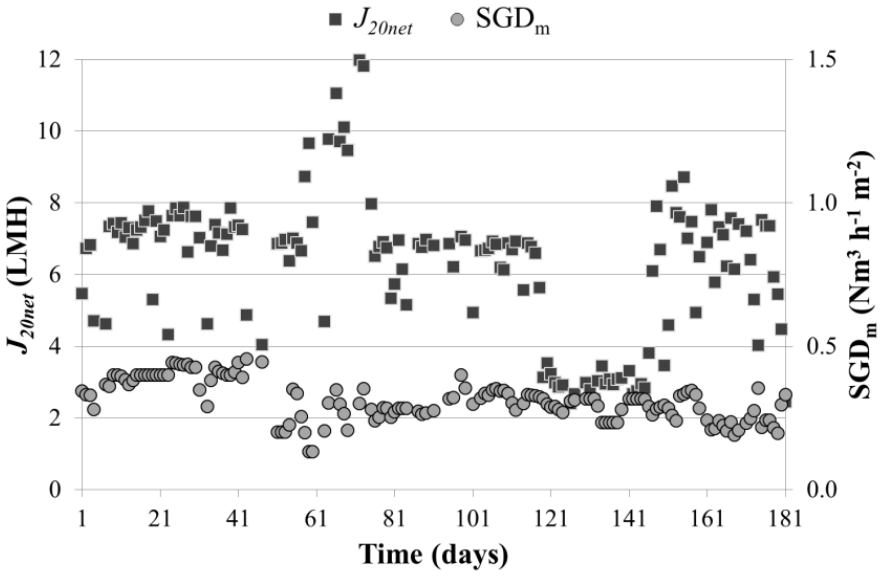

(a)

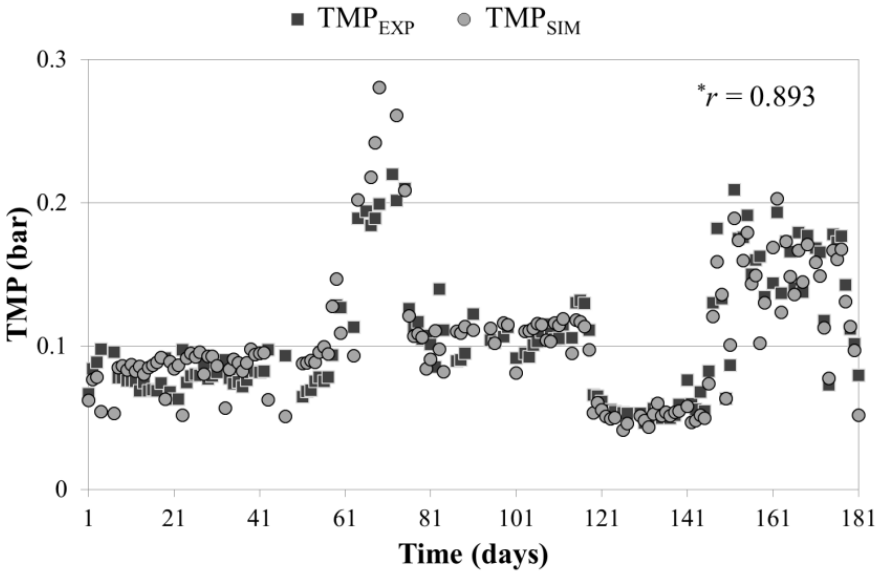

(b)

Figure 8.1 Long-term model validation using heavily-fouled membranes. Daily average values of: **(a)** J_{20} and SGD_m; and **(b)** TMP_{EXP} and TMP_{SIM}. * *r represents the Pearson Product-Moment correlation coefficient between* TMP_{EXP} *and* TMP_{SIM}.

$$SGD_{m_{CORRECTED}} = SGD_{m_{MEASURED}} \cdot frho \qquad \textbf{Eq. 8.5}$$

where:

- $frho = \sqrt{\frac{\rho_{AIR}}{\left(\rho_{CH_4}\cdot\%CH_4+\rho_{CO_2}\cdot\%CO_2+\rho_{H_2}\cdot\%H_2+\rho_{H_2S}\cdot\%H_2S+\rho_{N_2}\cdot\%N_2\right)/100}}$
- rho_{AIR}: volumetric weight of air (1.2930 kg m^{-3})
- rho_{CH4}: volumetric weight of CH_4 (0.7168 kg m^{-3})
- rho_{CO2}: volumetric weight of CO_2 (1.9768 kg m^{-3})
- rho_{H2}: volumetric weight of H_2 (0.0449 kg m^{-3})
- rho_{H2S}: volumetric weight of H_2S (1.5195 kg m^{-3})
- rho_{N2}: volumetric weight of N_2 (1.2505 kg m^{-3})

Figure 8.2a shows the average daily MLTS level (ranging from 15 to 25 g L^{-1}), and the simulated average daily values for ω_C and ω_I. The R_I (determined as the difference between R_T and R_M during back-flushing) obtained from experimental data, gave an initial ω_I of 0.03 kg $X_{m_I} m^{-2}$ (see Figure 8.2a). As it was expected (Figure 8.2a), the highest ω_C values occurred when operating at high J_{20net} (see operating days 60 – 75 in Figure 8.1a), which corresponds to the lowest SGD_m (0.13 – 0.2 $Nm^3 h^{-1} m^{-2}$, see Figure 8.1a). This is the result of an increasing convective transport of foulants (X_{TS} in the model) from the bulk to the membrane surface, combined with weak shear conditions in the membrane tank due to a reduction in the biogas sparging intensity. On the contrary, a considerable decrease in ω_C (due to increasing the membrane scouring rate) was observed when J_{20net} fell from about 7 to 3 LMH (see operating days 115 – 120 in Figure 8.1a). It must be emphasised that the membrane scouring velocity (q_{MS}) is a function of an exponential-type inhibition function that depends on both MLTS and J_{20} (Eq. 7.16), which is used to model the effect of filtering below or above critical conditions [8.7]. It can, therefore, be assumed that the membranes were operated supra-critically on operating days 60 – 75 and sub-critically on operating days 115 – 120.

Irreversible fouling is represented in the model as a direct function of X_{m_C}. Therefore, ω_C, which directly depends on J_{20net}, was assumed to be one key factor that finally determines the irreversible fouling of the membranes. In this respect, high ω_C values resulting from operating at high J_{20} values will result in a greater propensity to irreversible fouling than when operating at low J_{20} values.

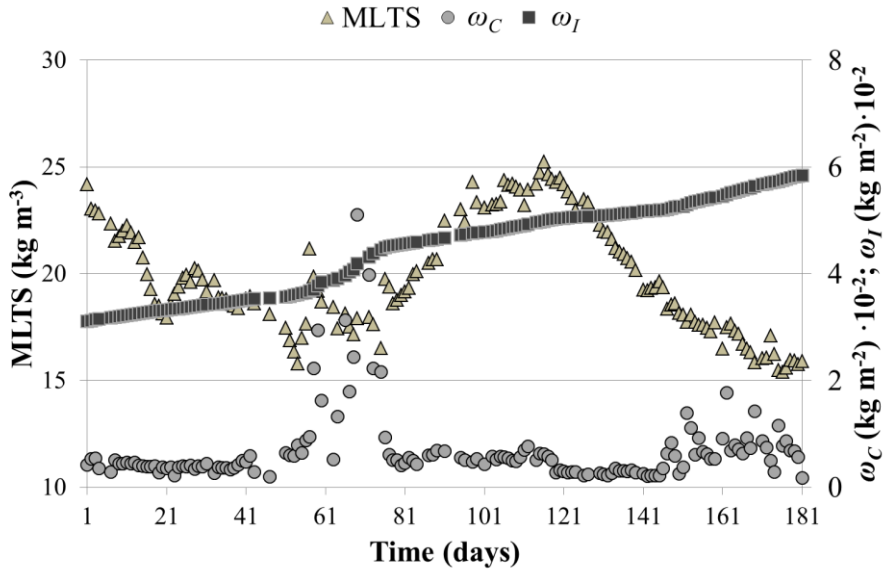

(a)

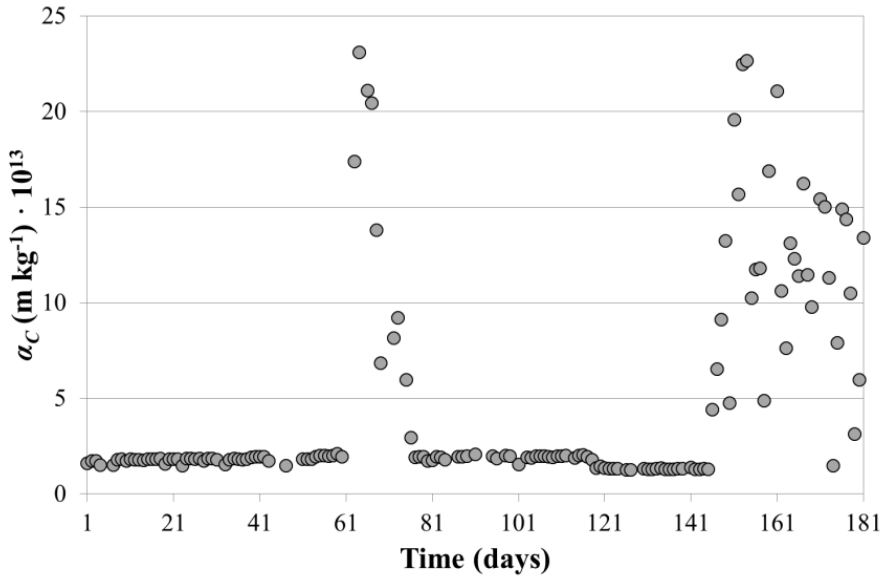

(b)

Figure 8.2 Long-term model validation using heavily-fouled membranes. Daily average values of: **(a)** MLTS, ω_C and ω_I; and **(b)** α_C.

As Figure 8.2a shows, the highest irreversible fouling rate modelled (0.0051 kg $X_{m_I}m^{-2}$ d^{-1}) was reached on operating days 63 – 73 (which coincides with the highest ω_C levels). In addition, a decrease in the irreversible fouling rate from 0.0015 to 0.0005 kg $X_{m_I}m^{-2}$ d^{-1} was observed (calculated on operating days 104 – 115 and 120 – 131, respectively) when J_{20net} decreased from about 7 to 3 LMH (see operating days 115 – 120 in Figure 8.1a): ω_C decreased from approx. 0.5 to 0.25 kg m^{-2}. Apart from J_{20net}, ω_C is also dependent on MLTS. Nevertheless, even when MLTS decreased from approx.

18.5 to 15 g L^{-1} on operating days 148 to 181, the model predicted an increase in the irreversible fouling rate from 0.0006 to 0.0019 kg $X_{m_I} m^{-2} d^{-1}$ (calculated on operating days 121 – 144 and 148 – 179, respectively) due to J_{20net} increasing from about 3 to 8 LMH (see operating days 145 – 150 in Figure 8.1a). The average irreversible fouling rate for the whole operating period (181 days of continuous operation) resulted in 0.00015 kg $X_{m_I} m^{-2} d^{-1}$.

It must be emphasised that modelling ω_C may make it possible to optimise overall membrane performance in SAnMBR technology because it enables operating and control strategies designed to minimise cake layer formation to be tested and developed.

Figure 8.2b shows the simulated average daily values of α_C. As this figure shows, α_C increased from approx. $2 \cdot 10^{13}$ to $25 \cdot 10^{13}$ m kg^{-1} when TMP increased from approx. 0.1 to 0.3 bar (see operating days 70 – 75 in Figure 8.1b). Similar behaviour was observed on operating days 143 – 181 (see Figure 8.1a), when TMP was 0.1 – 0.2 bars. The considerable increase in α_C due to the increase in TMP highlights the need to model not only cake build-up but also cake compression in filtration processes of this type [8.10; 8.11].

Figure 8.3a shows the average daily results (in absolute terms) of the simulation obtained at the different filtration resistances (R_T, R_M, R_C and R_I) considered in the model. As regards reversible fouling, Figure 8.3a shows a sharp increase in R_C (and consequently in R_T) on operating days 60 – 75, caused by the high values of ω_C and α_C observed (see Figure 8.2). Similar behaviour can be seen on operating days 141 – 181. In this period it was assumed that the membranes were operated around or above the critical flux level, resulting in the accumulation of more solids on the membrane surface than when operating sub-critically (see, for example, operating days 1 – 41 and 81 – 141). As regards irreversible fouling, Figure 8.3a shows a continuous increase in R_I over time as a result of the continuous increase in ω_I (see Figure 8.2a).

Since it is possible to simulate R_I and R_C from the predicted ω_C and ω_I values, the weighted average daily distribution for R_T can be modelled in the long-term (see Figure 8.3b). As Figure 8.3b shows, a constant slightly decrease in the weighted average contribution of R_M to R_T is observed throughout the operating period mainly as a result of the increasing contribution of R_I to R_T. On the other hand, the weighted average contribution of R_C to R_T remained around 0% on operating days 1 – 41 and 81 – 141 due to the fact that filtration conditions were sub-critical. This weighted average contribution

increased sharply when operating at fluxes around or above the critical flux level (see operating days 61 – 81 and 141 – 181).

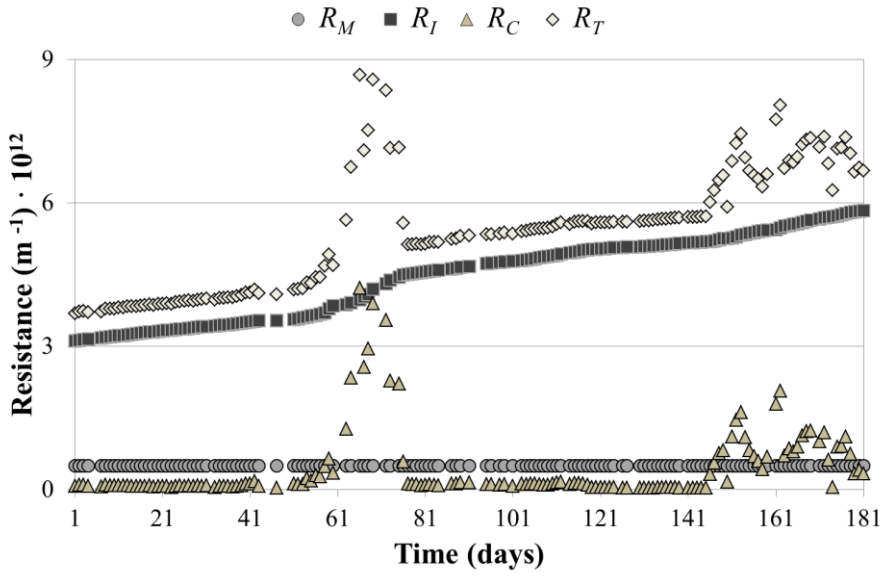

(a)

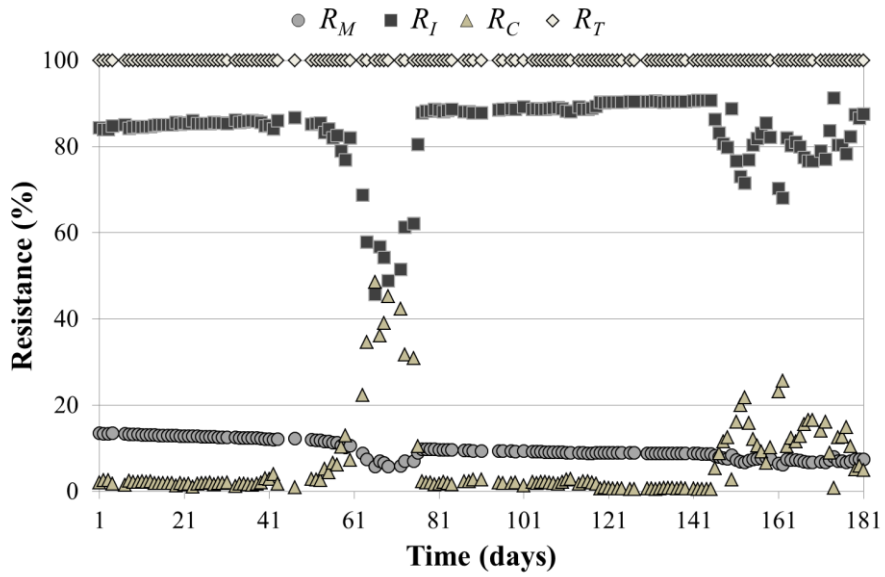

(b)

Figure 8.3 Long-term model validation using heavily-fouled membranes. Daily average values of R_M, R_I, R_C and R_T in: **(a)** absolute terms (m^{-1}); and **(b)** weighted average distribution (%).

8.3.2 Model validation using lightly-fouled membranes

Lightly-fouled membranes were used for the validation of the model when operating at SRT of 71.5 days and 33 ºC. Figure 8.4a shows the average daily values of J_{20net} (approx. 8 and 11 LMH) and SGD_m (0.23 $Nm^3\ h^{-1}\ m^{-2}$) in this operating period. Figure 8.4b shows the average daily values of TMP_{SIM} and TMP_{EXP}. Similar to the results obtained when operating using heavily-fouled membranes, Figure 8.4b illustrates how the model was able to correctly reproduce long-term membrane performance operating under completely different conditions (lightly-fouled membranes) than in Figure 8.1b (see Figure 8.4b), resulting in a Pearson's *r* coefficient between TMP_{EXP} and TMP_{SIM} of 0.987 .

Figure 8.5a shows the average daily MLTS level (ranging from 7 to 25 g L^{-1}), and the simulated average daily values of ω_C and ω_I. Using the R_I determined experimentally as mentioned before, gave an initial ω_I of about 0.006 kg $X_{m_I}m^{-2}$ (see Figure 8.5a). In this case, Figure 8.5a shows how ω_C increases as MLTS increases (a constant operating J_{20net} was maintained during the operating period, as, for instance, on operating days 57 – 141 in Figure 8.4a). Similar to the results shown in Figure 8.2, this is due to the increasing convective transport of foulants (X_{TS} in the model) to the membrane surface caused by an increase in the bulk concentration. On the other hand, a significant increase in ω_C can be seen after operating day 130. As mentioned before, q_{MS} is function of an exponential-type inhibition function that depends on both MLTS and J_{20}, which is used to model the effect of filtering at levels above or below critical conditions. Therefore, it can be assumed that the membranes were operated at near critical flux on operating days 131 – 141 (operating at 23 g L^{-1} of MLTS). Indeed, the critical flux was determined experimentally at these operating conditions (23 g L^{-1} of MLTS and SGD_m of 0.23 $Nm^3\ h^{-1}\ m^{-2}$) giving a value of about 13.5 LMH, which coincides with the gross operating J_{20} in this operating period.

As mentioned above, since the irreversible fouling rate is represented in the model as a direct function of ω_C, a higher propensity to irreversible fouling was observed when operating at high ω_C values due to operating at high MLTS levels (see operating days 131 – 141 in Figure 8.4a). In this respect, Figure 8.5a shows the highest irreversible fouling rate modelled in this operating period (0.0004 kg $X_{m_I}m^{-2}\ d^{-1}$) that was reached on operating days 131 – 141 (corresponding with the highest ω_C levels). On the other hand, an irreversible fouling rate of 0.0001 kg $X_{m_I}m^{-2}\ d^{-1}$) was modelled on operating days 1 – 131. The average irreversible fouling rate for the whole operating period (141 days of continuous operation) resulted in 0.00012 kg $X_{m_I}m^{-2}\ d^{-1}$.

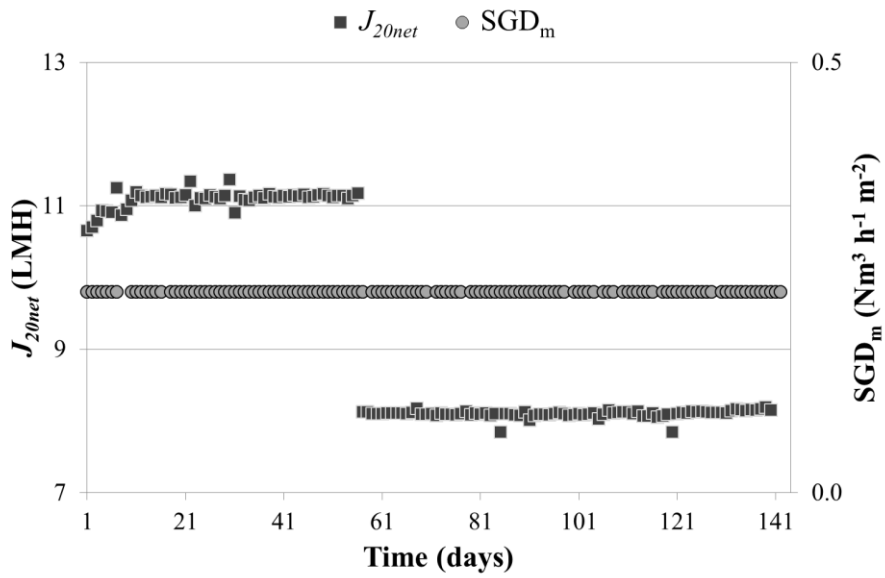

(a)

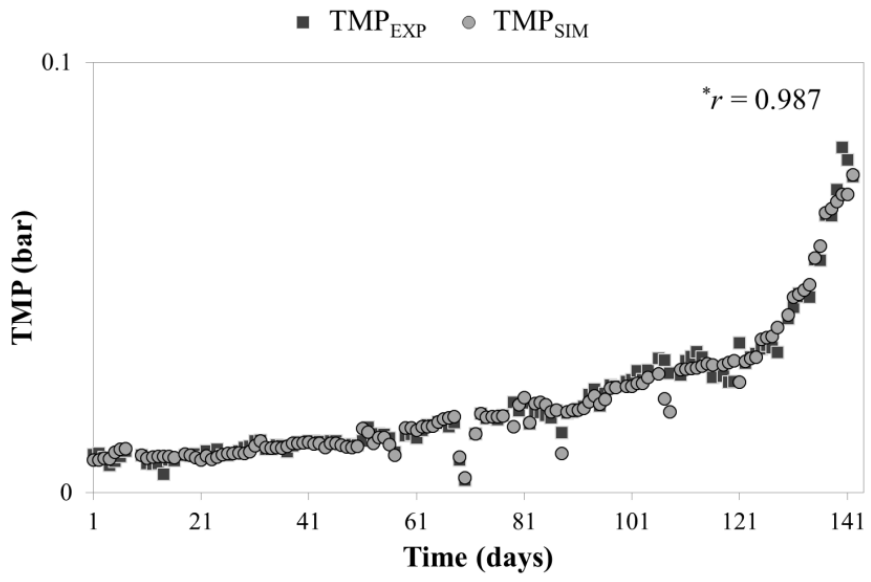

(b)

Figure 8.4 Long-term model validation using lightly-fouled membranes. Daily average values of: **(a)** J_{20} and SGD_m; and **(b)** TMP_{EXP} and TMP_{SIM}. * *r represents the Pearson Product-Moment correlation coefficient between TMP_{EXP} and TMP_{SIM}.*

It must be said that similar overall irreversible fouling rates were observed in both operating periods: when operating at SRT of 71.5 days and 33 ºC (0.00015 kg $X_{m_I}m^{-2}$ d^{-1}) and when operating at SRT of 38.5 days and 20 ºC (0.00012 kg $X_{m_I}m^{-2}$ d^{-1}). As mentioned before, this was mainly attributed to the presence of similar amounts of SMP and EPS in the mixed liquor (around 150 – 180 mg g^{-1} MLVS and 60 – 80 mg g^{-1} MLVS respectively), which resulted in similar propensities to irreversible fouling.

Nevertheless, further research is required in the long term to establish the exact dependence of $q_{IF,Max}$ upon T and SRT.

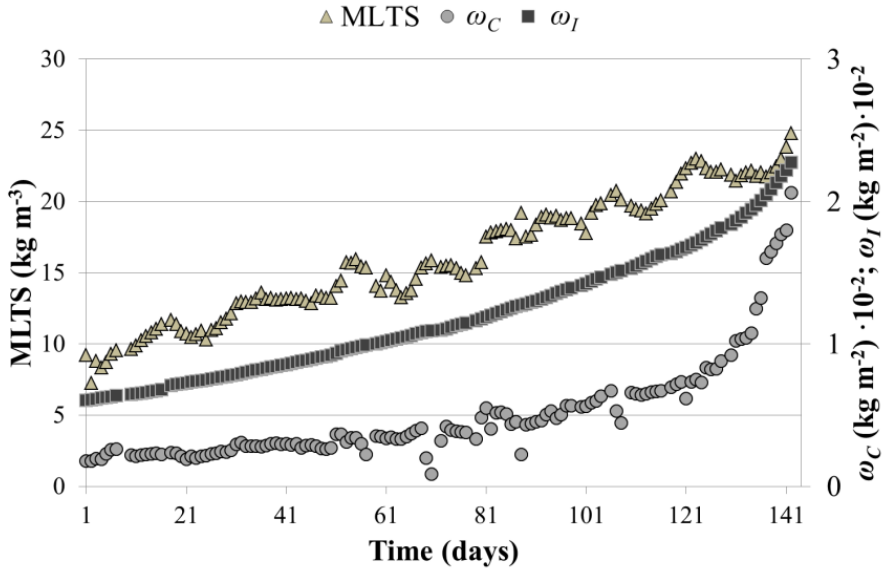

(a)

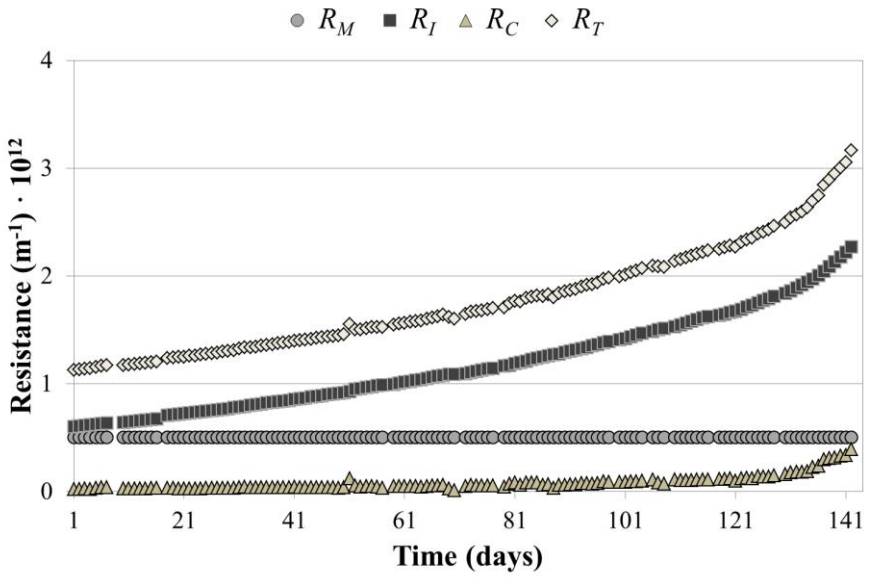

(b)

Figure 8.5 Long-term model validation using lightly-fouled membranes. Daily average values of: **(a)** MLTS, ω_C and ω_I; and **(b)** R_M, R_I, R_C and R_T.

The simulated average daily values for α_C were maintained from approx. $1.1 \cdot 10^{13}$ to $1.8 \cdot 10^{13}$ m kg^{-1} due to operating at low average TMP values (approx. 0.007 - 0.07 bar) throughout the whole operating period (α_C followed a similar behaviour to TMP).

Figure 8.5b shows the simulated average daily results (in absolute terms) recorded in this operating period at the different filtration resistances considered in the model (R_T, R_M, R_C and R_I). Regarding reversible fouling, Figure 8.5b shows low R_C values during the operating period resulting from the low values observed in ω_C and α_C. Concerning irreversible fouling, Figure 8.5b shows an increasing R_T value due to an increasing R_I value. The increase in R_I is the result of the continuous modelled increase in ω_I (see Figure 8.5a). This behaviour highlights the necessity of modelling the irreversible fouling phenomenon in the long-term to account for the actual variation of R_T over time. In this regard, a constant slightly increase in the weighted average contribution of R_I to R_T was observed throughout this operating period due to slightly increasing ω_I over time (see Figure 8.5a). On the other hand, the weighted average contribution of R_C to R_T remained close to 0% until operating day 131 when sub-critical filtration conditions were applied.

Finally, it is important to highlight that the model was able to reproduce the filtration process in a SAnMBR system across a wide range of operating conditions when working with both lightly- and heavily-fouled membranes. These results illustrate the potential of the proposed model for predicting membrane performance in the long term. Therefore, because it was possible to simulate the long-term average daily weighted distribution of R_T (including R_I), the proposed filtration model can indeed be used for the following objectives: to design and upgrade SAnMBR systems and to develop operating and control strategies designed to optimise the long-term performance of the process.

8.4 Conclusions

A filtration model has been validated in the long-term in an SAnMBR demonstration plant fitted with industrial-scale hollow-fibre membranes. The model was validated in a wide range of operating conditions using both heavily-fouled and lightly-fouled membranes. Model validation resulted in an adequate Pearson Product-Moment correlation coefficient (r) between experimental and simulated data. The simulation results revealed that irreversible fouling is the main component in the weighted average distribution of total filtration resistance in the long term.

8.5 Acknowledgements

This research has been supported by the Spanish Ministry of Economy and Competitiveness (MINECO Project CTM2011-28595-C02-01/02) jointly with the European Regional Development Fund (ERDF), which are gratefully acknowledged.

8.6 References

8.1 W. Naessens, T. Maere, I. Nopens, Critical review of membrane bioreactor models–Part 1: Biokinetic and filtration models, Bioresource Technol. 122 (2012) 95–106.

8.2 J. Ferrer, J.J. Morenilla, A. Bouzas, F. García-Usach, Calibration and simulation of two large wastewater treatment plants operated for nutrient removal, Water Sci. Technol. 50 (2004), 87–94.

8.3 K. Derbal, M. Bencheikh-lehocine, F. Cecchi, A.-H. Meniai, P. Pavan, Application of the IWA ADM1 model to simulate anaerobic co-digestion of organic waste with waste activated sludge in mesophilic condition, Bioresource Technol. 100 (2009), 1539–1543.

8.4 M.V. Ruano, J. Serralta, J. Ribes, F. Garcia-Usach, A. Bouzas, R. Barat, A. Seco, J. Ferrer, Application of the General Model "Biological Nutrient Removal Model No.1" to upgrade two full-scale WWTPs, Environ. Technol. 33(2012), 1005–1012.

8.5 G. Mannina, G. Di Bella, G. Viviani, An integrated model for biological and physical process simulation in membrane bioreactors (MBRs), J. Membr. Sci. 376 (2011), 56–69.

8.6 A.N.L. Ng, A.S. Kim, A mini-review of modeling studies on membrane bioreactor (MBR) treatment for municipal wastewaters, Desalination 212 (2007), 261–281.

8.7 A. Robles, M.V. Ruano, J. Ribes, A. Seco, J. Ferrer, A filtration model applied to submerged anaerobic MBRs (SAnMBRs). J. Membr. Sci. (2013), J. Membr. Sci. 444(2013), 139–147.

8.8 A. Robles, M.V. Ruano, J. Ribes, J. Ferrer, Factors that affect the permeability of commercial hollow-fibre membranes in a submerged anaerobic MBR (HF-SAnMBR) system, Water Res. 47 (2013), 1277–1288.

8.9 American Public Health Association/American Water Works Association/Water Environmental Federation, Standard methods for the Examination of Water and Wastewater, 21st edition, Washington DC, USA, 2005.

8.10 T.V. Bugge, M.K. Jørgensen, M.L. Christensen, K. Keiding, Modeling cake buildup under TMP-step filtration in a membrane bioreactor: Cake compressibility is significant, Water Res. 46 (2012), 4330–4338.

8.11 M.K. Jørgensen, T.V. Bugge, M.L. Christensen, K. Keiding, Modeling approach to determine cake buildup and compression in a high-shear membrane bioreactor, J. Membr. Sci. 409/410 (2012), 335–345.

8.12 M.L. Christensen, The Effect of Filter Cake Viscoelasticity on Filtration: a Study of Activated Sludge Dewatering, PhD thesis, Aalborg University, Department of Biotechnology, Chemistry and Environmental Engineering, Aalborg, Denmark, 2006.

8.13 LD. Hughes, R.W. Field, Crossflow filtration of washed and unwashed yeast suspensions at constant shear under nominally sub-critical conditions, J. Membr. Sci. 280 (2006), 89–98.

8.14 M. Sarioglu, G. Insel, D. Orhon, Dynamic in-series resistance modeling and analysis of a submerged membrane bioreactor using a novel filtration mode, Desalination 285 (2012), 285–294.

8.15 A. Robles, M.V. Ruano, F. García-Usach, J. Ferrer, Sub-critical filtration conditions of commercial hollow-fibre membranes in a submerged anaerobic MBR (HF-SAnMBR) system: The effect of gas sparging intensity, Bioresource Technol. 114 (2012) 247–254.

8.16 P. Le-Clech, V. Chen, T.A.G. Fane, Fouling in membrane bioreactors used in wastewater treatment, J. Membr. Sci. 284 (2006), 17–53.

8.17 A. Robles, M.V. Ruano, J. Ribes, J. Ferrer, Performance of industrial scale hollow-fibre membranes in a submerged anaerobic MBR (HF-SAnMBR) system at mesophilic and psychrophilic conditions, Sep. Purif. Technol. 104 (2013), 290–296.

8.18 F.G. Meng, S.R. Chae, A. Drews, M. Kraume, H.S. Shin, F.L. Yang, Recent advances in membrane bioreactors (MBRs): membrane fouling and membrane materials, Water Res. 43 (2009), 2405–2415.

CHAPTER 9:

Sensitivity analysis of a filtration model for submerged anaerobic MBRs (SAnMBRs) using a revised version of the Morris screening method

Abstract

In this paper we assess the results of a sensitivity analysis of a filtration model for submerged anaerobic MBRs (SAnMBRs). This study aimed to (1) identify the less-(or non-) influential parameters of the model in order to facilitate model calibration and (2) validate the modelling approach (i.e. to determine the need for each of the proposed parameters to be included in the model). The sensitivity analysis was conducted using a revised version of the Morris screening method. The dynamic simulations were conducted using long-term data obtained from a SAnMBR plant fitted with industrial-scale hollow-fibre membranes. Of the 14 parameters in the model, six were identified as influential, i.e. those calibrated using off-line protocols. A dynamic calibration (based on optimisation algorithms) of these influential parameters was conducted. The resulting estimated model parameters accurately predicted membrane performance

Keywords

Calibration; filtration model; industrial-scale hollow-fibre membranes; Morris screening method; sensitivity analysis; submerged anaerobic MBR

Highlights

A sensitivity analysis of a filtration model for SAnMBRs was conducted.
It was conducted using a revised version of the Morris screening method.
Sensitivity results significantly simplified the parameter subset to be calibrated.
Only one parameter could be removed from the model.

A. Robles, M.V. Ruano, J. Ribes, A. Seco, J. Ferrer
Sensitivity analysis of a filtration model for submerged anaerobic MBRs (SAnMBRs) using a revised version of the Morris screening method
Submitted to J. Membrane Sci.

9.1 Introduction

Understanding and optimising a complex system such as a membrane bioreactor (MBR) is a difficult and time-consuming process mainly because of the large number of sub-processes taking place simultaneously, which are generally highly dependent upon each other. In this respect, mathematical modelling is a powerful tool for studying such complex systems [9.1].

Certain models have been found to be useful for dealing with different aspects of WWTPs, *e.g.* R&D of wastewater treatment processes, design and upgrading of WWTPs, and the development of operating and control strategies designed to optimise process performance [9.2; 9.3; 9.4]. Computerised models make it possible to perform many virtual experiments in a short space of time. Therefore the mathematical modelling of filtration in submerged anaerobic MBRs (SAnMBRs) may help gain an insight into the key factors in membrane fouling [9.5], and are also invaluable for the design, prediction and control of the membrane technology used for treating wastewater [9.6]. However, predictions made on the basis of models are not free from uncertainty because models are an abstract approximation of reality and are usually based on a considerable number of assumptions. In this respect, sensitivity analysis provides useful information for modellers because it attempts to quantify how changes to a model's input parameters affect the model's output. In addition, due to the limited data available about full-scale systems, the subset of identifiable parameters can be reduced, which makes calibrating the model simpler.

The different sensitivity analysis strategies applied in literature are usually classified in two main categories: global sensitivity analysis which involves sampling and whose range of input uncertainty reflects the uncertainty in the output variables; and local sensitivity analysis, which is based on the local impact of parameters upon output variables.

The Morris screening method [9.7] is a one-factor-at-a-time (OAT) method of global sensitivity analysis which calculates the elementary effects (EE_i) of input factors upon the output of a model. EE_i is in itself a local measure of sensitivity, but this drawback is overcome by repeating EE_i calculations in the input region of interest using Morris's efficient random sampling strategy, which is obtained by using a trajectory-based design. Finally, the analysis of the distribution (F_i) of the elementary effects of each input factor will determine the relative importance of the input factors, which closely resembles a global sensitivity analysis. Moreover, the Morris screening method makes it possible to validate the modelling approach because it identifies the non-influential parameters, which could be

useful for improving the definition of the model by evaluating the usefulness of the non-influential parameters.

One key issue with the Morris screening method is that the sampling matrix is generated at random. This random sampling may not represent the sampling space well and result in an inadequate screening of non-influential parameters. In this regard, Campolongo *et al*. [9.8] proposed an improved sampling method which maximised the distances between the final trajectories (*r*) selected. However, this improved sampling was not suitable for large models because of the vast numbers of calculations needed to determine the best combinations. For this reason, Ruano *et al*. [9.9] proposed an improved sampling method based on trajectory design intended to overcome the great many calculations required by the Campolongo sampling method.

In this study, a revised version of the Morris screening method that includes an improved sampling method [9.9] was applied to a filtration model (resistance-in-series-based) for SAnMBRs [9.10; 9.11]. Although the model was proven to be robust, the Morris screening method was used not only to identify the less influential parameters of the model, but also to validate the modelling approach (*i.e.* to assess the need to include each of the proposed parameters in the model). In addition, a dynamic calibration (based on optimisation algorithms) of the most influential parameters was conducted.

9.2 Materials and methods

9.2.1 SAnMBR plant description

The filtration model evaluated in this study was developed, calibrated and validated using data obtained from the previously introduced SAnMBR system (see Chapter 2). For further details of this SAnMBR system, see Robles *et al*. [9.12].

9.2.2 Monitoring system

In addition to being monitored on line, grab samples of anaerobic sludge were taken once a day to assess filtration performance. MLTS concentration was determined according to Standard Methods [9.13] using procedure 2540 B.

9.2.3 Model description

The filtration model used in this study (see Chapter 7) gives the dynamic evolution of the transmembrane pressure (TMP) by applying Eq. 9.1 and Eq. 9.2.

$$TMP(t) = J \cdot \mu \cdot R_T \qquad \textbf{Eq. 9.1}$$

where:

- J is the transmembrane flux (m s^{-1}).
- μ is the permeate dynamic viscosity (kg m^{-1} s).
- $TMP\ (t)$ is the transmembrane pressure (Pa).
- R_T is the total filtration resistance (m^{-1}).

$$R_T = R_M + R_C + R_I = R_M + \omega_C \cdot \alpha_C + \omega_I \cdot \alpha_I \qquad \textbf{Eq. 9.2}$$

where:

- R_M is the intrinsic membrane resistance (m^{-1}).
- R_C is the cake layer resistance (m^{-1}).
- R_I is the irreversible fouling resistance (m^{-1}).
- ω_C is the mass of cake deposited per membrane area (kg m^{-2}).
- α_C is the average specific cake resistance (m kg^{-1}).
- ω_I is the mass of irreversible fouling per membrane area (kg m^{-2}).
- α_I is the average specific irreversible fouling resistance (m kg^{-1}).

To account for cake layer compression, α_C was defined as time- and TMP-dependent as per Bugge *et al*. [9.14] and Jørgensen *et al*. [9.15]. In addition, to account for sub-critical fouling, an additional dependence of α_C on time was considered in the model [9.10], as shown in Eq. 9.3 below:

$$\alpha_C(t) = \alpha_C(t-\Delta t) + \max\left(k_{SF}, k_t \cdot \left(\alpha_{C,0} \cdot \left(1 + \frac{TMP}{TMP_a}\right) - \alpha_C(t-\Delta t)\right)\right) \cdot \Delta t \qquad \textbf{Eq. 9.3}$$

where:

- $\alpha_C(t)$ is the specific resistance of the cake at time t (kg m^{-2}).
- $\alpha_C(t-\Delta t)$ is the specific resistance of the cake at a previous moment in time (kg m^{-2}).
- k_{SF} is the sub-critical fouling parameter (kg m^{-2} s^{-1}).
- $\alpha_{C,0}$ is the specific resistance of the cake at zero pressure (kg m^{-2}).

- TMP_a is the pressure needed to double the specific resistance (Pa).
- k_t is the time constant (s^{-1}).
- Δt is the time step (s).

To model the dynamics of ω_C and ω_I a black-box approach was adopted in the model. This approach considers 3 suspended components: MLTS concentration X_{TS} (kg TS m^{-3}); dry mass of cake on the membrane surface, X_{m_C} (kg TS); and dry mass of irreversible fouling on the surface of the membrane, X_{m_I} (kg TS). In addition, this approach includes four kinetically governed physical processes: (1) cake layer build-up during filtration; (2) cake layer removal using biogas sparging to scour the membrane; (3) cake layer removal during back-flushing; and (4) consolidation of irreversible fouling. Table 7.1 shows the stoichiometry and kinetic formulae of the four processes considered in the model.

Process 1 (cake layer build-up, see Table 7.1) is the convective transport of foulants (X_{TS} in the model) to the membrane, which is a function of the permeate flow-rate, Q_{20P} (m^3 s^{-1}), and bulk concentration (X_{TS}). Process 2 (membrane scouring by biogas sparging, see Table 7.1) is the impact of the hydrodynamic conditions in the membrane tank caused by biogas sparging (measured as BRF_V: biogas recycling flow per bulk volume in the membrane tank). Our study defined a maximum membrane scouring velocity ($q_{MS,Max}$) for process 2. In process 3 (see Table 7.1), the back-flushing removal rate is defined as a function of the back-flushing flow rate, Q_{20BF} (m^3 s^{-1}), and X_{m_C}. As per Sarioglu *et al.* [9.16], we defined a maximum back-flushing removal velocity, $q_{BF,Max}$ (m^{-3}), for process 3.

One half-saturation switching function ($M_{X_{m_C}}$, Eq. 9.4) for both membrane scouring (process 2) and back-flushing (process 3) was used to vary the removal of solids smoothly as the cake layer disappeared [9.16].

$$M_{X_{m_C}} = \frac{X_{m_C}}{K_{S,X_{m_C}} + X_{m_C}} \qquad \textbf{Eq. 9.4}$$

where:

- $K_{S,X_{m_C}}$ is the half-saturation coefficient of cake solids during membrane scouring and back-flushing (kg ST).

Process 2 includes one sigmoid inhibition function (I_{MS}, Eq. 9.5) to model the impact of filtering above or below critical conditions.

$$I_{MS} = \frac{1}{1 + K_F \cdot e^{\left(J_{20} \cdot \left(\beta_1 \cdot BRF_V + \beta_2 \cdot MLTS + \gamma\right)\right)}} \qquad \textbf{Eq. 9.5}$$

where:

- K_F is the adjustment parameter representing the fouling rate when the gross 20 ºC-normalised transmembrane flux (J_{20}) tends to zero (Pa s^{-1}).
- J_{20} is the gross 20 ºC-normalised transmembrane flux (m s^{-1}).
- BRF_V is the biogas recycling flow per bulk volume in the membrane tank (Nm^3 s^{-1} m^{-3}).
- $MLTS$ is the mixed liquor total solids concentration (kg m^{-3}).
- β_1 (s^2 m^{-1}), β_2 (s m^2 kg^{-1}) and γ (s m^{-1}) are the parameters of the model.

On the basis of long-term experimental results, the value of γ was defined as a function of R_I to account for the reduction over time in the filtering capacity of the membranes due to the onset of irreversible fouling. This dependence on irreversible fouling can be expressed as:

$$\gamma_t = \gamma_0 - \left(R_{I_t} - R_{I_0}\right) k_{RI} \qquad \textbf{Eq. 9.6}$$

where:

- γ_t is the value of γ at time t (s m^{-1}).
- γ_0 is the value of γ at the initial time (s m^{-1}).
- R_{I_t} is the irreversible fouling resistance at time t (m^{-1}).
- R_{I_0} is the irreversible fouling resistance at the initial time (m^{-1}).
- k_{RI} is the proportional constant (s).

Finally, irreversible fouling (process 4, see Table 7.1) was given in the evaluated model as a direct function of X_{m_C} and a maximum irreversible fouling kinetic constant, $q_{IF,Max}$ (s^{-1}).

This filtration model features a total of 14 parameters that must be calibrated for each specific system (see Table 7.4). These parameters were previously calibrated by off-line and dynamic calibration methods using short-term and long-term data from the SAnMBR plant (see Chapter 7). In addition, on the basis of expert knowledge, default values were assigned to those parameters that could not be estimated from the available data [9.10]. Table 7.4 shows these default values calibrated beforehand

and used in the sensitivity analysis carried out in this study. Uncertainty was set to 20% of the variability of these values in the dynamics simulations.

9.2.4 Simulation

Our study included 1 month of dynamic simulations using data obtained from the above-mentioned SAnMBR system. This period was selected as a compromise between obtaining reliable results and the cost of calculations. It is important to note that the simulation period must be sufficiently long to enable the effect of both reversible and irreversible fouling mechanisms to be evaluated [9.17].

Simulation entailed the following dynamic operating conditions: MLTS levels from approx. 15 – 18 g L^{-1}; biogas recycling flow (BRF) from 4 to 12 Nm^3 h^{-1}; and J_{20} from approx. 4 to 12 LMH. The dynamics in J_{20} considered the fluctuations in the influent flows of WWTPs. For this purpose, the standard dry-weather influent records (updated in 2006) recommended by Copp [9.18] were used as shown in Robles *et al*. [9.19].

9.2.5 Morris screening method

The Morris screening method [9.7] evaluates the distribution (F_i) of the elementary effects (EE_i) of each input factor upon model outputs, used to calculate the statistical parameters that provide sensitivity data. In this study the scaled elementary effect (SEE_i) proposed by Sin and Gernaey [9.20] was applied. The finite distribution of elementary effects associated with each input factor F_i is obtained by sampling different coordinates (X) from the parameter space at random. However, this random sampling of X may only cover a small part of the space. Therefore, we applied a modified version of the improved sampling proposed by Campolongo *et al*. [9.8]. This alternative methodology [9.9] has low calculation requirements and generates a combination of r trajectories from a defined group of initial Morris trajectories (M) that are very close to the ones with the highest spreads. Although the proposed sampling does not guarantee maximum overall distances between the final trajectories (r) selected (*i.e.* maximum dispersion in the input space), at least these distances are maximised locally [9.9].

As per Saltelli *et al*. [9.21], the mean (μ), standard deviation (σ) and absolute mean (μ^*) of the SEE_i values of each F_i were used in our study as sensitivity measures. μ^* was used to rank the parameters, in order to systematically differentiate between non-influential parameters (low μ^*) and influential

parameters (high μ^*). An optimal setting of r (r_{opt}) was sought with a constant resolution of $p = 4$. To this end, increasing numbers of elementary effect calculations (r) were carried out for each distribution F_i until the ranking of parameters (based on μ^*) remained more or less stable, *i.e.* type II error was minimised (type II error: identifying an important factor as insignificant). This stability was numerically evaluated using the position index $PF_{ri \to rj}$ [9.9] which enables an optimal value for r (r_{opt}) to be determined. For given rankings obtained by r_i and r_j, the index $PF_{ri \to rj}$ is defined by Eq. 9.7.

$$PF_{r_i \to r_j} = \sum_{k=1}^{k} \frac{Abs\left(P_{k,i} - P_{k,j}\right)}{\mu_{P_{k,i}, P_{k,j}}} \qquad \textbf{Eq. 9.7}$$

where:

- $P_{k,i}$ is the position of the k^{th} parameter in the ranking obtained by r_i
- $P_{k,j}$ is the position of the k^{th} parameter in the ranking obtained by r_j
- $\mu_{P_{k,i}, P_{k,j}}$ is the average of the positions of the k^{th} parameter in the ranking obtained by r_i and r_j.

Once r_{opt} was found, the graphical Morris approach was used to identify the parameters that influence the model. The μ and σ obtained for all SEE_i values of each F_i are plotted. Two lines were also plotted, corresponding to $\mu_i \pm 2SEM_i$, where SEM_i is the standard error of the mean that can be calculated thus: $SEM_i = \sigma_i / \sqrt{r}$. Parameters with low μ and low σ are deemed to be non-influential [9.7].

9.2.6 Dynamic calibration of the model being evaluated

The dynamic calibration (based on optimisation algorithms) of the influential parameters of the model consisted of adjusting the simulated TMP (TMP_{SIM}) to the experimental TMP (TMP_{EXP}) by means of the least squares method together with the subspace trust region method [9.22], based on the interior-reflective Newton method (implemented in MATLAB® LSQNONLIN), and the Runge-Kutta method (MATLAB® ode45 function). The objective function (OF) applied is shown in Eq. 9.8.

$$OF = \sum \sqrt{\left(TMP_{SIM} - TMP_{EXP}\right)^2} \qquad \textbf{Eq. 9.8}$$

To enhance the dynamic calibration, appropriate initial values for the model parameters had to be selected. In this respect, on the basis of the different Morris simulations carried out to select r_{opt}, the

optimum initial values chosen were those which combined to give the minimum least squares error between TMP_{SIM} and TMP_{EXP} (see Eq. 9.8).

9.3 Results and discussion

9.3.1 Sensitivity analysis results

The revised version of the Morris screening method was applied to different number of trajectories (r), chosen from M =1000 initial Morris trajectories, until the ranking of significant parameters remained more or less stable, as measured quantitatively by the index $PF_{ri \rightarrow rj}$. Parameter uncertainty was set to 20% of the variability of the default values shown in Table 7.4. This value was established on the basis of the results from different trials in which uncertainty ranged from 10 to 50%.

Table 9.1 shows the sensitivity measures (μ^* and σ) resulting from the model inputs calculated for the different number of runs selected for the Morris simulations. As Table 9.1 illustrates, higher numbers of runs (*i.e.* an increase in r) did not significantly modify the sensitivity measures of the inputs. For instance, increasing the number of runs from 10 to 40 had no significant impact on the rankings of the different model parameters.

Table 9.2 shows PFri→ $_{rj}$ for the different number of trajectories evaluated. As can be seen in Table 9.2, $PF_{ri \rightarrow rj}$ was low even when the number of runs was low (*e.g.* r = 10~40). This means that in this study, values of r below 40 (*e.g.* r = 10~30) give a suitable estimate of sensitivity measurements. These results tally with other applications of the Morris screening method involving few repetitions (*e.g.* r = 10~20) [9.23; 9.24].

On the basis of these results, r = 10 was selected as the optimal number of repetitions (r_{opt}) in this study. We considered r = 10 to be optimal not only because $PF_{10 \rightarrow 20}$ was low but also because of the significant stability of the parameters at the top of the ranking (see Table 9.1). When r_{opt} = 10, 140 simulations (simulations = $r \cdot (k+1)$; r = 10; k = 14) were required to evaluate the entire model. One simulation (covering 1 month's operations) took approximately 10 minutes to calculate using a PC with 8 GHz Intel® CORE™ i5 processor. Therefore, in this study, it was possible to estimate the sensitivity measures adequately with a low number of repetitions (requiring few calculations). These results suggest adequate coverage of the input space and, therefore, that possible problems related to

type I error (*i.e.* considering a factor to be significant when it is not) and type II error (*i.e.* failing to identify a parameter that influences the model considerably) are avoided.

Table 9.1 Sensitivity analysis results: sensitivity measures of the model parameters for the different values of *r* evaluated (r_{opt} = 10).

r = 10			***r = 20***		
Parameter	μ^*	σ	**Parameter**	μ^*	σ
γ_0	0.496	0.160	γ_0	0.547	0.185
β_2	0.151	0.082	β_2	0.159	0.090
k_{SF}	0.096	0.040	β_1	0.119	0.068
β_1	0.092	0.067	k_{SF}	0.089	0.051
K_F	0.046	0.035	$q_{\mathrm{MS,Max}}$	0.060	0.038
$q_{\mathrm{MS,Max}}$	0.046	0.029	K_F	0.051	0.034
$\alpha_{C,0}$	0.016	0.005	$\alpha_{C,0}$	0.018	0.005
k_{RI}	0.010	0.007	k_{RI}	0.010	0.004
TMP_a	0.009	0.004	TMP_a	0.009	0.009
$K_{S,XmC}$	0.004	0.002	$K_{S,XmC}$	0.007	0.009
$q_{\mathrm{IF,Max}}$	0.004	0.004	$q_{\mathrm{IF,Max}}$	0.005	0.003
α_I	0.003	0.000	α_I	0.004	0.000
k_t	0.000	0.000	k_t	0.000	0.000
$q_{\mathrm{BF,Max}}$	0.000	0.000	$q_{\mathrm{BF,Max}}$	0.000	0.000
r = 30			***r = 40***		
Parameter	μ^*	σ	**Parameter**	μ^*	σ
γ_0	0.599	0.190	γ_0	0.527	0.162
β_2	0.182	0.086	β_2	0.159	0.084
β_1	0.128	0.061	β_1	0.116	0.069
k_{SF}	0.097	0.050	k_{SF}	0.090	0.045
K_F	0.068	0.041	$q_{\mathrm{MS,Max}}$	0.054	0.037
$q_{\mathrm{MS,Max}}$	0.062	0.036	K_F	0.051	0.035
$\alpha_{C,0}$	0.015	0.006	$\alpha_{C,0}$	0.015	0.005
TMP_a	0.015	0.013	k_{RI}	0.010	0.009
k_{RI}	0.008	0.004	TMP_a	0.008	0.004
$q_{\mathrm{IF,Max}}$	0.006	0.000	$K_{S,XmC}$	0.005	0.003
$K_{S,XmC}$	0.005	0.003	$q_{\mathrm{IF,Max}}$	0.003	0.004
α_I	0.005	0.006	α_I	0.003	0.000
k_t	0.000	0.000	k_t	0.000	0.000
$q_{\mathrm{BF,Max}}$	0.000	0.000	$q_{\mathrm{BF,Max}}$	0.000	0.000

Table 9.2 Sensitivity analysis results: position factors ($PF_{ri \rightarrow rj}$) for the *r* evaluated.

$r_i \rightarrow r_j$	$10 \rightarrow 20$	$20 \rightarrow 30$	$30 \rightarrow 40$
$PF_{ri \rightarrow rj}$	0.93	0.79	0.79

Figure 9.1 shows the graphical Morris approach for the optimal number of repetitions selected for the sensitivity evaluation. This figure shows the most influential parameters in the model. Figure 9.1a shows the 6 most influential parameters, which lie outside the wedge formed by two lines plotted according to $\mu_i = \pm 2SEM_i$. They have means substantially different from 0 and relatively small standard deviations. It consisted of: (1) the model parameter related to reversible fouling γ_0 (μ^* = 0.496 and σ = 0.160); (2) the model parameter related to reversible fouling β_2 (μ^* = 0.151 and σ = 0.082); (3) the parameter related to sub-critical fouling k_{SF} (μ^* = 0.096 and σ = 0.040); (4) the model parameter related to reversible fouling β_1 (μ^* = 0.092 and σ = 0.067); (5) the maximum membrane scouring velocity $q_{\mathrm{MS,Max}}$ (μ^* = 0.046 and σ = 0.035); and (6) the fouling rate when J_{20} tends to zero K_F (μ^* = 0.046 and σ = 0.029). It is important to note that 3 of the 4 model parameters in the sigmoid inhibition function (see Eq. 9.5) included in process 2 (cake layer removal using biogas sparging to scour the membrane) had the highest mean and standard deviation values: γ_0, β_2 and β_1. These results highlight the importance of these parameters for an adequate representation of the filtration results achieved using the model we developed. It is important to note that the calibration method proposed for these parameters (in addition to K_F) entailed off-line experiments based on the data obtained from different flux-step trials according to Robles *et al*. [9.26]. The next in importance were k_{SF}, $q_{\mathrm{MS,Max}}$ and K_F. These 3 parameters are also related to the reversible fouling mechanisms modelled.

In particular, it is important to highlight the great influence of the parameter γ_0, which has the highest μ^* and σ. According to the Morris theory, parameters with high σ are expected to have a non-linear or interactive impact on output. Indeed, based on the defined model, γ_0 modifies the impact of other inputs on the model output (interactions between input factors). Finally, γ_0 determines the critical filtration conditions for given MLTS and BRF, and thus affects the final value of ω_C at given operating conditions. Therefore, γ_0 indirectly determines the final value of ω_I, which is a direct function of ω_C and $q_{\mathrm{IF,Max}}$. Both ω_C and ω_I finally determine the model output (TMP). Behaviour similar to γ_0 but to a lesser extent was observed for β_2 and β_1 (both affect critical filtration conditions). On the other hand, the impacts of k_{SF}, $q_{\mathrm{MS,Max}}$ and K_F upon output are expected to be more linear and additive: their mean is quite high and their standard deviation not very high. This behaviour is desirable when estimating parameters on the basis of optimisation algorithms.

Six model parameters were identified as less influential parameters (see Figure 9.1b): (1) specific resistance of cake at zero pressure $\alpha_{C,0}$ (μ* = 0.016 and σ = 0.005); (2) proportional constant k_{RI} (μ* = 0.010 and σ = 0.007); (3) pressure needed to double specific resistance TMP_a (μ* = 0.009 and σ = 0.004); (4) half-saturation coefficient for cake solids during membrane scouring and back-flushing $K_{S,X_{mC}}$ (μ* = 0.004 and σ = 0.002); (5) maximum irreversible fouling kinetic constant $q_{\text{IF,Max}}$ (μ* = 0.004 and σ = 0.004); and (6) average specific irreversible fouling resistance α_I (μ* = 0.003 and σ = 0.000). It is important to highlight that 3 of the 7 parameters identified as less influential are related to irreversible fouling: $q_{\text{IF,Max}}$, α_I and k_{RI}. The low impact of these parameters on the model output was attributed to the expected non-linear or interactive impact on the output of the influential input factors related to reversible fouling.

One aspect to highlight is that only two model parameters, the time constant k_t and the maximum back-flushing removal velocity $q_{\text{BF,Max}}$, were identified as non-influential with a value of zero for both sensitivity measures (μ and σ). The value of k_t is related to the time required for compressing the cake to its equilibrium value for a given TMP level (*i.e.* increasing α_C to $\alpha_{C,TMP}$). In this respect, it was assumed that $\alpha_{C,TMP}$ was always achieved independently of the value established for k_t within the selected input uncertainty. The effect of this input factor (k_t) on the output is therefore expected to be negligible, therefore this result suggests it is not necessary to calibrate this input factor in this particular application of the model. On the other hand, $q_{\text{BF,Max}}$ gives the maximum back-flushing removal velocity. Since this parameter was identified as non-influential, it can be assumed that for the back-flushing duration interval evaluated in this study (from 30 to 50 seconds), the reversible cake-layer was completely removed from the membrane surface. Moreover, it is interesting to note that low back-flushing frequencies (1 back-flushing for each 10 filtration-relaxation cycles on average) were applied, therefore this input factor was expected to influence the output less than other inputs (*e.g.* the input factors related to the removal of fouling by using biogas sparging to scour the membrane).

Parameters identified as less influential can be set to default values based on optimisation algorithms. It must be emphasised that these parameters are for the input factors whose values were not calibrated off-line beforehand. To be precise, these parameters were either dynamically calibrated ($\alpha_{C,0}$ and TMP_a), or calculated on the basis of experimental data ($q_{\text{IF,Max}}$, $K_{S,X_{mC}}$ and k_{RI}), or set to default values (α_I, $q_{\text{BF,Max}}$ and k_t).

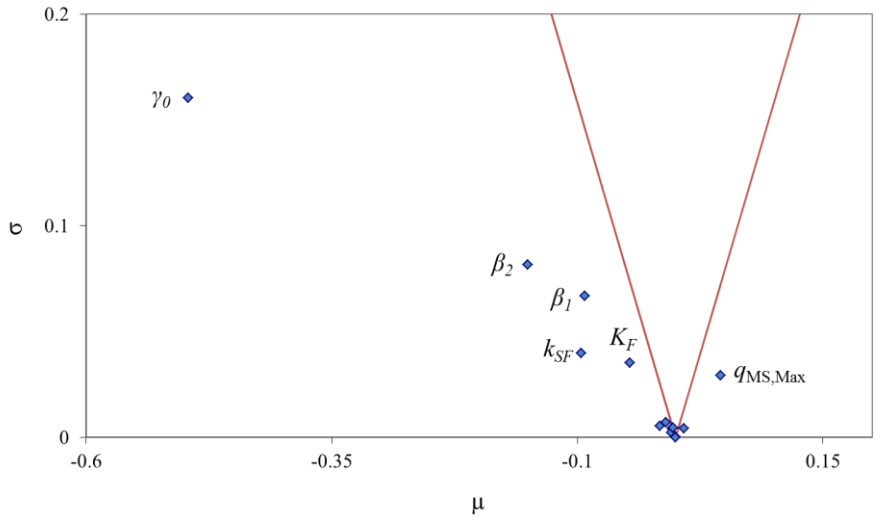

(a)

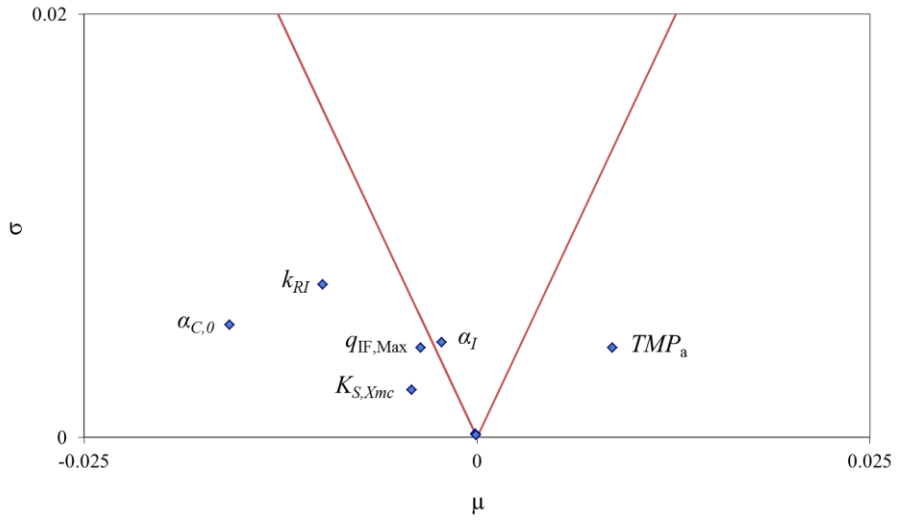

(b)

Figure 9.1 **(a)** Sensitivity analysis results: μ versus σ for the final value of r_{opt} of 10. **(b)** Zoom of the sensitivity analysis results in the range of - 0.025 < μ < 0.025 and 0 < σ < 0.02. Lines correspond to $\mu_i = \pm 2\ SEM_i$.

9.3.2 Assessment of the modelling approach

As mentioned before, one main characteristic of the model evaluated in our study is that it was developed on the basis of the operating results of an SAnMBR system fitted with industrial-scale membranes. Hence, most of the parameters included in the model were defined in order to represent all possible filtration process performances. Indeed, the results of the sensitivity analysis tally with our knowledge of the process because most of the proposed model parameters defined and calibrated by

off-line experiments were identified as the most influential parameters. In this respect, the parameters related to membrane scouring (β_1, β_2, γ_0, K_F and $q_{MS,Max}$) were defined in the model on the basis of trials designed to identify the critical filtration conditions of the SAnMBR plant.

As regards the less influential input factors, those related to cake layer build-up and compression during filtration (k_{SF}, $\alpha_{C,0}$ and TMP_a) and cake layer removal during back-flushing ($K_{S,X_{m_C}}$) were included in the model on the basis of experimental results found in recent literature [9.14; 9.15; 9.16]. As regards irreversible fouling mechanisms, parameters $q_{IF,Max}$, α_I and k_{RI} were included in the model on the basis of experimental results concerning long-term membrane performance (*i.e.* on the basis of the results showing an increase in the total filtering resistance of the system and a decrease in the critical flux determined in experiments throughout the operating period of the plant).

As regards the input factors identified in this study as non-influential (k_t and $q_{BF,Max}$), the result obtained for k_t predicts that this parameter can be fixed to a constant value in the model. The result for $q_{BF,Max}$ suggests that this input factor is not required in the model definition although this parameter was identified as non-influential in this specific study in which low back-flushing frequencies were applied. Therefore, it must be said that this input factor is expected to model the output in other specific situations or model applications (*e.g.* operating with variable duration, high back-flushing frequencies, modelling short-term process performance, etc.).

9.3.3 Model calibration

For the experimental period evaluated in this study, the 6 influential parameters (β_1, β_2, γ_0, K_F, $q_{MS,Max}$, k_{SF}) were calibrated by an optimisation algorithm, and the other parameters were set to the optimised initial values. Table 9.3 shows the initial values used in this dynamic calibration (column 1) and the calibrated values for the influential parameters mentioned above (column 2).

Table 9.3 Initial and dynamically calibrated values for the different model parameters in the experimental period evaluated in this study.

Parameter	Unit	Initial value	Calibrated value
$q_{MS,Max}$		5.89	4.71
$q_{BF,Max}$	m^{-3}	1.07	
$q_{IF,Max}$	s^{-1}	$3 \cdot 60^{-07}$	
$K_{S,XmC}$	kg SST	0.19	
$\alpha_{C,0}$	m kg^{-1}	$1.08 \cdot 10^{13}$	
TMP_a	kPa	20.1	
k_t	s^{-1}	1.2	
k_{SF}	m kg^{-1} s^{-1}	$3.81 \cdot 10^{10}$	$2.30 \cdot 10^{10}$
K_F	Pa s^{-1}	$4.5 \cdot 10^{-4}$	$5.4 \cdot 10^{-4}$
β_1	s^2 m^{-1}	$-2.31 \cdot 10^{8}$	$-1.85 \cdot 10^{8}$
β_2	s m^2 kg^{-1}	$4.1 \cdot 10^{4}$	$4.9 \cdot 10^{4}$
γ_0	s m^{-1}	$2.62 \cdot 10^{6}$	$3.14 \cdot 10^{6}$
k_{RI}	s	$1.9 \cdot 10^{-07}$	
α_I	m kg^{-1}	$1 \cdot 20^{14}$	

Figure 2 shows the results of the dynamic model calibration. Figure 2a shows the average daily values of J_{20net}, BRF, and MLTS. Figure 2b shows the average daily TMP_{SIM} and TMP_{EXP}. Hence, Figure 2 shows that, even when operating at different MLTS, J_{20net} and BRF levels (see Figure 2a), the model accurately predicted the membrane performance using the calibrated values for the model parameters (see Figure 2b): an adequate Pearson Product-Moment correlation coefficient (R) between TMP_{EXP} and TMP_{SIM} was obtained (0.936). Nevertheless, the model also gave accurate results when using the default values (Pearson's R coefficient was 0.898). Hence, the performance of the model was only slightly enhanced by dynamically calibrating the influential model parameters because the initial parameter values had been calibrated previously using long-term data [9.10].

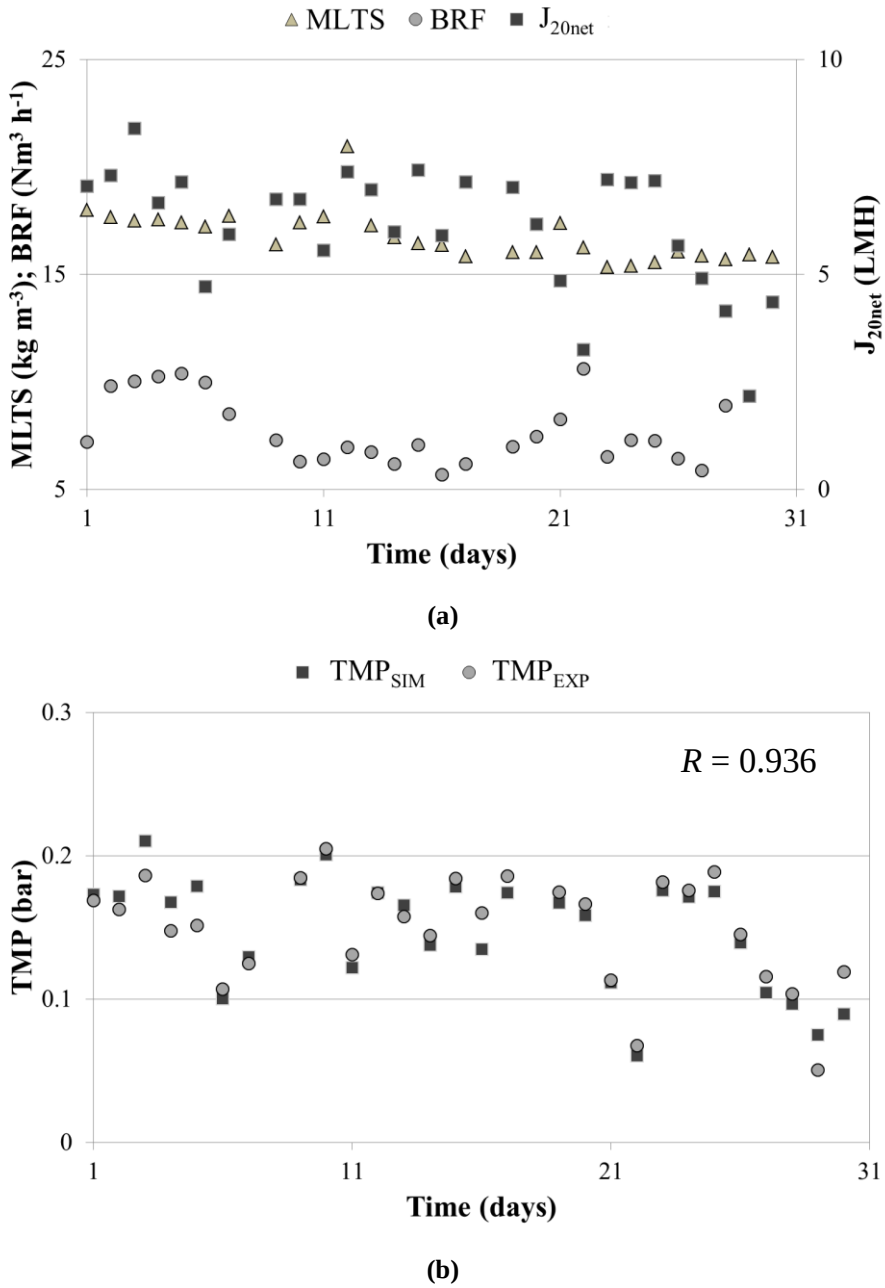

Figure 9.2 Model validation using the optimised model parameters values. Average daily values of **(a)** MLTS, J_{20net} and BRF and **(b)** TMP_{EXP} and TMP_{SIM}. * *R represents the Pearson Product-Moment correlation coefficient between TMP_{EXP} and TMP_{SIM}.*

9.4 Conclusions

A sensitivity analysis of a filtration model for SAnMBRs using a revised version of the Morris screening method was conducted. The optimal number of repetitions found in this study (r_{opt} = 10) was similar to the number of repetitions mainly used in other applications of the Morris screening method.

Using the Morris screening method enabled us to validate the model: 6 of the model's 14 parameters were identified as influential, *i.e.* the parameters calibrated using off-line methods. This tallied with our knowledge of the process because the model was developed on the basis of experimental results. After the dynamic calibration (based on optimisation algorithms) of the highly influential parameters, the predictions generated by the model were slightly more accurate.

9.5 Acknowledgements

This research work has been supported by the Spanish Ministry of Economy and Competitiveness (MINECO, Projects CTM2011-28595-C02-01/02) jointly with the European Regional Development Fund (ERDF) which are gratefully acknowledged.

9.6 References

9.1 W. Naessens, T. Maere, I. Nopens, Critical review of membrane bioreactor models – Part 1: Biokinetic and filtration models, Bioresour. Technol. 122 (2012) 95–106.

9.2 J. Ferrer, J.J. Morenilla, A. Bouzas, F. García-Usach, Calibration and simulation of two large wastewater treatment plants operated for nutrient removal, Water Sci. Technol. 50 (2004), 87–94.

9.3 K. Derbal, M. Bencheikh-lehocine, F. Cecchi, A.-H. Meniai, P. Pavan, Application of the IWA ADM1 model to simulate anaerobic co-digestion of organic waste with waste activated sludge in mesophilic condition, Bioresour. Technol. 100 (2009), 1539–1543.

9.4 M.V. Ruano, J. Serralta, J. Ribes, F. Garcia-Usach, A. Bouzas, R. Barat, A. Seco, J. Ferrer, Application of the General Model "Biological Nutrient Removal Model No.1" to upgrade two full-scale WWTPs, Environ. Technol. 33(2012), 1005–1012.

9.5 G. Mannina, G. Di Bella, G. Viviani, An integrated model for biological and physical process simulation in membrane bioreactors (MBRs), J. Membr. Sci. 376 (2011), 56–69.

9.6 A.N.L. Ng, A.S. Kim, A mini-review of modeling studies on membrane bioreactor (MBR) treatment for municipal wastewaters, Desalination 212 (2007), 261–281.

9.7 M. Morris, Factorial sampling plans for preliminary computational experiments, Technometrics. 33 (1991), 239 – 245.

9.8 F. Campolongo, J. Cariboni, A. Saltelli, An effective screening design for sensitivity analysis of large models, Environ. Modell. Softw. 22 (2007), 1509–1518.

9.9 M.V. Ruano, J. Ribes, A. Seco, J. Ferrer, An improved sampling strategy based on trajectory design for the application of Morris method to systems with many input factors, Environ. Modell. Softw. 37 (2012), 103–109.

9.10 A. Robles, M.V. Ruano, J. Ribes, A. Seco, J. Ferrer, A filtration model applied to submerged anaerobic MBRs (SAnMBRs), J. Membr. Sci. 444(2013), 139–147.

9.11 A. Robles, M.V. Ruano, J. Ribes, A. Seco, J. Ferrer, Mathematical modelling of filtration in submerged anaerobic MBRs (SAnMBRs): long-term validation, J. Membr. Sci., DOI: 10.1016/j.memsci.2013.07.001.

9.12 A. Robles, M.V. Ruano, J. Ribes, J. Ferrer, Factors that affect the permeability of commercial hollow-fibre membranes in a submerged anaerobic MBR (HF-SAnMBR) system, Water Res. 47 (2013), 1277–1288.

9.13 American Public Health Association/American Water Works Association/Water Environmental Federation, Standard methods for the Examination of Water and Wastewater, 21st edition, Washington DC, USA, 2005.

9.14 T.V. Bugge, M.K. Jørgensen, M.L. Christensen, K. Keiding, Modeling cake buildup under TMP-step filtration in a membrane bioreactor: Cake compressibility is significant, Water Res. 46 (2012), 4330–4338.

9.15 M.K. Jørgensen, T.V. Bugge, M.L. Christensen, K. Keiding, Modeling approach to determine cake buildup and compression in a high-shear membrane bioreactor, J. Membr. Sci. 409/410 (2012), 335–345.

9.16 M. Sarioglu, G. Insel, D. Orhon, Dynamic in-series resistance modeling and analysis of a submerged membrane bioreactor using a novel filtration mode, Desalination 285 (2012), 285–294.

9.17 A. Drews, Membrane fouling in membrane bioreactors – Characterisation, contradictions, cause and cures, J. Membr. Sci. 363 (2010), 1–28.

9.18 J.B. Copp, Development of standardised influent files for the evaluation of activated sludge control strategies, IAWQ Scientific and Technical Report Task Group: Respirometry in Control of the Activated Sludge Process – internal report, 1999.

9.19 A. Robles, M.V. Ruano, J. Ribes, J. Ferrer, Advanced control system for optimal filtration in submerged anaerobic MBRs (SAnMBRs), J. Membr. Sci. 430 (2013), 330–341.

9.20 G. Sin, KV. Gernaey, Improving the Morris method for sensitivity analysis by scaling the elementary effects, In: proceedings of the 19th European Symposium on Computer Aided Process Engineering (ESCAPE 19), Elsevier (2009), 925–930.

9.21 A. Saltelli, S. Tarantola, F. Campolongo, M. Ratto, Sensitivity analysis in practice: a guide to assessing scientific models, Chicester: Wiley (2004).

9.22 T.F. Coleman, Y. Li, An interior, trust region approach for nonlinear minimization subject to bounds. SIAM J. Optim. 6 (1996), 418–445.

9.23 F. Campolongo, A. Saltelli, J. Cariboni, From screening to quantitative sensitivity analysis. A unified approach, Comput. Phys. Commun. 182 (2011), 978–988.

9.24 M.V. Ruano, J. Ribes, J. Ferrer, G. Sin, Application of the Morris method for screening the influential parameters of fuzzy controllers applied to WWTPs. Wat. Scien. Tech. 63 (2011), 2199–2206.

9.25 R. Cropp, R. Braddock, The New Morris method: an efficient second-order screening method. Reliab. Eng. Syst. Safe., 78 (2002), 77–83.

9.26 A. Robles, M.V. Ruano, F. García-Usach, J. Ferrer, Sub-critical filtration conditions of commercial hollow-fibre membranes in a submerged anaerobic MBR (HF-SAnMBR) system: The effect of gas sparging intensity, Bioresour. Technol. 114 (2012) 247–254.

CHAPTER 10:

Advanced control system for optimal filtration in submerged anaerobic MBRs (SAnMBRs)

Abstract

The main aim of this study was to develop an advanced controller to optimise filtration in submerged anaerobic MBRs (SAnMBRs). The proposed controller was developed, calibrated and validated in a SAnMBR demonstration plant fitted with industrial-scale hollow-fibre membranes with variable influent flow and load. This 2-layer control system is designed for membranes operating sub-critically and features a lower layer (on/off and PID controllers) and an upper layer (knowledge-based controller). The upper layer consists of a MIMO (multiple-input-multiple-output) control structure that regulates the gas sparging for membrane scouring and the frequency of physical cleaning (ventilation and back flushing). The filtration process is monitored by measuring the fouling rate on-line. This controller demonstrated its ability to keep fouling rates low (close to 0 mbar min^{-1}) by applying sustainable gas sparging intensities (approx. 0.23 Nm^3 h^{-1} m^{-2}). It also reduced the downtimes needed for ventilation and back-flushing (less than 2% of operating time).

Keywords

Advanced control system; energy savings; industrial-scale hollow-fibre membranes; knowledge-based controller; submerged anaerobic MBR.

Highlights

An advanced control system for optimal filtration in SAnMBRs has been developed.
The controller was validated using industrial-scale hollow-fibre membranes.
The gas sparging intensity and the frequency of physical cleaning were regulated.
The fouling rate was low by applying sustainable SGDm (approx. 0.23 Nm^3 h^{-1} m^{-2}).
Low downtimes for physical cleaning (less than 2% of operating time) were achieved.

A. Robles, M.V. Ruano, J. Ribes, J. Ferrer
Advanced control system for optimal filtration in submerged anaerobic MBRs (SAnMBRs)
J. Membrane Sci. 430 (2013), 330 – 341.

10.1 Chapter nomenclature

Alk	*carbonate alkalinity*
AnR	*anaerobic reactor*
B	*back-flush*
B-1	*biogas recycling blower*
BRF	*biogas recycling flow*
$\boldsymbol{BRF_{MAX}}$	*maximum BRF*
$\boldsymbol{BRF_{MIN}}$	*minimum BRF*
$\boldsymbol{BRF_{SP}}$	*BRF set point*
$\boldsymbol{BRF_{SP}\ (t)}$	BRF_{SP} *at sample time*
$\boldsymbol{BRF_{SP}\ (t - CT)}$	BRF_{SP} *at previous sample time*
$\boldsymbol{\Delta BRF_{SP}}$	*modification in the BRF set point*
c	*centre of Gaussian membership function*
CI	*confidence interval*
CIP	*clean in place*
COD	*chemical oxygen demand*
$\boldsymbol{COD_S}$	*soluble COD*
$\boldsymbol{COD_T}$	*total COD*
CT	*control time*
DV	*degasification vessel*
$\boldsymbol{eFR_C}$	*error in* FR_C
$\boldsymbol{\Delta eFR_C}$	*difference in* FR_C
ΔeFRC (t)	*difference in fouling rate error at control time*
$\boldsymbol{\Sigma eFR_C}$	*accumulated error in* FR_C
ΣeFRC (t)	*accumulated error in fouling rate at control time.*
ΣeFRC (t – CT)	*accumulated error in fouling rate at previous control time*
EPS	*extracellular polymeric substances*
FC	*frequency converter*
FC-P11	*rotating speed of permeate pump*
FC-P12	*rotating speed of sludge recycling pump*
FIT	*flow indicator transmitters*
FIT-P11	*permeate flow*
$\boldsymbol{FIT\text{- }P11_{SP}}$	*permeate flow set point*
FIT-P12	*sludge flow entering membrane tank*
F-R	*filtration-relaxation*
FR	*fouling rate*
$\boldsymbol{FR_C}$	*FR related to cake-layer formation*

$\boldsymbol{FR_C\,(t)}$	*FR_C at sample time*
$\boldsymbol{FR_{C\_SP}}$	*FR_C set point*
$\boldsymbol{FR_{M'}}$	*intrinsic variation of FR due to change in J_{20}*
$\boldsymbol{FR_{M'}\,(t)}$	*$FR_{M'}$ at sample time*
$\boldsymbol{FR_T}$	*measured FR*
$\boldsymbol{FR_T\,(t)}$	*measured FR at sample time*
FS	*flat sheet*
HF	*hollow fibre*
HN	*high negative*
HP	*high positive*
HRT	*hydraulic retention time*
$\boldsymbol{HS^-}$	*total sulphide expressed as HS^-*
$\boldsymbol{J}$	*transmembrane flux*
$\boldsymbol{J_{20}}$	*20 ºC-normalised J*
$\Delta\boldsymbol{J_{20}}$	*change in J_{20}*
$\left(\frac{\partial J_{20}}{\partial t}\right)$	*decrease in J_{20} between two sample times*
$\left(\frac{\partial J_{20}}{\partial t}\right)_{MAX}$	*maximum decrease in J_{20}*
$\boldsymbol{J_{20,MIN}}$	*minimum J_{20}*
$\boldsymbol{J_{20,MIN}\,(t)}$	*$J_{20,MIN}$ at sample time*
$\boldsymbol{J_{20\ SP}}$	*J_{20} set point*
$\boldsymbol{J_{20\ SP}\,(t)}$	*$J_{20\ SP}$ at sample time*
$\boldsymbol{\%J_{20\ SP}}$	*maximum decrease in J_{20} referred to the established $J_{20\ SP}$*
$\boldsymbol{\%J_{20\ SP}\,(t)}$	*$\%J_{20\ SP}$ at sample time*
$\boldsymbol{J_C}$	*critical flux*
K	*permeability*
$\boldsymbol{K_{20}}$	*20 ºC-normalised K*
$\boldsymbol{\%K_{20}}$	*maximum decrease in highest K_{20} recorded during filtration*
$\boldsymbol{K_{20,MAX,BF}}$	*maximum back-flushing K_{20}*
$\boldsymbol{K_{20,MAX,F}}$	*maximum K_{20} during filtration*
$\boldsymbol{K_{20,MIN}}$	*minimum K_{20}*
$\boldsymbol{K_C}$	*controller gain*
$\boldsymbol{K_{M',20}}$	*intrinsic membrane permeability*
LMH	*litre per square metre of membrane per hour*
LN	*low negative*
LP	*low positive*
MBR	*membrane bioreactor*
MIMO	*multiple-input-multiple-output*

MLTS	*mixed liquor total solids*
$MLTS_{AnR}$	*MLTS in AnR (MLTS entering MT)*
$MLTS_{MT}$	*MLTS in MT*
$MLTS_{MT,SP}$	*set point of MLTS returning to AnR*
MT	*membrane tank*
N	*negative*
NH_4-N	*ammonium measured as nitrogen*
OLR	*organic loading rate*
OPC	*OLE for process control*
P	*positive*
P-11	*permeate pump*
P-12	*sludge recycling pump*
PID	*proportional-integrative-derivative*
PIT	*pressure indicator transmitter*
PLC	*programmable logic controller*
PO_4-P	*orthophosphate measured as phosphorous*
R_C	*cake-layer resistance*
R_I	*irreversible layer resistance*
R_M	*membrane resistance*
R_T	*total membrane resistance*
SAnMBR	*submerged anaerobic MBR*
SCADA	*supervisory control and data acquisition*
SD	*standard deviation*
SGD_m	*specific gas demand per membrane area*
SGD_p	*specific gas demand per permeate volume*
SISO	*single-input-single-output*
SIT	*solids concentration indicator transmitter*
SMP	*soluble microbiological products*
SO_4-S	*sulphate measured as sulphur*
SRF	*sludge recycling flow*
SRF_{MAX}	*maximum SRF*
SRF_{MIN}	*minimum SRF*
SRF_{SP}	*SRF set point*
SRT	*sludge retention time*
ST	*sample time*
T	*temperature*
TS	*total solids*
TSS	*total suspended solids*

$t_{F,MAX}$	*maximum filtering time*
Δt_{FR}	*time interval used in FR calculations*
TMP	*transmembrane pressure*
TMP (t)	*TMP at sample time*
TMP (t - Δt_{FR})	*TMP at start of Δt_{FR}*
Δ***TMP***	*change in TMP*
$\Delta TMP_{M'}$	*change in TMP associated with $K_{M',20}$ due to a change in J_{20}*
$\Delta TMP_{M'}$ **(t)**	*$\Delta TMP_{M'}$ at sample time*
TMP_{MAX}	*maximum TMP*
u	*control action*
V	*ventilation*
VFA	*volatile fatty acids*
VS	*volatile solids*
VS	*volatile suspended solids*
WWTP	*wastewater treatment plant*
Z	*zero*
z_{MIN}	*minimum quantity of filtration phase data*
σ	*amplitude of Gaussian membership function*
δ	*modifying algebraic factor*
η	*permeate viscosity*
$\mu(p)$	*degree of membership of input variable p*
t_I	*constant of integrative time*
t_D	*constant of derivative time*

10.2 Introduction

In recent years there has been increased interest in the feasibility of using SAnMBRs to treat municipal wastewater at ambient temperatures, focussing not only on the main advantages of MBRs (*i.e.* clarified and partially disinfected effluent; smaller environmental footprint of WWTPs) but also on the greater sustainability of anaerobic rather than aerobic processes: low sludge production due to the low anaerobic biomass yield, low energy consumption because no aeration is needed, and biogas generation that can be used as an energy resource.

MBRs usually operate at high MLTS levels which contribute to membrane fouling: one of the main handicaps of membranes [10.1]. Fouling reduces K and increases operating and maintenance costs [10.2]. In this respect, MBR installations still consume more energy than conventional activated sludge systems, calling for further study into economical and sustainability considerations [10.3].

Therefore, one key operating challenge of SAnMBR technology is how membrane performance can be optimised whilst minimising membrane fouling – in particular the irreversible/permanent component that cannot be eliminated by chemical cleaning and ultimately determines the membrane lifespan [10.4; 10.5; 10.6].

One such fouling control strategy consists of operating membranes at sub-critical filtration conditions [10.7] delimited by J_C [10.8; 10.9]. On the other hand, in order to minimise membrane fouling, a suitable physical and chemical membrane cleaning protocol must be applied to given filtration conditions. Gas sparging intensity, usually measured as SGD_m or SGD_p, is one of the factors that affects J_C most (at a specific MLTS level). The gas sparging intensity in each operating range must, therefore, be optimised in order to minimise membrane fouling and maximise energy savings in SAnMBR systems. It is important to emphasise that aeration can account for up to 50 – 75% of all the energy consumed by aerobic MBR technology [10.10]. Furthermore, minimising total operating downtime whilst using other physical cleaning protocols (relaxation and back-flushing) is a major challenge that must be solved if SAnMBR technology is to become economically feasible.

Several studies published recently have theoretically analysed and experimentally validated the energy savings of different types of advanced control (mainly model-based or knowledge-based) in aerobic MBR technology.

One of the model-based control systems, Drews *et al*. [10.11; 10.12], aimed to improve the efficiency of the filtration process in MBR technology by applying mathematical models to enable appropriate action to increase permeability over time. Busch *et al*. [10.13] proposed a model-based run-to-run (or run-by-run, batch-to-batch) process control system that optimised the adjusted variables (filtration and back-flushing stages) after each filtration cycle. However, the main drawback of such approaches is that the complexity of the mechanisms involved makes it impossible to describe fouling exactly or build a deterministic filtration model [10.14]. Due to the highly non-linear relations found throughout the physical separation processes and the large number of filtration mechanisms, the results achieved by model-based controllers are only acceptable when the process dynamics are bounded by a well-defined linear zone.

A variety of knowledge-based control laws, on the other hand, have been widely implemented in wastewater treatment in recent decades and been successful in several MBR applications. Huyskens *et al*. [10.3] validated an advanced knowledge-based control system that evaluated the reversible fouling propensity by using MBR-VITO (a specific on-line fouling measuring tool) [10.15]; Monclús *et al*.

[10.16] developed and validated a knowledge-based control module for optimising MBR start-up procedures and minimising fouling; and Ferrero *et al*. [10.17, 10.18, 10.19] developed a knowledge-based control system to supervise filtration in aerobic MBRs, achieving considerable energy savings (up to 21%) in membrane scouring.

Several simple operating strategies to control membrane fouling instead of advanced controllers have been experimentally validated. Jeison and van Lier [10.20] developed an on-line cake-layer management protocol that monitored critical flux constantly and prevented excessive cake-layer from building up on the membrane surface; Smith *et al*. [10.21] developed a control system to optimise back-flushing which reduced the water needed for back-flushing by up to 40%; Vargas *et al*. [10.22] established a control algorithm for fouling prevention which regulated back-flushing by constantly measuring TMP and J; and Park *et al*. [10.23] studied how membrane fouling could be reduced by successively increasing and decreasing the gas sparging intensities, and recorded the effectiveness in reducing membrane fouling.

Nevertheless, further study is required into control strategies of this type (designed to save energy in SAnMBR technology on an industrial scale) due to the lack of knowledge about fouling in anaerobic MBRs. In this respect, knowledge-based controllers may be a powerful tool for filtration control in SAnMBR technology because they are easily applied to non-linear processes. Fuzzy-logic controllers [10.24] in particular can optimise a variety of processes in dynamic operating and loading conditions by applying valuable expert knowledge [10.25; 10.26; 10.27]. In addition, control strategies of this type do not require a large amount of data and/or a rigorous mathematical model, and also allow MIMO control schemes to be developed.

To gain more insight into the optimisation of a SAnMBR system on an industrial scale, we designed a new control approach to minimise energy consumption during sub-critical filtration in a SAnMBR demonstration plant. To obtain representative results that could be extrapolated to full-scale plants, the SAnMBR system featuring industrial HF membrane units was operated using effluent from the pre-treatment of the Carraixet WWTP (Valencia, Spain). The main aim was to design a competitive and feasible control system capable of enhancing filtration in industrial-scale SAnMBR systems with minimum operating costs. This advanced control system was developed taking advantage of the industrially feasible on-line sensors now available for monitoring key physical variables in filtration processes (*i.e.* pressure, flow and total solids).

10.3 Materials and methods

10.3.1 SAnMBR plant description

Figure 10.1 shows a simplified lay-out of the SAnMBR plant used in this study including the main instrumentation and controllers. As previously introduced, the plant consists of an anaerobic reactor with a total volume of 1.3 m^3 connected to two membrane tanks each with a total volume of 0.8 m^3. Each membrane tank (MT) has one industrial HF ultrafiltration membrane unit (PURON®, Koch Membrane Systems (PUR-PSH31) with 0.05 μm pores). Each module has a total membrane surface of 30 m^2. To recover the bubbles of biogas in the permeate leaving the membrane tank, two degasification vessels (DV) were installed: one between each MT and the respective vacuum pump. The funnel-shaped section of conduit makes the biogas accumulate at the top of the DV. The resulting permeate is stored in the CIP tank. The two parallel membrane tanks make plant operating very flexible because it can work with one membrane tank or the other or both. Moreover, each tank enables the resulting permeate to be constantly recycled back into the anaerobic reactor, enabling different transmembrane fluxes to be tested without affecting HRT. The filtration results given in this paper are experimental data obtained from a membrane tank constantly recycling permeate back into the system. The HRTs tested to assess biological performances were, therefore, obtained from another membrane tank running in parallel.

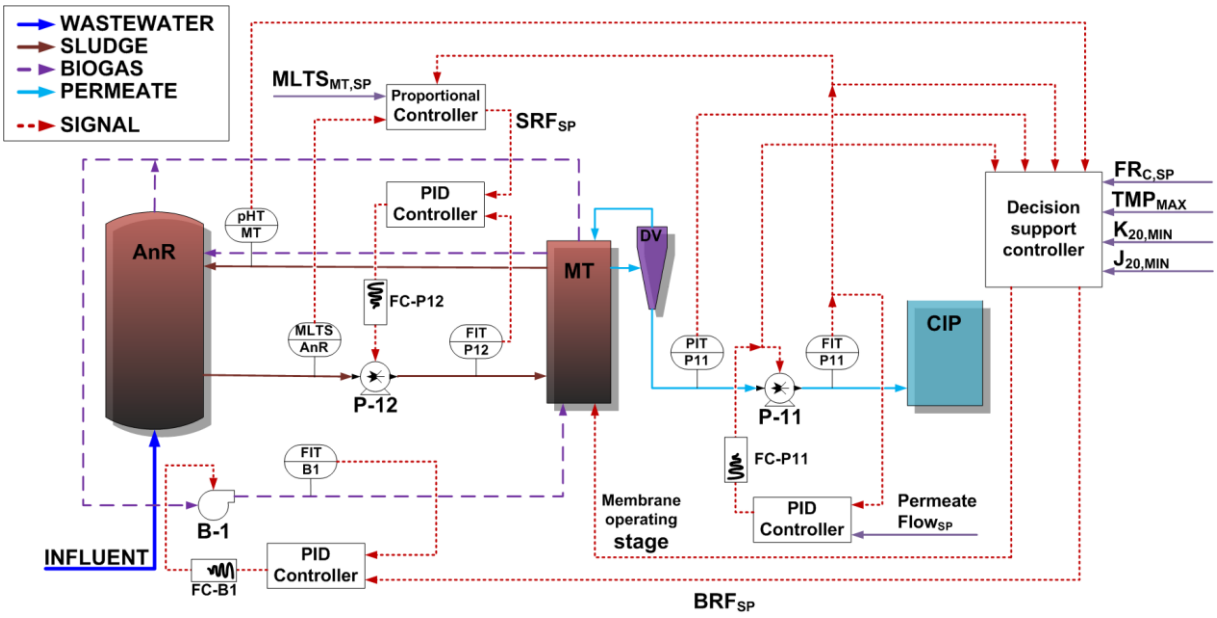

Figure 10.1 Simplified lay-out of the SAnMBR demonstration plant where the control system was designed.

Aspects of membrane operation taken into account included not only the classic membrane operating stages (filtration, relaxation and back-flushing) but also ventilation. In the ventilation stage, permeate is pumped into the membrane tank through the degasification vessel instead of through the membrane. The aim of ventilation is to recover the biogas that accumulates in the degasification vessel. Thus, in terms of membrane cleaning, ventilation acts as a relaxation since no transmembrane flux is applied whilst maintaining a given gas sparging intensity.

For further details about this SAnMBR system, see Chapter 2 or Giménez *et al*. [10.28].

10.3.2 Monitoring system description

Many on-line sensors and automatic devices were installed in order to automate and control plant operating and provide on-line information about the state of the process (see Figure 10.1). All instrumentation is labelled according to the name of the tank or equipment (*i.e.* pump or blower) where the sensor is installed. The main features of the installed equipment are: on-line availability and industrial feasibility, low-cost, corrosion resistance, long lifespan, and low and easy maintenance. The instrumentation is connected to a network system featuring several transmitters, a PLC and a PC to perform multi-parameter control and data acquisition. Both the operating data logging and the plant control are carried out by a SCADA system installed in the PC, which centralises all the signals from the sensors and actuators installed in the plant. In addition, the SCADA is linked to an OPC system that enables communication with external dedicated applications featuring upper-layer controllers.

The group of on-line sensors used in this study, shown in Figure 10.1, consists of the following: one solids concentration indicator transmitter (Hach Lange model TSS EX1 sc), $MLTS_{AnR}$, located in the anaerobic reactor; two flow indicator transmitters (Endress+Hauser model Proline Promag 50), FIT-P11 and FIT-P12, *i.e.* one for the permeate pump (JUROP VL02 NBR, P-11) and another for the mixed liquor feed pump (CompAir NEMO, P-12); one flow indicator transmitter (Iberfluid model VORTEX 84F), FIT-B1, for the membrane tank blower (FPZ 30HD, B-1); one pH-temperature sensor (Endress+Hauser model Liquiline M pH-ORP CM42), pHT-MT, located in the membrane tank; and one liquid pressure indicator transmitter (Endress+Hauser model Cerabar M PMC41), PIT-P11, to monitor the TMP. The group of actuators used in this study consists of a group of on/off flow-direction valves to control the different membrane operating stages (filtration, back-flushing, ventilation…), and three frequency converters (Micromaster Siemens 420) FC-P11, FC-P12 and FC-B1 to control the rotating speed of the permeate pump (P-11), the mixed liquor feed pump (P-12) and the membrane tank blower (B-1), respectively.

The composition of the biogas (CH_4, CO_2, H_2 and H_2S) was measured online using an X-STREAM enhanced analyser (EMERSON PROCESS Analytical GmbH). This equipment combines four measuring channels: two non-dispersive infrared channels for measuring CH_4 and CO_2; one thermal conductivity channel for measuring H_2; and one non-dispersive ultraviolet channel for measuring H_2S.

10.3.3 Sampling and analytical monitoring

The performance of the biological treatment was assessed by taking 24-hour composite samples of influent and effluent plus grab samples of biogas and anaerobic sludge once a day. The following parameters of influent, effluent and anaerobic sludge were analysed: TS, VS, TSS, VSS, VFA, Alk, SO_4-S, total sulphide (expressed as HS^-), nutrients (NH_4-N and PO_4-P), and COD_T and COD_S.

Levels of solids, COD, sulphate, total sulphide and nutrients were determined by Standard Methods [10.29], and Alk and VFA levels by titration according to the method proposed by WRC [10.30].

10.3.4 Operating conditions

The SAnMBR plant in this study was fed with effluent from the pre-treatment phase of a full-scale urban WWTP (screening, degritter and grease removal). Table 10.1 shows the average properties of this influent wastewater. This highlights its significant sulphate content in comparison with typical domestic wastewater, and also the wide variation in influent loads as shown by the high standard deviation of each parameter. The uncertainty of each value takes into account both the SD of the different samples analysed and the variation coefficient of the analytical methods. Table 10.1 also shows the median, minimum and maximum values and 95 % CI.

During the 3-year experimental period, the plant was operated continuously under a variety of operating conditions to study the biological process performance: SRT ranged from 20 to 70 days; HRT ranged from 5 to 24 hours, resulting in OLR of 0.5 to 2 kgCOD m^{-3} d^{-1}; and temperatures, from 14 to 33ºC.

Table 10.1 Average influent wastewater properties.

Parameter	Unit	Mean	SD	CI (95%)	Median	(	min	-	max	)
TSS	mgTSS L^{-1}	323	176	16	286	(	44	-	1060	)
VSS	%	80.4	7.9	0.7	81.4	(	44.1	-	100.0	)
NH_4-N	mgN L^{-1}	32.2	8.9	0.9	32	(	4.1	-	69.9	)
PO_4-P	mgP L^{-1}	4.0	1.6	0.2	3.89	(	0.58	-	13.32	)
SO_4-S	mgS L^{-1}	105	13	2	103	(	70	-	139	)
Total COD	mgCOD L^{-1}	585	253	43	537	(	211	-	1472	)
Soluble COD	mgCOD L^{-1}	80	20	4	77	(	32	-	132	)
pH	un. pH	7.7	0.2	0.02	7.7	(	6.8	-	8.2	)
Alk	mg$CaCO_3$ L^{-1}	332	58	5	331	(	139	-	707	)
VFA	mgCOD L^{-1}	7.9	10.5	0.9	6.3	(	0	-	198	)

10.4 Advanced control system description

The proposed controller aims to optimise the filtration process in a SAnMBR system, maintaining sub-critical filtration conditions and minimising operating costs. In this respect, this control system aims to operate membranes at fouling rates close to zero by modifying not only the gas sparging intensity for membrane scouring in the membrane tank, but also the starting time and frequency of both ventilation and back-flushing.

As Figure 10.1 shows, the proposed control system consists of a combination of 5 lower-layer controllers (3 PID, 1 proportional and 1 on/off) and 1 upper-layer controller (decision-support controller). The lower-layer controllers are based on classic on-off and feedback PID (proportional-integral-derivative) controllers consisting of SISO control structures. The upper-layer controller allows the different set points for the controlled variables in the lower-layer controllers to be established according to the data gathered from the different sensors installed in the plant. The upper-layer controller is based on knowledge-based theory and consists of a MIMO control structure.

10.4.1 Lower-layer controllers

The group of lower-layer controllers used in this study, shown in Figure 10.1, consists of the following: three PID controllers to adjust the rotating speed of the sludge recycling pump (P-12), the permeate pump (P-11) and the biogas recycling blower (B-1) by the corresponding frequency

converter (FC-P12, FC-P11 and FC-B1 respectively) in order to keep the corresponding flow close to its set point value; one on-off controller that determines the membrane operating stage by changing both the position of the corresponding on-off valves and the flux direction of the permeate pump; and one proportional controller that determines the SRF_{SP} through the membrane tank depending on the $FIT\text{-}P11_{SP}$ and the MLTS in the anaerobic reactor (measured by $MLTS_{AnR}$). The PID controllers were fine-tuned by trial and error.

The aim of the proportional controller is to reduce the energy consumption of both sludge and permeate pumping. When the anaerobic reactor is operated at high MLTS levels, the SRF must be high enough not only to maintain suitable levels of MLTS in the membrane tank, but also to minimise the energy consumed by permeation. It must be emphasised that, depending on the sludge concentration factor (the ratio between the sludge flow entering the membrane tank and the net permeate flow), the MLTS in the membrane tank could reach prohibitive levels. It must also be said that MLTS is a key operating factor as regards membrane permeability [10.31] which therefore affects the energy required for permeate pumping. Nonetheless, SRF must be minimised in order to maximise energy savings since sludge pumping energy accounts for 15 – 20% of all the energy consumed by aerobic MBR technology [10.10]. Hence, it is advisable for SRF to be regulated in order to optimise the economic feasibility of full-scale SAnMBR systems. Therefore, the proposed advanced control system features a control strategy based on proportional action taking into account both the MLTS entering the membrane tank and the permeate flux.

This proportional controller calculates the SRF_{SP} by applying a simple mass balance (MLTS mass balance) to the membrane tank (see Eq. 10.1). The left and right sides of Eq. 10.1 are the input and output terms of the mass balance, respectively. In this mass balance, the effluent MLTS concentration is assumed to be zero (see second term on the right side of Eq. 10.11). Accumulation and generation terms are not considered.

$$MLTS_{AnR} \cdot SRF = MLTS_{MT} \cdot (SRF - FITP11) + 0 \cdot FITP11 \qquad \textbf{Eq. 10.1}$$

Hence Eq. 10.1 can be used to calculate the SRF_{SP} theoretically required to maintain a given $MLTS_{MT,SP}$ as a function of the recorded values of $MLTS_{AnR}$ and FIT-P11 (see Eq. 10.2).

$$SRF_{SP} = \frac{FITP11 \cdot MLTS_{MT,SP}}{MLTS_{MT,SP} - MLTSAnR} \qquad \textbf{Eq. 10.2}$$

SRF_{SP} was only modified within a pre-defined range delimited by the minimum and maximum flows provided by the sludge recycling pump: SRF_{MIN} (1.0 m^3 h^{-1}) and SRF_{MAX} (2.7 m^3 h^{-1}), respectively.

10.4.2 Upper-layer controller

The flow chart of the proposed upper-layer controller (Figure 10.2) shows how this upper-layer controller is divided in three subsections: (i) initialisation where the control variables are calculated; (ii) a preliminary group of knowledge-based rules; and (iii) a fuzzy-logic controller. As mentioned before, this control system aims to operate membranes sub-critically, keeping the fouling rate close to zero. Basically, the fouling rate is controlled by adjusting the BRF through the membrane tank by means of the fuzzy-logic controller, and the membrane operating stage (filtration, ventilation or back-flushing) by the preliminary knowledge-based rules. In addition to the FR, the control variables of this MIMO control structure are TMP, K and J.

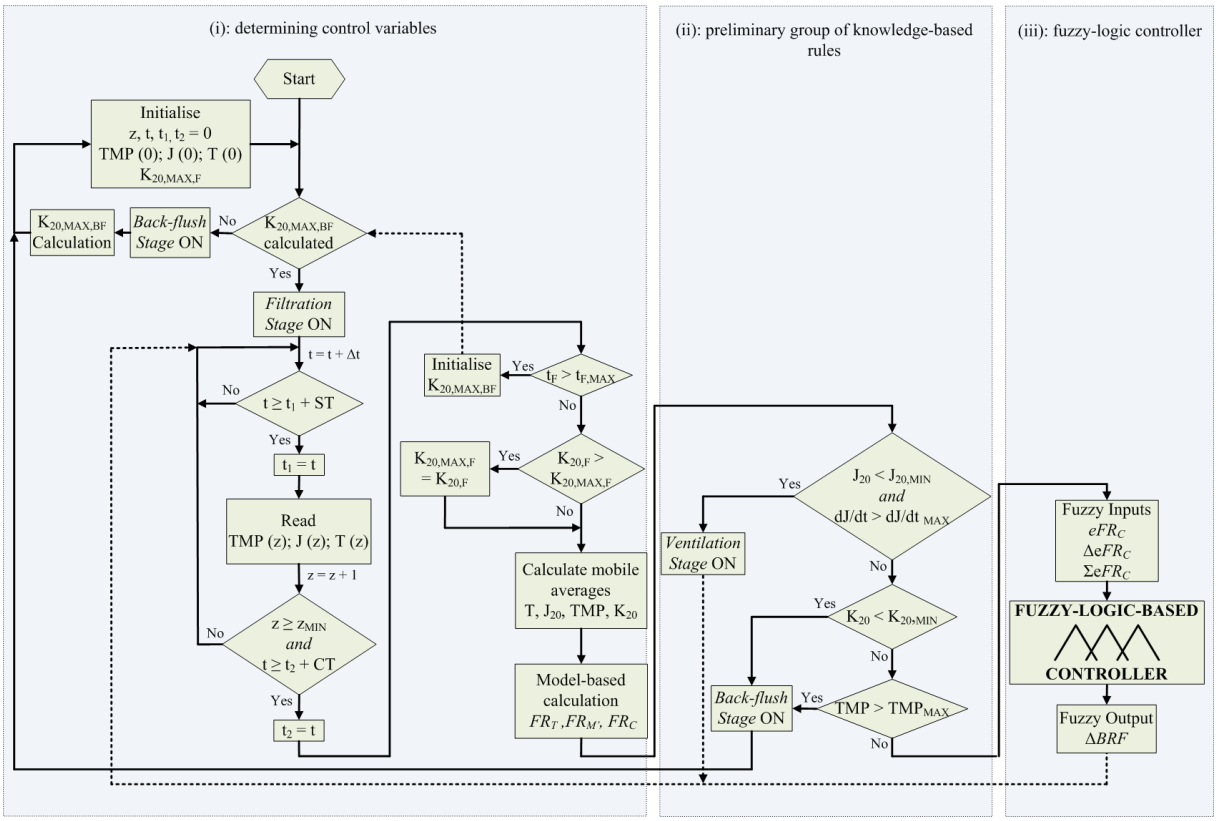

Figure 10.2 Flow chart of the proposed filtration control system.

10.4.2.1 Determining the control variables

Control variables TMP and J were calculated by a 15 second moving average in order to filter the typical signal noise from the corresponding sensors (ST set to 5 seconds). Therefore, a minimum quantity of filtration phase data (z_{MIN}) was needed to calculate the control parameter. The J_{20} was calculated using Eq. 10.3 in order to reflect the dependence of η on T, and the K_{20} was calculated using a simple filtration model (Eq. 10.4) that takes into account the TMP and J_{20} data monitored on-line. In this classic filtration model, R_T was theoretically represented by R_M, R_I, and R_C.

$$J_{20} = J_T \cdot e^{-0.0239\,(T-20)} \qquad \textbf{Eq. 10.3}$$

$$K_{20} = \frac{1}{\eta \cdot R_T} = \frac{1}{\eta \cdot (R_M + R_I + R_C)} = \frac{J_{20}}{TMP} \qquad \textbf{Eq. 10.4}$$

As regards the control variable, *i.e.* the fouling rate, several techniques to monitor membrane fouling are described in literature. In most of them, however, membrane fouling cannot be measured on-line because they are too invasive and require subsequent chemical cleaning, or require new instrumentation which increases their operating costs [10.32]. In our study membrane fouling was measured on-line as the change in TMP over time (Eq. 10.5).

$$FR_T\,(t) = \frac{\Delta \mathrm{TMP}}{\Delta t} = \frac{TMP\,(t) - TMP\,(t - \Delta t_{FR})}{\Delta t_{FR}} \qquad \textbf{Eq. 10.5}$$

From Eq. 10.4 it can be assumed that any change in J_{20} (ΔJ_{20}) results in a proportional change in TMP (ΔTMP) when treating clean water. In this case, $K_{M',20}$ can be assumed to be constant and proportional to the sum of both the membrane and irreversible fouling resistances in series (see Eq. 10.6). Membrane and irreversible fouling resistances can be assumed to be constant because the tortuosity of both the membrane and the irreversible fouling layer is not expected to increase due to pressure in low-pressure filtration processes.

$$K_{M',20} = \frac{1}{\eta \cdot (R_M + R_I)} = \frac{\Delta J_{20}}{\Delta TMP} \qquad \textbf{Eq. 10.6}$$

On the basis of this assumption, the fouling rate calculated by Eq. 10.5 was not adopted as the control variable of the control system. The control variable adopted was FR_C calculated by Eq. 10.7. The

intrinsic variation of the fouling rate caused by a change in J_{20} was not considered in order to minimise the total energy consumption since this fouling rate component cannot be remedied/minimised by increasing BRF. FR_C variable is obtained from the total measured fouling rate (Eq. 10.5) and the intrinsic variation of the fouling rate due to a change in J_{20} ($FR_{M'}$, Eq. 10.8).

$$FR_C\,(t) = FR_T\,(t) - FR_{M'}\,(t) \qquad \textbf{Eq. 10.7}$$

$$FR_{M'}\,(t) = \frac{\Delta TMP_{M'}\,(t)}{\Delta t_{FR}} \qquad \textbf{Eq. 10.8}$$

In order to calculate $\Delta TMP_{M'}$ using Eq. 10.6, $K_{M',20}$ must be estimated. This is done by using the simple filtration model given in Eq. 10.4 during back-flushing, determining the maximum back-flushing permeability, *i.e.* $K_{20,MAX,BF}$ which is considered to be the maximum filtering permeability of the membrane under study. This assumption is based on the fact that after a significant back-flushing period, cake layer resistance is negligible, and the resulting membrane resistance is the sum of both membrane and irreversible fouling resistances. This permeability is therefore calculated when the TMP during back-flushing remains stable over time at a given J. This calculation is done once a day when the maximum filtering time ($t_{F,MAX}$) is reached (see Figure 10.2). This maximum filtering time (set to 1 day in this study) is defined in order to apply at least one back-flush per day, when the filtration stage is not interrupted by other conditions defined in the control system.

Calculating maximum back-flushing permeability is an useful way of monitoring the reduction in permeability during long-term membrane operation and deciding the right time to conduct chemical membrane cleaning or recovery.

In addition to $K_{20,MAX,BF}$, $K_{20,MAX,F}$ was another input variable for the preliminary knowledge-based rules. This variable was defined as the maximum K_{20} calculated by Eq. 10.4 during each filtration stage.

Thus, as Figure 10.2 shows, the first subsection of the flow chart (i) represents all the calculations needed to obtain the final values of the control variables at each *CT*: FR_C, K_{20}, TMP and J_{20}. In this study, *CT* was set to 20 seconds.

10.4.2.2 Preliminary knowledge-based rules

Similar to Vargas *et al*. [10.22], different knowledge-based rules have been included in the proposed advanced control system. The aim of these control rules was to decide when to initiate both ventilation (also acting as relaxation) and back-flushing. An additional rule designed to determine the right time for the chemical cleaning or recovery of membranes was also taken into account.

As Figure 10.2 shows (subsection ii), at each time interval between two control actions (*CT*), the control system applies the different knowledge-based rules to decide whether or not to start ventilation or back-flushing.

10.4.2.3 Ventilation initiation

As mentioned above, the aim of ventilation is to recover the biogas that accumulates in the degasification vessel thus reducing the amount of methane expelled with the effluent. For this reason, a degasification vessel was installed in the membrane tank. This degasification vessel accumulates the biogas released from the extracted permeate.

Ventilation takes place when the system detects that some of the biogas accumulated in the degasification vessel is extracted with the effluent during filtration. This is revealed by the rotating speed of the permeate pump suddenly increasing to its maximum operating value without reaching the permeate flow set point. Ventilation is activated at this stage in order to recover the biogas remaining in the degasification vessel by recycling it into the membrane tank. As mentioned before, ventilation causes membrane permeability to fall to previous values because it acts as relaxation in terms of membrane physical cleaning. The corresponding control action is expressed by Rule 1.

$$IF\ \left[J_{20}\ (t) < J_{20,MIN}\ (t)\right]\ AND\ \left[\left(\frac{\partial\ J_{20}}{\partial t}\right) > \left(\frac{\partial\ J_{20}}{\partial t}\right)_{MAX}\right] THEN\ [Ventilation\ stage] \qquad \text{(Rule 1)}$$

$J_{20,MIN}\ (t)$ is calculated by Eq. 10.9.

$$J_{20,MIN}\ (t) = \%J_{20_{SP}} \cdot J_{20_{SP}}\ (t) \qquad \textbf{Eq. 10.9}$$

$\%J_{20\ SP}\ (t)$ was set to 95% in our study.

10.4.2.3.1 Back-flushing initiation

Back-flushing minimises the long-term build-up of a reversible cake layer on the membrane surface. Two different rules for back-flushing initiation were defined in the proposed advanced control system: (1) when membrane permeability is below a minimum value (Rule 2); and (2) when a maximum TMP value (Rule 3) is reached.

$IF\ [K_{20}\ (t) <\ K_{20,MIN}\ ]\ THEN\ [Back - flushing\ stage]$ (Rule 2)

$K_{20,MIN}$ is calculated by Eq. 10.10.

$$K_{20,MIN} = \%K_{20} \cdot\ K_{20,MAX,F} \quad \textbf{Eq. 10.10}$$

$\%K_{20}$ was set to 65% in our study.

$IF\ [TMP\ (t) >\ TMP_{MAX}\ ]\ THEN\ [back - flushing\ stage]$ (Rule 3)

TMP_{MAX} was set to 450 mbar in our study.

10.4.2.4 Fuzzy-logic controller

The fuzzy-logic controller determines the variation in the set point of the biogas recycling flow (*i.e.* ΔBRF_{SP}) on the basis of three inputs obtained from the estimated fouling rate caused by cake-layer formation, *i.e.* error (Eq. 10.11), accumulated error (Eq. 10.12) and error difference (Eq. 10.13). The structure of this controller is, therefore, a fuzzy version of the classical PID.

$$eFR_C\ (t) =\ FR_C\ (t) - FR_{C\_SP} \quad \textbf{Eq. 10.11}$$

$$\Sigma eFR_C\ (t) = \Sigma eFR_C\ (t - CT)\ + CT\ \cdot\ eFR_C\ (t) \quad \textbf{Eq. 10.12}$$

$$\Delta eFR_C\ (t)\ = eFR_C\ (t) - \delta\ \cdot\ eFR_C\ (t - CT) \quad \textbf{Eq. 10.13}$$

The fouling rate error difference variable calculated by Eq. 10.13 will be negative or positive depending on whether or not the fouling rate error tends to zero because this equation features a modifying algebraic factor (δ) which is defined in Eq. 10.14.

$$\delta = \frac{eFR_C\ (t)\ \cdot\ eFR_C\ (t - CT)}{|eFR_C\ (t)\ \cdot\ eFR_C\ (t - CT)|} \qquad \textbf{Eq. 10.14}$$

Although a classical PID controller could have been used, the fuzzy-logic based controller was preferred because of strong non-linear relations between the input and output of the filtering process (several factors affect membrane performance considerably). Fuzzy-logic controllers are suitable for systems which are extremely non-linear and also for processes that are too complex to be analysed using conventional quantitative techniques or when available sources of information are subjective, inexact or unreliable. Well-developed fuzzy logic controllers can generalise to a great extent and can easily be developed and fine-tuned by an experienced plant operator because fuzzy logic is much closer to human reasoning and natural language than traditional control algorithms.

10.4.2.5 Description of fuzzy-logic controller structure

The fuzzy-logic controller has five stages. In the first stage the input variables (eFR_C, ΔeFR_C and ΣeFR_C) are calculated from the estimated fouling rate due to cake-layer formation (see Eq. 10.11, Eq. 10.12 and Eq. 10.13). Once the input variables are calculated, in the *fuzzification* stage (stage 2) the input variables are converted into linguistic variables (fuzzy set) represented by membership functions. The proposed controller used Gaussian membership functions (see Eq. 10.15) because they produce smooth controller output. Three Gaussian membership functions were considered for each input: *N*, *Z* and *P*.

$$\mu(p) = exp\left(-\frac{(p-c)^2}{2\cdot\sigma^2}\right) \qquad \textbf{Eq. 10.15}$$

The output variable of the controller is ΔBRF_{SP}. In the *defuzzification* stage of this output variable, four singleton membership functions were defined as output linguistic variables: *HN*, *LN*, *LP* and *HP*.

In stage 3, the inference engine, a set of rules is applied to the fuzzy sets obtained in stage 2. Table 10.2 shows the inference rules defined for the proposed fuzzy-logic controller. As Table 10.2 shows, each inference rule consists of an *if-then* fuzzy implication. Each inference rule is built by the fuzzy intersection (*AND*) of two input fuzzy sets (*N, Z, P*) from the input variables (eFR_C, ΔeFR_C, ΣeFR_C). Each fuzzy intersection results in one fuzzy output set (*HN, LN, LP, HP*) for the output variable (ΔBRF_{SP}). The degree of membership (μ) of each input fuzzy set is given by the corresponding

Gaussian membership function in the range [0, 1]. When μ is zero, the corresponding rule is inactive and does not contribute to the output.

Because the proposed filtration control system is hierarchical, the priorities for applying Table 10.2 rules are different from those of the preliminary group of knowledge-based rules. The filtration control system prioritises the preliminary group of knowledge-based rules, so when a knowledge-based rule is initiated the controller is initialised and no fuzzy-logic controller action is applied (see Figure 10.2, subsection ii). Otherwise, when no knowledge-based rule is initiated, Table 10.2 rules are applied (see Figure 10.2, subsection iii).

Table 10.2 Inference rules of control system.

Inference Rules
1. If eFR_C is *P* and ΣeFR_C is *P* then ΔBRF_{SP} is *LP*
2. If eFR_C is *N* and ΣeFR_C is *N* then ΔBRF_{SP} is *LN*
3. If eFR_C is *Z* and ΣeFR_C is *Z* then ΔBRF_{SP} is *LN*
4. If eFR_C is *P* and ΔeFR_C is *P* then ΔBRF_{SP} is *HP*
5. If eFR_C is *N* and ΔeFR_C is *P* then ΔBRF_{SP} is *HN*

The output linguistic variables (fuzzy output sets) were obtained in this stage by applying Larsen's fuzzy inference method [10.33] using the Max-Prod operator. Hence, for each rule defined in Table 10.2, the operator represented by Eq. 10.16 was applied (where *i* represents each inference rule defined and *j* represents each of the input fuzzy sets in rule *i*).

$$\mu_i = \prod_1^j \mu_j \qquad \textbf{Eq. 10.16}$$

The operator expressed in Eq. 10.17 (where *k* represents each of the linguistic variables defined for the output variable) was then applied to establish just one linguistic output value when the consequences of different rules are the same (*i.e.* the consequence results in the same linguistic output variable).

$$\mu_k = Max(\mu_i) \qquad \textbf{Eq. 10.17}$$

During *defuzzification* (stage 4), linguistic variables are converted into the corresponding numerical control actions. Hence, in order to obtain a single output value from the fuzzy linguistic set, the Height Defuzzifier method [10.34] was employed (see Eq. 10.18).

$$\Delta BRF_{SP}\ (t) = \frac{\sum(c_k \cdot \mu_k)}{\sum(\mu_k)} \qquad \textbf{Eq. 10.18}$$

Finally, stage 5 is the output stage where the numerical control action of the fuzzy-logic controller is obtained, *i.e.* the set point of the biogas recycling flow. The control action of the fuzzy logic controller is expressed by Eq. 10.19, giving the integral output action necessary for set-point tracking.

$$BRF_{SP}(t) = BRF_{SP}(t - CT) + \Delta BRF_{SP}\ (t) \qquad \textbf{Eq. 10.19}$$

The biogas recycling flow was only modified within a defined range to avoid operating problems, taking into account the following constraints: the minimum biogas recycling flow needed for the membranes to operate and the maximum biogas recycling flow provided by the blower. These are BRF_{MIN} (5.5 $Nm^3\ h^{-1}$, *i.e.* an SGD_m of 0.18 $Nm^3\ h^{-1}\ m^{-2}$) and BRF_{MAX} (11 $Nm^3\ h^{-1}$, *i.e.* an SGD_m of 0.37 $Nm^3\ h^{-1}\ m^{-2}$), respectively.

10.5 Results and discussion

To account for the considerable fluctuations in the influent flows of WWTPs, we used the standard dry weather influent records (updated in 2006) recommended by Copp [10.35] which are generally accepted for evaluating control algorithms in WWTPs. The influent flow dynamics were calculated by applying a dynamic peak flow factor (calculated on the basis of the above-mentioned influent file) to an influent flow base of 225 L h^{-1}. The permeate flow was then set using the same time-series behaviour as for the influent.

The influent flow base (225 L h^{-1}) was established on the basis of the lifetime of the membranes used. It is important to emphasise that the proposed control system was calibrated and validated using a two-and-a-half-year-old membrane. Permeability was expected to be low because this membrane was used constantly and never underwent any physical or chemical cleaning.

10.5.1 Performance of sludge recycling flow controller

Figure 10.3 illustrates the performance of the sludge recycling flow controller during one day of operation (day 16). This figure shows the evolution of SRF_{SP} and SRF throughout the membrane tank, FIT-P11 and $FIT\text{-}P11_{SP}$, and FC-P12. As Figure 10.3 shows, SRF was adjusted proportionately to permeate flow. In this operating period $MLTS_{AnR}$ remained almost constant, varying from around 17.2

to 17.5 g L^{-1}, whilst $MLTS_{MT,SP}$ was set to 20 g L^{-1}. From hours 3 to 9, and 10.5 to 11.5, the minimum rotating speed for the sludge recycling pump and maximum SRF were reached, respectively. Therefore, the controller was not able to set the SRF to the expected set point. Nevertheless, the controller generally allowed MLTS to remain close to its set point in the membrane tank (checked by the corresponding lab measurements), thereby enabling an overall reduction in the energy consumed during filtration.

For instance, for our case study, comparing the results shown in Figure 10.3 (average SRF of 1.7 m^3 h^{-1}) with those obtained when operating at a set SRF of 2.7 m^3 h^{-1}, energy savings of up to 50% are obtained in sludge pumping (calculated theoretically using the classical mechanical energy balance). This means that the energy demand for sludge pumping could be reduced from approximately 0.06 to 0.03 kWh m^{-3}.

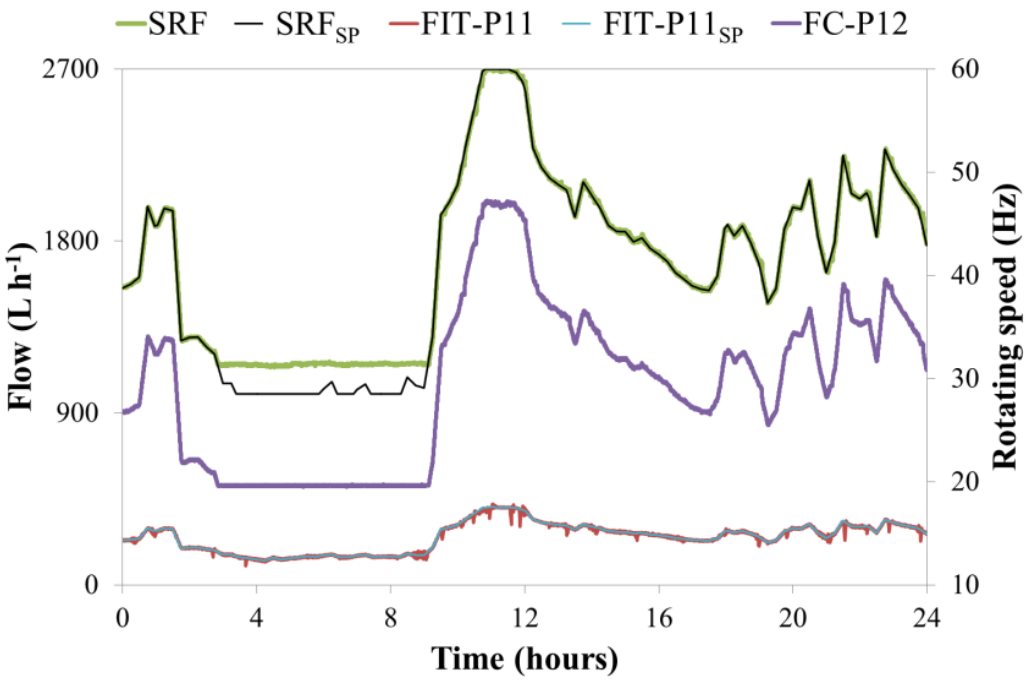

Figure 10.3 Performance of the sludge recycling controller. Evolution of sludge recycled through the membrane tank (*SRF*), set point of the sludge recycled through the membrane tank (SRF_{SP}), permeate flow (*FIT-P11*), permeate flow set point ($FIT\text{-}P11_{SP}$), and rotating speed of the sludge recycling pump (*FC-P12*).

10.5.2 Performance of knowledge-based rules

As mentioned before, the aim of the knowledge-based rules is to determine the best time to start ventilation and back-flushing.

10.5.2.1 Ventilation initiation

Figure 10.4 shows how the knowledge-based rule concerning ventilation initiation performed on one operating day (day 16). Figure 10.4a shows $FIT\text{-}P11_{SP}$ and the membrane operating mode. Figure 10.4b shows the recorded J_{20} and $J_{20,SP}$, $J_{20,MIN}$, and FC-P11.

Figure 10.4a shows how ventilation frequency increases as permeate flow increases. This increase in ventilation frequency is related to the amount of biogas in the permeate leaving the system. In this respect, the higher the permeate flow, the greater the amount of biogas extracted. Therefore, ventilation frequency increases in order to recover as much biogas as possible from the top of the degasification vessel. No ventilation was conducted between hours 4 and 9 approximately due to the lower vacuum strength applied for filtration (*i.e.* low transmembrane fluxes were applied), resulting in little biogas being extracted with the effluent. On the other hand, it must be emphasised that each ventilation stage constituted a relaxation stage in terms of membrane scouring, resulting in a partial improvement in membrane permeability.

Figure 10.4b shows the ventilation initiation times calculated by the respective knowledge-based rule. As mentioned before, the controller triggers ventilation when a sharp increase in the rotating speed of the permeate pump is detected but the corresponding J_{20} set point is not maintained. This situation was observed 24 times during the operating period shown in Figure 10.4. It is important to emphasise that Figure 10.4 illustrates the higher ventilation frequency observed throughout the experimental period that includes controller validation. This frequency means a ventilation downtime of around 1.4% of operating time. This value is considerably lower than the average full-scale results from aerobic MBR technology found in literature. For instance, Judd and Judd [1] reported a relaxation downtime of around 10% of the operating time in both FS and HF configurations. Therefore, considerable energy savings may be achieved by using the rule-based controller rather than the fixed membrane operating sequences provided by membrane suppliers.

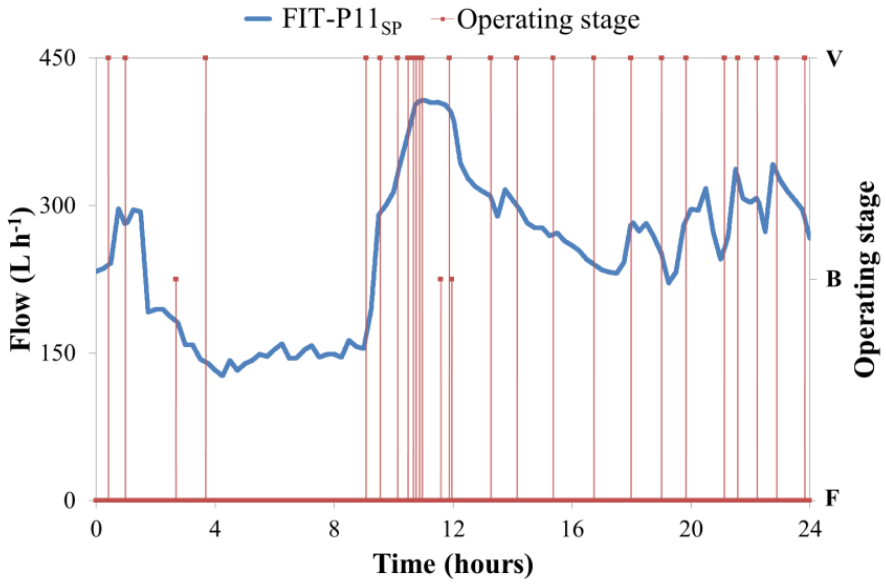

(a)

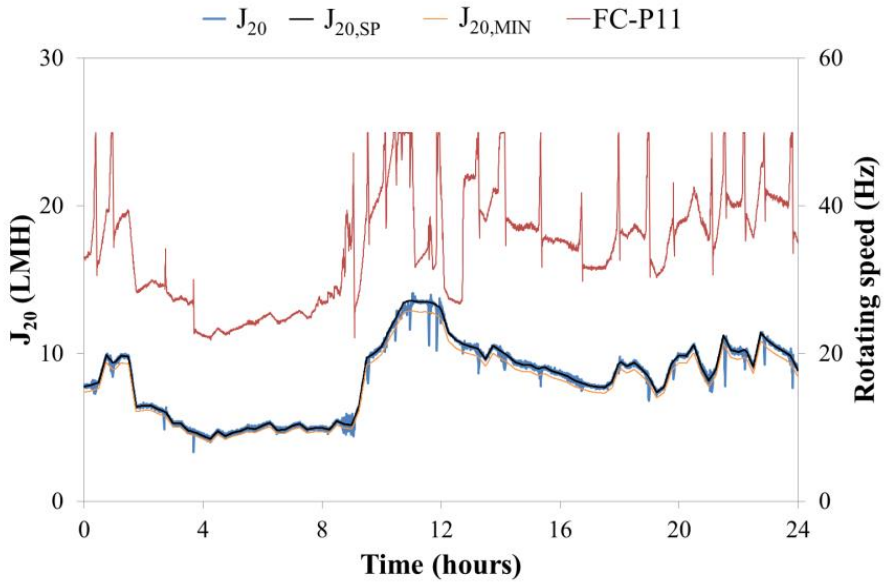

(b)

Figure 10.4 Ventilation initiation time determined by knowledge-based rule. Evolution of: **(a)** permeate flow set point (*FIT-P11$_{SP}$*) and membrane operating stage (*V: ventilation; B: back-flushing; and F: filtration*); and **(b)** 20 ºC-normalised transmembrane flux (J_{20}), 20 ºC-normalised transmembrane flux set point ($J_{20,\,SP}$), 20 ºC-normalised minimum transmembrane flux set point ($J_{20,\,SP}$), and rotating speed of the permeate pump (*FC-P11*).

10.5.2.2 Back-flushing initiation

Figure 10.5 shows how the knowledge-based rules concerning the start of back-flushing performed during one day of operation (day 16). Figure 10.5a shows TMP, TMP_{MAX} and membrane operating

mode. Figure 10.5b shows $K_{20,MAX,F}$ and $K_{20,MIN}$, and K_{20} calculated over time using on-line T, TMP and J data.

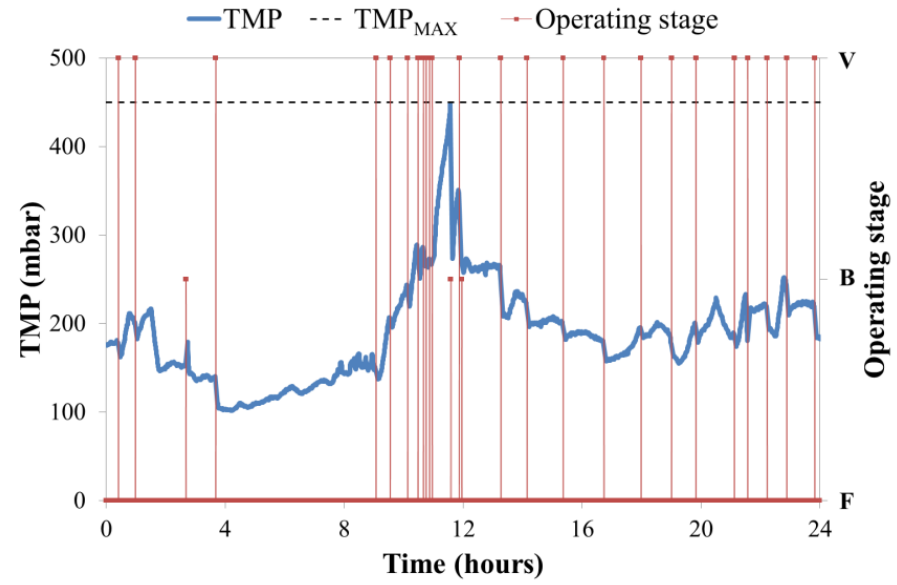

(a)

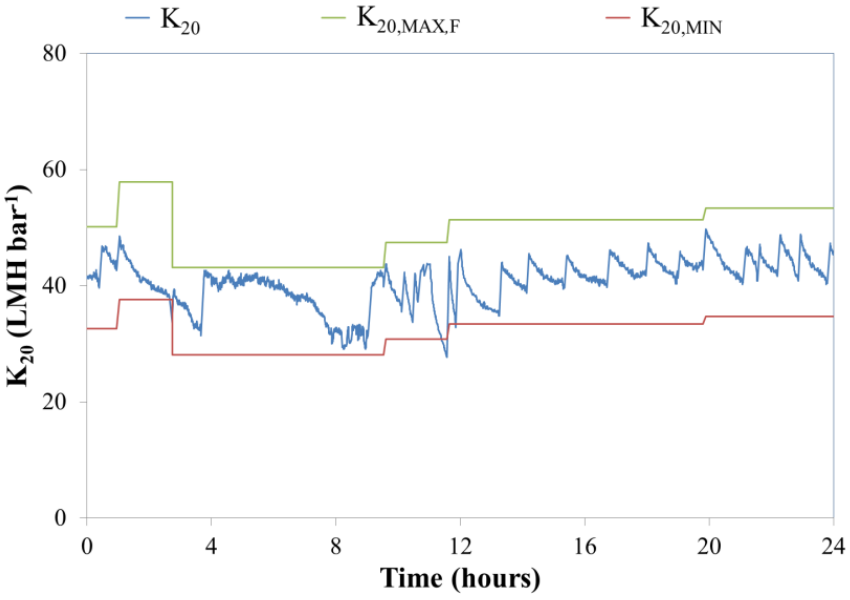

(b)

Figure 10.5 Back-flushing initiation time triggered by knowledge-based rules. Evolution of: **(a)** transmembrane pressure (*TMP*) and membrane operating stage (*V: ventilation; B: back-flushing; and F: filtration*); and **(b)** membrane permeability (K_{20}), maximum filtration membrane permeability recorded between consecutive back-flushing ($K_{20,MAX,F}$), and maximum calibrated back-flushing membrane permeability ($K_{20,MAX,BF}$).

Figure 10.5a shows three back-flushing starts during the experimental period. Rule 2 was applied at hours 2.7 and 12. As Figure 10.5b shows, K_{20} declined considerably (35%) during filtration, which triggered back-flushing. On the other hand, Rule 3 triggered back-flushing at hour 11.5 because the maximum TMP set for membrane operation (0.45 bars) had been reached.

Hence, as Figure 10.5 shows, back-flushing downtime accounted for around 0.2% of operating time. Similar results were observed throughout the experimental period in which controller validation took place. This downtime is also considerably lower than the average results reported for full-scale aerobic MBR technology in literature, *i.e.* back-flushing downtime of around 6 – 9% of operating time dedicated to treating urban wastewater aerobically [10.1]. This gives a total average downtime for physical cleaning (relaxation and back-flushing) of around 16 – 19% of operating time when using HF technology to treat urban wastewater aerobically (instead of the downtime of approx. 1.6% obtained in the period shown in Figures 4 and 5).

10.5.3 Performance of fuzzy-logic controller

An example of how the control system performed after calibration (day 16) is shown in Figure 10.6. The fuzzy-logic controller was adjusted by means of the classic trial and error method.

Figure 10.6a illustrates the evolution of FIT-P11 and $FIT\text{-}P11_{SP}$ (fixed by the dry weather influent dynamics records proposed by Copp), and also BRF and BRF_{SP} resulting from the control action. Figure 10.6b also shows BRF and BRF_{SP}, plus FR_C and FR_{C_SP}. The fouling rate set point was set to 0 mbar min^{-1} in order to keep filtration conditions sub-critical.

As can be observed in Figure 10.6, a fast controller response was achieved to compensate the fouling rate error (see, for instance, hours 20 to 24). In this respect, even when a dynamic influent flow set point was applied, the control response was able to keep the controlled variable close to the established set point by modifying BRF.

As Figure 10.6b shows, the controller operated mainly at the minimum threshold value established for BRF (5.5 $Nm^3\ h^{-1}$) as, for instance, in hours 2 to 7. In this period an excessive gas sparging intensity could have been applied for membrane scouring because the minimum BRF was reached. Between hours 9 to 12, on the other hand, BRF reached its maximum established value (11 $Nm^3\ h^{-1}$). During this period the fouling rate increased because it was not possible to maintain the controlled variable around its set point. This behaviour can be also observed from hours 20 to 24. In this situation, it can

be assumed that critical filtration conditions were exceeded. It must once again be emphasised that the controller was validated using a two-and-a-half-year-old membrane, resulting in low membrane permeability due to the irreversible fouling on the surface of the membrane during its lifetime. Consequently, it is expected that the permeate flux could be set to considerably higher values after chemical membrane cleaning, probably requiring no increase of the gas sparging intensity.

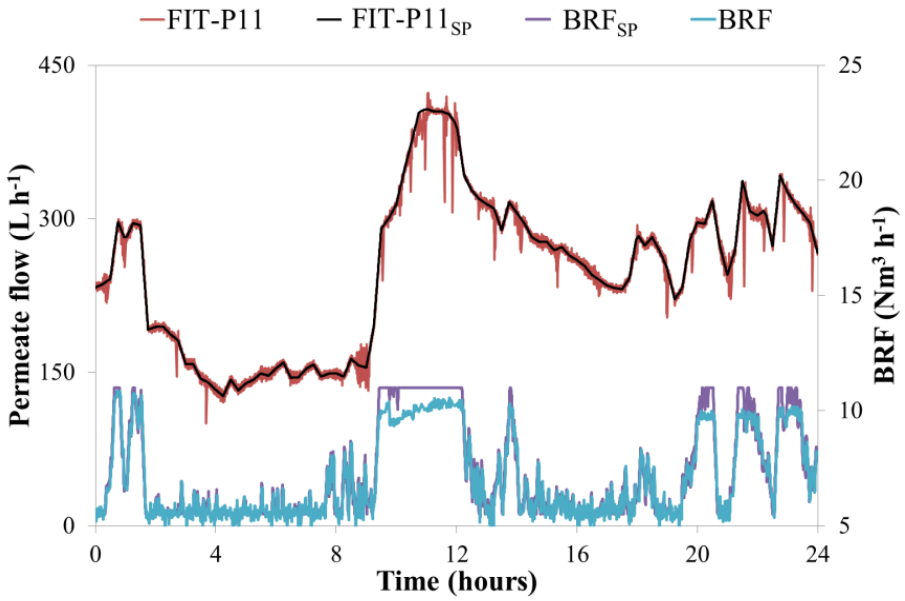

Figure 10.6 Fuzzy-logic controller performance. Evolution of: **(a)** permeate flow (*FIT-P11*), permeate flow set point ($FIT\text{-}P11_{SP}$), biogas recycling flow set point (BRF_{SP}) and biogas recycling flow (*BRF*); and **(b)** fouling rate (FR_C), fouling rate set point (FR_{C_SP}), biogas recycling flow set point (BRF_{SP}) and biogas recycling flow (*BRF*).

Figure 10.6 shows that the fuzzy-logic controller proposed in this study performed adequately: the fouling rate remained close to its set point when there were no constraints on the gas sparging intensity. Indeed, in spite of the considerable variation in the permeate flux the controlled variable remained at quite suitable values, highlighting that the proposed fuzzy-logic controller performed well under conditions similar to those expected in full-scale SAnMBR systems.

10.5.4 Overall performance of the advanced control system

Figure 10.7 shows the average daily membrane performance logged whilst using the control system for one month. The average MLTS concentration entering the membrane tank during the operating period ranged from around 16 to 18 g L^{-1}. This variation in MLTS was caused by the dynamics of the influent flow and load entering the demonstration plant. The results shown in Figure 10.7 can be divided in two different periods: whilst the controller was not calibrated (until day 9) and when fully adjusted (after day 9). Before the advanced control system was implemented, the membranes were operated by time-based filtration sequences (resulting in a J_{20} of 8 LMH) with constant gasification intensity (SGD_m of 0.35 Nm^3 h^{-1} m^{-2}). The time-based filtration sequences entailed a specific schedule consisting of a combination of different individual stages (back-flushing, degasification and ventilation) taken from a basic F-R cycle. The time-based operating mode was as follows: a 300-second basic F-R cycle (250 s filtration and 50 s relaxation), 30 seconds of back-flush every 10 F-R cycles, 40 seconds of ventilation every 10 F-R cycles, and 30 seconds of degasification every 50 F-R cycles.

The savings made in specific gas demand (SGD_m, SGD_P) after implementing the proposed control system (in comparison with the previous time-based membrane operating mode) is shown in Figure 10.7 as a clear area (*i.e.* the difference between the applied specific gas demand and the maximum y-axis value: 0.35 Nm^3 h^{-1} m^{-2}). Comparing the results shown in Figure 10.7 with those of the previous operating period in which membranes were operated at a fixed BRF of 0.35 Nm^3 h^{-1} m^{-2}, reveals energy savings during membrane scouring of up to 60% (calculated theoretically by considering the energy needed for adiabatic compression according to the classic mechanical energy balance). Indeed, the energy demand for membrane scouring was reduced from approx. 0.36 to 0.15 kWh m^{-3}.

As Figure 10.7 shows, even whilst operating sub-optimally (until day 9), the controller allowed a slight reduction in the energy required for membrane scouring. On the other hand, after tuning the control system, an SGD_m of around 0.23 Nm^3 h^{-1} m^{-2} was enough to operate the two-and-a-half-year-old membranes sub-critically (see Figure 10.7a). As a result, the SGD_P was reduced by up to 25%.

These values resulted in an SGD_P of around 30, operating with average permeability of 40 LMH bar^{-1}. In this respect, quite stable average TMP values (around 0.18 bars) were achieved when operating with an average J_{20} of 8 LMH.

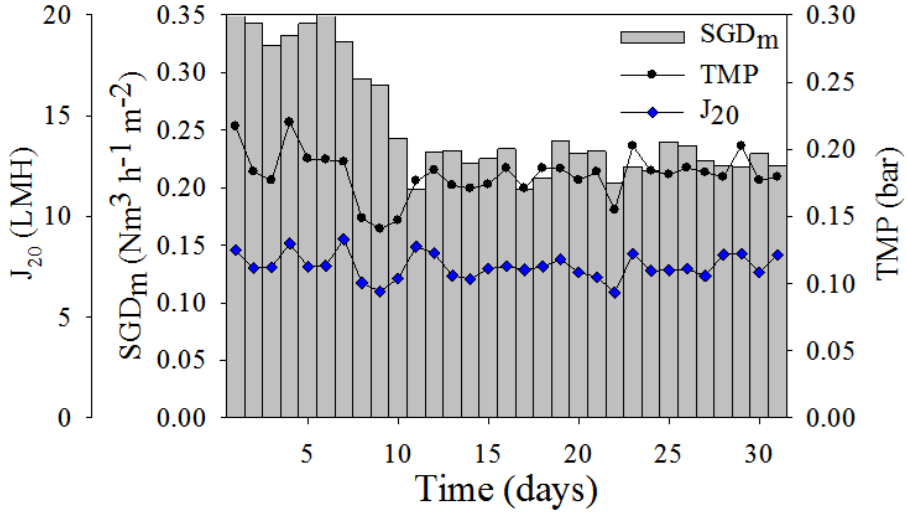

(a)

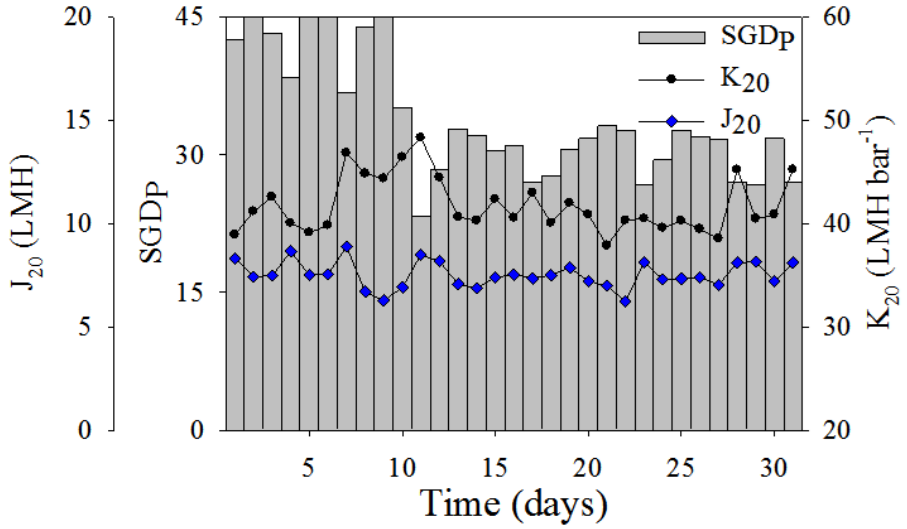

(b)

Figure 10.7 Overall advanced control system results. Evolution of: **(a)** 20 ºC-normalised transmembrane flux (J_{20}), specific gas demand per membrane area (SGD_m), and transmembrane pressure (TMP); and **(b)** 20 ºC-normalised transmembrane flux (J_{20}), specific gas demand per permeate volume (SGD_p), and membrane permeability (K_{20}).

Taking into account how long membranes last if not chemically cleaned or recovered (as reflected by the low permeability values), the results shown in this study predict that operating a full-scale SAnMBR using the proposed advanced control system would be quite sustainable. For instance, Judd

and Judd [10.1] reported average SGD_m and SGD_P values of 0.57 $Nm^3\ h^{-1}\ m^{-2}$ and 27.5, respectively, in full-scale WWTPs treating urban wastewater with submerged aerobic MBRs featuring flat-sheet membranes. The same authors reported average SGD_m and SGD_P values of 0.3 $Nm^3\ h^{-1}\ m^{-2}$ and 16, respectively, when the membranes were hollow-fibre. These full-scale aerobic operating results are similar to the results obtained in our study because the MLTS levels applied in our study (approx. 20 g L^{-1}) were higher than those in aerobic MBRs (ranging from around 12 to 18 g L^{-1}). In addition, the lifespan of the membranes in our study must be taken into account.

As regards the physical cleaning stages, the average ventilation and back-flushing frequencies were about 21 and 5, respectively. The total downtime caused by physical cleaning therefore accounted for less than 2% of operating time.

Table 10.3 Overall SAnMBR operating results with control system on and off.

Operating results	**Time-based operating mode**	**Control system action**
Average SGD_m ($Nm^3\ h^{-1}\ m^{-2}$)	0.35	0.25
Average SGD_P	45	30
Average SRF ($m^3\ h^{-1}$)	2.7	1.7
Energy for membrane scouring (kWh m^3)	0.36	0.15
Energy for pumping sludge (kWh m^3)	0.06	0.03
Ventilation frequency (initiations/day)	27	21
Back-flushing frequency (initiations/day)	27	5
Downtime for ventilation (%)	1.6	1.4
Downtime for back-flushing (%)	1.2	0.2
Overall downtime for physical cleaning (%)	2.8	1.6

Table 10.3 summarises the average SAnMBR performance when operating on a time-based mode and the performance of the proposed filtration control system, showing that far greater energy savings could be achieved by the proposed control system than the time-based fixed operating mode.

The proposed advanced control system enables adequate filtration performance; makes use of the on-line equipment available in the plant; and is user-friendly and adaptable to new operating requirements.

10.5.5 Overall performance of the SAnMBR system

As mentioned earlier, the filtration system controller was tested using a membrane tank that continuously recycled the permeate back into the system. As Figure 10.4a shows, the permeate flow ranged from about 135 to 400 L h^{-1} (225 L h^{-1} on average). As regards designing a full-scale plant, the findings set forth in this paper would be useful for determining the reaction volume giving the HRT needed to ensure that the biological process performs adequately.

Previous research on this SAnMBR system has shown that acceptable COD removal efficiencies (of around 90%) can be accomplished in a wide range of operating conditions: SRT of 20 - 70 days, ambient temperature conditions (14 - 33 ºC), OLR of 0.5 - 2 kgCOD m^{-3} d^{-1}, and HRT of 5 - 24 hours. These results shows that this SAnMBR system would be able to treat the organic load occurring at the peak flow simulated in this study by applying Copp's influent data.

Biogas was produced at a significant rate on average (around 100 L d^{-1}) throughout the experimental period. A fraction of the biogas stored in the anaerobic reactor head space was recycled through the membrane tanks to scour them which enabled the ORP and pH in the mixed liquor to remain relatively stable at around 450-500 mV and 6.5-7.1, respectively. An equilibrium between liquid and gas phases in SAnMBR systems was observed [10.36], *i.e.* the CO_2 content of the effluent was similar to the CO_2 saturation point. Hence, most of the CO_2 produced remained in the mixed liquor and acted as a pH buffer. This was confirmed by the high Alk content of the mixed liquor (around 600 mg$CaCO_3$ L^{-1} during the operating period), in comparison with the influent Alk (around 332 mg$CaCO_3$ L^{-1}). This behaviour highlights the importance of scouring the membranes with a fraction of the biogas produced by SAnMBR systems because according to recent literature, pH is a key factor in membrane fouling [10.37; 10.38].

As regards the impact of SRT on membrane fouling, a considerably higher propensity to irreversible fouling was observed when SRT was 20 days rather than 70 days. This was attributed mainly to the fact that EPS and SMP concentrations were higher when SRT was lower (data not shown). Furthermore, it is well known that at any given reactor volume, the higher the SRT, the higher the MLTS in the system. MLTS directly reduces K [10.31], resulting in higher operating costs. Therefore, a compromise must be struck between SRT and MLTS levels in order to minimise both irreversible membrane fouling and operating costs. On the basis of the results obtained, we propose that SAnMBR systems be operated with MLTS levels of approximately 15 to 20 g L^{-1} in the membrane tank and a minimum SRT of 40 days.

10.6 Conclusions

An advanced control system designed to control filtration in SAnMBR systems has been developed, fine-tuned and validated. It consists of lower-layer controllers (classical on-off and PID controllers) and an upper-layer (knowledge-based) control. The results of this study suggest that the proposed control system is promising: low fouling rates (almost 0 mbar min^{-1}) were achieved by applying sustainable gas sparging intensities (approx. 0.23 Nm^3 h^{-1} m^{-2}). Moreover, ventilation and back-flushing downtimes were reduced considerably (to around 2% of total operating time) in comparison with full-scale aerobic MBRs.

10.7 Acknowledgements

This research has been supported by the Spanish Research Foundation (CICYT Projects CTM2008-06809-C02-01 and CTM2008-06809-C02-02, and MICINN FPI grant BES-2009-023712) and Generalitat Valenciana (Projects GVA-ACOMP2010/130 and GVA-ACOMP2011/182), which are gratefully acknowledged.

10.8 References

10.1 S. Judd, C. Judd, The MBR Book: Principles and Applications of Membrane Bioreactors for Water and Wastewater Treatment, second ed., Elsevier, ISBN: 978-0-08-096682-3, 2011.

10.2 I.S. Chang, P. L. Clech, B. Jefferson, S. Judd, Membrane fouling in membrane bioreactors for wastewater treatment, J. Environ. Eng. 128(2002), 1018–1029.

10.3 C. Huyskens, E. Brauns, E. Van Hoof, L. Diels, H. De Wever, Validation of a supervisory control system for energy savings in membrane bioreactors, Water Res. 45 (2011), 1443–1453.

10.4 S. Judd, The status of membrane bioreactor technology, Trends Biotechnol. 26 (2008), 109–116.

10.5 A. Drews, Membrane fouling in membrane bioreactors–Characterisation, contradictions, cause and cures, J. Membr. Sci. 363 (2010), 1–28.

10.6 S.I. Patsios, A.J. Karabelas, An investigation of the long-term filtration performance of a membrane bioreactor (MBR): The role of specific organic fractions, J. Membr. Sci. 253 (2011), 102–115.

10.7 A. Robles, M.V. Ruano, F. García-Usach, J. Ferrer, Sub-critical filtration conditions of commercial hollow-fibre membranes in a submerged anaerobic MBR (HF-SAnMBR) system: The effect of gas sparging intensity, Bioresource Technol. 114 (2012), 247–254.

10.8 P. Bachin, P. Aimar, V. Sanchez, Model for colloidal fouling of membranes, AIChE J. 41 (1995), 368–377.

10.9 R.W. Field, D. Wu, J.A. Howell, B.B. Gupta, Critical flux concept for microfiltration fouling, J. Membr. Sci. 100 (1995), 259–272.

10.10 B. Verrecht, T. Maere, I. Nopens, C. Brepols, S. Judd, The cost of a large-scale hollow fibre MBR, Water Res. 44 (2010), 5274–5283.

10.11 A. Drews, H. Arellano-Garcia, J. Schöneberger, J. Schaller, M. Kraume, G. Wozny, Improving the efficiency of membrane bioreactors by a novel model-based control of membrane filtration, 17th European Symposium on Computer Aided Process Engineering–ESCAPE 17(2007), 345–350.

10.12 A. Drews, H. Arellano-Garcia, J. Schöneberger, J. Schaller, G. Wozny, M. Kraume, Model-based recognition of fouling mechanisms in membrane bioreactors, Desalination 236 (2009), 224–233.

10.13 J. Busch, A. Cruse, W. Marquardt, Run-to-Run Control of Membrane Filtration Processes, AIChE J. 53 (2007), 2316–2328.

10.14 G. Ferrero, I. Rodriguez-Roda, J. Comas, Automatic control systems for submerged membrane bioreactors: A state-of-the-art review, Water Res. 46 (2012), 3421–3433.

10.15 C. Huyskens, E. Brauns, E. Van Hoof, H. De Wever, A new method for the evaluation of the reversible and irreversible fouling propensity of MBR mixed liquor, J. Membr. Sci. 323 (2008), 185–192.

10.16 H. Monclús, G. Buttiglieri, G. Ferrero, I. Rodriguez-Roda, J. Comas, Knowledge-based control module for start-up of flat sheet MBRs, Bioresource Technol. 106 (2012), 50–54.

10.17 G. Ferrero, H. Monclús, G. Buttiglieri, S. Gabarron, J. Comas, I. Rodriguez-Roda, Development of a control algorithm for air-scour reduction in membrane bioreactors for wastewater treatment, J. Chem. Technol. Biotechnol. 86 (2010), 784–789.

10.18 G. Ferrero, H. Monclús, G. Buttiglieri, J. Comas, I. Rodriguez-Roda, Automatic control system for energy optimization in membrane bioreactors, Desalination 268 (2011), 276–280.

10.19 G. Ferrero, H. Monclús, L. Sancho, J.M. Garrido, J. Comas, I. Rodriguez-Roda, A knowledge-based control system for air-scour optimisation in membrane bioreactors, Water Sci. Technol. 63 (2011), 2025–2031.

10.20 D. Jeison, J.B. van Lier, On-line cake-layer management by trans-membrane pressure steady state assessment in Anaerobic Membrane Bioreactors for wastewater treatment, Biochem. Eng. J. 29 (2006), 204–209.

10.21 P.J. Smith, S. Vigneswaran, H.H. Ngo, R. Ben-Aim, H. Nguyen, A new approach to backwash initiation in membrane systems, J. Membr. Sci. 278 (2006), 381–389.

10.22 A. Vargas, I. Moreno-Andrade, G. Buitrón, Controlled backwashing in a membrane sequencing batch reactor used for toxic wastewater treatment, J. Membr. Sci. 320 (2008), 185–190.

10.23 H-D. Park, Y.H. Lee, H-B. Kim, J. Moon, C-H. Ahn, K-T. Kim, M-S. Kang, Reduction of membrane fouling by simultaneous upward and downward air sparging in a pilot-scale submerged membrane bioreactor treating municipal wastewater, Desalination 251 (2010), 75–82.

10.24 L.A. Zadeh, Fuzzy sets, Information and Control 8 (1965), 338–353.

10.25 H.B. Verbruggen, P.M. Bruijn, Fuzzy control and conventional control: What is (and can be) the real contribution of Fuzzy Systems?, Fuzzy Set. Syst. 90 (1997), 151–160.

10.26 M.V. Ruano, J. Ribes, G. Sin, A. Seco, J. Ferrer, A systematic approach for fine-tuning of fuzzy controllers applied to WWTPs, Environ. Modell. Softw. 25 (2010), 670–676.

10.27 M.V. Ruano, J. Ribes, A. Seco, J. Ferrer, An advanced control strategy for biological nutrient removal in continuous systems based on pH and ORP sensors, Chem. Eng. J. 183 (2012), 212–221.

10.28 J.B. Giménez, A. Robles, L. Carretero, F. Durán, M.V. Ruano, M.N. Gatti, J. Ribes, J. Ferrer, A. Seco, Experimental study of the anaerobic urban wastewater treatment in a submerged hollow-fibre membrane bioreactor at pilot scale, Bioresource Technol. 102 (2011), 8799–8806.

10.29 American Public Health Association/American Water Works Association/Water Environmental Federation, Standard methods for the Examination of Water and Wastewater, 21st edition, Washington DC, USA, 2005.

10.30 Water Res. Commission, University of Cape Town, Simple titration procedures to determine H2CO3* alkalinity and short-chain fatty acids in aqueous solutions containing known concentrations of ammonium, phosphate and sulphide weak acid/bases, Report No. TT 57/92, Pretoria, Republic of South Africa, 1992.

10.31 A. Robles, F. Durán, M.V. Ruano, J. Ribes, J. Ferrer, Influence of total solids concentration on membrane permeability in a submerged hollow-fibre anaerobic membrane bioreactor, Water Sci. Technol. 66 (2012), 377–384.

10.32 H. Monclús, G. Ferrero, G. Buttiglieri, J. Comas, I. Rodriguez-Roda, On-line monitoring of membrane fouling in submerged MBRs, Desalination 277 (2011), 414–419.

10.33 P.M. Larsen, Industrial application of fuzzy logic control, Int. J. Man. Mach. Stud. 12 (1980), 3–10.

10.34 J.M. Mendel, Fuzzy logic systems for engineering: a tutorial, Proc. IEEE 83 (1995), 345–375.

10.35 J.B. Copp, Development of standardised influent files for the evaluation of activated sludge control strategies, IAWQ Scientific and Technical Report Task Group: Respirometry in Control of the Activated Sludge Process–internal report, 1999.

10.36 J.B. Giménez, N. Martí, J. Ferrer, A. Seco, Methane recovery efficiency in a submerged anaerobic membrane bioreactor (SAnMBR) treating sulphate-rich urban wastewater: Evaluation of methane losses with the effluent, Bioresource Technol. 118 (2012), 67–72.

10.37 W.J. Jane Gao, H.J.Lin, K.T. Leunga, B.Q. Liao, Influence of elevated pH shocks on the performance of a submerged anaerobic membrane bioreactor, Process Biochem. 45 (2010), 1279–1287.

10.38 A. Sweity, W. Ying, S. Belfer, G. Oron, M. Herzberg, pH effects on the adherence and fouling propensity of extracellular polymeric substances in a membrane bioreactor, J. Membr. Sci.378 (2011), 186–193.

CHAPTER 11:

Model-based automatic tuning of a filtration control system for submerged anaerobic MBRs (SAnMBRs)

Abstract

This paper describes a model-based optimisation method for filtration in submerged anaerobic MBRs (SAnMBRs). The method is applied to an advanced knowledge-based control system and considers three statistical methods: (1) sensitivity analysis (Morris screening method) to identify an input subset for the advanced controller; (2) Monte Carlo method (using trajectory-based random sampling) to find adequate initial values for the control inputs; and (3) optimisation algorithm (performing as supervisory controller) to re-calibrate these control inputs in order to minimise plant operating costs. The proposed model-based supervisory controller allowed filtration to be optimised with low computational demands (about 5 minutes). Energy savings of up to 25% were achieved during membrane scouring by gas sparging. The downtime for physical cleaning was about 2.4% of operating time. The operating cost of the SAnMBR system after implementing the proposed supervisory controller was about €0.028 per m^{-3}, 85.7% of which were energy costs.

Keywords

Industrial-scale hollow-fibre membranes; model-based supervisory controller; Monte Carlo procedure; Morris screening method; submerged anaerobic MBR (SAnMBR)

Highlights

A model-based optimisation method for filtration in SAnMBRs is proposed.
It includes the Morris method, Monte Carlo procedure and an optimisation algorithm.
The computational demand of control system optimisation was low.
Energy savings during membrane scouring of up to 25%.
The supervisory controller resulted in SAnMBR operating costs of about €0.028 per m^{-3}.

A. Robles, M.V. Ruano, J. Ribes, A. Seco, J. Ferrer
Model-based automatic tuning of a filtration control system for submerged anaerobic MBRs (SAnMBRs)
Submitted to J. Membrane Sci.

11.1 Introduction

Mathematical modelling is a powerful tool for studying complex systems such as anaerobic MBRs (AnMBRs) [11.1] and may help provide an insight into the factors that play a key role in membrane fouling [11.2]. Indeed, certain models have been found to be useful for different objectives related to WWTPs, such as the development of operation and control strategies designed to optimise process performance [11.3; 11.4; 11.5]. Hence, the mathematical modelling of filtration in AnMBRs may be very useful for the design, prediction and control of membrane technology applied to wastewater treatment [11.6].

The main challenge of AnMBR technology is to control membrane fouling whilst optimising energy consumption but few scientific papers and innovations aimed at minimising operating costs and enhancing AnMBR efficiency have been published or patented [11.7]. In addition, these contributions address mainly different types of advanced controllers (mainly model-based and knowledge-based) that enable energy savings in aerobic MBR (AeMBR) technology, therefore further research is needed in the anaerobic field. As regards the model-based control of filtration in AeMBR technology, Drews *et al*. [11.8; 11.9] developed a control system designed to improve filtration efficiency by applying mathematical models enabling appropriate actions to increase permeability over time. On the other hand, Busch *et al*. [11.10] proposed a model-based run-to-run control system that optimised the adjusted variables (filtration and back-flushing stages) after each filtration cycle. However, further research is needed into model-based control strategies for filtration in AnMBR technology due to the limited knowledge about fouling in systems of this type. As regards knowledge-based control of filtration in AeMBR technology, Huyskens *et al*. [11.11] validated an advanced control system that evaluated the reversible fouling propensity by using a specific on-line fouling measuring tool [11.12]; Ferrero *et* al. [11.13; 11.14; 11.15] developed a controller to supervise filtration and achieved considerable energy savings (up to 21%) in membrane scouring; and Soleimani *et al*. [11.16] optimised membrane operation by combining neural networks and genetic algorithms.

As regards the knowledge-based control of filtration in AnMBR technology, in a previous paper we presented a knowledge-based advanced control system (including a fuzzy-logic controller) that reduced both the energy consumption related to membrane scouring and the downtime needed for back-flushing [11.17]. To minimise long-term operating costs, the set points of this knowledge-based advanced control system should be modified over time to account for the dynamic operating conditions typically observed in WWTPs. Furthermore, it is well known that the automatic recalibration of control parameters is advisable in the event of variable operating conditions [11.18].

Therefore, optimising the advanced controller involves adjusting not only the set-point values, but also the values of the different control parameters included in the fuzzy-logic controller (*i.e.* control time (*CT*), sampling time (*ST*), centre and amplitude of each input fuzzy set, and singleton value of each output fuzzy set).

Fuzzy-logic controllers applied to wastewater treatment usually contain large numbers of control parameters – which complicates their calibration. Therefore, before fine-tuning these controllers, regardless of the optimisation method applied, a selection must be made of the most important parameters to be adjusted in each particular application. This is when the main challenge arises, *i.e.* how to select an identifiable input subset from amongst the significant number of control parameters.

Sensitivity analysis provides useful information for modellers because it attempts to quantify how changes in the input factors of a model affect its outputs. Hence, sensitivity analysis is an attempt to determine the most influential parameters of a model. These parameters are the identifiable input factors, *i.e.* those with the greatest impact on the outputs of a model. Sensitivity analysis can also be used to identify the most important parameters in advanced control systems such as those based on fuzzy logic. For instance, different applications of the Morris screening method [11.19] in determining the most influential parameters in fuzzy-logic controllers can be found in the literature [11.20; 11.21]. Furthermore, this sensitivity analysis has been incorporated into a control system calibration method in order to find an adequate parameter subset for fine-tuning fuzzy-logic controllers [11.22].

In this study, we propose a model-based supervisory controller which is to be applied to the above-mentioned knowledge-based advanced control system in order to optimise filtration in submerged AnMBRs (SAnMBRs). This supervisory system uses a resistance-in-series-based filtration model developed for SAnMBR technology [11.23] in order to find the optimum combination of set points for the advanced controller resulting in minimum operating costs (evaluated by a specific objective function). In addition, the optimum combination of values of fuzzy-logic control parameters resulting in the minimum integral absolute error (*IAE*) over time was also obtained for each change in the advanced controller set points.

The optimisation method proposed in this study is based on model simulations and considers three statistical methods: (1) sensitivity analysis (Morris screening method) to find an identifiable input subset for the control system; (2) Monte Carlo procedure (using trajectory-based random sampling technique) to find adequate initial conditions; and (3) optimisation algorithm (performing as

supervisory controller) to obtain the optimum input value combination that minimises both *IAE* and operating costs.

11.2 Materials and methods

As mentioned above, in this study we propose a model-based supervisory controller for filtration in SAnMBR systems. This supervisory controller was applied to an advanced fuzzy-logic control system for filtration in SAnMBRs [11.17]. It uses a resistance-in-series-based filtration model developed in SAnMBRs [11.23] for selecting the optimum set points for the advanced controller resulting in minimum operating costs. To obtain representative results that could be extrapolated to full-scale plants, both the advanced control system and the filtration model were validated beforehand in a SAnMBR system fitted with industrial-scale hollow-fibre membranes and fed with urban wastewater from the pre-treatment of the Carraixet WWTP (Valencia, Spain) [11.17; 11.23].

11.2.1 SAnMBR plant description and monitoring

This study was carried out using data from the previously introduced SAnMBR system (see Chapter 2).

In addition to being monitored on line, grab samples of anaerobic sludge were taken once a day to assess filtration performance. MLTS concentration was determined according to Standard Methods [11.24] using procedure 2540 B.

11.2.2 Advanced control system description

The advanced control system (see Chapter 10 and Robles *et al*. [11.17]) used in this study aims to minimise operating costs in SAnMBR technology by modifying not only the gas sparging intensity used in membrane scouring but also the back-flushing frequency. The advanced controller consists of a MIMO control structure including a number of lower-layer controllers and one upper-layer controller. The lower-layer controllers are based on classic on-off and feedback PID (proportional-integral-derivative) controllers consisting of SISO control structures. The upper-layer controller is based on knowledge-based theory and consists of a MIMO control structure including fuzzy-logic control and knowledge-based rules. The upper-layer controller allows the different set points of the

controlled variables in the lower-layer controllers to be established according to the data gathered from the different sensors installed in the plant.

The inputs of this advanced controller include, besides the fuzzy-logic control parameters, the fouling rate set point related to cake layer formation (FR_{C_SP}), maximum operating transmembrane pressure (TMP_{MAX}), maximum decrease in membrane permeability during filtration ($\%K_{20}$) and the sludge recycling flow set point through the membrane tank (SRF_{SP}).

11.2.2.1 Lower-layer controllers

The group of lower-layer controllers included in the advanced control system consists of the following: three PID controllers to adjust the rotating speed of the sludge recycling pump, the permeate pump and the biogas recycling blower by the corresponding frequency converter in order to keep the corresponding flow close to its set point value; and one on-off controller that determines the membrane operating stage by changing both the position of the corresponding on-off valves and the flux direction of the permeate pump. The PID controllers were tuned by trial and error, resulting in good performance under different situations.

11.2.2.2 Upper-layer control structure

The upper-layer controller can be divided into two subsections: (i) a preliminary group of knowledge-based rules, where the membrane operating stage is established (filtration or back-flushing); and (ii) fuzzy-logic control, where FR_C is controlled by adjusting the set point of the biogas recycling flow for membrane scouring (BRF_{SP}).

11.2.2.2.1 Control variables

The 20 ºC-normalised transmembrane flux (J_{20}) was defined as shown in Eq. 11.1 in order to reflect the dependence of permeate viscosity (μ) on temperature (T).

$$J_{20} = J_T \cdot \exp\left(-0.0239 \cdot (T - 20)\right) \qquad \textbf{Eq. 11.1}$$

where J_T is the transmembrane flux at temperature T.

The resistance-in-series model considered in this study is shown in Eq. 11.2 In this classic filtration model, the total filtering resistance (R_T) was theoretically represented by intrinsic membrane resistance (R_M), irreversible fouling resistance (R_I) and cake-layer resistance (R_C).

$$K_{20} = \frac{1}{\mu_{20} \cdot R_T} = \frac{1}{\mu_{20} \cdot \left(R_M + R_I + R_C\right)} = \frac{J_{20}}{TMP} \qquad \textbf{Eq. 11.2}$$

where K_{20} is 20 ºC-normalised membrane permeability, TMP is transmembrane pressure and μ_{20} is permeate viscosity at 20 ºC.

In this study, FR_C at time t was calculated as follows:

$$FR_C(t) = \frac{\partial TMP_C}{\partial t} = \frac{n \cdot \sum_1^n \left(TMP_{C,i} \cdot t_i\right) + \sum_1^n TMP_{C,i} \cdot \sum_1^n t_i}{n \cdot \sum_1^n {TMP_{C,i}}^2 - \left(\sum_1^n TMP_{C,i}\right)^2} \qquad \textbf{Eq. 11.3}$$

where TMP_C is the TMP through the cake-layer and n is the number of points considered for estimating FR_C (5 points in this study).

The evolution of TMP_C over time was represented as follows:

$$TMP_C(t) = J_{20}(t) \cdot \mu_{20} \cdot R_C(t) = J_{20}(t) \cdot \mu_{20} \cdot \alpha_C(t) \cdot \omega_C(t) \qquad \textbf{Eq. 11.4}$$

where $\alpha_C\ (t)$ and $\omega_C\ (t)$ are the average specific cake resistance and the mass of cake deposited per membrane area at time t, respectively.

The sampling time was set as the fifth part of the control time, *i.e.* $ST = CT/5$.

11.2.2.2.2 <u>*Preliminary knowledge-based rules*</u>

Two different knowledge-based rules for back-flushing initiation were defined in the advanced control system: (1) when K_{20} is below a minimum value ($K_{20,MIN}$), *i.e.* a function of the maximum K_{20} during the corresponding filtration stage ($K_{20,MAX}$, see Eq. 11.5); and (2) when TMP_{MAX} is reached.

$$K_{20,MIN} = \%K_{20} \cdot K_{20,MAX} \qquad \textbf{Eq. 11.5}$$

11.2.2.2.3 Fuzzy-logic controller description

The fuzzy-logic controller only acts during filtration since the aim is to control FR_C. The output variable of the fuzzy-logic controller is the variation in the biogas recycling flow (*VBRF*). This controller determines *VBRF* on the basis of three inputs obtained from the estimated FR_C, *i.e.* error (*FRE*), accumulated error (*FRAE*) and error difference (*FRDE*). Three Gaussian membership functions were considered for each input of the fuzzy-logic controller: negative (*N*), zero (*Z*) and positive (*P*). Therefore, 9 Gaussian membership functions were defined in the *fuzzification* stage. As each Gaussian membership function is defined by two parameters (centre, *c*, and amplitude, *a*), the fuzzy-logic controller has a total of 18 parameters corresponding to the *fuzzification* stage. Four singleton membership functions were defined as output linguistic variables in the *defuzzification* stage: high negative (*HN*), low negative (*LN*), low positive (*LP*) and high positive (*HP*). In this case, each singleton membership function is defined by only one parameter (s, singleton value). Therefore, the fuzzy-logic controller has a total of 4 parameters for the *defuzzification* stage. Including the control actuation time (*CT*), a total of 23 parameters need to be adjusted in the fuzzy-logic controller (as mentioned before, sampling time was set to *CT*/5 in this study). Hence, reducing the number of tuning parameters is essential.

When classifying the parameters of the fuzzy-logic controller, acronyms for each parameter were constructed as follows: "abbreviation of input/output variable of the controller" + "c/a/s" (centre/amplitude/singleton) + "input/output membership function abbreviation in the *fuzzification*/*defuzzification* stage". For instance, *FREaN* is the acronym of the amplitude of the Negative Gaussian membership function for the error of FR_C; and *VBRFsHP* is the acronym of the singleton value of the High Positive singleton membership function for the variation in BRF_{SP}.

11.2.3 Model-based optimisation method

Figure 11.1 is a schematic representation of the model-based optimisation method proposed in our study. As Figure 11.1a shows, Morris simulations are conducted (Step A) in order to select the highly-influential control inputs (Step B) from the knowledge-based advanced control system (including both set points and fuzzy-logic control parameters). Screening the slightly/non-influential parameters of the control system is essential in order to reduce the computational cost of the model-based supervisory controller. Once the highly-influential control input subset is selected, a Monte Carlo procedure (using trajectory-based random sampling technique) is conducted (Step C) to establish adequate initial values (Step D) for the advanced control system. Then the inputs of the advanced controller are updated (Step

E). The model-based supervisory controller is initiated (Step F) each optimiser time (*OT*) in order to optimise plant performance by updating the optimal inputs of the advanced control system (Step G).

Figure 11.1b is a schematic representation of the model-based supervisory controller. As this figure shows, the real-time optimiser adjusts the advanced controller set points periodically (Step H) and calculates an objective function (Step I) by applying the above-mentioned filtration model (Step J). In addition, the fuzzy-logic controller was previously tuned by trial and error methods based on technical knowledge of process and controller performance. Therefore, as Figure 11.1b shows, the model-based supervisory controller also adjusts the highly-influential fuzzy-logic control parameters (Step K) and calculates another objective function (Step L) by applying a filtration model (Step M). In order to minimise the control error, the fuzzy-logic control parameters must be calibrated for each set point combination.

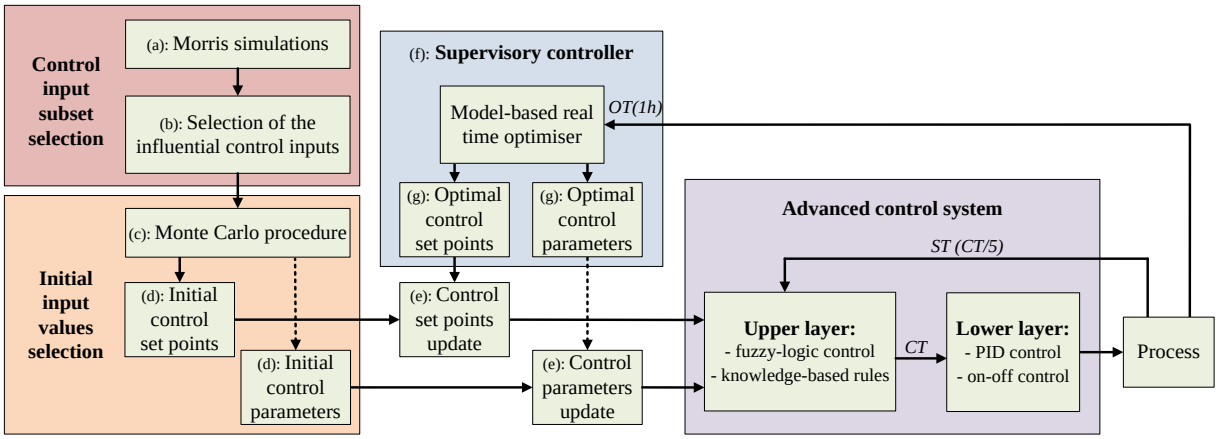

(a)

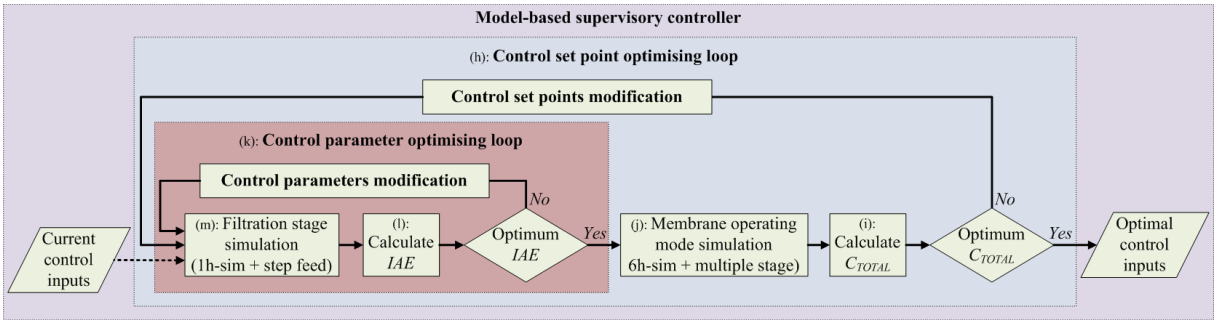

(b)

Figure 11.1 **(a)** Flow chart of proposed methodology for real-time optimisation of filtration in SAnMBRs. **(b)** Flow chart of model-based supervisory controller.

11.2.3.1 Model description

The filtration model used in this study [11.23] gives the dynamic evolution of TMP by applying Eq. 11.6 and Eq. 11.7 (see Chapters 7 and 8).

$$TMP(t) = J \cdot \mu \cdot R_T \qquad \textbf{Eq. 11.6}$$

$$R_T = R_M + R_C + R_I = R_M + \omega_C \cdot \alpha_C + \omega_I \cdot \alpha_I \qquad \textbf{Eq. 11.7}$$

where ω_I is the mass of irreversible fouling per membrane area and α_I is the average specific irreversible fouling resistance.

To model the dynamics of ω_C and ω_I a black-box approach was considered in the model. This approach features 3 suspended components: MLTS concentration (X_{TS}); dry mass of cake on the membrane surface (X_{m_C}); and dry mass of irreversible fouling on the membrane surface (X_{m_I}). In addition, a total of four kinetically governed physical processes are included in the model approach: (1) cake layer build-up during filtration; (2) cake layer removal using biogas sparging to scour the membrane; (3) cake layer removal during back-flushing; and (4) irreversible fouling consolidation.

Further details of this filtration model can be found in Chapter 7 and Robles *et al*. [11.23]. The model parameters were calibrated beforehand at the same pilot plant [11.23], and the same values were used in this study.

11.2.3.2 Objective functions of the supervisory controller

The aim of dynamically optimising the inputs of the advanced controller was to minimise the operating costs and control error in each specific scenario. To this end, two different objective functions were evaluated in the model-based supervisory controller (see step I and L in Figure 11.1b): controller performance (*IAE*, Eq. 11.8) and overall operating cost (C_{TOTAL}, Eq. 11.14). Eq. 11.8 was used to select the optimum combination of fuzzy-logic control parameters resulting in the lowest *IAE*.

$$IAE = \int |eFR_C| dt \qquad \textbf{Eq. 11.8}$$

where $|eFR_C|$ is the absolute error of FR_C.

Eq. 11.14 was used in order to identify the optimum combination of set points for the advanced controller resulting in minimum operating costs. The unit chosen for the evaluation of the objective function was the net volume of treated wastewater (V_T, m^3), taking into account both filtration (positive term) and back-flushing (negative term). Taking into account the main parameters that affect the costs of membrane technology [11.25; 11.26; 11.27], the following terms were considered when defining this function: cost of membrane scouring by biogas sparging (€ m^{-3}); cost of pumping sludge through the membrane tank (€ m^{-3}); cost of pumping permeate during filtration and back-flushing (€ m^{-3}); cost of chemical reagent required to remove the corresponding irreversible fouling generated during filtration (€ m^{-3}); and cost of replacing membrane at end of membrane lifespan related to the corresponding irreversible fouling generated during filtration (€ m^{-3}).

The operating cost of the blower (adiabatic compression), sludge recycling pump and permeate pump was calculated by applying Eq. 11.9, Eq. 11.10 and Eq. 11.11, respectively. The energy term (E_{COST}) considered in this study was €0.138 per kWh (in keeping with current electricity rates and prices in Spain).

$$C_B = \frac{M \cdot R \cdot T_{gas}}{(\alpha - 1)\eta_{blower}} \left[\left(\frac{P_2}{P_1} \right)^{\frac{\alpha-1}{\alpha}} - 1 \right] \cdot \frac{E_{COST}}{V_T} \qquad \textbf{Eq. 11.9}$$

where C_B (€ m^{-3}) is the operating cost of membrane scouring by biogas sparging, M (mol s^{-1}) is the molar flow rate of biogas, R (kJ mol^{-1} K^{-1}) is the gas constant for biogas, P_1 (atm) is the absolute inlet pressure, P_2 (atm) is the absolute outlet pressure, T_{gas} (K) is the biogas temperature, α is the compression index and η_{blower} is the overall mechanical and electrical efficiency of the blower.

$$C_{SRF} = q \cdot \rho_{sludge} \cdot g \frac{\left[\left(\frac{(L + L_{eq}) f \cdot V^2}{D \cdot 2 \cdot g} \right)_{asp} + \left(\frac{(L + L_{eq}) f \cdot V^2}{D \cdot 2 \cdot g} \right)_{imp} \right] + [z_1 - z_2]}{\eta_{pump}} \cdot \frac{E_{COST}}{V_T} \qquad \textbf{Eq. 11.10}$$

where C_{SRF} (€ m^{-3}) is the operating cost of pumping the sludge, q (m^3 s^{-1}) is the volumetric flow rate, ρ_{sludge} (kg m^{-3}) is the sludge density, g (m s^{-1}) is the acceleration of gravity, L (m) is the pipe length, L_{eq} (m) is the equivalent pipe length of accidental pressure drops, V (m s^{-1}) is the fluid velocity, f is the friction factor, D (m) is the pipe diameter, Z_1-Z_2 (m) is the difference in height and η_{pump} is the overall mechanical and electrical efficiency of the pump.

$$C_{stage} = \frac{q_{stage} \cdot TMP_{stage}}{\eta_{pump}} \cdot \frac{E_{COST}}{V_T} \qquad \textbf{Eq. 11.11}$$

where C_{stage} (€ m^{-3}) is the operating cost of pumping permeate during the corresponding operating stage (*i.e*. filtration or back-flushing), TMP_{stage} (Pa) is the TMP during the corresponding operating stage (*i.e*. filtration or back-flushing), q_{stage} (m^3 s^{-1}) is the volumetric flow rate during the corresponding operating stage (*i.e*. filtration or back-flushing) and η_{pump} is the overall mechanical and electrical efficiency of the pump.

As regards membrane cleaning, the proportional cost of the reagents needed to clean the irreversible fouling produced during filtration was contemplated when evaluating total operating costs (Eq. 11.12). The upper threshold of irreversible fouling resistance at which membrane cleaning starts ($\Delta R_{I,MAX}$) was set to 10^{13} m^{-1} (established on the basis of experimental results). Two reagents were contemplated for cleaning the membranes: citric acid and sodium hypochlorite (NaOCl). The cleaning protocol considered consisted of a 5-hour cleaning session with acid (2000 ppm of citric acid) at pH 2.5, followed by a 5-hour oxidising cleaning session (2000 ppm of NaOCl) at pH 12.

$$C_{REAGENTS} = \frac{\Delta R_{I,filtration}}{\Delta R_{I,MAX}} \cdot \frac{\left(X_{AC} \cdot AC_{COST} + X_{NaOCl} \cdot NaOCl_{COST}\right)}{V_T} \qquad \textbf{Eq. 11.12}$$

where $C_{REAGENTS}$ (€ m^{-3}) is the proportional cost of the reagents needed to clean the irreversible fouling produced during filtration, $\Delta R_{I,filtration}$ is the increase in the irreversible fouling resistance during filtration, X_{AC} (kg cleaning^{-1}) is the amount of citric acid required for membrane cleaning, AC_{COST} (€ kg^{-1}) is price of citric acid (constant), X_{NaOCl} (kg cleaning^{-1}) is the amount of NaOCl required for membrane cleaning and $NaOCl_{COST}$ (€ kg^{-1}) is the price of NaOCl (constant).

As regards membrane lifespan, the cost of replacing the membrane was contemplated in order to evaluate the entire operating cost (Eq. 11.13). The maximum total contact with chlorine permissible before membrane replacement according to the supplier is 500,000 ppm-hours cumulative.

$$C_{LIFESPAN} = \frac{\Delta R_{I,filtration}}{\Delta R_{I,MAX}} \cdot \frac{M_{COST} \cdot A \,/\, N_{C,MAX}}{V_T} \qquad \textbf{Eq. 11.13}$$

where $C_{LIFESPAN}$ (€ m^{-3}) is the cost of membrane replacement due to irreversible fouling, M_{COST} (€ m^{-2}) is the price per square metre of membrane area, A (m^{-2}) is the membrane area and $N_{C,MAX}$ is the

maximum number of times the membrane can be cleaned (50 times = 500,000 ppm of maximum accumulated chloride tolerance / 2000 ppm of citric acid per cleaning / 5 hrs contact).

The prices of the membrane area and chemical reagents used in our full-scale calculations were those given by the respective suppliers.

On the basis of the different terms contemplated when evaluating total costs (C_{TOTAL}, € m^{-3}), the following objective function was defined in this study:

$$C_{TOTAL} = C_B + C_{SRF} + C_{stage} + C_{REAGENTS} + C_{LIFESPAN} \quad \textbf{Eq. 11.14}$$

11.2.3.3 Morris screening method

The Morris screening method [11.19] is a one-factor-at-a-time (OAT) method of global sensitivity analysis that evaluates the distribution of the elementary effects (EE_i) of each input factor in a model upon each output, and produces basic statistics then used to gather sensitivity information. In this study the scaled elementary effect (SEE_i) concept proposed by Sin and Gernaey [11.28] was applied. EE_i is in itself a local measure of sensitivity, but this drawback is overcome by repeating EE_i calculations in the input region of interest using Morris's efficient random sampling strategy, which is obtained by using a trajectory-based design. This sampling strategy then evaluates the EE_i of each parameter with the same step size but at different initial points in the parameter region of interest. Finally, the analysis of the distribution (F_i) of the elementary effects of each input factor will determine the relative importance of the input factors, providing a good approximation of a global sensitivity analysis.

In this study we applied a modified version of the trajectory-based sampling strategy proposed in Campolongo *et al.* [11.29]. This methodology [11.30] consists of maximising distances between *r* Morris trajectories that are selected from a defined group of *M* initial trajectories (*i.e.* maximising their dispersion in the input space). Further details of this sampling strategy can be found in Ruano *et al.* [11.21].

In accordance with Saltelli *et al.* [11.30], the mean (μ), standard deviation (σ) and absolute mean (μ^*) of the SEE_i values of each distribution F_i were considered in this study to be sensitivity measures. The measure μ^* was used to rank the parameters in order to systematically differentiate slightly/non-

influential parameters (low μ^*) from highly-influential parameters (high μ^*). The optimal number of repetitions of elementary effects calculations (r_{opt}) for each F_i was calculated using a constant resolution of p = 4. To this end, r was increased until the ranking of parameters (based on μ^*) remained more or less stable, *i.e.* the type II error was minimised (type II error means identifying an important factor as insignificant). This stability was numerically evaluated using the position index $PF_{ri \to rj}$, which enables an optimal value for r (r_{opt}) to be determined [11.31]. For given rankings obtained by r_i and r_j, the index $PF_{ri \to rj}$ is defined by Eq. 11.15.

$$PF_{r_i \to r_j} = \sum_{k=1}^{k} \frac{Abs\left(P_{k,i} - P_{k,j}\right)}{\mu_{P_{k,i},P_{k,j}}} \qquad \textbf{Eq. 11.15}$$

where $P_{k,i}$ is the position of the k^{th} parameter in the ranking obtained by r_i; $P_{k,j}$ is the position of the k^{th} parameter in the ranking obtained by r_j; and $\mu_{P_{k,i},P_{k,j}}$ is the average of the positions of the k^{th} parameter in the ranking obtained by r_i and r_j.

Once r_{opt} was found, the graphical Morris approach was used to identify the highly-influential parameters of the controller. In this approach, the values of μ and σ obtained for all SEE_i values of each F_i are shown, together with two lines corresponding to $\mu_i \pm 2SEM_i$, where SEM_i is the standard error of the mean that can be calculated thus: $SEM_i = \sigma_i / \sqrt{r}$. Parameters lying outside the wedge formed by the two lines corresponding to $\mu_i = \pm 2SEM_i$ are deemed in this study to be slightly/non-influential [11.19].

The Morris screening method was applied to different number of r, chosen from M =1000 initial Morris trajectories, until the ranking of significant parameters remained more or less stable, as measured quantitatively by the index $PF_{ri \to rj}$. In this sensitivity study, two output variables were used: overall operating cost (Eq. 11.14), which is related to the advanced controller set points; and *IAE* (Eq. 11.8), which evaluates the performance of the fuzzy-logic controller.

In this study, the distribution of the elementary effects of each input factor in the model upon the corresponding output was evaluated by modifying all the input factors of the advanced controller, *i.e.* set points (FR_{C_SP}, TMP_{MAX}, $\%K_{20}$ and SRF_{SP}) and fuzzy-logic control parameters (*CT*, centre and amplitude for each input fuzzy set, and singleton value for each output fuzzy set). Nevertheless, two differentiated rankings were established in order to evaluate the influence of the different control inputs: one featuring the set points and other, the fuzzy-logic control parameters.

11.2.3.4 Monte Carlo method

In order to optimise a controller, suitable initial values must be selected for inputs identified as highly-influential. In addition, slightly/non-influential inputs must be set to adequate values in order to enhance the optimisation process. The Monte Carlo method based on trajectory-based random sampling was used in our study to select adequate values for both highly-influential and slightly/non-influential inputs. Hence, the combination of advanced controller set points and fuzzy-logic control parameters giving the minimum operating cost (Eq. 11.14) and minimum *IAE* (Eq. 11.8), respectively, was selected as the initial values of the model-based supervisory controller. This Monte Carlo method was applied to the different Morris simulations carried out in search of r_{opt} because a suitable coverage of the input region was assumed.

11.2.3.5 Dynamic optimisation of the advanced control system

The optimisation of the set points of the advanced control system consisted of minimising C_{TOTAL} (see Eq. 11.14) and was obtained using 6-hour simulations (see step J Figure 11.1b) during the different stages of membrane operations. As mentioned before, apart from optimising the set points of the controller, the fuzzy-logic control parameters must be adjusted for each operating scenario. This step consisted of minimising *IAE* (see Eq. 11.8) and was carried out using 1-hour filtration-stage simulations (see step M in Figure 11.1b) since, as mentioned before, the fuzzy-logic controller only works during filtration. These 1-hour filtration-stage simulations included intakes with a J_{20} step to evaluate *IAE* over time in each operating scenario.

Both optimisation algorithms were applied using the subspace trust region method [11.31], based on the interior-reflective Newton method (implemented in MATLAB® LSQNONLIN function), and the Runge-Kutta method (MATLAB® ODE45 function). The termination tolerance on the function value of 1% was selected in this study.

11.2.3.6 Simulation strategy

MATLAB® was used in this study to simulate the above-mentioned filtration model. The Runge-Kutta method (MATLAB® ode45 function) was selected as the integration method.

11.2.3.6.1 Morris screening method and Monte Carlo method

The simulation strategy applied to the Morris screening method and the Monte Carlo method entailed 24 hours of continuous operation and was conducted using data for the following dynamic operating scenarios: MLTS entering the membrane tank: 17 g L^{-1}; biogas recycling flow (BRF): approx. 4 to 12 Nm^3 h^{-1}; and J_{20} from approx. 4 to 12 LMH. The dynamics of J_{20} considered the fluctuations typical in the intake of WWTPs. For this purpose, the standard dry weather influent records (updated in 2006) recommended by Copp [11.32] were used as shown in Robles *et al*. [11.17].

Table 11.1 shows the default values of the inputs to the advanced control system and the uncertainty used for the sensitivity analysis. All the input factors were varied according to a uniform distribution with an uncertainty equal to 50% of the default value. The uncertainty factor for the advanced controller set points was established on the basis of technical knowledge of the process and operating constraints associated with process and controller performance. In addition, the uncertainty factor for the fuzzy-logic control parameters was selected taking into account that the set points of the advanced control system were also modified in the simulations.

Table 11.1 Control inputs (including advanced controller set points and fuzzy-logic control parameters): default values, interval of variation or uncertainty, respectively, and initial values of model-based supervisory controller. [**] *corresponding to dynamically optimised inputs identified as influential.*

Parameter	Units	Default value	Minimum	Maximum	Initial values
FR_{C_SP}	mbar min^{-1}	4	0	8	0 **
$\%K_{20}$	%	0.65	0.5	0.8	0.6
TMP_{MAX}	bar	0.45	0.3	0.6	0.3 **
SRF_{SP}	L h^{-1}	2200	1700	2700	2367 **
CT	s	20	10	30	23.3 **
FREaN	mbar min^{-1}	0.4	0.2	0.6	0.33
FREaP	mbar min^{-1}	0.4	0.2	0.6	0.2
FREaZ	mbar min^{-1}	0.4	0.2	0.6	0.2
FREcN	mbar min^{-1}	-1	-1.5	-0.5	-0.5
FREcP	mbar min^{-1}	0	-0.5	0.5	1.5
FREcZ	mbar min^{-1}	1	0.5	1.5	0.17
FRDEaP	mbar min^{-1}	0.9	0.45	1.35	1.35
FRDEcP	mbar min^{-1}	2	1	3	1
FRAEaN	mbar min^{-1}	1.6	0.8	2.4	0.8
FRAEaP	mbar min^{-1}	1.6	0.8	2.4	1.87
FRAEaZ	mbar min^{-1}	1.6	0.8	2.4	1.87
FRAEcN	mbar min^{-1}	-4	-6	-2	-6
FRAEcP	mbar min^{-1}	0	-2	2	2 **
FRAEcZ	mbar min^{-1}	4	2	6	-2
VBRFsHN	Nm^3 h^{-1}	-0.4	-0.6	-0.2	-0.33
VBRFsHP	Nm^3 h^{-1}	-0.16	-0.24	0.08	0.2 **
VBRFsLN	Nm^3 h^{-1}	0.16	0.08	0.24	-0.08
VBRFsLP	Nm^3 h^{-1}	0.4	0.2	0.6	0.13

11.2.3.6.2 Model-based supervisory controller

The performance of the model-based supervisory controller was assessed by running the above-mentioned filtration model for 24 hours continuously. In order to validate this supervisory controller, the MLTS entering the membrane tank was set to 20 g L^{-1} whilst J_{20} varied according to the dynamics typical of WWTP intake.

In this study, *OT* was set to 1 hour. The overall computational cost for dynamically optimising the advanced controller was around 5 minutes (using a PC with 8 GHz Intel® CORE™ i5 processor).

11.3 Results and discussion

11.3.1 Sensitivity analysis results

Table 11.2 shows the resulting sensitivity measures (μ^* and σ) of the fuzzy-logic control parameters. As can be seen in this table, an increase in *r* resulted in a greater similarity between the sensitivity measures of the control parameters (see, for instance, the positions of *CT* and *FREaP* in the significance rankings). Table 11.3 shows the $PF_{ri \rightarrow rj}$ of the different number of trajectories evaluated. $PF_{ri \rightarrow rj}$ tended to decrease as the number of runs increased (from 50 to 80), which indicates a greater similarity between the positions of the parameters in the compared rankings. This reveals that, as regards this fuzzy-logic control, low values of *r* did not enable a suitable estimate of sensitivity measures because either the system was very non-linear or the input factors involved considerable uncertainty. It is therefore necessary to find an appropriate *r* in order to avoid type I and type II errors (false positive and false negative, respectively). For instance, in this study, when $r = 60$, *CT* was 10th in the sensitivity ranking, whereas when $r = 80$, it was 3rd.

$r = 80$ was selected as the optimal number of repetitions (r_{opt}) for the fuzzy-logic control evaluation: not only because of the low $PF_{70 \rightarrow 80}$ but also because it was a compromise between the stability of the parameters ranked highest (see Table 11.3) and computational cost. These results tally with previous studies of similar fuzzy-logic controllers [11.21]. When $r_{opt} = 80$, the overall cost of evaluating the model was 1920 simulations (simulations = $r \cdot (k+1)$; $r = 80$; $k = 23$). The computational cost of one simulation (involving 24 hours of operation) was approximately 1 minute when using a PC with 8 GHz Intel® CORE™ i5 processor.

Table 11.2 Sensitivity analysis results of fuzzy-logic control parameters: sensitivity measures at different values of *r*.

r = 50			***r = 60***		
Parameter	***μ****	***σ***	**Parameter**	***μ****	***σ***
FREaZ	0.746	1.755	***FREaP***	0.916	1.886
CT	0.671	1.340	***VBRFsLP***	0.833	1.854
FREcZ	0.658	1.651	***VBRFsHP***	0.780	1.989
FRAEaP	0.632	2.008	***FRAEcP***	0.776	2.140
VBRFsLN	0.609	1.826	***FREcP***	0.689	1.714
VBRFsLP	0.608	1.371	***FRAEaN***	0.662	1.882
FRAEcP	0.604	1.369	***FRAEcZ***	0.654	1.566
FREaP	0.543	1.189	***FRDEcP***	0.610	1.116
FRAEcZ	0.539	1.349	***FRDEaP***	0.596	1.331
FRDEaP	0.515	1.589	***CT***	0.549	1.050
FRAEcN	0.506	1.221	***FREaN***	0.508	1.215
FRDEcP	0.497	1.139	***VBRFsHN***	0.492	1.468
FRAEaZ	0.472	1.133	***FRAEaP***	0.479	1.045
FREcP	0.438	0.832	***FREcZ***	0.454	1.136
VBRFsHN	0.431	1.492	***FREaZ***	0.452	0.989
VBRFsHP	0.396	0.831	***VBRFsLN***	0.408	1.038
FRAEaN	0.319	0.702	***FRAEaZ***	0.405	0.979
FREcN	0.308	0.721	***FREcN***	0.398	0.849
FREaN	0.299	0.604	***FRAEcN***	0.390	0.861
r = 70			***r = 80***		
Parameter	***μ****	***σ***	**Parameter**	***μ****	***σ***
VBRFsLP	1.163	1.285	***FREaP***	0.846	1.763
FREaP	0.950	2.002	***VBRFsLP***	0.843	1.808
FREcP	0.803	1.742	***CT***	0.836	1.887
CT	0.724	1.731	***FRAEcP***	0.835	2.254
VBRFsHP	0.717	1.804	***FRAEcZ***	0.681	1.645
FRDEcP	0.708	1.880	***VBRFsHP***	0.639	1.741
FRAEcP	0.707	0.859	***FREcP***	0.612	1.542
FREaZ	0.669	1.424	***FRDEcP***	0.577	1.062
FRAEcZ	0.646	1.658	***FRDEaP***	0.576	1.249
FRAEaN	0.636	1.666	***FREaZ***	0.570	1.596
FRDEaP	0.632	1.355	***FRAEaN***	0.559	1.672
FREaN	0.601	1.707	***FRAEaZ***	0.519	1.457
FREcN	0.595	1.264	***VBRFsHN***	0.506	1.433
FRAEaZ	0.553	1.741	***FREaN***	0.476	1.238
VBRFsHN	0.507	1.373	***VBRFsLN***	0.454	1.081
FRAEaP	0.479	1.302	***FRAEaP***	0.426	0.951
FRAEcN	0.469	1.415	***FREcZ***	0.349	0.849
VBRFsLN	0.453	1.290	***FREcN***	0.345	0.761
FREcZ	0.437	0.649	***FRAEcN***	0.343	0.806

Table 11.3 Sensitivity analysis results of fuzzy-logic control parameters: position factors ($PF_{ri \rightarrow rj}$) at different variations in *r*.

$r_i \rightarrow r_j$	50 → 60	60 → 70	70 → 80
$PF_{ri \rightarrow rj}$	15.2	7.1	5.7

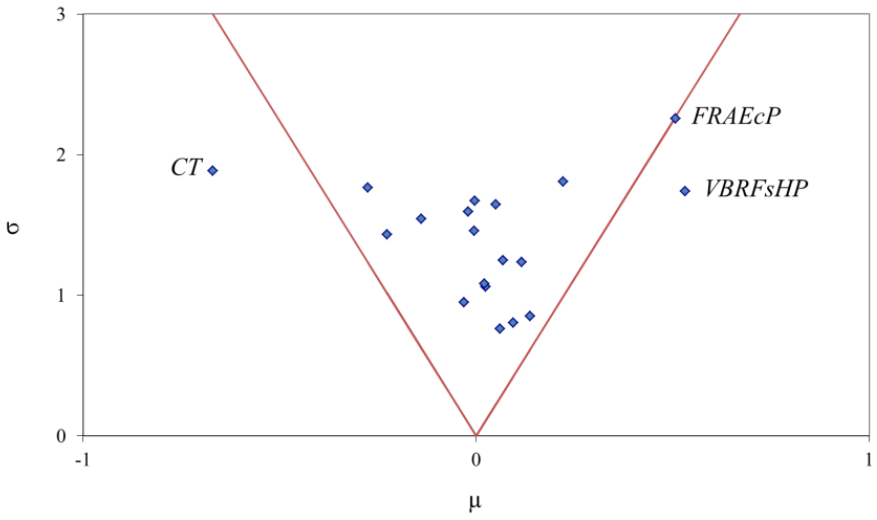

(a)

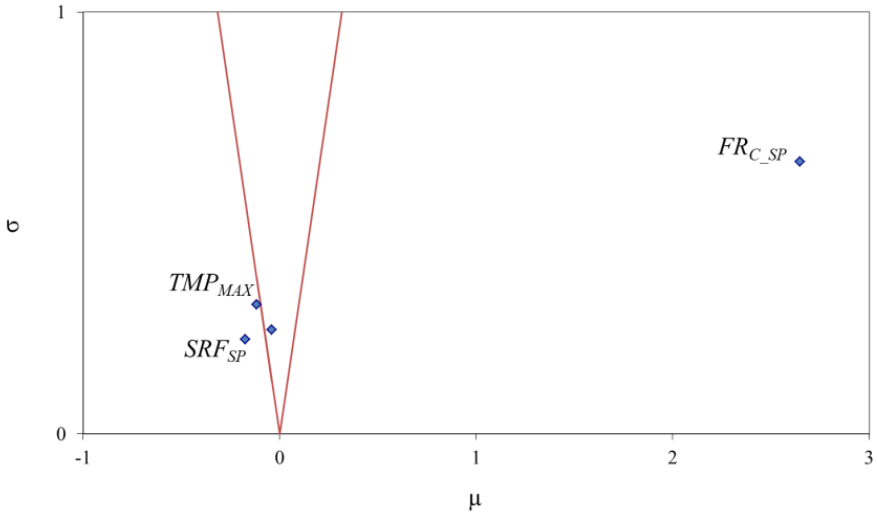

(b)

Figure 11.2 Sensitivity analysis results of: **(a)** fuzzy-logic control parameters (μ versus σ when final value of r = 80); and **(b)** advanced controller set points (μ versus σ when final value of r = 40). Lines plotted according to μ_i = ± 2 SEM_i.

Figure 11.2a shows the graphical Morris approach (using r = 80) applied to evaluate the sensitivity of the fuzzy-logic controller. In this case, 3 control parameters were identified as highly-influential: (1)

positive membership function centre of the accumulated FR_C error (FRAEcP, μ^* = 0.835 and σ = 2.254); (2) *high positive singleton value of the increase in BRF* (*VBRFsHP,* μ^* = 0.639 and σ = 1.741); and (3) *control time* (*CT,* μ^* = 0.836 and σ = 1.887). These results tally with experienced-based knowledge about control systems of this type, since *CT* is usually recognised as one of the most important parameters. High *CT* values would result in a slow response to changes in process variables, whilst low values might cause an overly fast response resulting in instabilities. *VBRFsHP* is important in the control system because it enables *BRF* to respond quickly to increasing fouling rates. The value of *FRAEcP* is important because it aims to identify possible increases in reversible fouling on the membrane surface. It is important to mention that the build-up of reversible fouling affects not only operating costs related to filtration, but also membrane chemical cleaning and membrane replacement cost due to higher irreversible fouling propensities (high reversible fouling usually means high irreversible fouling propensities).

The other fuzzy-logic control parameters lay inside the wedge formed by the two lines plotted according to $\mu_i = \pm 2SEM_i$ and were therefore classified as slightly/non-influential.

Table 11.4 Sensitivity analysis results of advanced controller set points: sensitivity measures at different values of *r*.

r = 10			***r = 20***		
Parameter	***μ ****	***σ***	**Parameter**	***μ ****	***σ***
$\boldsymbol{FR_{C\_SP}}$	2.772	0.571	$\boldsymbol{FR_{C\_SP}}$	2.556	0.519
$\boldsymbol{\%K_{20}}$	0.211	0.348	$\boldsymbol{\%K_{20}}$	0.239	0.316
$\boldsymbol{TMP_{MAX}}$	0.157	0.233	$\boldsymbol{TMP_{MAX}}$	0.215	0.354
$\boldsymbol{SRF_{SP}}$	0.127	0.141	$\boldsymbol{SRF_{SP}}$	0.191	0.193
r = 30			***r = 40***		
Parameter	***μ ****	***σ***	**Parameter**	***μ ****	***σ***
$\boldsymbol{FR_{C\_SP}}$	2.602	0.490	$\boldsymbol{FR_{C\_SP}}$	2.650	0.645
$\boldsymbol{TMP_{MAX}}$	0.276	0.375	$\boldsymbol{SRF_{SP}}$	0.217	0.225
$\boldsymbol{SRF_{SP}}$	0.186	0.166	$\boldsymbol{TMP_{MAX}}$	0.213	0.306
$\boldsymbol{\%K_{20}}$	0.142	0.235	$\boldsymbol{\%K_{20}}$	0.188	0.246

Table 11.4 shows the sensitivity measures (μ^* and σ) of the advanced controller set points. As can be seen in this table, an increase in the number of elementary effects calculations (*i.e.* an increase in *r*) also modified the sensitivity measures of the inputs. Table 11.5 shows the $PF_{ri \rightarrow rj}$ values of the

different r values evaluated. As Table 11.5 shows, $PF_{ri \rightarrow rj}$ was close to zero when r was increased (from 30 to 40) and remained at zero at higher values of r (data not shown). Therefore, r = 40 was selected as r_{opt} for evaluating the advanced controller set points.

Table 11.5 Sensitivity analysis results of advanced controller set points: position factors ($PF_{ri \rightarrow rj}$) at different variations in r.

$r_i \rightarrow r_j$	$10 \rightarrow 20$	$20 \rightarrow 30$	$30 \rightarrow 40$
$PF_{ri \rightarrow rj}$	0	1.35	0.8

Figure 11.2b shows the graphical Morris approach (using r = 40) adopted to evaluate the sensitivity of the advanced controller at the four set points. This graphical Morris approach was used to identify the highly-influential parameters of this controller, which lay outside the wedge formed by two lines plotted according to $\mu_i = \pm 2SEM_i$. Three of these 4 input factors were identified as highly-influential: (1) FR_{C_SP} (μ^* = 2.650 and σ = 0.645); (2) SRF_{SP} (μ^* = 0.217 and σ = 0.225); and (3) TMP_{MAX} (μ^* = 0.213 and σ = 0.306). According to the Morris theory, parameters with a high μ^* and low σ are expected to be linear and additive. This is the case of FR_{C_SP}, which affects the control output considerably. This behaviour is desirable when using optimisation algorithms to estimate parameters. Hence, in our study, the cost function is affected considerably by slight changes in FR_{C_SP}.

The results shown in Figure 11.2b tally with our knowledge of the process. FR_{C_SP} is the most important control set point due to its final impact on overall operating costs. High FR_{C_SP} values result in low membrane scouring costs, but higher chemical cleaning costs and membrane replacement costs due to increasing fouling propensity. On the other hand, operating at low FR_{C_SP} values requires high gas sparging intensities in order to minimise cake-layer build-up, which, consequently, minimises the cost of membrane chemical cleaning and membrane replacement due to reducing fouling propensity. TMP_{MAX} is important because it affects the energy required to pump permeate (*i.e.* an increase in TMP increases the energy needed to pump permeate). However, TMP_{MAX} also determines the start of back-flushing, *i.e.*, the higher the TMP_{MAX}, the lower the back-flushing frequency. Hence, it is also necessary to optimise the value of this parameter. The value of SRF_{SP} is important because it affects not only the cost of pumping sludge through the membrane tank, but also the energy needed to minimise the build-up of cake. In this respect, SRF_{SP} determines the MLTS concentration in the membrane tank ($MLTS_{MT}$) at a given J_{20}, thus affecting the energy required for membrane scouring (*i.e.* an increase in $MLTS_{MT}$ means an increase in BRF_{SP} at a given FR_{C_SP}).

Only one advanced controller set point lay inside the wedge formed by the two lines plotted according to $\mu_i = \pm 2SEM_i$. It was identified as slightly/non-influential and tallied with $\%K_{20}$. This was attributed to the interactive effects between TMP_{MAX} and $\%K_{20}$ (*i.e*. both of them determine when back-flushing starts). In this respect, since TMP_{MAX} was identified as highly-influential, the impact of $\%K_{20}$ on the output was contemplated implicitly. Nevertheless, $\%K_{20}$ was included in the advanced control system because it adjusts the back-flushing frequency by taking into account fluctuations in membrane permeability over time and not merely a single fixed threshold value (e.g. TMP_{MAX}). TMP_{MAX} was originally defined as the security threshold.

11.3.2 Monte Carlo method results

As mentioned before, the Monte Carlo method was used to select the initial values of the inputs to the advanced control system (including set points and fuzzy-logic control parameters).

As regards the advanced controller set points, considerable variations were observed in the total operating cost of the simulations conducted in this study. They ranged from €0.17 to 0.32 per m^3 depending on the set-point value combination. Therefore, considerable energy savings could be made by selecting adequate initial values for these control inputs.

As regards the fuzzy-logic control, adequate initial values must be selected for the control parameters in order to reduce *IAE* and fine-tune the controller. In this respect, although most of the simulations resulted in low *IAE* values, it was observed that *IAE* rose from 0.013 to 7.728 when inadequate combinations of these control inputs were selected.

The combination of control inputs selected by the Monte Carlo method is shown in Table 11.1 (those values giving the lowest output variables, *IAE* and operating costs). Although this method does not give the optimum input combination, because it is based on a discrete search, the output variables were at least partly optimised after a global search (based on trajectory-based random sampling). From this initial point in the parameter space, further optimisation was carried out but the highly-influential parameters were modified, as explained in the following section.

11.3.3 Performance of model-based supervisory controller

11.3.3.1 Optimisation of fuzzy-logic controller

Figure 11.3 shows the evolution of the optimised values of the fuzzy-logic control parameters identified as highly-influential using the Morris screening method. As mentioned before, the fuzzy-logic control parameters were calibrated over time to fine-tune the advanced controller. Figure 11.3 shows that the greatest set-point modification occurred during the operating period when daily J_{20} was highest (see hours 10 to 13 in Figure 11.4a). In this respect, it is important to highlight that the operating J_{20} affects not only the daily net volume of treated water, but also the operating costs (e.g. the energy needed for membrane scouring). Therefore, it is essential to optimise the performance of the fuzzy-logic controller periodically in order to enhance the performance of the advanced control system.

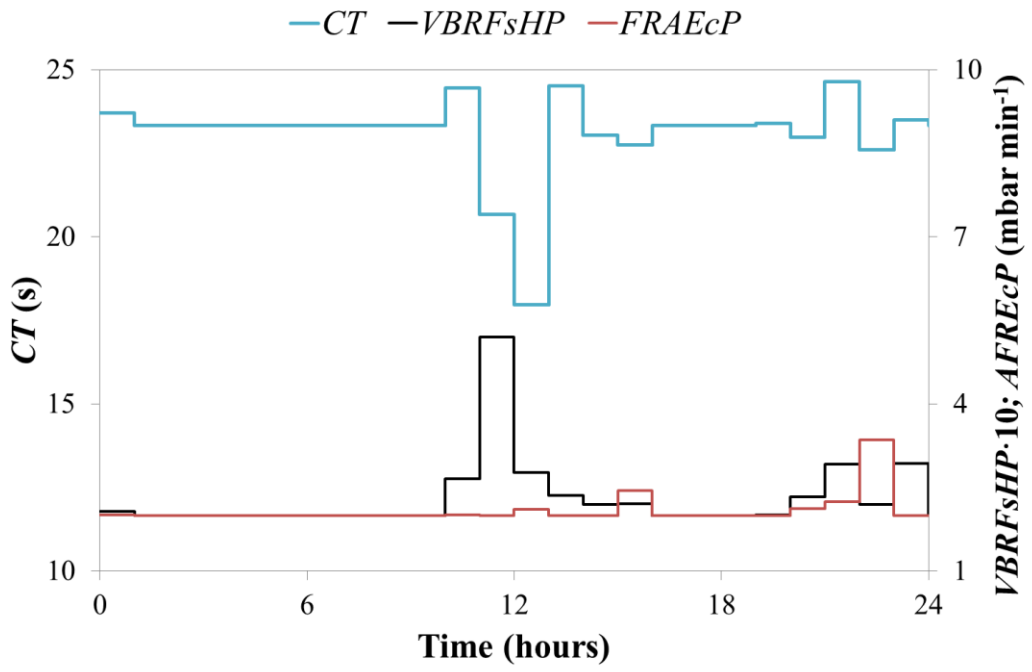

Figure 11.3 Evolution of optimised values of fuzzy-logic control parameters identified as highly-influential using the Morris screening method.

11.3.3.2 Optimisation of set points of advanced controller

Figure 11.4 shows the optimised values for the advanced controller set points identified as highly-influential using the Morris screening method, as well as the simulation results of the main operating variables when performing the model-based supervisory controller.

Figure 11.4a shows the evolution of SRF_{SP}, $MLTS_{MT}$ and J_{20}. As this figure shows, the behaviour of SRF_{SP} was similar to J_{20} but this evolution was not proportional. In this respect, the model-based supervisory controller set SRF_{SP} to a value that allowed total operating costs to be minimised whilst taking the values of the other control set points into account (*i.e.* FR_{C_SP} and TMP_{MAX}). Indeed, the supervisory controller optimised SRF_{SP} in order to establish adequate $MLTS_{MT}$ levels (see Figure 11.4a) that minimise the energy required not only for pumping sludge, but also for gas sparging and filtration.

Figure 11.4b shows the evolution of FR_{C_SP}, FR_C and *BRF*. It can be seen that the highest FR_{C_SP} occurred in hours 2 to 9, when the minimum J_{20} was applied. This made it possible to reduce the operating *BRF* considerably with no significant increase in FR_C. On the contrary, the lowest FR_{C_SP} was applied when operating at high J_{20} values (see Figure 11.4a) since a reduction in fouling enables irreversible fouling to be minimised and therefore the membrane lifespan to be maximised. As Figure 11.4b shows, the controller operated most of the time at the minimum threshold value established for *BRF* (4 $Nm^3\ h^{-1}$). From 0.5 to 9 hours, excessive gas sparging was used to scour the membrane because the minimum *BRF* was reached, and this prevented the controller from setting FR_C to the expected set point. In these conditions, the supervisory controller suggests that operating with intermittent gas sparging would be the best option (it was not considered in this study). Working with intermittent gas sparging would decrease operating costs considerably whilst allowing the advanced controller to set FR_C to the set point established by the model-based supervisory controller. Between hours 10.5 and 11.5, on the other hand, *BRF* reached its maximum established value (14 $Nm^3\ h^{-1}$). During this period FR_C increased because it was not possible to maintain the controlled variable around its set point. Nevertheless, the controller performed properly, *i.e.* the fouling rate remained close to its set point, when there were no constraints on the gas sparging intensity.

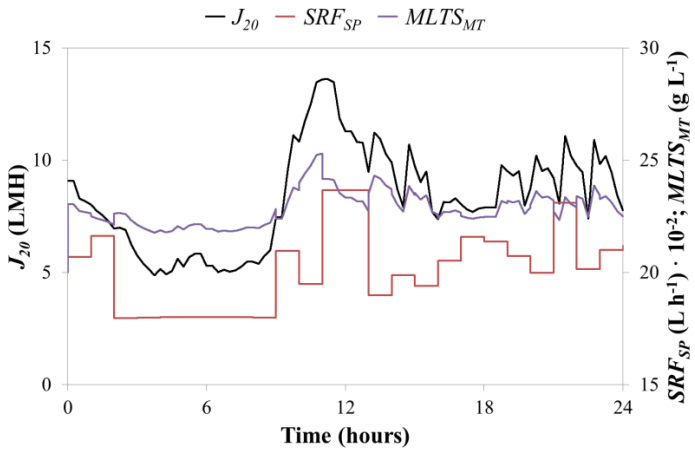

(a)

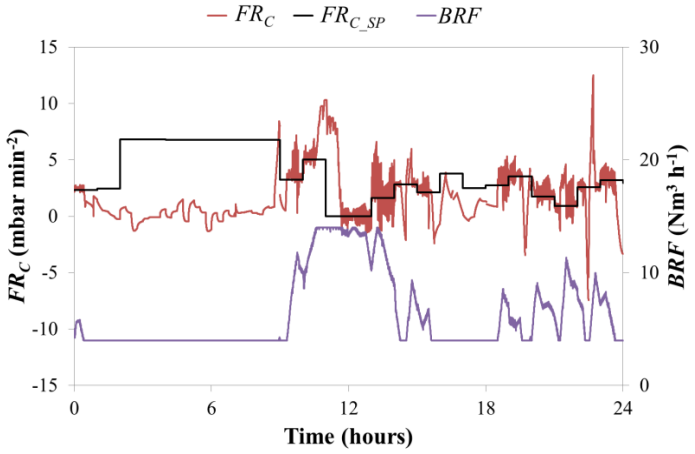

(b)

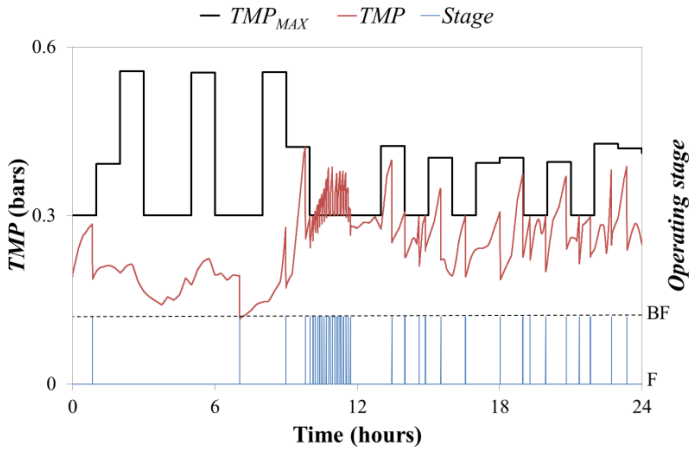

(c)

Figure 11.4 Optimised values of advanced controller set points identified as highly-influential using the Morris screening method and modelled results of main operating variables when the model-based supervisory controller was running. Evolution of: **(a)** SRF_{SP}, $MLTS_{MT}$ and J_{20}; **(b)** FR_{C_SP}, FR_C and BRF; and **(c)** TMP_{MAX}, TMP and membrane operating stage.

Figure 11.4c shows the evolution of TMP_{MAX}, *TMP* and membrane operating stage. It is important to highlight that the model-based supervisory controller modified the back-flushing frequency (indirectly set by TMP_{MAX}) according to variations in operating conditions. Hence, a higher back-flushing frequency was established when operating at high J_{20} and $MLTS_{MT}$ levels (see hours 9.5 to 11.5 in Figure 11.4a) in order to minimise irreversible fouling (directly affected by reversible fouling). Figure 11.4c shows that from hours 10 to 11.5 the established TMP_{MAX} was exceeded. This highlights the capability of the model-based supervisory controller to identify system constrains. In this respect, TMP_{MAX} was exceeded in order to fulfil the minimum filtration time set point required for back-flushing initiation (set to 200 s in this study). During this operating period the gas sparging intensity related to the maximum operating *BRF* was reached. Therefore, the fuzzy-logic controller was not able to set FR_C to the expected set point, which resulted in TMP_{MAX} being exceeded.

11.3.4 Overall performance

Figure 11.5 shows the evolution of the energy requirements and operating costs of the SAnMBR system when the model-based supervisory controller was running.

Figure 11.5a shows the evolution of total energy consumption (W_{TOTAL}), blower energy consumption (W_B), sludge recycling flow energy consumption (W_{SRF}), filtration energy consumption ($W_{filtration}$) and back-flushing energy consumption ($W_{back\text{-}flushing}$). As this figure shows, the behaviour of W_{TOTAL} was similar to J_{20}. From hours 0.5 to 9, Figure 11.5a illustrates an increase in W_{TOTAL} despite a decrease in J_{20}. As mentioned before, from hours 0.5 to 9 the controller was not able to set FR_C to the expected set point because of operating at the minimum threshold established for *BRF* (4 $Nm^3\ h^{-1}$). Therefore, during this period the process performance was not optimised, resulting in an increase in W_B due to an increase in the ratio between blower energy consumption and the net volume of treated wastewater, which confirms the advisability of using intermittent gas sparging in this study. On the other hand, a considerable decrease in W_{TOTAL} was observed from hours 10.5 to 11.5 (see Figure 11.5a). In this case, the controller could not set FR_C to the expected set point either – due to operating at the maximum *BRF* threshold (14 $Nm^3\ h^{-1}$). This behaviour resulted in a decrease in the ratio between blower energy consumption and net volume of treated wastewater due to an increase in J_{20} whilst maintaining a constant *BRF*, resulting in a considerable decrease in W_B. However, it must be said that during this operating period the membranes were operated at FR_C values higher than the optimal value, thereby increasing the propensity to irreversible fouling. A higher propensity to irreversible fouling leads to higher operating costs related to membrane chemical cleaning and membrane replacement.

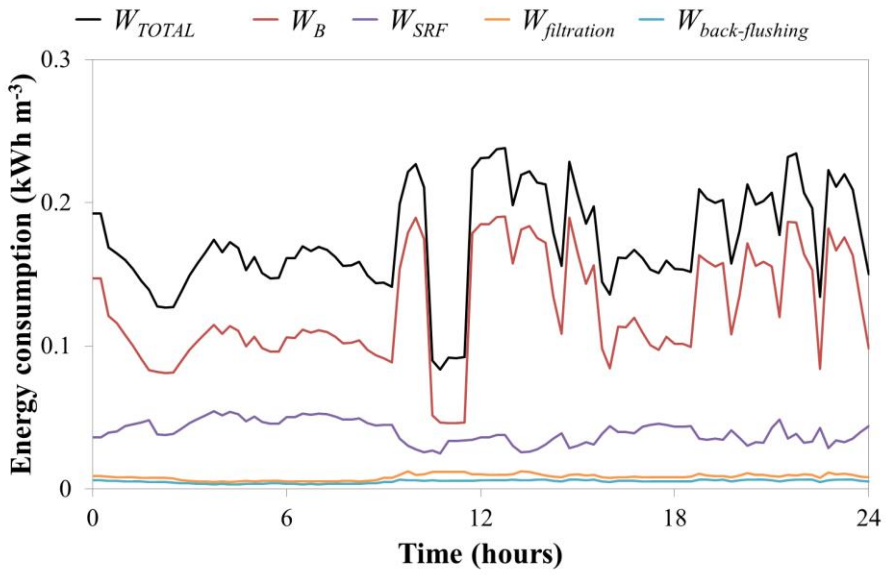

(a)

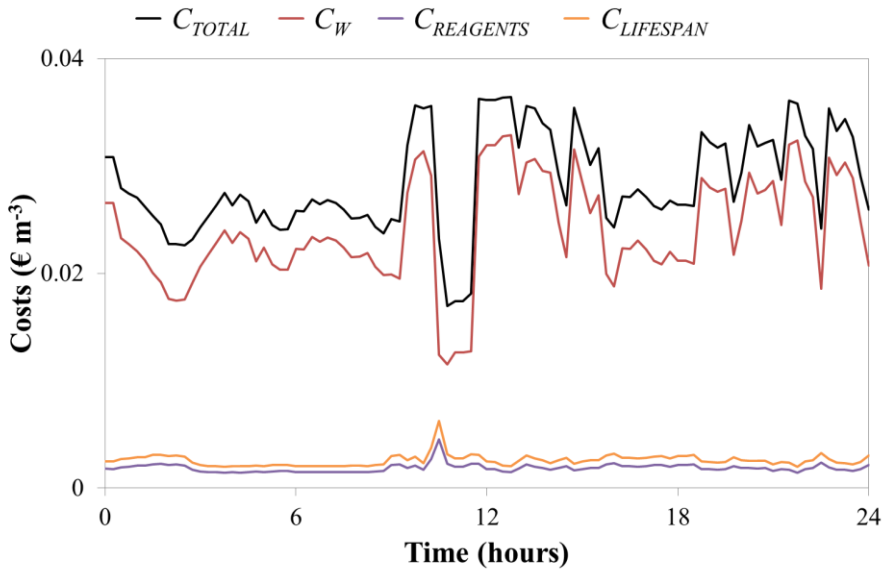

(b)

Figure 11.5 Model-based supervisory control performance. Evolution of: **(a)** total energy consumption (W_{TOTAL}), blower energy consumption (W_B), sludge recycling flow energy consumption (W_{SRF}), filtration energy consumption ($W_{filtration}$) and back-flushing energy consumption ($W_{back\text{-}flushing}$); and **(b)** total operating costs (C_{TOTAL}), energy costs (C_W), reagents costs ($C_{REAGENTS}$) and membrane replacement costs ($C_{LIFESPAN}$).

The average energy consumption of the plant when the proposed supervisory controller was running was 0.17 kWh m^{-3}. On the basis of this figure, the energy requirements for membrane scouring, sludge pumping and permeate pumping (including filtration and back-flushing) were 0.12, 0.04 and 0.01 kWh m^{-3}, respectively. Membrane scouring accounted for a considerable part of total energy requirements,

which highlights the need to optimise the intensity of gas sparging in each operating scenario. Indeed, the average energy needed to pump sludge and permeate was similar to the energy needed when the advanced controller was running alone in similar conditions (about 0.04 kWh m^{-3}); whilst the average energy for membrane scouring was considerably reduced (from about 0.16 to 0.12 kWh m^{-3}). Therefore, energy savings of up to 25% in membrane scouring can be achieved by this model-based real time supervisory controller. In addition, as mentioned before, these energy savings could be increased if intermittent gas sparging was incorporated into the advanced control system.

On the other hand, the model-based supervisory controller established a total downtime for physical cleaning of approximately 2.4% of operating time, which is slightly higher than when the advanced controller was running alone. This was because not only energy consumption but also membrane cleaning and membrane replacement were optimised (*i.e.* an increase in the frequency of physical cleaning often means a reduction in the fouling propensity).

Figure 11.5b shows the evolution of total operating costs (C_{TOTAL}), energy costs (C_W), reagents costs ($C_{REAGENTS}$) and lifespan costs ($C_{LIFESPAN}$). As expected, operating costs behave like energy requirements. In this study, the average operating cost of the SAnMBR after implementing the proposed model-based supervisory controller was about €0.028 per m^3, of which about 85.7 % was the cost of energy (about €0.024 per m^3). These results highlight the need to optimise short-term membrane filtration because it could determine the feasibility of using SAnMBR technology to treat urban wastewater.

The performance of the proposed model-based supervisory controller showed that far greater energy savings could be achieved by using the proposed model-based supervisory controller in conjunction with the advanced controller rather than using the latter alone. The proposed supervisory control system enables adequate filtration and can be adapted to new operating requirements. Moreover, the proposed supervisory controller fulfils the main requirements of real-time optimisation [11.33]: (1) robustness (*i.e.* it always finds a solution); (2) fast problem solving; (3) in certain operating conditions, it always reaches the same solution, even from different starting points; and (4) ability to identify system constraints.

11.4 Conclusions

This paper describes a model-based method for the optimisation of filtration in submerged anaerobic MBRs (SAnMBRs) that considers three statistical methods: (1) sensitivity analysis (Morris screening

method); (2) Monte Carlo method (trajectory-based random sampling); and (3) optimisation algorithm (performing as supervisory controller). The Morris screening method enabled highly-influential inputs of the advanced control system to be identified. The Monte Carlo method enabled suitable initial values to be selected for the inputs to the advanced controller. The optimisation algorithm enabled the advanced controller to be enhanced with moderate computational requirements (approx. 5 minutes) by minimising operating costs. The theoretical energy consumption of the SAnMBR when running the proposed supervisory controller was 0.17 kWh m^{-3}. Energy savings of up to 25% were achieved during membrane scouring in comparison with using the advanced controller alone. The downtime for physical cleaning was approx. 2.4% of operating time. The average operating cost of the SAnMBR system after implementing the proposed supervisory controller was approx. €0.028 per m^3, of which approx. 85.7 % were energy costs. In addition, the proposed supervisory controller fulfils the main requirements for real-time optimisation, *i.e.* robustness (*i.e.* it can always find a solution), fast problem solving, consistent conversion, and ability to identify system constraints.

11.5 Acknowledgements

This research work has been supported by the Spanish Ministry of Economy and Competitiveness (MINECO, Projects CTM2011-28595-C02-01/02) jointly with the European Regional Development Fund (ERDF), which are gratefully acknowledged.

11.6 References

11.1 W. Naessens, T. Maere, I. Nopens, Critical review of membrane bioreactor models – Part 1: Biokinetic and filtration models, Bioresour. Technol. 122 (2012) 95–106.

11.2 G. Mannina, G. Di Bella, G. Viviani, An integrated model for biological and physical process simulation in membrane bioreactors (MBRs), J. Membr. Sci. 376 (2011), 56–69.

11.3 J. Ferrer, J.J. Morenilla, A. Bouzas, F. García-Usach, Calibration and simulation of two large wastewater treatment plants operated for nutrient removal, Water Sci. Technol. 50 (2004), 87–94.

11.4 K. Derbal, M. Bencheikh-lehocine, F. Cecchi, A.-H. Meniai, P. Pavan, Application of the IWA ADM1 model to simulate anaerobic co-digestion of organic waste with waste activated sludge in mesophilic condition, Bioresour. Technol. 100 (2009), 1539–1543.

11.5 M.V. Ruano, J. Serralta, J. Ribes, F. Garcia-Usach, A. Bouzas, R. Barat, A. Seco, J. Ferrer, Application of the General Model "Biological Nutrient Removal Model No.1" to upgrade two full-scale WWTPs, Environ. Technol. 33(2012), 1005–1012.

11.6 A.N.L. Ng, A.S. Kim, A mini-review of modeling studies on membrane bioreactor (MBR) treatment for municipal wastewaters, Desalination 212 (2007), 261–281.

11.7 G. Ferrero, I. Rodríguez-Roda, J. Comas, Automatic control systems for submerged membrane bioreactors: A state-of-the-art review, Water Res. 46 (2012), 3421–3433.

11.8 A. Drews, H. Arellano-Garcia, J. Schöneberger, J. Schaller, M. Kraume, G. Wozny, Improving the efficiency of membrane bioreactors by a novel model-based control of membrane filtration, 17th European Symposium on Computer Aided Process Engineering – ESCAPE 17(2007), 345–350.

11.9 A. Drews, H. Arellano-Garcia, J. Schöneberger, J. Schaller, G. Wozny, M. Kraume, Model-based recognition of fouling mechanisms in membrane bioreactors, Desalination 236 (2009), 224–233.

11.10 J. Busch, A. Cruse, W. Marquardt, Run-to-Run Control of Membrane Filtration Processes, AIChE J. 53 (2007), 2316–2328.

11.11 C. Huyskens, E. Brauns, E. Van Hoof, L. Diels, H. De Wever, Validation of a supervisory control system for energy savings in membrane bioreactors, Water Res. 45 (2011), 1443–1453.

11.12 C. Huyskens, E. Brauns, E. Van Hoof, H. De Wever, A new method for the evaluation of the reversible and irreversible fouling propensity of MBR mixed liquor, J. Membr. Sci. 323 (2008), 185–192.

11.13 G. Ferrero, H. Monclús, G. Buttiglieri, S. Gabarron, J. Comas, I. Rodriguez-Roda, Development of a control algorithm for air-scour reduction in membrane bioreactors for wastewater treatment, J. Chem. Technol. Biotechnol. 86 (2010), 784–789.

11.14 G. Ferrero, H. Monclús, G. Buttiglieri, J. Comas, I. Rodriguez-Roda, Automatic control system for energy optimization in membrane bioreactors, Desalination 268 (2011), 276–280.

11.15 G. Ferrero, H. Monclús, L. Sancho, J.M. Garrido, J. Comas, I. Rodriguez-Roda, A knowledge-based control system for air-scour optimisation in membrane bioreactors, Water Sci. Technol. 63 (2011), 2025–2031.

11.16 R. Soleimani, N.A. Shoushtari, B. Mirza, A. Salahi, Experimental investigation, modeling and optimization of membrane separation using artificial neural network and multi-objective optimization using genetic algorithm, Chem. Eng. Res. Des. 91 (2013), 883–903.

11.17 A. Robles, M.V. Ruano, J. Ribes, J. Ferrer, Advanced control system for optimal filtration in submerged anaerobic MBRs (SAnMBRs), J. Membr. Sci. 430 (2013), 330–341.

11.18 K.J. Åström, T. Hägglund, C.C. Hang, W.K. Ho, Automatic tuning and adaptation for PID controllers - a survey, Control Engineering Practice 1(1993), 699–714.

11.19 M. Morris, Factorial sampling plans for preliminary computational experiments, Technometrics. 33 (1991), 239–245.

11.20 M.V. Ruano, J. Ribes, J. Ferrer, G. Sin, Application of the Morris method for screening the influential parameters of fuzzy controllers applied to WWTPs. Wat. Scien. Tech. 63 (2011), 2199–2206.

11.21 M.V. Ruano, J. Ribes, A. Seco, J. Ferrer, An improved sampling strategy based on trajectory design for the application of Morris method to systems with many input factors, Environ. Modell. Softw. 37 (2012), 103–109.

11.22 M.V. Ruano, J. Ribes, G. Sin, A. Seco, J. Ferrer, A systematic approach for fine-tuning of fuzzy controllers applied to WWTPs, Environ. Modell. Softw. 25 (2010), 670–676.

11.23 A. Robles, M.V. Ruano, J. Ribes, A. Seco, J. Ferrer, A filtration model applied to submerged anaerobic MBRs (SAnMBRs), J. Membr. Sci. 444(2013), 139–147.

11.24 American Public Health Association/American Water Works Association/Water Environmental Federation, Standard methods for the Examination of Water and Wastewater, 21st edition, Washington DC, USA, 2005.

11.25 B. Verrecht, T. Maere, I. Nopens, C. Brepols, S. Judd, The cost of a large-scale hollow fibre MBR, Water research 44 (2010), 5274–5283.

11.26 T. Maere, B. Verrecht, S. Moerenhout, S. Judd, I. Nopens, BSM-MBR: A benchmark simulation model to compare control and operational strategies for membrane bioreactors, Water Res. 45 (2011), 2181–2190.

11.27 S. Judd, C. Judd, The MBR Book: Principles and Applications of Membrane Bioreactors for Water and Wastewater Treatment, second ed., Elsevier, ISBN: 978-0-08-096682-3, 2011.

11.28 G. Sin, KV. Gernaey, Improving the Morris method for sensitivity analysis by scaling the elementary effects, In: proceedings of the 19th European Symposium on Computer Aided Process Engineering (ESCAPE 19), Elsevier (2009), 925–930.

11.29 F. Campolongo, J. Cariboni, A. Saltelli, An effective screening design for sensitivity analysis of large models, Environ. Modell. Softw. 22 (2007), 1509–1518.

11.30 A. Saltelli, S. Tarantola, F. Campolongo, M. Ratto, Sensitivity analysis in practice: a guide to assessing scientific models, Chicester: Wiley (2004).

11.31 T.F. Coleman, Y. Li, An interior, trust region approach for nonlinear minimization subject to bounds. SIAM J. Optim. 6 (1996), 418–445.

11.32 J.B. Copp, Development of standardised influent files for the evaluation of activated sludge control strategies, IAWQ Scientific and Technical Report Task Group: Respirometry in Control of the Activated Sludge Process–internal report, 1999.

11.33 G. Towler, R.K. Sinnott, Chemical Engineering Design: Principles, Practice and Economics of Plant and Process Design, second ed., Elsevier Science, ISBN: 978-0-08-096659-5, 2012.

CHAPTER 12:

Summary and general discussion: Implications for full-scale implementation and recommendations for further research

12.1 Research work motivation

During the developing period of this Ph.D. thesis several laboratory- and bench-scale studies on submerged anaerobic MBR (SAnMBR) technology for urban wastewater treatment have been published. Literature demonstrates the potentials of SAnMBR technology for efficiently treating a wide variety of wastewaters, and producing both high-quality, pathogen-free treated water and methane-rich biogas, which can be used as renewable energy resource. However, there are still some barriers or challenging issues that limit the widespread practical application of this emerging technology for urban wastewater treatment. In addition, pilot-scale studies are limited and full-scale implementation has not been reported yet [12.1]. Therefore, the objective of this Ph.D. thesis is to further investigate the feasibility of full-scale SAnMBR systems as core technology for urban wastewater treatment. Specifically, this thesis focussed on modelling, simulation and control of filtration process in SAnMBRs. The main point of this research work was to operate a SAnMBR plant that includes industrial-scale membrane modules and is fed with urban wastewater at ambient temperature.

12.2 Instrumentation, control, and automation (ICA) for submerged anaerobic MBR (SAnMBR)

One key step for adequately implementing SAnMBR technology on an industrial scale is developing appropriate instrumentation, control, and automation (ICA) systems that facilitate system management and save manpower and energy. In this respect, this Ph.D. thesis proposes an ICA system for SAnMBRs which was developed taking into account the main parameters that affect the process performance (*e.g.* transmembrane pressure (TMP), transmembrane flux (J), etc.). Moreover, it was possible to detect and solve two critical issues in systems of this type: (1) the initial flow-rate instabilities derived from those proportional-integral-derivative (PID) controllers whose normal operating mode means intermittent operation of the associated equipment (*i.e.* permeate pumps); and (2) the process disturbance related to head-space pressure variations in the anaerobic reactor, which are associated to variable mixed liquor level in the reactor (typical of closed systems). The first issue, which critically affected the filtration process performance, was successfully solved by implementing a correcting action each time the pump was started up. This correcting action consists in operating the pumps at fixed frequency for a short period of time before starting the corresponding flow-rate PID controller. This way, a start-up of the PID controller from an initial situation far from the established flow rate set-point is avoided, which allows the set-point to be reached in a short period of time and a

high stability performance. Regarding the second issue, to avoid possible disturbances on the mixed liquor volume in the anaerobic reactor, the proposed control strategy established a J proportional to the influent wastewater flow rate. This control strategy avoids possible variations in the mixed liquor level, which results in the following disturbances: (1) incorrect biogas wasted flow rate due to oscillations in the biogas wasting valve, which is controlled by a head-space pressure controller; (2) variations in the mixed liquor total solids (MLTS) concentration (affecting the physical separation process performance); (3) variations in the water column resistance to be overcome by the gas flow entering the membrane tank, thus affecting the energy consumption required to maintain fixed biogas flow rate; and (4) variations in the biogas recirculation to the membrane tank when operating in fixed pressure control mode, which can result in insufficient gas sparging intensities for membrane scouring, weak mixing intensities in the SAnMBR system, death zones in the anaerobic reactor, and so on.

As regards control in membrane separation process, it is important to highlight that appropriate instrumentation and automation equipment is necessary to automatically implement enhanced membrane operating mode, which is essential for an optimised process performance. Indeed, the proposed ICA offers high process stability towards perturbations, which improves the overall controllability of the SAnMBR technology and allows optimising membrane performance.

12.3 Sustainable membrane operation

In this Ph.D. thesis, the long-term performance of an SAnMBR system with industrial-scale membrane modules has been assessed. The main advantage of submerged membrane configurations is that the energy required for the crossflow filtration is not required, although biogas needs to be recycled from the headspace to underneath the membranes to provide gas bubble shear to minimise membrane fouling [12.2]. Nevertheless, submerged configurations usually lead to lower shear rates compared to crossflow configurations, and hence to lower operating J.

On the other hand, SAnMBRs are generally designed at lower J than submerged aerobic MBRs (SAeMBRs) [12.3]. However, this leads to greater installed membrane areas, although lower operating costs [12.4]. Therefore, it is necessary to optimise the membrane operating mode, thus optimising the operating J, in order to avoid possible uneconomical membrane performances when scaling-up SAnMBR technology for urban wastewater treatment. In this respect, membrane fouling must be minimised since it finally determines the operating sustainability of the filtration process in the long term. Specifically, reversible fouling related to cake layer build-up was found to be the key physical process governing the applicable J in the SAnMBR evaluated in this research work. Hence, it is

critical to find economical ways of reducing cake layer building-up for optimising SAnMBR technology treating urban wastewater at full scale.

12.3.1 Membrane scouring by gas sparging

Membrane scouring by gas sparging (usually measured as specific gas demand per square metre of membrane area (SGD_m) or as specific gas demand per permeate volume (SGD_P)) is the most widely used technique for reducing membrane fouling in submerged hollow fibre systems. Selecting the adequate gas sparging intensity in each operating range is essential for making SAnMBR technology economically feasible in the long term since considerable energy savings could be achieved.

It has been shown that it is theoretically possible to operate the membranes at a J up to 13 LMH when operating at SGD_m of 0.17 $Nm^3\ h^{-1}\ m^{-2}$ (almost half of the lowest threshold suggested by membrane suppliers (0.3 $Nm^3\ h^{-1}\ m^{-2}$) for the typical operating range for aerobic MBRs). Moreover, the fouling rate values shown in this Ph.D. thesis predict that it is theoretically possible to maintain sub-critical filtration conditions (*i.e.* to operate at sustainable J values) when operating membranes at quite high MLTS levels, without applying a prohibitive SGD_m. For instance, it was theoretically possible to operate membranes sub-critically at 28 g L^{-1} of MLTS when J was 10 LMH and SGD_m about 0.25 $Nm^3\ h^{-1}\ m^{-2}$. By contrast, it was theoretically possible to operate sub-critically at MLTS of 23 g L^{-1} with J between 12 and 19 LMH and SGD_m ranging from 0.17 to 0.50 $Nm^3\ h^{-1}\ m^{-2}$. Thus, a considerable increase in J can be achieved in sub-critical filtration conditions by increasing SGD_m and/or slightly reducing MLTS.

The results shown in this Ph.D. thesis confirm that the gas sparging intensity poses a major challenge since it must be minimised in order to maximise energy savings of SAnMBR systems at full-scale. In this regard, it is important to emphasise that aeration energy can account for up to 50 - 75% of all the energy consumed by SAeMBR technology [12.5]. Specifically, in this Ph.D. thesis the energy consumption related to membrane scouring by gas sparging resulted in about 0.10-0.15 kWh m^{-3} when working with strongly fouled membranes.

On the other hand, optimising gas sparging intensity for every operating range as well as for every membrane operating mode enables not only considerable energy savings but also adequate long-term operating, since it is possible to minimise the onset of irreversible/irrecoverable fouling problems. In this respect, the effect of other key operating parameters entailing the membrane operating mode on membrane performance was also assessed at different MLTS levels: frequency and duration of the

physical cleaning stages (back-flushing and relaxation); and sludge recycling velocity through the membrane tank.

12.3.2 Sludge recycling velocity through the membrane tank

Controlling the sludge recycling velocity through the membrane tank is essential since this operating variable is related to the sludge concentration factor resulting from the ratio between the sludge flow entering the membrane tank and the net permeate flow. In this regard, the MLTS in the membrane tank could reach prohibitive values when the concentration in the sludge entering the membrane tank has considerably high values. For instance, when the MLTS entering the membrane tank is 25 g L^{-1} and the ratio between the sludge recycling flow rate and the permeate flow rate is 9 (the maximum studied value), the MLTS recycled to the anaerobic reactor is expected to be around 28 g L^{-1}.

Therefore, the operating sludge recycling velocity must be selected carefully depending on the operating conditions. Nonetheless, sludge recycling ratio must be minimised in order to maximise energy savings in full-scale SAnMBR systems since pumping energy accounts for up to 15 – 20% of all the energy consumed in SAeMBR technology [12.5]. Specifically, in this Ph.D. thesis the energy consumption related to sludge pumping resulted in about 0.03-0.04 kWh m^{-3} when working with strongly fouled membranes.

12.3.3 Duration and frequency of the physical cleaning stages

The results of this Ph.D. thesis suggest that, when membranes are operated supra-critically at low SGD_m, the duration and/or frequency of the physical cleaning stages (relaxation and back-flushing) must be increased considerably. For instance, when operating at MLTS levels above 24 g L^{-1}, a significant decrease in K was detected, making necessary to increase the back-flushing frequency from 1:30 (Back-flushing : Filtration-Relaxation) to 1:10 in order to keep the filtration process working below the operating TMP safety value. Nevertheless, MLTS around 30 g L^{-1} are not advisable since increasing the back-flushing frequency from 1:30 to 1:10 did not improve the membrane performance.

As regard relaxation stage, it was observed that K was not critically affected by relaxation stages duration between 30 and 50 seconds when operating at MLTS levels below 25 g L^{-1}. This behaviour was mainly the result of combining relaxation stages with an appropriate back-flushing frequency what allowed keeping TMP stable at quite low values. On the other hand, decreasing the relaxation

stage duration from 50 to 30 seconds at MLTS levels of 28 g L^{-1} resulted in a slight increase in the reversible fouling component that accumulated on the membrane surface. Therefore, MLTS above 28 g L^{-1} are not advisable due to a decrease in the efficiency of membrane scouring by gas sparging.

It is worth pointing out that the downtime for physical cleaning affects the economic feasibility of the process because of the resulting decrease in the net volume of treated water. Hence, it is advisable to control duration and frequency of the physical cleaning stages in each operating MLTS level to ensure that the membrane is properly cleaned whilst minimising the operating cost per unit of treated water (*e.g.* reducing SGD_P).

12.3.4 The dilemma of operating sub-critically or supra-critically

Two opposite design strategies could be applied depending on the operating regime adopted. If the design strategy is based on sub-critical operating, the installed filtration area must be increased – which increases the initial investment cost. On the other hand, if the design strategy selected is based on operating supra-critically, then high back-flushing frequencies and/or unsustainable SGD_m are required – which increases operating and maintenance/replacement costs. Thus, this design decision may result in low process efficiency per unit of treated water or high energy consumption, respectively.

Results shown in this Ph.D. thesis demonstrates that working at sub-critical filtration conditions is an adequate operating strategy for SAnMBR technology treating urban wastewater because no considerable irreversible/irrecoverable fouling rates are reached whilst working at low energy requirements. Indeed, membranes did not required chemical cleaning after being operated for more than two years. Nevertheless, an exhaustive economic analysis should be carried out in any specific scenario to accurately demonstrate the feasibility of working at sub-critical or supra-critical levels.

12.3.5 Full-scale application of hollow-fibre membranes

The results obtained in this Ph.D. thesis are quite similar to the results from full-scale applications of SAeMBR technology treating urban wastewater. In this regard, the SAnMBR system evaluated in this research work resulted in reasonably adequate J and K by applying moderate SGD_P. Moreover, the average downtime for physical cleaning obtained in this Ph.D thesis (about 18% of the operating time) remained in a similar range to full-scale SAeMBR applications [12.3].

As mentioned above, it is important to emphasise that – despite operating at high MLTS levels and with temperature shocks that affected the physical properties of the sludge – the membranes did not require chemical cleaning after being operated for more than two years, which is a considerably longer period than the ones usually employed in SAeMBR technology. Hence, hollow-fibre (HF) membrane technology can be considered a promising, competitive technology for the anaerobic treatment of urban wastewater.

12.4 Minimising the onset of irreversible/irrecoverable fouling

It was expected that SAnMBRs could present lower sludge filterability than SAeMBRs, thus resulting in more intense membrane fouling propensities [12.3]. In this respect, some studies suggested that the cake layer formed with aerobic and anaerobic sludge might present different removability (see, for instance, Meng *et al*. [12.10]). Nevertheless, based on the results obtained in this Ph.D. thesis, which are comparable to the results from the aerobic operation of HF membranes at full scale [12.3], it can be assumed that, for this case study, differences between anaerobic and aerobic sludge properties (*i.e.* extracellular polymeric substances (EPS), soluble microbial products (SMP), biomass concentration, sludge viscosity, etc.) did not critically determine the removability of the cake layer from the membrane surface.

The experimental period shown in this research work can be divided in two different long-term operating periods according to the irreversible/irrecoverable fouling rate observed. During the first operating period (up to operating day 300) no significant irreversible/irrecoverable fouling was observed, which indicated that the total filtering resistance was mainly related to cake layer resistance. This behaviour means that MLTS level is a key factor affecting K in this HF-based SAnMBR system. Indeed, a linear dependency of K on MLTS was observed [12.6; 12.7]. The low onset of irreversible fouling during this first operating period was mainly attributed to the low amounts of EPS and SMP present in the mixed liquor. EPS and SMP levels were low due to the high sludge retention time (SRT) in this first period (set to 70 days). On the other hand, a progressive accumulation of irreversible/irrecoverable fouling over the membrane surface was detected after operating day 300. During this operating period higher amounts of EPS and SMP were observed. It was attributed to operating at lower SRTs than in the first period (it was set to 30 – 40 days).

The results obtained in this research work revealed that EPS and SMP affected not only the three-dimensional floc matrix, but also the fouling propensity (K decreased as EPS and SMP increased). On the other hand, the EPS and SMP levels observed when operating at mesophilic conditions were

higher than at psychrophilic conditions. Nonetheless, irreversible/irrecoverable fouling was in general low during the whole experimental period shown in this research work. These results revealed that membrane fouling was successfully controlled mainly due to applying physical cleaning mechanisms (relaxation, back-flushing and gas sparging) and operating membranes sub-critically.

Apart from operating at sub-critical filtration conditions and establishing an adequate membrane operating mode, other factors were identified as key parameters minimising possible irreversible/irrecoverable fouling problems in this HF-SAnMBR system, such as the relatively low operating pH (around 6.7). This low pH reduces chemical precipitation propensity. Besides chemical precipitation propensity, recent literature [12.8; 12.9] has demonstrated that pH affects the anaerobic sludge properties thus affecting the biofouling propensity. It has been shown that pH can influence on either the dispersion of sludge flocs resulting in sub-products generation (colloids and solutes or biopolymers) or the adherence ability and fouling propensity of EPS.

12.5 Modelling filtration process

In this Ph.D. thesis a resistance-in-series-based model was developed, calibrated and validated on the basis of the experimental data available from the before-mentioned SAnMBR plant fitted with industrial-scale membrane units. The proposed model will be useful for several applications, such as design, upgrading and scaling-up of SAnMBR-based systems, and development of operating and control strategies designed to optimise full-scale process performance not only in the short term, but also in the long term. It is worth pointing out that studies aimed to numerically simulate SAnMBR technology for urban wastewater entailing full-scale membranes were not previously reported.

The model was validated in both the short and the long term, which demonstrated the potentials of the proposed model. Although considerably high variations were applied to J and SGD_m, the proposed model was able to correctly reproduce the filtration performance of the evaluated SAnMBR system. Moreover, the model was capable of reproducing the reduction in TMP caused by relaxation or back-flushing. In this respect, since the proposed filtration model was developed on the basis of the operating results from an SAnMBR system fitted with industrial-scale membranes, most of the parameters included in the model were defined in order to represent somehow all possible filtration process performances.

A sensitivity analysis of the proposed filtration model was also assessed. The sensitivity analysis consisted in a revised version of the Morris screening method, which is considered as a one-factor-at-

a-time (OAT) method for global sensitivity analysis. This assessment aimed to (1) identify the less (or non) influential parameters of the model to facilitate model calibration and (2) validate the modelling approach (*i.e.* assessing the necessity of including in the model each of the proposed parameters). Indeed, by applying the Morris screening method it was possible to validate the evaluated model: 6 of the 14 model parameters were identified as influential, corresponding to those model parameters which were calibrated using direct off-line experiments.

Important to highlight is that biological modelling on anaerobic filtration-based systems is quite recent, which makes difficult to obtain reliable information about the interaction between biological and filtration processes. Therefore, enhancing biological modelling of anaerobic processes of this type may allow improving the quality of the proposed filtration model since a greater amount of useful data related to different fouling mechanisms would be available (*e.g.* EPS, SMP, colloidal matter, etc.).

12.6 Optimising filtration process

Although the membrane module costs have decreased dramatically in the last years, further research is needed in energy consumption of SAnMBR technology on an industrial scale. It is worth pointing out that SAnMBRs can lead to energy-sustainable urban wastewater management, even in mild climate regions. Hence, it is essential to develop control systems aimed to optimise filtration process under the minimum operating costs in order to optimise the economic feasibility of full-scale SAnMBR systems.

Since most of the recently-published studies on monitoring and control strategies designed to save energy in filtration have been developed for SAeMBR technology (see, for instance, Ferrero *et al*. [12.11; 12.12]; Huyskens *et al*. [12.13]), in this Ph.D. thesis an advanced control system was developed aimed to optimise filtration in full-scale SAnMBRs.

The results from the developed controller are promising. Energy savings of up to 50% were obtained in sludge pumping (energy demand for sludge pumping was reduced from approximately 0.06 to 0.03 kWh m^{-3}). The total downtime caused by physical cleaning (relaxation and back-flushing) accounted for less than 2% of operating time when performing the control system, which is considerably lower than the average full-scale results from SAeMBR technology found in the literature (around 16 – 19% of operating time) [12.3]. Moreover, considerable savings in gas sparging intensity for membrane scouring were achieved after implementing the proposed control system (up to 60% of SGD_m). Indeed, the energy demand for membrane scouring was reduced from approx. 0.36 to 0.15 kWh m^{-3}.

In addition, a model-based supervisory controller was proposed for real-time optimising the above-mentioned advanced controller by an automatic tuning procedure. This model-based supervisory system, which uses the filtration model developed in this Ph.D. thesis, is based on an optimising methodology that considers the following three statistical methods: (1) sensitivity analysis (Morris screening method) to find an identifiable input subset for the advanced controller; (2) Monte Carlo procedure (using trajectory-based random sampling technique) to find adequate initial values for the control inputs; and (3) optimising algorithm to minimise an operating cost objective function. The Morris screening method allowed for identifying the strongly-influential inputs of the advanced control system; the Monte Carlo procedure allowed for selecting suitable initial values for the advanced controller inputs; and the optimising algorithm allowed the advanced controller to be enhanced with moderate computational demand (around 5 minutes) by minimising an operating cost objective function.

Energy savings during membrane scouring by gas sparging of up to 25% were achieved with this automatic tuning methodology in comparison with the energy consumption resulting from running the advanced controller alone. The average operating cost of the SAnMBR after implementing the proposed model-based supervisory controller was about €0.028 per m^3 (the energy term considered in this study was €0.138 per kWh, according to the current electricity rates and prices in Spain), from which about 85.7 % corresponded to the cost related to energy requirements (about €0.024 per m^3). Moreover, the proposed supervisory controller proposed in this Ph.D. thesis accomplishes the main requirements for a real-time optimisation [12.14]: (1) robustness (i.e. it always finds a solution); (2) fast problem solving; (3) in certain operating conditions, it always reaches the same solution, even from different starting points; and (4) ability to identify system constraints.

Therefore, in accordance to recent literature in the field [12.15; 12.16], the results obtained in this Ph.D. thesis are promising since it is expected that SAnMBR treating urban wastewater can be successfully implemented at full scale under minimum operating costs related to filtration process.

12.7 Moving towards sustainable urban wastewater treatment

The urban wastewater treatment industry is moving towards sustainability, including greater emphasis on the energy/water nexus, potentially leading to greater use of anaerobic processes [12.17]. Specifically, there are now net-energy-producing urban WWTPs where the electricity consumed for wastewater treatment is exceeded by the energy recovered in the form of methane [12.18]. Therefore,

further research needs to be directed toward methane recovery in SAnMBR systems. In this respect, it has been reported that the energy recovery from high strength wastewater can represent up to 7 times the required energy to operate an SAnMBR system [12.19]. In addition, recovering the dissolved methane leaving the system in the effluent is of great interest (particularly for dilute wastewater) because it can be used for meeting energy requirements, but also because it is mandatory for reducing the greenhouse gases emissions. Hence, development of effective and economical methane recovery technologies would further improve the economic feasibility of SAnMBR for urban wastewater treatment at full scale [12.20]. In this regard, different processes have been reported in recent literature aimed to capture the dissolved methane present in the effluent, such as stripping of SAnMBR effluent through post-treatment aeration [12.21], methane recovery using a degassing membrane [12.22], and the use of a down-flow hanging sponge reactor [12.23].

12.8 References

12.1 G. Skouteris, D. Hermosilla, P. López, C. Negro, A. Blanco, Anaerobic membrane bioreactors for wastewater treatment: A review, Chem. Eng. J. 198/199 (2012), 138–148.

12.2 I. Vyrides, D.C. Stuckey, Saline sewage treatment using a submerged anaerobic membrane reactor (SAMBR): effects of activated carbon addition and biogas sparging time, Water Res. 43 (2009), 933–942.

12.3 S. Judd, C. Judd, The MBR Book: Principles and Applications of Membrane Bioreactors for Water and Wastewater Treatment, 2nd edition, Elsevier, ISBN: 978–0–08–096682–3, 2011.

12.4 D.C. Stuckey, Recent developments in anaerobic membrane reactors, Bioresource Technol. 122 (2012), 137–148.

12.5 B. Verrecht, T. Maere, I. Nopens, C. Brepols, S. Judd, The cost of a large-scale hollow fibre MBR. Water Res. 44 (2010), 5274–5283.

12.6 A. Robles, F. Durán, M.V. Ruano, J. Ribes, J. Ferrer, Influence of total solids concentration on membrane permeability in a submerged hollow–fibre anaerobic membrane bioreactor, Water Sci. Technol. 66 (2012), 377–384.

12.7 A. Robles, M.V. Ruano, J. Ribes, J. Ferrer, Performance of industrial hollow–fibre membranes in a submerged anaerobic MBR (HF–SAnMBR), system under mesophilic and psychrophilic conditions, Sep. Purif. Technol. 104 (2013), 290–296.

12.8 W.J. Jane Gao, H.J. Lin, K.T. Leunga, B.Q. Liao, Influence of elevated pH shocks on the performance of a submerged anaerobic membrane bioreactor, Process Biochem. 45 (2010) 1279–1287.

12.9 A. Sweity, W. Ying, S. Belfer, G. Oron, M. Herzberg, pH effects on the adherence and fouling propensity of extracellular polymeric substances in a membrane bioreactor, J. Membr. Sci. 378 (2011) 186–193.

12.10 F. Meng, S.R. Chae, A. Drews, M. Kraume, H.S. Shin, F. Yang, Recent advances in membrane bioreactors (MBRs): Membrane fouling and membrane material, Water Res. 43 (2009), 1489–1512.

12.11 G. Ferrero, H. Monclús, G. Buttiglieri, J. Comas, I. Rodriguez–Roda, Automatic control system for energy optimization in membrane bioreactors, Desalination 268 (2011), 276–280.

12.12 G. Ferrero, H. Monclús, J.M. Garrido, L. Sancho, J. Comas, I. Rodriguez–Roda, A knowledge–based control system for air scour optimization in membrane bioreactors. Water Sci. Technol. 63 (2011), 2025–2031.

12.13 C. Huyskens, E. Brauns, E. Van Hoof, E. Diels, H. De Wever, Validation of a supervisory control system for energy saving in membrane bioreactors, Water Res. 45 (2011), 1443–1453.

12.14 G. Towler, R.K. Sinnott, Chemical Engineering Design: Principles, Practice and Economics of Plant and Process Design, second ed., Elsevier Science, ISBN: 978-0-08-096659-5, 2012.

12.15 H. Lin, J. Chen, F. Wang, L. Ding, H. Hong, Feasibility evaluation of submerged anaerobic membrane bioreactor for municipal secondary wastewater treatment, Desalination 280 (2011), 120–126.

12.16 I. Martin, M. Pidou, A. Soares, S. Judd, B. Jefferson, Modelling the energy demands of aerobic and anaerobic membrane bioreactors for wastewater treatment, Environ. Technol. 32 (2011), 921–932.

12.17 J.T. Kraemer, A.L. Menniti, Z.K. Erdal, T.A. Constantine, B.R. Johnson, G.T. Daigger, G.V. Crawford, A practitioner's perspective on the application and research needs of membrane bioreactors for municipal wastewater treatment, Bioresource Technol. 122 (2012), 2–10.

12.18 WERF, Best Practices for Sustainable Wastewater Treatment: Initial Case Study Incorporating European Experience and Evaluation Tool Concept, Report OWS04R07a, Water Environ. Res. Foundation, Alexandria, VA, 2010.

12.19 P.J. Van Zyl, M.C.Wentzel, G.A. Ekama, K.J. Riedel, Design and start-up of a high rate anaerobic membrane bioreactor for the treatment of a low pH, high strength, dissolved organic waste water, Water Sci. Technol. 57 (2008) 291–295.

12.20 H. Lin, W. Peng, M. Zhang, J. Chen, H Huachang, Y. Zhang, A review on anaerobic membrane bioreactors: Applications, membrane fouling and future perspectives, Desalination 314 (2013), 169–188.

12.21 P.L. McCarty, J. Bae, J. Kim, Domestic wastewater treatment as a net energy producer–can this be achieved? Environ. Sci. Technol. 45 (2011) 7100–7106.

12.22 W.M.K.R.T.W. Bandara, H. Satoh, M. Sasakawa, Y. Nakahara, M. Takahashi, S. Okabe, Removal of residual dissolved methane gas in an upflow anaerobic sludge blanket reactor treating low-strength wastewater at low temperature with degassing membrane, Water Res. 45 (2011) 3533–3540.

12.23 M. Hatamoto, H. Yamamoto, T. Kindaichi, N. Ozaki, A. Ohashi, Biological oxidation of dissolved methane in effluents from anaerobic reactors using a down-flow hanging sponge reactor, Water Res. 44 (2010) 1409–1418.

CHAPTER 13:

General conclusions

This Ph.D. thesis aimed to investigate the potential of submerged anaerobic membrane bioreactors (SAnMBRs) as core technology for urban wastewater treatment. The main features studied in this Ph.D. thesis focussed on modelling, simulation and control of filtration process in SAnMBRs. From this, the following conclusions can be drawn:

Instrumentation, control, and automation (ICA) for submerged anaerobic membrane bioreactors (SAnMBRs)

1. Establishing an adequate instrumentation, control and automation (ICA) system for SAnMBR is required for enabling suitable and stable process performance towards perturbations.
2. Various modifications to the classical proportional-integral-derivative (PID) control from the lower layer controllers are required to enhance global process performance.

Sub-critical filtration conditions of commercial hollow-fibre membranes in a submerged anaerobic MBR (HF-SAnMBR) system: the effect of gas sparging intensity

3. A linear dependency between the critical flux (J_C) and the specific gas demand per square metre of membrane area (SGD_m) was observed.
4. At mixed liquor total solids (MLTS) concentrations above 22 g L^{-1}, J_C ranged from 12 to 19 LMH at quite low SGD_m values compared to aerobic MBRs (between 0.17 and 0.5 Nm^3 h^{-1} m^{-2}, respectively).

Factors that affect the permeability of commercial hollow-fibre membranes in a submerged anaerobic MBR (HF-SAnMBR) system

5. Low gas sparging intensities (around 0.23 Nm^3 h^{-1} m^{-2}) and low back-flushing (BF) frequencies (30 seconds of BF every 10 basic filtration-relaxation (F-R) cycle) were enough to operate membranes sub-critically even at high levels of MLTS (up to 25 g L^{-1}).
6. Membrane performance in the studied SAnMBR system was similar to the aerobic HF membranes operated in full-scale MBR plants (for instance, similar specific gas demand per permeate volume (SGD_P) were achieved).

Sub-critical long-term operation of industrial scale hollow-fibre membranes in a submerged anaerobic MBR (HF-SAnMBR) system

7. After more than two years of continuous operation no significant irreversible fouling problems were detected, and low fouling rates were observed even when MLTS was high.
8. This was mainly attributed to: operating at sub-critical filtration conditions; establishing an adequate membrane operating mode; and working at pH values of less than 7 as a result of part of the biogas produced being recycled for in-situ sparging.

Performance of industrial scale hollow-fibre membranes in a submerged anaerobic MBR (HF-SAnMBR) system at mesophilic and psychrophilic conditions

9. MLTS was identified as one key factor affecting membrane permeability (K).
10. Higher membrane fouling propensities were observed under mesophilic than under psychrophilic conditions due to higher soluble microbial products (SMPs) production.

A filtration model applied to submerged anaerobic MBRs (SAnMBRs)

11. The short- and long-term validation of the resistance-in-series-based filtration model proposed in this Ph.D. thesis resulted in satisfactory correlation coefficients (R) of 0.981 and 0.964 respectively.
12. The developed model was able to accurately reproduce the filtration process in a SAnMBR plant fitted with industrial-scale hollow-fibre membranes.

Mathematical modelling of filtration in submerged anaerobic MBRs (SAnMBRs): long-term validation

13. The developed filtration model was adequately validated in a wide range of operating conditions using both heavily-fouled and lightly-fouled industrial-scale membrane units.
14. The simulation results revealed that irreversible fouling was the main component in the weighted average distribution of total filtration resistance in the long term.

Sensitivity analysis of a filtration model for submerged anaerobic MBRs (SAnMBRs) using a revised version of the Morris screening method

15. By applying the Morris screening method it was possible to validate the developed model: 6 of the 14 model parameters were identified as highly influential, corresponding to those parameters which were calibrated using direct off-line experiments.

Advanced control system for optimal filtration in submerged anaerobic MBRs (SAnMBRs)

16. The advanced control system for filtration in SAnMBR systems proposed in this Ph.D. thesis revealed promising results: low fouling rates (almost 0 mbar min^{-1}) were achieved by applying sustainable gas sparging intensities (approx. 0.23 Nm^3 h^{-1} m^{-2}); physical cleaning downtimes were reduced considerably to around 2% of the total operating time.

Model-based automatic tuning of a filtration control system for submerged anaerobic MBRs (SAnMBRs)

17. The model-based supervisory controller proposed in this Ph.D. thesis allowed the above-mentioned advanced controller to be enhanced by an automatic tuning with moderate computational demand (around 5 minutes).
18. Energy savings during membrane scouring of up to 25% were achieved compared to the advanced controller running alone.
19. The average operating cost of the SAnMBR system after implementing the proposed supervisory controller was about €0.028 per m^3, from which about 85.7 % corresponded to the energetic costs.

Demonstration Plant
Modelling
Cake-layer
Fouling
Knowledge-based Control
Automation
Fuzzy-logic
Monte Carlo
Relaxation
Membrane Scouring
Hollow-fibre Membranes
Resistance-in-series
Critical Flux
Model-based Control
Commercial Membranes
Back-flushing
Set-point
Dynamic Calibration
Flux-step Method
Simulation
Transmembrane Flux
Mesophilic
Energy Savings
Biogas Sparging
Morris Method
Off-line Calibration
SAnMBR
Instrumentation Control
Sensitivity Analysis
Filtration
SGD
Psychrophilic
OLR
Permeability
Real-time Optimiser
TMP
Filtering Resistance
On-line Monitoring
Model Validation
EPS
Optimisation
Submerged
Mltsm
SMP
Advanced Control System
Urban Wastewater
Ventilation